



UNIL | Université de Lausanne

Unicentre

CH-1015 Lausanne

<http://serval.unil.ch>

Year : 2012

ANALYSIS OF CD4+ AND CD8+ T CELLS BY DEFINED MHC- PEPTIDE COMPLEXES

DOJCINOVIC Danijel

DOJCINOVIC Danijel, 2012, ANALYSIS OF CD4+ AND CD8+ T CELLS BY DEFINED MHC-
PEPTIDE COMPLEXES

Originally published at : Thesis, University of Lausanne

Posted at the University of Lausanne Open Archive.
<http://serval.unil.ch>

Droits d'auteur

L'Université de Lausanne attire expressément l'attention des utilisateurs sur le fait que tous les documents publiés dans l'Archive SERVAL sont protégés par le droit d'auteur, conformément à la loi fédérale sur le droit d'auteur et les droits voisins (LDA). A ce titre, il est indispensable d'obtenir le consentement préalable de l'auteur et/ou de l'éditeur avant toute utilisation d'une oeuvre ou d'une partie d'une oeuvre ne relevant pas d'une utilisation à des fins personnelles au sens de la LDA (art. 19, al. 1 lettre a). A défaut, tout contrevenant s'expose aux sanctions prévues par cette loi. Nous déclinons toute responsabilité en la matière.

Copyright

The University of Lausanne expressly draws the attention of users to the fact that all documents published in the SERVAL Archive are protected by copyright in accordance with federal law on copyright and similar rights (LDA). Accordingly it is indispensable to obtain prior consent from the author and/or publisher before any use of a work or part of a work for purposes other than personal use within the meaning of LDA (art. 19, para. 1 letter a). Failure to do so will expose offenders to the sanctions laid down by this law. We accept no liability in this respect.



UNIL | Université de Lausanne

Faculté de biologie
et de médecine

Centre Ludwig de l'Université de Lausanne pour la recherche sur le cancer

**ANALYSIS OF CD4+ AND CD8+ T CELLS
BY DEFINED MHC-PEPTIDE COMPLEXES**

Thèse de doctorat ès sciences de la vie (PhD)

présentée à la

Faculté de biologie et de médecine
de l'Université de Lausanne

par

Danijel DOJCINOVIC

Biologiste diplômé de l'Arizona State University, USA

Jury

Prof. Dr. Sanjiv Luther, président
Dr. Immanuel F. Luescher, directeur de thèse
Prof. Dr. Hans Acha-Orbea, rapporteur
Prof. Dr. Daniel Speiser, expert interne
Prof. Dr. Pedro Romero, expert interne
Prof. Dr. Ed Palmer, expert externe

Lausanne , le 13 septembre 2012

Imprimatur

Vu le rapport présenté par le jury d'examen, composé de

<i>Président</i>	Monsieur Prof. Sanjiv Luther
<i>Directeur de thèse</i>	Monsieur Dr Immanuel Luescher
<i>Rapporteur</i>	Monsieur Prof. Hans Acha-Orbea
<i>Experts</i>	Monsieur Prof. Daniel Speiser
	Monsieur Prof. Pedro Romero
	Monsieur Prof. Ed Palmer

le Conseil de Faculté autorise l'impression de la thèse de

Monsieur Danijel Dojcinovic

Master of Science de Arizona State University, USA

intitulée

**ANALYSIS OF CD4+ AND CD8+ T CELLS
BY DEFINED MHC-PEPTIDE COMPLEXES**

Lausanne, le 13 septembre 2012

pour Le Doyen
de la Faculté de Biologie et de Médecine

Prof. Sanjiv Luther

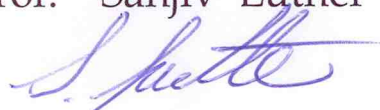


Table of contents

ACKNOWLEDGMENTS	1
SUMMARY	2
RÉSUMÉ	4
LIST OF ABBREVIATIONS	6
1. INTRODUCTION	8
1.1 General introduction to immunity	8
1.2 T cell receptor.....	9
1.2.1 Structural aspects of T cell receptors.....	9
1.2.2 T cell receptor triggering	10
1.2.3 T cell receptor signaling	12
1.3 MHC-peptide complexes.....	14
1.3.1 Structural aspects of MHC-peptide complexes	14
1.3.2 Pathways of antigen presentation	17
1.4 CD8 and CD4 coreceptors.....	18
1.5 T cells	21
1.5.1 Origin and development of T cells	21
1.5.2 Activation and differentiation of T cells.....	22
1.5.3 CD8+ T cells.....	23
1.5.4 CD4+ T cells – subsets and functions	23
1.6 Fluorescent MHC-peptide oligomers (“tetramers”).....	25
1.7 Thesis aims.....	28
2. MATERIALS AND METHODS	29
2.1 General materials and methods	29
2.1.1 Reagents and consumables	29
2.1.2 Antibiotics	29
2.1.3 Enzymes.....	29
2.1.4 Kits.....	30
2.1.5 Solutions and cell culture media.....	30
2.1.6 Instruments	33
2.1.7 FPLC columns	33

2.1.8 HPLC columns	33
2.1.9 Software.....	33
2.1.10 Molecular biology methods	34
2.2 Materials and methods, Chapter I	35
2.3 Materials and methods, Chapter II	48
3. Detection of antigen-specific CD4+ T cells by novel types of MHC class II–peptide complexes	56
3.1 Results	56
3.1.1 State of the art of MHC-peptide multimer staining of specific CD4+ T cells.....	56
3.1.2 Loading of “empty” MHC class II molecules with specific peptides and impact of peptide loading efficiency on multimer staining	59
3.1.3 Purification of <i>bona fide</i> MHC class II-peptide complexes and impact on staining of antigen-specific CD4+ T cells.....	62
3.1.3.1 Purification via a His-tag at the peptide N-terminus	62
3.1.3.2 Reversible N-terminal peptide tags	66
3.1.3.3 Purification of MHC-peptide monomers via N-terminal acidic tags.....	69
3.1.3.4 MHC-peptide monomer purification via a N-terminal DTB tag	73
3.1.4 NTAmers: a novel class of reversible MHC class II-peptide staining reagents	74
3.1.4.1 Principles of the new strategy.....	75
3.1.4.2 Staining performance of reversible NTAmers and staining reversibility	77
3.1.5 Improving peptide loading of MHC class II molecules via conditional peptide ligands.....	80
3.1.5.1 Design of conditional photocleavable peptide ligands	80
3.1.5.2 Relative affinity of conditional peptide ligands for DR4 and efficiency of photocleavage.....	81
3.1.5.3 Dissociation of photocleaved peptide depends on temperature and pH	82
3.1.5.4 Increased peptide binding of UV-irradiated, photosensitive DR4/HA*5 peptide complexes	84
3.1.5.5 Detection of antigen-specific T cells with peptide exchange multimers	85
3.2 Discussion	88
3.3 Conclusion and perspectives	91
4. Essential role of the CD8α transmembrane domain for efficient CD8 coreceptor function	93
4.1 Results	93
4.1.1 Role of transmembrane domains for CD8 coreceptor function.....	93
4.1.2 Cell surface expression of CD8 α and CD8 α_{TAc} on T1 T cell hybridomas	94
4.1.3 K ^d /PbCS(ABA) multimer binding.....	95

4.1.4 Calcium flux and IL-2 production is impaired on hybridomas expressing CD8 α_{Tac}	98
4.1.5 Assessment of the proximity of CD8 and TCR:CD3 by FRET	99
4.1.6 Multimer and CD8 β co-localize on CD8 $\alpha\beta$ and CD8 $\alpha_{\text{Tac}}\beta$ hybridomas	101
4.1.7 Expression of CD3 ζ -CFP in hybridomas harboring CD8 β -YFP and CD8 α or CD8 α_{Tac}	102
4.1.8 Antigen-dependent responses of hybridomas expressing CD8 β -YFP, CD3 ζ -CFP and CD8 α or CD8 α_{Tac}	104
4.1.9 Antigen-induced CD8-CD3 ζ interaction is reduced on CD8 $\alpha_{\text{Tac}}\beta$ hybridoma	106
4.1.10 CD8 $\alpha_{\text{Tac}}\beta$ associates with less p56 ^{Lck} and partitions less in rafts than the CD8 $\alpha\beta$	107
4.2 Discussion	109
4.3 Conclusion and perspectives	112
5. REFERENCES.....	113

ACKNOWLEDGMENTS

First, I'd like to thank Immanuel Luescher for giving me the opportunity to do my PhD thesis in his laboratory and to extend the work started in the Tetramer Production Facility. His guidance, stimulating discussions and generous support during my thesis years were invaluable.

It would have been impossible to carry out this work without the deep involvement of a highly skilled peptide chemist. For this reason, I am immensely grateful to and hugely indebted to my colleague, Julien Schmidt, for all the complicated peptides he synthesized and his help with the experiments.

Special thanks to Philippe Guillaume, for introducing me to the not-always-easy world of MHC-peptide biochemistry and for always being there for a piece of wisdom or just a vial of multimers.

It was a pleasure to work with Danila Valmori and Maha Ayyoub, who were the most efficient collaborators I had the chance to meet.

I am grateful to Emily Navid for her dedicated technical help, and to all Luescher lab members, past and present; particularly to Marek Cebecauer, Laurence Goffin, Laurence Neff, Melita Irving, Raphaël Genolet and Luca Cariolato for their helpful advice, encouragement, support and company.

As this research area is highly collaborative, needing an interplay of people with different skill sets, it was a pleasure to work with Gilles Bioley, Camilla Jandus, Amandine Legat and Nicole Montandon who were great partners in trying out and testing different MHC class II-peptide multimers and providing cells and reagents for many exploratory experiments. My warmest expressions of gratitude go to Daniel Speiser and Pedro Romero who were always ready to provide sound judgment for research directions.

I am also thankful to Michel Mallaun from Ed Palmer's laboratory for his kindness in providing constructs, microscopy training sessions and advice. For many hours of assistance to my fluorescence microscopy experiments, I would extend my warmest gratitude to Florence Morgenthaler from the Cellular Imaging Facility (CIF) at the University of Lausanne.

In particular, I would like to thank Anne Wilson for critical reading of the thesis manuscript and together with Isabel Ferrero, Emma Fiorini and Donata Rimoldi for encouragement all along the way.

Special thanks to Alexandre Rey for his generous help in French translations.

Finally, to my parents who are always supportive to my endeavors whatever they might be.

SUMMARY

MHC class II-peptide multimers are important tools for the detection, enumeration and isolation of antigen-specific CD4⁺ T cells. However, their erratic and often poor performance impeded their broad application and thus in-depth analysis of key aspects of antigen-specific CD4⁺ T cell responses. In the first part of this thesis we demonstrate that a major cause for poor MHC class II tetramer staining performance is incomplete peptide loading on MHC molecules. We observed that peptide binding affinity for “empty” MHC class II molecules poorly correlates with peptide loading efficacy. Addition of a His-tag or desthiobiotin (DTB) at the peptide N-terminus allowed us to isolate “immunopure” MHC class II-peptide monomers by affinity chromatography; this significantly, often dramatically, improved tetramer staining of antigen-specific CD4⁺ T cells. Insertion of a photosensitive amino acid between the tag and the peptide, permitted removal of the tag from “immunopure” MHC class II-peptide complex by UV irradiation, and hence elimination of its potential interference with TCR and/or MHC binding. Moreover, to improve loading of self and tumor antigen-derived peptides onto “empty” MHC II molecules, we first loaded these with a photocleavable variant of the influenza A hemagglutinin peptide HA₃₀₆₋₃₁₈ and subsequently exchanged it with a poorly loading peptide (e.g. NY-ESO-1₁₁₉₋₁₄₃) upon photolysis of the conditional ligand. Finally, we established a novel type of MHC class II multimers built on reversible chelate formation between 2xHis-tagged MHC molecules and a fluorescent nitrilotriacetic acid (NTA)-containing scaffold. Staining of antigen-specific CD4⁺ T cells with “NTAmers” is fully reversible and allows gentle cell sorting.

In the second part of the thesis we investigated the role of the CD8 α transmembrane domain (TMD) for CD8 coreceptor function. The sequence of the CD8 α TMD, but not the CD8 β TMD, is highly conserved and homodimerizes efficiently. We replaced the CD8 α TMD with the one of the interleukin-2 receptor α chain (CD8 α_{Tac}) and thus ablated CD8 α TMD interactions. We observed that T1 T cell hybridomas expressing CD8 $\alpha_{\text{Tac}}\beta$ exhibited severely impaired intracellular calcium flux, IL-2 responses and K^d/PbCS(ABA) P255A tetramer binding. By means of fluorescence resonance energy transfer experiments (FRET) we established that CD8 $\alpha_{\text{Tac}}\beta$ associated with TCR:CD3 considerably less efficiently than CD8 $\alpha\beta$, both in the presence and the absence of K^d/PbCS(ABA) complexes. Moreover, we observed that CD8 $\alpha_{\text{Tac}}\beta$ partitioned substantially less in lipid rafts, and related to this,

associated less efficiently with p56^{Lck} (Lck), a Src kinase that plays key roles in TCR proximal signaling. Our results support the view that the CD8 α TMD promotes the formation of CD8 $\alpha\beta$ -CD8 $\alpha\beta$ dimers on cell surfaces. Because these contain two CD8 β chains and that CD8 β , unlike CD8 α , mediates association of CD8 with TCR:CD3 as well as with lipid rafts and hence with Lck, we propose that the CD8 α TMD plays an important and hitherto unrecognized role for CD8 coreceptor function, namely by promoting CD8 $\alpha\beta$ dimer formation. We discuss what implications this might have on TCR oligomerization and TCR signaling.

RÉSUMÉ

Les multimères de complexes MHC classe II-peptide sont des outils importants pour la détection, le dénombrement et l'isolation des cellules T CD4+ spécifiques pour un antigène d'intérêt. Cependant, leur performance erratique et souvent inadéquate a empêché leur utilisation généralisée, limitant ainsi l'analyse des aspects clés des réponses des lymphocytes T CD4+. Dans la première partie de cette thèse, nous montrons que la cause principale de la faible efficacité des multimères de complexes MHC classe II-peptide est le chargement incomplet des molécules MHC par des peptides. Nous montrons également que l'affinité du peptide pour la molécule MHC classe II "vide" n'est pas nécessairement liée au degré de chargement. Grâce à l'introduction d'une étiquette d'histidines (His-tag) ou d'une molécule de desthiobiotine à l'extrémité N-terminale du peptide, des monomères MHC classe II-peptide dits "immunopures" ont pu être isolés par chromatographie d'affinité. Ceci a permis d'améliorer significativement et souvent de façon spectaculaire, le marquage des cellules T CD4+ spécifiques pour un antigène d'intérêt. L'insertion d'un acide aminé photosensible entre l'étiquette et le peptide a permis la suppression de l'étiquette du complexe MHC classe-II peptide "immunopure" par irradiation aux UV, éliminant ainsi de potentielles interférences de liaison au TCR et/ou au MHC. De plus, afin d'améliorer le chargement des molécules MHC classe II "vides" avec des peptides dérivés d'auto-antigènes ou d'antigènes tumoraux, nous avons tout d'abord chargé les molécules MHC "vides" avec un analogue peptidique photoclivable issu du peptide HA₃₀₆₋₃₁₈ de l'hémagglutinine de la grippe de type A, puis, sous condition de photolyse, nous l'avons échangé avec de peptides à chargement faible (p.ex. NY-ESO-1₁₁₉₋₁₄₃). Finalement, nous avons construit un nouveau type de multimère réversible, appelé "NTAmère", basé sur la formation chélatante réversible entre les molécules MHC-peptide étiquetés par 2xHis et un support fluorescent contenant des acides nitrilotriacétiques (NTA). Le marquage des cellules T CD4+ spécifiques pour un antigène d'intérêt avec les "NTAmères" est pleinement réversible et permet également un tri cellulaire plus doux.

Dans la deuxième partie de cette thèse nous avons étudié le rôle du domaine transmembranaire (TMD) du CD8 α pour la fonction coréceptrice du CD8. La séquence du TMD du CD8 α , mais pas celle du TMD du CD8 β , est hautement conservée et permet une homodimérisation efficace. Nous avons remplacé le TMD du CD8 α avec celui de la chaîne α

du récepteur à l'IL-2 ($CD8\alpha_{Tac}$), éliminant ainsi les interactions du TMD du $CD8\alpha$. Nous avons montré que les cellules des hybridomes T T1 exprimant le $CD8\alpha_{Tac}\beta$ présentaient une atteinte sévère du flux du calcium intracellulaire, des réponses d'IL-2 et de la liaison des tétramères $K^d/PbCS(ABA)$ P255A. Grâce aux expériences de transfert d'énergie entre molécules fluorescentes (FRET), nous avons montré que l'association du $CD8\alpha_{Tac}\beta$ avec le TCR:CD3 est considérablement moins efficace qu'avec le $CD8\alpha\beta$, et ceci aussi bien en présence qu'en absence de complexes $K^d/PbCS(ABA)$. De plus, nous avons observé que le $CD8\alpha_{Tac}\beta$ se distribuait beaucoup moins bien dans les radeaux lipidiques, engendrant ainsi, une association moins efficace avec $p56^{Lck}$ (Lck), une kinase de la famille Src qui joue un rôle clé dans la signalisation proximale du TCR. Nos résultats soutiennent l'hypothèse que le TMD du $CD8\alpha$ favorise la formation des dimères de $CD8\alpha\beta$ à la surface des cellules. Parce que ces derniers contiennent deux chaînes $CD8\beta$ et que $CD8\beta$, contrairement à $CD8\alpha$, favorise l'association du CD8 au TCR:CD3 aussi bien qu'aux radeaux lipidiques et par conséquent à Lck, nous proposons que le TMD du $CD8\alpha$ joue un rôle important, jusqu'alors inconnu, pour la fonction coreceptrice du CD8, en encourageant la formation des dimères $CD8\alpha\beta$. Nous discutons des implications possibles sur l'oligomérisation du TCR et la signalisation du TCR.

LIST OF ABBREVIATIONS

ABA	azidobenzoic acid
Ahx	ϵ -aminocaproyl
AP	alkaline phosphatase
APC	antigen-presenting cell
APS	ammonium persulfate
β 2m	beta2-microglobulin
BSA	bovine serum albumin
BSP	biotinylation sequence peptide
CD	cluster of differentiation
CDR	complementarity determining region
CTL	cytotoxic T lymphocyte
kD	kiloDalton
DMEM	Dulbecco's modified Eagle medium
DNA	deoxyribonucleic acid
DMSO	dimethylsulfoxide
EBVB	EBV-transformed lymphoblastoid B cell
ECL	enhanced chemoluminescence
ELISA	enzyme-linked immunosorbent assay
ER	endoplasmic reticulum
FCS	fetal calf serum
FACS	fluorescence activated cell sorting
FPLC	fast protein liquid chromatography
FITC	fluorescein isothiocyanate
HA	influenza A hemagglutinin
HEPES	N-2-hydroxyethylpiperazine-N-2-ethansulfonic acid
HPLC	high pressure liquid chromatography
HRP	horseradish peroxidase
ICS	intracellular staining
Ig	immunoglobulin
IP	immunoprecipitation
ITAM	immunoreceptor tyrosine activation motif
IMDM	Iscove's modified Dulbecco's medium
LB	Luria-Bertani
MFI	mean fluorescence intensity
MHC	major histocompatibility complex
MW	molecular weight
NPG	nitrophenylglycine
NPPA	nitrophenylpropionic acid
mAb	monoclonal antibody
OD	optical density
PAGE	polyacrylamide gel electrophoresis
PbCS	<i>Plasmodium berghei</i> circumsporozoite
PBMC	peripheral blood mononuclear cell
PCR	polymerase chain reaction
PE	phycoerythrin

LIST OF ABBREVIATIONS

PHA	phytohemagglutinin
RPMI	Roswell Park Memorial Institute medium
RT	room temperature
SA	streptavidin
SDS	sodium dodecyl sulfate
TCR	T cell receptor
TMD	transmembrane domain
Temed	N,N,N,N' tetramethyl ethylenediamine
Tris	tris(hydroxymethyl)aminomethane

1. INTRODUCTION

1.1 General introduction to immunity

The immune system provides the body with protection against viral, bacterial and fungal pathogens, multicellular parasites, tumor cells and foreign transplanted tissue. Immune-specific organs, cells and molecules are capable of efficiently eliminating interlopers recognized as non-self while minimizing damage to proper tissues. Epithelial surfaces are the first barriers to entry of pathogens, with mechanical (e.g. mucus), chemical (e.g. pH, enzymes, defensins) and microbiological (e.g. normal microbiota) mechanisms. Beyond this constitutive component of non-specific nature, the first cell-mediated line of defense is innate immune system, which is capable of mounting appropriate responses within the time span of minutes to hours. Innate immunity is armed with inducible mechanisms triggering phagocytosis, destruction and inflammation responses. The innate immune system is capable of recognizing and reacting to evolutionary conserved, broad non-self-features such as lipopolysaccharides present in the bacterial cell wall or unmethylated CpG DNA present in bacterial or viral genomes (Medzhitov, 2007).

Recognition of pathogen-specific molecular signatures or antigens is pertinent to adaptive immunity in the medium to long term, and is present in vertebrates. A hallmark of adaptive immunity is memory, the ability to provide a long-lasting record of past encounters with an antigen in the form of specialized populations of cells which can rapidly elicit a recall response upon antigen re-encounter. The two cornerstones of adaptive immunity are B and T lymphocytes, constituting humoral and cellular immunity, respectively. In humans and mice, both types of cells arise from a common hematopoietic stem cell precursor from the bone marrow which can differentiate into mature, naive B cells in the bone marrow and three main subsets of T cells (CD4+, CD8+ and NKT) in a specialized organ, the thymus. After completing thymic development, T lymphocytes circulate through the blood stream and populate peripheral lymphoid organs such as the spleen, lymph nodes and other lymphatic tissues which are sites of antigen encounter.

Both types of lymphocytes harbor specific receptors for recognition of antigens referred to as the B cell receptor (BCR) and the T cell receptor (TCR). TCRs can recognize antigens only in the form of peptides bound to major histocompatibility complex (MHC) proteins, a group of polygenic and highly polymorphic proteins. Fluorescent oligomeric recombinant MHC-

peptide complexes, usually referred to as “tetramers”, are used to detect and sort antigen-specific T cells by flow cytometry. The first subject of this thesis pertains to methods on how to improve the quality of MHC-peptide class II complexes, and therefore multimer binding to specific cells. The second subject of this thesis concerns the CD8 coreceptor molecule, where the importance of the CD8 α chain transmembrane domain is investigated for its coreceptor function.

1.2 T cell receptor

1.2.1 Structural aspects of T cell receptors

The T cell receptor (TCR) belongs to the immunoglobulin superfamily of proteins. Two forms have been identified: $\alpha\beta$ TCR and $\gamma\delta$ TCR. The $\alpha\beta$ TCR is expressed on CD4+, CD8+ T and NKT cells, while the $\gamma\delta$ TCR is expressed on a subset of intraepithelial lymphocytes, found predominantly in the skin and gut. The $\alpha\beta$ TCR is a membrane-bound heterodimeric protein composed of α and β chain, which are linked by a disulfide bond. The chains are encoded by genes formed by rearrangement of variable (V), diversity (D) (in β chain only), joining (J) and constant (C) segments that are highly similar to immunoglobulin chain formation. During T cell development, these segments are rearranged in a controlled and stepwise manner, resulting in 2×10^6 and 2.5×10^8 different TCR specificities in peripheral T cells of mice and humans, respectively (Casrouge et al., 2000; Robins et al., 2009). Structural studies of TCRs revealed four major differences from canonical immunoglobulin structures (Garboczi et al., 1996; Garcia et al., 1996a; Rudolph et al., 2006): i) a protruding, 13 residue long, FG loop in the constant domain of TCR β ; ii) rather flat surface of TCR α constant domain as a consequence of lacking several residues; iii) the absence of surface protrusions in the variable domain of TCR α because of a strand switch; iv) absence of flexibility in the hinge region of TCR β . The TCR binds antigens in the form of peptides non-covalently bound to MHC proteins, known as MHC-peptide complexes. The binding site for MHC-peptide complexes is formed by six loops, called complementary determining regions (CDR). Each chain forms three CDRs. Two CDR loops are encoded by V gene segments (CDR1 and CDR2) and one by recombined V, (D on the β chain) and J segments (CDR3). Consequently, the CDR3 loop is the most polymorphic. While the CDR1 and CDR2 loops typically contact the helices of the MHC molecule, the highly polymorphic CDR3 loop interacts primarily with the MHC-bound peptide. TCRs tend to bind MHC-peptide complexes in a “diagonal” orientation, in which the peptide runs diagonally between the two CDR3 loops, extending

from CDR1 α to CDR1 β (Fig. 1.1). This orientation implies conserved atomic interactions between TCR V regions (mainly V α) and residues of the MHC helices (mainly α 2). However, binding modes of TCRs to MHC-peptide complexes vary considerably. In some cases CDR1 and/or CDR2 loops make no or little contact and the orientation of TCR binding to MHC-peptide is nearly perpendicular (Rudolph et al., 2006).

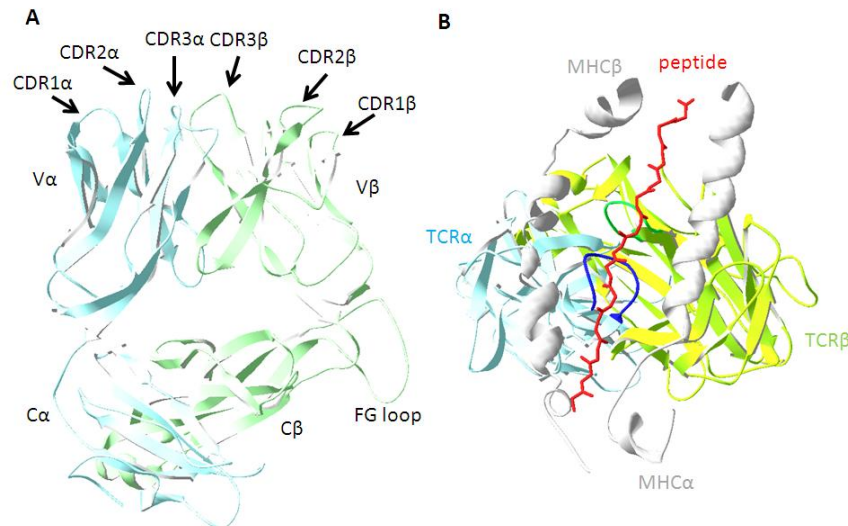


Figure 1.1 *T cell receptor structure and diagonal ligand binding mode.* A, Side view of the HA1.7 T cell receptor (TCR). The TCR α chain is in light blue and the TCR β chain in light green. The constant and variable domains of both chains are labeled as C α , C β and V α , V β respectively. CDR loops from each chain are indicated by arrows. B, Top view of HA1.7 TCR with bound DR4/HA₃₀₆₋₃₁₈. The TCR α is light blue and TCR β is yellow-green. The HA₃₀₆₋₃₁₈ peptide (PKYVKQNTLKLAT) is represented by a backbone in red and parts of the MHC (DR4) chains are shown in grey. Only residues Leu45 to Arg76 of MHC α (DR α) and Pro56 to Tyr96 (DR4 β) are shown for clarity. The CDR3 α loop (Glu94 to Leu104) is shown in dark blue and the CDR3 β loop (Ser96 to Tyr106) in dark green. The protein backbone is represented as ribbons. Coordinates are from the PDB file ID code 1J8H.

1.2.2 T cell receptor triggering

Surface plasmon resonance studies on purified recombinant molecules showed that TCRs typically bind MHC-peptide complexes with low affinity (K_D from 10^{-4} to 10^{-6} M) and exhibit fast on-rates (10^3 to 10^4 s $^{-1}$) and considerably slower off-rates (from 0.02 to 5 s $^{-1}$) at room temperature. The rapid dissociation of TCR:MHC-peptide complexes allows the T cell to quickly scan MHC-peptide complexes on presenting cells and engage in TCR triggering in a rapid succession, which is usually referred to as serial triggering (Fremont et al., 1996b; Luescher et al., 1995b; Rudolph et al., 2002). Coordinate binding of CD8 to TCR-associated MHC-peptide greatly strengthens MHC-peptide binding to the TCR, mainly by decreasing TCR-MHC-peptide complex dissociation (Luescher et al., 1995b), allowing the recognition of weak and/or rare peptide ligands.

T cells are highly sensitive and can be triggered by just a few cognate MHC-peptide complexes (Irvine et al., 2002; Purbhoo et al., 2004). For CD4⁺ and CD8⁺ T cells it has been shown that MHC-peptide null ligands (i.e. ligands that bind to the TCR, but are too weak to trigger activation) significantly increase the sensitivity of antigen recognition (Cebecauer et al., 2005b; Krosggaard et al., 2005; Wulfing et al., 2002). These and other findings support a model in which CD4 cross-links MHC-peptides engaged by TCRs by associating with one TCR and binding to the MHC-peptide engaging another TCR (Krosggaard et al., 2005).

A general mechanism to trigger receptors is dimerization (e.g. for erythropoietin receptor, growth hormone receptors and the pre-TCR) (Livnah et al., 1999; Yamasaki et al., 2006). There is also substantial evidence that TCR:CD3 can form dimers and higher aggregates (Minguet et al., 2007; Reich et al., 1997; Schamel et al., 2006; Yokosuka et al., 2005). Studies with soluble MHC-peptide complexes have shown that TCR triggering requires that these are at least dimeric, i.e. can induce TCR cross-linking (Cebecauer et al., 2005b; Cochran et al., 2001; Krosggaard et al., 2005). TCR and coreceptor co-aggregation induces cross-linking mediated activation of Src kinases, such as coreceptor-associated Lck and TCR-associated p59^{fyn} (Fyn). This initial tyrosine kinase activity mediates phosphorylation of CD3 ITAMs, which allows docking of SH2 containing kinases like Syk-family ZAP-70, which upon activation phosphorylate diverse additional signaling molecules. TCR micro clusters can be observed in APC-T cell contact areas as the sites where initial phosphorylation events and intracellular calcium flux emerge (Kane et al., 2000; Palacios and Weiss, 2004). The emerging view is that TCR aggregation elicits structural changes in CD3 complex (composed an $\epsilon\gamma$, an $\epsilon\delta$ and a $\zeta\zeta$ dimer), which renders their ITAMs more amenable to kinases and adaptors (Minguet et al., 2007). Observations of T cell:APC synapses by confocal microscopy led to a third category of models which invoke segregation of large tyrosine phosphatases (e.g. CD45 or CD148) from the T cell:APC contact zones which would favor net phosphorylation of ITAMs by p56^{Lck}. The exclusion of tyrosine phosphatases can be mediated purely on the basis of size of their ectodomains (the CD45 ectodomain is 540 residue long in mice, Uniprot ID P06800) or by lipid-raft (also referred to as diffusional trapping) exclusion. Originally, this model was based on the observation that CD45 and CD148 are excluded from T cell:APC contact sites (Lin and Weiss, 2003; Varma et al., 2006). Further support to this model is provided by experiments where the truncation of CD45 and CD148 ectodomains inhibits TCR triggering (Irles et al., 2003; Lin and Weiss, 2003); elongation of MHC-peptide complexes inhibits TCR triggering (Choudhuri et al.,

2009; Choudhuri et al., 2005); surface-bound MHC-peptide ligands induce TCR triggering better than soluble ones (Geppert and Lipsky, 1987; Ma et al., 2008) and the recognition of epitopes by engineered TCRs is better when they are positioned close to the target cell (Bluemel et al., 2010; James et al., 2008). The role of lipid rafts in T cell triggering has been subject to debate, as conflicting studies have been published. Nonetheless, it is recognized that they do play a role, albeit on a smaller scale than previously thought (Glebov and Nichols, 2004; Hashimoto-Tane et al., 2010; Pizzo et al., 2002; Zhu et al., 2005).

1.2.3 T cell receptor signaling

The TCR itself possesses no signal transduction capabilities (Fig. 1.2). Expression of a TCR on the cell membrane requires association with the CD3 complex. The intracellular tails of the CD3 chains contain immunoreceptor tyrosine activation motifs (ITAMs) crucial for initiation of TCR signaling. The CD3 complex consists of an $\epsilon\gamma$, an $\epsilon\delta$ and a $\zeta\zeta$ dimer (Call and Wucherpfennig, 2004, 2005). The $\epsilon\delta$ and $\zeta\zeta$ dimers associate with the TCR α chain and the $\epsilon\gamma$ dimer with the TCR β chain (Kuhns et al., 2010). Upon TCR triggering, the ITAM motifs (Y-x-x-L/I) on the long cytoplasmic tails of CD3 units are phosphorylated at their tyrosines by Src tyrosine kinases Lck and/or Fyn. Phosphorylated ITAMs bind SH2 domain containing kinases, such as ZAP-70 (ζ -chain-associated protein of 70 kDa) and Syk (Kane et al., 2000; Pitcher and van Oers, 2003). Lck can also phosphorylate ZAP-70 directly, thereby increasing its enzymatic activity (LoGrasso et al., 1996), as well as a negative regulator of ZAP-70 and Lck itself, SHP1, a tyrosine phosphatase (Kosugi et al., 2001). Activated ZAP-70 phosphorylates tyrosines on LAT (linker of activation of T cells) which serves as a scaffold for organization of a proximal signaling complex consisting of PLC γ 1, PI3K, GRB2, Gads and SLP-76. The activated plasma-membrane-associated PLC γ 1 hydrolyzes PI(4,5)P₂ (phosphoinositol-4,5-diphosphate), a membrane constituent, whose products, IP₃ (inositol-3-phosphate) and DAG (diacyl-glycerol) activate downstream signaling pathways. IP₃ triggers elevation of intracellular Ca²⁺ by activating IP₃-dependent calcium channels in the endoplasmic reticulum (ER), thereby releasing Ca²⁺ from the ER into the cytosol. This influx of Ca²⁺ from intracellular stores triggers Ca²⁺ channels in the cell plasma membrane aptly termed CRACs (Ca²⁺-release activated Ca²⁺ channels). Elevated concentration of Ca²⁺ triggers release of cytotoxic granules, directly activates transcription factors MEF2 and DREAM, and signaling proteins calcineurin and CaMK (Ca²⁺/calmodulin-dependent protein kinase) which phosphorylates NFAT (nuclear factor of activated T cells), an important

transcription factor. The other signaling product of PI(4,5)P₂ hydrolysis, DAG, activates the MAPK (mitogen-activated protein kinase) pathway through Ras. Another important pathway activated by DAG is the PKC θ -dependent pathway, with ends in activation of the NF- κ B transcription factor and is mediated by the CARMA1/Bcl10/MALT1 complex, also referred to as the lymphocyte-specific activation complex. Negative regulation of TCR signaling is mediated by the Csk (C-terminal Src kinase) kinase that inactivates Lck by phosphorylation at Tyr505, and CD45 phosphatase that can directly dephosphorylate ITAMs. The end result of all this transcription factor activation is the production of cytokines (e.g. IL-2, IFN γ) and chemokines that activate long-range intercellular effector and signaling molecules of the immune system; reviewed in (Smith-Garvin et al., 2009).

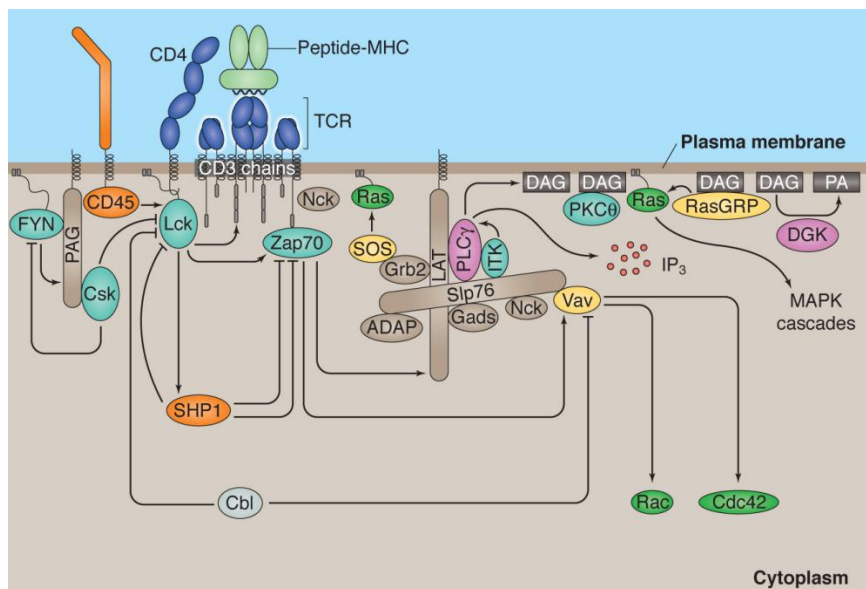


Figure 1.2 *T cell receptor proximal signaling pathways.* T cell receptor (TCR) triggering induces a series of changes that activate ζ -chain associated protein of 70 kDa (ZAP-70) which phosphorylates linker of activator of T cells (LAT) to assemble various components of the proximal signaling complex. A component of the complex, the phospholipase C γ 1 (PLC γ 1) breaks down PIP₂ (phosphoinositol-4,5-diphosphate) into two major small signaling molecules: inositol-triphosphate (IP₃) and diacylglycerol (DAG). IP₃ triggers Ca²⁺ channels in the ER and indirectly all Ca²⁺-dependent signaling pathways. DAG acts on the mitogen-activated protein kinase (MAPK) cascade via Ras. All these pathways end on transcription factors which relocate to the nucleus and activate transcription of target genes such as interleukin 2 (IL-2). Parts of these pathways branch out and act on cytoskeletal proteins, cell proliferation and survival. Proteins are represented by oval shapes. Small molecules are in rectangles or not associated by shapes. Activating receptors are blue; ligands in light green; structural, scaffold and regulatory proteins are shown in brown; kinases in blue-green; phosphatases in orange; GTP-exchange factors in yellow; GTP-ases in dark green and lipid modifying enzymes in purple. After (Huse, 2009).

1.3 MHC-peptide complexes

1.3.1 Structural aspects of MHC-peptide complexes

MHC-peptide complexes, ligands for $\alpha\beta$ TCRs, are non-covalent complexes composed of major histocompatibility proteins (MHC) and antigen-derived peptides. There are two classes of MHC proteins, encoded by genes clustered in the >4 million basepair MHC locus located on chromosome 6 in humans (HLA) and chromosome 17 in the mouse (H-2). There are multiple, highly polymorphic genes for human MHC class I and class II proteins. In humans, there are three main HLA class I loci, referred to as A, B and C and three HLA class II loci, called DR, DP and DQ; reviewed in (Kumanovics et al., 2003). According to the IMGT/HLA database at the European Institute for Bioinformatics (<http://www.ebi.ac.uk/imgt/hla>), release 3.8.0 of April 12, 2012, there are 5880 HLA class I alleles (including minor E, F and G loci) coding for 4291 different proteins and 1647 HLA class II alleles (including DM and DQ loci) coding for 1208 different proteins (Fig. 1.3). In laboratory inbred strains of mice, the diversity of H-2 proteins is much smaller (Table 1.1). Both classes are comprised of non-covalently associated protein chains and share common structural features, i.e. a TCR-facing peptide-binding cleft formed by two α -helices and a β -sheet on the bottom, variable and constant immunoglobulin domains, transmembrane helices and short intracellular tail(s). Bound peptides interact with MHC protein primarily via a network of hydrogen bonds (Fig 1.4). Some peptide amino acid residues with bulky side chains are buried in deep, frequently hydrophobic, pockets. MHC class I proteins consist of a heavy and a light chain, also referred to as β 2-microglobulin, and bind peptides usually of 8 to 10 amino acid residues, whereas MHC class II proteins are comprised of two equally sized membrane-bound chains and bind larger peptides, from 9 to >20 amino acid residues in length, in an extended, poly-proline helix II-like conformation. Whereas MHC class I proteins have at least two prominent binding pockets accommodating peptide's amino acid side chains, MHC class II proteins have typically four binding pockets at positions P1, P4, P6 and P9, where the pocket P1 is the primary with the other being secondary binding pockets. Amino acid residues whose side chains bind into these pockets are termed anchor residues. Residues at positions P2, P3, P5 and P8 are typically solvent-exposed, i.e. available to contact the TCR. In many HLA-DR molecules, the pocket 1 is occupied by a bulky, hydrophobic side chain (F, Y or W) and defines the peptide binding register. Because MHC class II molecules do not impose any length constraints to bound peptides and the binding pockets can accommodate multiple

amino acid residues as anchors, a single peptide can bind in different registers giving rise to various conformers of the MHC class II-peptide complex (Lovitch and Unanue, 2005). The best studied examples of such conformers are those of I-A^k/HEL₄₈₋₆₂ and I-A^{g7}/B₉₋₂₃ complexes (Mohan and Unanue, 2012). Following immunization of mice with hen egg-white lysozyme (HEL), two types of CD4⁺ T cells specific for the dominant HEL₄₈₋₆₂ peptide are induced: type A, which react against APCs pulsed with the HEL protein or the HEL₄₈₋₆₂ peptide, whereas the type B cells react only with the APCs pulsed with the HEL₄₈₋₆₂ peptide (Pu et al., 2002; Viner et al., 1996). In the non-obese diabetic (NOD) mouse, CD4⁺ T cells specific for the insulin beta chain (B) are key for the initiation of diabetes (Nakayama et al., 2005). As in the HEL system, CD4⁺ T cells specific for the dominant B₉₋₂₃ peptide can be found as type A and type B. In this case, it has been demonstrated that type A cells recognize the strongly binding B₁₃₋₂₁ register and type B cells the weakly binding B₁₂₋₂₀ register (Levisetti et al., 2007; Mohan et al., 2010; Mohan et al., 2011). Peptide-pulsed APCs present peptide loaded in early endosomes where H2-M is not present (see section 1.3.2) that would normally edit out the B₉₋₂₃ peptide bound in the weakly binding register (Pu et al., 2004). The existence of type A and B cells has been linked to autoimmunity where the type B cells for self-antigens, able to escape thymic negative selection and present in the periphery, could be activated by APCs presenting extracellularly-generated peptides and trigger autoimmune reactions.

These features of MHC class II molecules related to peptide binding have several important consequences for the design of fluorescent MHC-peptide class II multimers (section 1.6).

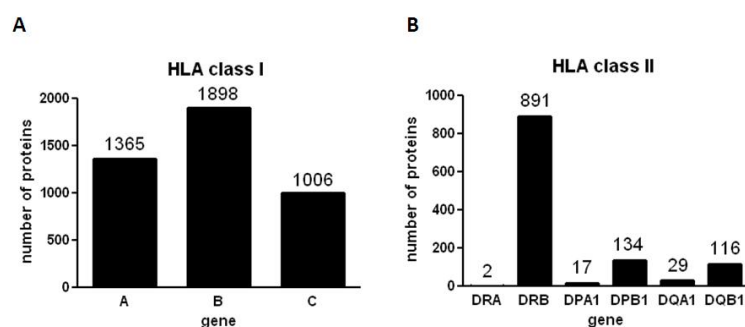


Figure 1.3 *Human leukocyte antigen diversity in populations of the world.* Bar charts representing the number of different proteins encoded by class I genes (A) or class II genes (B). Minor class I genes E, F, G and class II genes DM and DQ are not shown. Data are from the IMGT/HLA database, release 3.8.0, April 12, 2012.

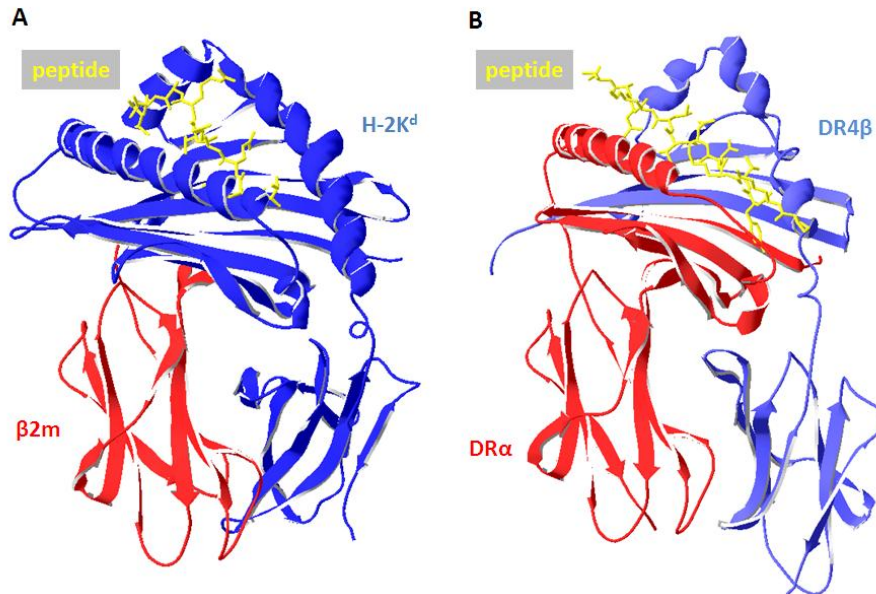


Figure 1.4 *Structural features of MHC-peptide complexes.* A, Structure of the K^d in complex with the influenza nucleoprotein peptide 147-155 (TYQRTRALV). The β 2-microglobulin (β 2m) is in red and the H-2K^d heavy chain in blue. The peptide is shown in yellow. Coordinates are from the PDB file ID code 2FWO. B, Structure of the DR4/HA₃₀₆₋₃₁₈ complex. The DR α chain is shown in red, the DR4 β in blue and the peptide in yellow. Coordinates are from the PDB file ID code 1J8H. Backbones of protein chains are represented as ribbons and peptide backbones with side chains as sticks.

Table 1.1 *Murine H-2 proteins in common strains of laboratory mice.* Due to inbreeding, laboratory mice (Balb/c, C57BL/6, C3H/He, CBA) have a limited number of alleles in the H-2 class I (K, D and L) and class II (I-A and I-E) genes.

strain	appearance	haplotype	H-2 Class I			H-2 class II	
			K	D	L	I-A	I-E
Balb/c	albino	d	K ^d	D ^d	L ^d	I-A ^d	I-E ^d
C57BL/6	black	b	K ^b	D ^b	-	I-A ^b	-
C3H/He	agouti	k	K ^k	D ^k	-	I-A ^k	I-E ^k
CBA	agouti	k	K ^k	D ^k	-	I-A ^k	I-E ^k

1.3.2 Pathways of antigen presentation

The pathways of antigen presentation by MHC molecules have been extensively reviewed in (Neefjes et al., 2011). MHC class I molecules present peptides derived from (immuno)proteasomal degradation of intracellular proteins (Fig. 1.5A). Two ATP-dependent peptide transporters, TAP1 and TAP2, pump these peptides into the ER lumen where newly synthesized empty MHC class I proteins are present. Nascent MHC class I heavy chains are stabilized in association with calreticulin, tapasin and ERp57. Upon successful binding of a peptide ligand, MHC-peptide class I complexes bind β 2-microglobulin and are exported and displayed on the cell surface. MHC class I proteins can also present peptides derived by extracellular antigens by a process termed cross-presentation.

While all cells are able to express MHC class I molecules in a constitutive manner, MHC class II expression is under control of the MHC class II transactivator (CIITA), being constantly expressed only in DCs, macrophages, monocytes and B-cells (termed professional APCs) and is inducible under certain conditions, e.g. exposure to IFN γ , in all other cell types. MHC class II molecules present peptides derived from extracellular proteins degraded by endosomal cysteine proteases known as cathepsins (Fig. 1.5B). Extracellular antigens are taken up via IgG or Fc receptor-mediated endocytosis in B cells and DCs respectively, or by phagocytosis in macrophages. Recently, autophagy has been identified as a mechanism that also allows MHC class II proteins to present peptides derived from intracellular antigens (Klein et al., 2010). Cathepsins are activated by acidification of endosomal vesicles and/or fusion with acid lysosomes.

Nascent MHC class II molecules are first associated with the invariant chain (Ii) that is degraded by cathepsins and other proteases to leave a fragment referred to as CLIP (PVSKMRMATPLLMQA), bound to the peptide-binding groove of the MHC protein. Exchange of CLIP with an antigen-derived peptide is favored by acidic pH and is catalyzed by an MHC class II homologue referred to as HLA-DM in humans and H2-M in the mouse, in specialized multi-vesicular and/or multilamellar compartments termed MIICs (MHC class II compartments). Another MHC class II-like molecule, HLA-DO in humans and H2-O in mice, can prevent interaction with MHC class II-CLIP complexes by physical association with HLA-DM/H2-M thereby acting as a negative regulator (Porter et al., 2011; Xiu et al., 2011). To date, the exact role of HLA-DO/H2-O in antigen presentation is still unclear.

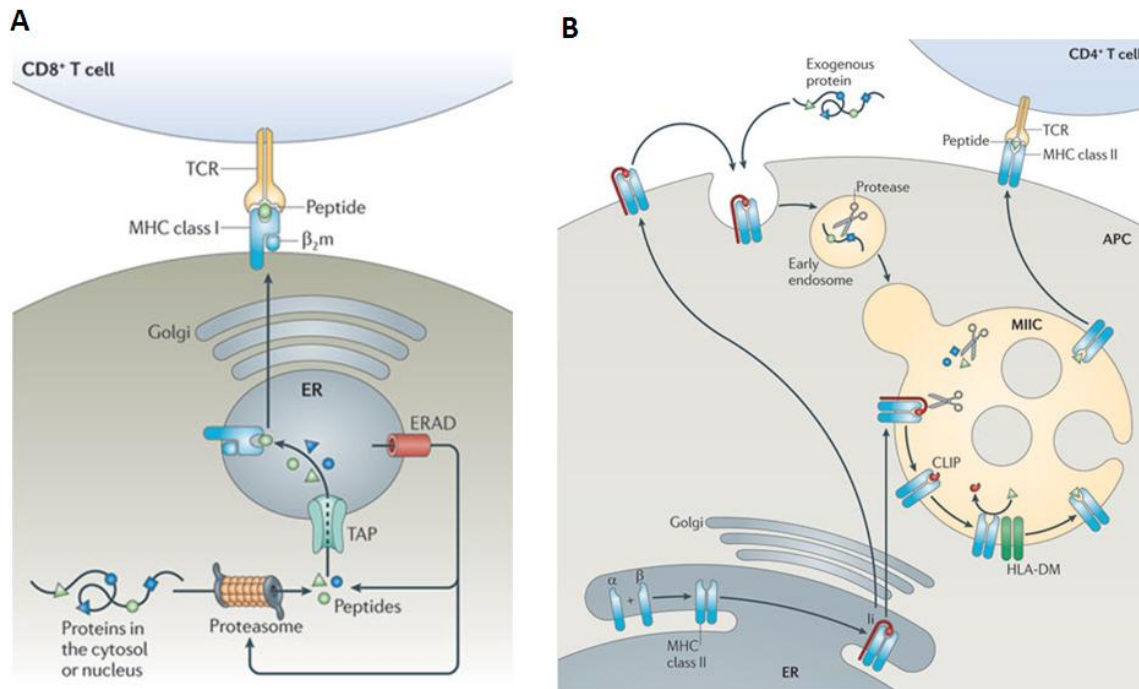


Figure 1.5 Antigen presentation pathways. A, Basic pathway of antigen presentation by MHC class I molecules. Cytosolic antigens are degraded by the proteasome and pumped by peptide transporters associated with antigen presentation (TAP) into the endoplasmic reticulum (ER) where nascent MHC class I molecules are loaded. Defective or denatured intra-ER proteins are degraded by ER-associated protein degradation mechanisms (ERAD). Upon stable peptide binding, MHC class I molecules bind β 2-microglobulin (β 2m) and are released from the ER and transported through the Golgi to the plasma membrane for binding to T cell receptors (TCRs) on CD8⁺ T cells. B, Basic pathway of antigen presentation by MHC class II molecules. MHC class II α - and β -chains assemble with the invariant chain (Ii) into a heterotrimeric complex in the endoplasmic reticulum (ER) of an antigen-presenting cell (APC). Subsequently, the MHC class II-Ii complexes are transported via the Golgi to the MHC class II compartment (MIIC) directly or passing by the plasma membrane. Endocytosed antigens and the MHC class II-associated Ii are degraded by resident proteases in the MIIC and the Ii fragment CLIP is exchanged for an antigenic peptide at acidic pH with the help of the HLA-DM (H2-M in mice). Such MHC class II-complexes are exported to the plasma membrane and presented as ligands to specific T cell receptors (TCRs) on CD4⁺ T cells. After (Neefjes et al., 2011).

1.4 CD8 and CD4 coreceptors

The developmental fate of T cells bearing the $\alpha\beta$ TCR depends on the surface expression of CD4 and CD8 molecules. T cells expressing CD4 are selected on MHC class II-peptide complexes while those expressing CD8 recognize their antigen in complex with MHC class I proteins. CD8 and CD4 are also referred to as coreceptors because they influence antigen recognition by the TCR.

CD8 can occur in two forms. Homodimeric CD8 $\alpha\alpha$ consisting of disulfide-linked CD8 α chains, is expressed on some intraepithelial lymphocytes (IEL), dendritic cells (DC), natural killer (NK) and NKT cells (Romero et al., 2005). Conversely, heterodimeric CD8 $\alpha\beta$, consisting of a disulfide linked α and β chain, is expressed on some IEL in the gut and

importantly, on all $\alpha\beta$ TCR thymus-derived T cells (Fig. 1.6A). Both CD8 chains consist of an extracellular domain in which a long, heavily glycosylated stalk can be clearly distinguished from an N-terminal globular domain (Chang et al., 2005), a single transmembrane domain important for chain association and a cytoplasmic tail. The cytoplasmic tail of CD8 β , but not of CD8 α , contains the binding site for Lck, a Src tyrosine kinase that plays a crucial role in phosphorylation of the CD3 ITAMs, and hence initiating TCR signaling. While both CD8 forms bind with comparable affinity (11-67 μ M) (Garcia et al., 1996b; Kern et al., 1999) to the $\alpha 3$ constant domain of MHC class I molecules, they have completely different roles and activities. CD8 $\alpha\beta$ is the *bona fide* coreceptor, greatly increasing sensitivity and breadth of antigen recognition. By contrast, the biological role of CD8 $\alpha\alpha$ remains a matter of debate (Cheroutre and Lambolez, 2008; Romero et al., 2005) and when expressed on T cells tends to have an inhibitory role. The reasons for these differences include: i) the cytoplasmic tail of CD8 β is palmitoylated, thereby promoting partitioning of CD $\alpha\beta$ to lipid rafts and association with Lck and the linker of activation of T cells (LAT) ii) as a consequence lipid raft partitioning, there is about five times more Lck molecules associated with CD $\alpha\beta$ than with CD8 $\alpha\alpha$ (Bosselut et al., 2000); iii) differences in stalk length (Rettig et al., 2009) and flexibility between the two forms (the CD8 β stalk is shorter than that of CD8 α) and, iv) by co-ordinated binding to TCR-associated MHC-peptide complexes, CD8 $\alpha\beta$, but not CD8 $\alpha\alpha$, strongly increases MHC-peptide binding activity (Arcaro et al., 2000).

Acting as a coreceptor, CD8 associates with the TCR:CD3 complex and the MHC-peptide simultaneously. Immunoprecipitation experiments demonstrated that CD8 $\alpha\beta$ but not CD8 $\alpha\alpha$ associates with the TCR:CD3 (Anel et al., 1997; Arcaro et al., 2001). Observations by FRET microscopy (Yachi et al., 2005) and micropipette adhesion frequency assay (Jiang et al., 2011) revealed the inducible nature of this interaction. Interestingly, the anergic state of tumor-infiltrated human CD8 $^{+}$ CTLs can be at least partly explained by lack of association of TCR with CD8 (Demotte et al., 2008).

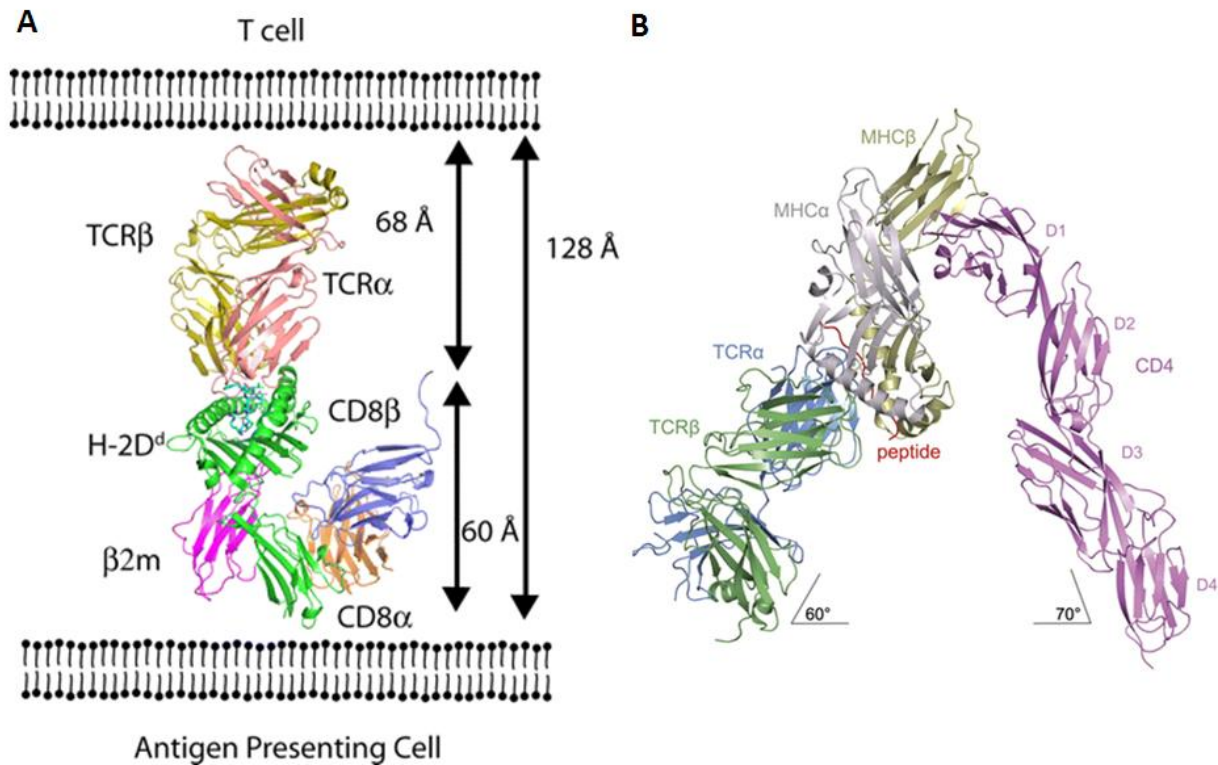


Figure 1.6 CD8 and CD4 coreceptors in molecular context. A, CD8 $\alpha\beta$ immunoglobulin domain in complex with H-2D^d/P18-I10 (RGPGRAFVTI) with murine β 2-microglobulin (β 2m) bound to a specific T cell receptor (TCR). CD8 $\alpha\beta$ interacts with the acidic loop on the α 3 domain of H-2D^d (residues 222-228). The CD8 α chain is in ochre; CD8 β in blue; H-2D^d in green; β 2m in magenta; TCR α in rose and TCR β in gold. Protein backbones represented as ribbons. The peptide is in light blue, represented as sticks. Distance in angstroms between the antigen presenting cell and the CD8⁺ T cell as a sum of heights of the TCR (68 Å) and the MHC-peptide (60 Å) is represented. After (Wang et al., 2009). B, Ternary complex between the extracellular part of CD4 (domains D1-D4) bound to the HLA-DR4/MBP₁₁₄₋₁₂₆ (FSWGAEGRPGFG) and the MS2-3C8 TCR. The CD4 is a high-affinity variant which harbors two point mutations in the D1 domain (Gln40Tyr/Thr45Trp) increasing its avidity to HLA-DR4 to 10.1 μ M. Most of the contacts between CD4 and the HLA-DR4 are with β 2 domain (residues 104, 114, 116, 142-145, 148, 158, 160, 162) with some in the α 1 domain (residues 88, 90, 176). It is notable that the structure has an inverted V-shape. The TCR:MHC-peptide axis is tilted to 60° against the plasma membrane and the CD4, the apical angle is 70°. CD4 is shown in magenta, the MHC α in grey, MHC β in gold, TCR α in blue, TCR β in green. Peptide backbone is shown in red. After (Yin et al., 2012).

CD8 $\alpha\beta$ can also function as an adhesion molecule. As first demonstrated in a plate adhesion assay, CD8⁺ CTLs avidly adhere to plastic coated with non-cognate MHC-peptide complexes after sub-optimal TCR triggering, e.g. by low concentrations of a soluble anti-TCR or CD3 antibody (O'Rourke et al., 1990). Subsequent studies showed that CD8-mediated adhesion is driven by partial TCR signaling. It has been shown that CD8 is associated with the actin cytoskeleton (Geppert and Lipsky, 1991; O'Rourke et al., 1991), arguing that cytoskeletal rearrangements are important for CD8-mediated adhesion. A recent finding indicates that kinetically, CD8 adhesion events precede engagement by the TCR by approx. 1 second (Jiang et al., 2011).

CD8 coreceptor function can be modulated during T cell development and differentiation by changes in CD8 glycosylation and sialylation. In particular the O-linked glycosylation and sialylation of CD8 β increases when CD4, CD8 double positive thymocytes convert into CD8 single positive thymocytes and T cells and decreases again upon T cell activation (Moody et al., 2001; Shore et al., 2005). CD8 coreceptor function can also be regulated by tuning the CD8 surface expression and perhaps by over expression of CD8 α (or down-modulation of CD8 β) (Maile et al., 2005).

CD4 consists of four immunoglobulin domains (D1 to D4), a transmembrane and cytoplasmic domain, similar to that of CD8 β , can be palmitoylated (Fig. 1.6B). The interaction of CD4 with the constant domains of MHC class II molecules is nearly 10-fold lower as compared to the interaction of CD8 with MHC class I molecules ($K_D > 200 \mu\text{M}$ versus 50-150 μM for CD8 $\alpha\beta$) (Fremont et al., 1996b). Whereas CD8 substantially strengthens the binding of MHC class I-peptide complexes to cell-associated TCR, CD4 has no influence on the MHC class II-peptide binding. CD4 can form dimers and tetramers, which are highly active as coreceptors (Maekawa et al., 2006). Moreover, CD4 and CD8 can both associate with TCR:CD3, which involves CD3 δ and enhances MHC-peptide binding and T cell activation (Doucey et al., 2003).

1.5 T cells

1.5.1 Origin and development of T cells

T cell development, reviewed extensively in (Koch and Radtke, 2011), originates from hematopoietic stem cells (HSC) precursors, which are located in the bone marrow. As multipotent stem cell (MSCs) progenitors leave the bone marrow and enter the thymus, they lose self-renewal potential and start their differentiation pathways, circulating through distinct anatomical parts: cortex, subcapsular zone, medulla and back to the cortex. Thymic seeding progenitors (TSPs), derived from MSCs, pass through four developmental stages termed double negative (DN1 to DN4) where cells do not express coreceptor proteins, i.e. are CD8 $-$ CD4 $-$. The DN stages can be differentiated by their differential expression of CD44 and CD25. During that time, T cell precursors rearrange their TCR β chains and express them on the cell surface along with an invariant pT α chain and the CD3 complex, forming a pre-TCR. It is only after productive pre-TCR triggering and cellular expansion that both coreceptors are expressed and cells acquire a double positive (CD8 $+$ CD4 $+$) phenotype (DP). The TCR α chain then rearranges and such cells express clonotypic fully mature $\alpha\beta$ TCRs and are ready to

engage in a selection process, (also referred to as “central tolerance”) to finally become single positive (SP) and commit to CD8⁺ or CD4⁺ T cell lineages.

During positive selection, DP thymocytes interact with MHC-self-peptide complexes expressed on the surface of thymic epithelial cells (TECs). In the case of successful engagement in low avidity interactions with presented MHC-self-peptide complexes, DP thymocytes receive a survival signal and continue their differentiation program further. Those that cannot engage die passively, i.e. undergo “death-by-neglect”. By contrast, in the case of overly strong interactions, the stimulatory signal received results in apoptosis. This process, called negative selection, is extensively reviewed in (Palmer, 2003). It is extremely important as it prevents harmful, autoreactive T cells from reaching body tissues where they would potentially trigger autoimmune reactions. Substantial evidence from experiments using altered peptide ligands on S14, T1 and OT-I transgenic TCRs showed that there is an affinity threshold of ~6 μ M between positive and negative selection (Naeher et al., 2007; Palmer and Naeher, 2009). Above this threshold, for TCR:MHC-peptide affinities of <6 μ M, negative selection occurs. It is estimated that because of death-by-neglect and apoptosis during negative selection only 5% of initial DP thymocytes reach maturity.

1.5.2 Activation and differentiation of T cells

After exit from the thymus, naïve T cells populate defined areas of secondary lymphoid organs and recirculate back through body tissues via the bloodstream. Upon their very first antigen encounter, in addition to TCR:CD3 signaling triggered by recognition of cognate MHC-peptide class I or class II complexes, a second signal is needed. This additional requirement is termed costimulation, namely productive triggering of CD28 expressed on the surface of the T cell by CD80 (B7.1) and CD86 (B7.2) on the APC. In the absence of this second signal, T cells fail to activate and enter a non-functional state termed anergy.

Activated cells upregulate CD25, the alpha chain of the receptor for IL-2 (a key growth-promoting factor), and downregulate CCR7, a receptor important for homing in secondary lymphoid organs. IL-2 is produced in a paracrine fashion as well. Furthermore, a common surface antigen, CD45 changes to a shorter splicing isoform (from CD45RA to CD45RO). Activated cells can further differentiate into short-lived effectors and long-lived memory cells. Memory cells are antigen-experienced and can rapidly respond to antigen in a costimulation-independent way.

1.5.3 CD8+ T cells

The main function of CD8+ T cells consists in killing pathogen infected or transformed cells, so they are therefore known as cytotoxic T cells (CTLs), which display antigenic peptides derived from endogenously produced antigens bound to MHC class I molecules, as reviewed in (Harty et al., 2000). Activated CD8+ CTLs kill target cells primarily by releasing perforin and granzymes, which in a synergistic manner induce target cell death via caspase-dependent apoptosis. CTL can also kill other cells by expressing FasL, which binds to Fas on target cells and induces apoptosis. Fas-dependent killing can also be used by helper T cells (Th) and other cells, e.g. to maintain homeostasis and to regulate development. Activated CTLs also release cytokines, such as TNF, IFN γ and variable amounts of other interleukins. Perforin-dependent killing is rapid (from a few minutes to a few hours) and can be elicited by a few MHC-peptide complexes on target cells. By contrast, cytokine production and FasL synthesis involve gene transcription, which requires sustained TCR signaling for extended periods of time. Fas-dependent cytolysis is slower than perforin dependent cytolysis (6–18 h) and TNF-mediated killing is slower still (after 16 h). In some cases Fas–FasL-dependent killing involves translocation of preformed, intracellular FasL to the cell surface or release of soluble FasL.

1.5.4 CD4+ T cells – subsets and functions

The principal function of CD4+ T cells is to support and regulate cellular and humoral immune responses. Th cells control B cell antibody class switching and support antibody production (Lederman et al., 1996). They also promote proliferation, differentiation and activation of cytotoxic T cells (CTLs), and increase bactericidal activity of macrophages (Constant and Bottomly, 1997; Dong and Flavell, 2001; Tato et al., 2006) and produce cytokines. Originally Th cells were divided into Th1 and Th2 cells (type 1 and type 2 Th) (Dong and Flavell, 2001; Reinhardt et al., 2006; Susan L, 1999). Th1 cells produce proinflammatory cytokines, mainly interferon- γ (IFN γ) and tumor necrosis factor- β (TNF β). Th1 cytokines augment the cytotoxicity of macrophages and proliferation of cytotoxic CD8+ T cells. Th1 cells also express CD40 ligand (CD154) and Fas ligand (CD178) on cell surface, thereby mediating costimulation and apoptosis, respectively. Differentiation of Th1 is driven by IL-12, IL-18 and IL-27, cytokines produced by APCs such as macrophages and DCs. Activated Th2 cells produce IL-4, IL-5, IL-6 and IL-13. These cytokines stimulate B cells to

proliferate, to induce antibody class switching, and to increase antibody production, i.e. are crucial for humoral immunity, including IgE-mediated allergic reactions. Many of the Th2 cytokines also act on CD4⁺ T cells and other immune cells and can be part of regulatory mechanisms (e.g. IL-4 promotes the production of Th2 cytokines (including itself), and Th1 cytokines (IFN γ , TNF β) inhibit differentiation into Th1. It was proposed to separate a specific subset, referred to as Th9, which arises from Th2 cells and secretes broadly inhibitory cytokines IL-9 and IL-10, previously assigned to the Th2 subset itself (Dardalhon et al., 2008; Veldhoen et al., 2008). These cytokines negatively affect secretion of IL-2 and IFN γ by Th cells and IL-12 by DC and macrophages). Th1 and Th2 cells express different sets of chemokine receptors, which govern their migration to different sites (Dong and Flavell, 2001). Th1 cells preferentially express CCR5, CXCR3 and CCR1, which allow them to migrate to inflammatory sites. By contrast Th2 cells express CCR3, CCR4 and CCR8, which are important for recruitment to site of allergic reactions. Th1 and Th2 cells are well characterized at the level of specific transcription factors driving their distinct gene expression programs. Th1 cells express Stat1, Stat4 and T-bet and Th2 cells express Stat5, Stat6 and GATA3 transcription factors. T-bet and GATA3 are master transcription factors and *de facto* represent their lineage markers. Additional CD4⁺ Th cell subsets were recently defined, such as Th3, which produce mainly TGF β (transforming growth factor β); Th17, which by secreting IL-17A and other cytokines, promoting protective immunity against extracellular bacteria and fungi, mainly at mucosal surfaces. They also promote autoimmune and inflammatory diseases. Further subsets are Tfh (follicular helper cells) which due to CXCR5 expression migrate to B cell follicles to support B cell development by secreting IL-21 and Th22 cells which secrete IL-22 and were identified in inflammatory skin diseases. Under certain conditions leading to expression of eomesodermin (EOMES), such as repeated exposure to antigen (e.g. EBV, HIV-1, CMV infections), Th1 cells can acquire full cytolytic machinery (Qui et al., 2011). Regulatory T cells comprise thymus-derived nTreg cells (natural regulatory T cells), and iTreg (induced regulatory T cells) that arise from naïve Th cells in the periphery. nTregs express constitutively high levels of CD25, secrete TGF β and IL-10 inhibitory cytokines (Bacchetta et al., 2005; Grazia Roncarolo et al., 2006). A distinct subset of iTregs, Tr1 cells, are suppressive cells generated under experimental conditions *in vitro* from naïve T cells in the presence of TGF β and IL-27 or in the presence of the immunosuppressive drugs vitamin D3 and dexamethasone. These cells do not undergo negative thymic selection and therefore have relatively high affinities for self-antigens. The

transcription factor FoxP3 is required for regulatory T cell development and is a master regulator of the genetic program for this lineage, along with the transcription factors Smad3 and Stat5. iTregs are also CD25⁺ and FoxP3⁺ and differentiate from naïve peripheral CD4⁺ cells, namely under the influence of TGFβ and IL-2.

Regulatory T cells play a crucial role in T cell homeostasis and in suppressing T cell mediated immunity against self-antigens (Randolph and Fathman, 2006; Wahl and Chen, 2005). A major mechanism of inhibition is via secretion of inhibitory cytokines, namely IL-10 and TGFβ. IL-10 inhibits CD28-mediated tyrosine phosphorylation and hence CD28-mediated co-stimulation. TGFβ suppresses the activity of most immune cells. Regulatory T cells also express high levels of inhibitory coreceptors such as CTLA-4 (cytotoxic T-lymphocyte associated molecule-4), GITR (glucocorticoid-induced TNF receptor) and PD-1 (programmed cell death-1) inhibitory coreceptors (Yamazaki et al., 2006), acting negatively on T cells by contact inhibition. Treg have a greater TCR diversity than effector T cells, with recognition biased towards self-peptides (Föhse et al., 2011). Regulatory T cells actively suppress activation of immune responses against self-antigens and thus prevent autoimmune disease. Genetic deficiency in Tregs results in severe autoimmune syndromes. The balance in the differentiation of the various CD4⁺ effector and regulatory T cells is controlled to a large extent by DCs (de Jong et al., 2005). Immature DCs reside in different tissues and in the blood and can be activated by pathogens, e.g. via Toll-like receptors (TLR), which are members of the IL-1 receptor/TLR superfamily. Upon activation DCs acquire effector functions, including production of proinflammatory cytokines and support local innate immune responses; they also up-regulate MHC class II, CD80 and CD86 thereby efficiently promoting the differentiation of CD4⁺ T cells into effector cells.

1.6 Fluorescent MHC-peptide oligomers (“tetramers”)

The invention of MHC-peptide tetramers (Altman et al., 1996) revolutionized CD8⁺ T cell immunology (Klenerman et al., 2002). Tetramers made possible enumeration and isolation of antigen-specific T cells. MHC-peptides are natural ligands for T cell receptors (TCRs). Because TCR:MHC-peptide interactions are of low affinity (micromolar dissociation constants) and relatively short lived (off-rates in the range of seconds) (Merwe and Davis, 2003), fluorescently labeled monomeric MHC-peptide complexes cannot be used to stain T cells. Oligomerization of biotinylated MHC-peptides on fluorescent streptavidin provides such conjugates with sufficiently stable binding to allow detection of cell-bound complexes

by flow cytometry. Streptavidin-phycoerythrin conjugates (e.g. phycoerythrin or allophycocyanin) are most commonly used because of their intense fluorescence. Because of the large size of these fluorochromes, such conjugates are typically heterogeneous and hence the resulting staining reagents are multimeric (Guillaume et al., 2003).

Applying the same strategy to MHC class II-peptide complexes encountered numerous difficulties, only some of which have been solved (Guillaume et al., 2009; Kwok, 2003; Vollers and Stern, 2008). Soluble recombinant MHC class II monomers proved more difficult to produce than their class I counterparts. While MHC class I heavy chains can be readily refolded from heavy and light chains produced in *E. coli* in the presence of a given binding peptide, this method is generally not applicable to the production of MHC class II-peptide complexes, except for rare cases such as for HLA-DR1 (Frayser et al., 1999). The most successful expression system proved to be based on *Drosophila* S2 cells, probably at least in part because of their ability to grow between 20 and 28 °C (optimum at 26 °C) which favors thermolabile MHC class II proteins. Naturally, transmembrane domains (TMDs) have an important role in the formation and stabilization of the MHC class II heterodimer. In soluble recombinant MHC II molecules, acidic and basic leucine zippers replace the TMDs to promote chain pairing. One of the leucine zippers is C-terminally fused with an Avi-Tag (also referred to as BSP tag), which is recognized and biotinylated by the *E. coli* BirA enzyme in the presence of ATP. There are two approaches to produce MHC-class II peptide complexes. One is to encode the peptide fused via a flexible (often thrombin-cleavable) linker to the MHC class II β chain and the other is to load the “empty” molecules with the peptide *in vitro*. The so-called “peptide tethered-on” approach is sometimes necessary if “empty” MHC class II molecules of a particular allele are very unstable, and is favored by crystallographers; such complexes are more amenable to crystallization. Disadvantages are that a separate β chain construct is required for every different MHC-peptide complex and that linker length imposes constraints on the peptide (Cunliffe et al., 2002). To prepare MHC-class II peptide complexes by loading is a more flexible strategy.

While it is possible to detect antigen-specific CD8⁺ T cells directly *ex vivo*, for most specificities frequencies of effector CD4⁺ T cells are at or just above 0.02%, i.e. detection limit of flow cytometers (Vollers and Stern, 2008). Higher frequencies of specific cells can be found in diseased tissues (e.g. lung parenchyma of mice infected by Sendai virus (Cauley et al., 2002) or human synovial fluid from individuals affected by Lyme disease (Meyer et al., 2000)). CD4⁺ memory cells are very rare; their frequencies in peripheral blood are estimated

at 1/100,000 or lower (Vollers and Stern, 2008). Naïve cells counts are also well below flow cytometric detection limits (Moon et al., 2007). Usually strategies such as peptide-stimulated expansion *in vitro* or tetramer-guided MACS (Day et al., 2003) are required to visualize antigen-specific CD4⁺ T cells by flow cytometry.

It is not clear why antigen-specific CD4⁺ T cells are at least an order of magnitude less frequent than CD8⁺ T cells in blood. A possible explanation could be the way peptides are presented by MHC class II molecules. Because their peptide-binding grooves are open-ended, MHC class II molecule-bound peptides are not of defined length. Peptides are presented as nested truncates (Chicz et al., 1992; Rudensky et al., 1991) with a common nonamer core binding sequence flanked by residues of variable length. Such core peptide-flanking residues have been shown to play a role in TCR recognition, MHC binding and MHC-peptide conformation (Arnold et al., 2002; Durinovic-Bello et al., 2006; Lovitch et al., 2006; Rötzschke et al., 1999). Changes in peptide-dependent conformation can be observed by NMR (Schmitt et al., 1999), mass spectrometry (Carven and Stern, 2005), differences in SDS-resistance (Natarajan et al., 1999b), measurements of hydrodynamic radii (Zarutskie et al., 1999), differential antibody reactivity (Carven et al., 2004) or T cell recognition (Lovitch and Unanue, 2005).

Another reason is that in CD8⁺ T cells, epitope immunodominance is highly pronounced, leading to high frequencies of CD8⁺ T cells specific for immunodominant epitopes. This is less so in the CD4⁺ T cell compartments, along with more limited burst sizes than CD8⁺ T cells.

Coordinate binding of CD8 to TCR-associated MHC class I-peptide complexes provides a substantial increase in avidity of MHC class I-peptide multimer binding (Merwe and Davis, 2003). This is not the case for MHC class II-peptide multimer binding, mainly because CD4:MHC class II-peptide interactions are very weak ($K_D > 200 \mu\text{M}$) (Xiong et al., 2001). Moreover, data comparing binding of several class I and class II MHC-peptide binding to their cognate TCRs showed on average weaker interactions of class II MHC-peptide:TCR (Cole et al., 2007). As those data are limited, it is not possible to generalize to all TCR:MHC class II-peptide interactions, but it is conceivable that MHC class II multimers can efficiently bind only to CD4⁺ T cells expressing TCRs of sufficiently high avidity.

Refolding of MHC class I heavy chains in the presence of $\beta 2$ -microglobulin and peptide is an “all-or-none” process. Preparations of purified MHC class I-peptide complexes are highly molecularly homogenous. Conversely, register sliding has been demonstrated in mouse and

human recombinant MHC class II-peptide complexes, even with covalently bound long peptides (Cecconi et al., 2010; Landais et al., 2009; Stadinski et al., 2010). Adoption of alternate binding registers consequently yields heterogeneous mixtures of MHC class II-peptide conformers giving multimers with suboptimal avidity. Heterogeneity arises as well when “empty” MHC molecules are loaded with peptides of interest, which is investigated in this thesis.

1.7 Thesis aims

The objectives of the thesis research include : 1) establishment of methods to reliably produce molecularly defined MHC class II-peptide multimers to further analysis of antigen-specific CD4⁺ T cells, 2) to invent a novel type of reversible MHC class II-peptide multimers for special applications, 3) elucidation of the role of the CD8 α transmembrane domain for CD8 coreceptor function.

2. MATERIALS AND METHODS

2.1 General materials and methods

2.1.1 Reagents and consumables

β -mercaptoethanol	Gibco/Invitrogen Life Technologies, US
DMEM	Gibco/Invitrogen Life Technologies, US
RPMI 1640	Gibco/Invitrogen Life Technologies, US
IMDM	Gibco/Invitrogen Life Technologies, US
Sf900 II SFM	Gibco/Invitrogen Life Technologies, US
Fetal calf serum	Omnilab, CH
Human serum	Swiss Blood Bank, CH
Mouse recombinant IL-2	Peprtech, UK
Human recombinant IL-2	Peprtech, UK
Polybrene	Sigma, US
Human β 2-microglobulin	courtesy of Dr. P. Guillaume
GelCode Blue Stain reagent	Pierce, US
Precision Plus Protein Standards All Blue	Bio-Rad, US
Centrifugal filter devices (Amicon Ultra-4/Ultra-15 ; Amicon concentration cell)	Merck Millipore, US
NHS-Cy5	GE Healthcare Life Sciences, SE
CnBr Sepharose 4B	GE Healthcare Life Sciences, SE
PD-10 columns	GE Healthcare Life Sciences, SE
SigmaFAST pNPP substrate	Sigma, US
Amersham Hyperfilm ECL	GE Healthcare Life Sciences, SE
ECL detection solutions	GE Healthcare Life Sciences, SE
16% formaldehyde, MetOH free	PolySciences, US

All other chemicals were from Sigma, if not otherwise mentioned.

2.1.2 Antibiotics

Ampicillin	Applichem, DE
Penicillin/streptomycin	Gibco/Invitrogen Life Technologies, US
Puromycin	Sigma, US

2.1.3 Enzymes

<i>V. cholerae</i> neuraminidase	Roche, CH
Restriction enzymes and accompanying buffers	New England Biolabs or Promega, US
T4 DNA polymerase Klenow fragment	New England Biolabs, US
Quick DNA ligase	Promega, US

2.1.4 Kits

MaxiPrep, MiniPrep, RNAeasy Mini, QiaPrep, OmniScript RT, Qiashredder kits	Qiagen, DE
Mouse IL-2 and human IFN- γ ELISA	Mabtech, SE

2.1.5 Solutions and cell culture media

TBE

45 mM Tris-borate
1 mM EDTA

PBS

137 mM NaCl
2.7 mM KCl
8.0 mM Na₂HPO₄
1.5 mM KH₂PO₄

TBS

20 mM Tris pH 8.0
100 mM NaCl

Stacking gel solution

30% acrylamide solution
1 M Tris pH 6.8
10% SDS
10% APS
0.25% TEMED

Separating gel solution

30% acrylamide solution
1.5M Tris pH 8.8
10% SDS
10% APS
0.25% TEMED

SDS-PAGE running buffer

25 mM Tris pH 8.3
250 mM glycine pH 8.3
0.1% SDS

SDS gel loading buffer

50 mM Tris pH 6.8
100 mM β -mercaptoethanol
2% SDS
10% glycerol
0.1% bromophenol blue

Semi-dry transfer buffer

38 mM glycine
48 mM Tris pH 8.3
0.4% SDS
20% methanol

Western Blocking solution

5% fat-free dry milk
0.05% Tween 20
1xPBS

ELISA incubation buffer

0.1% BSA
0.05% Tween 20
1xPBS

ELISA wash buffer

0.05% Tween 20
1xPBS

FACS buffer

0.5% BSA
2 mM EDTA
0.02% NaN₃

LB medium

1% peptone
0.5% yeast extract
90 mM NaCl

LB freezing medium

LB medium
40% glycerol

TSS solution

10% w/v PEG 3350
5% v/v DMSO
20 mM MgCl₂
pH 6.5 in LB broth

5xKCM buffer

0.5 M KCl
0.15 M CaCl₂
0.25 M MgCl₂

Cell lysis buffer

1% Triton X-100 or Brij96
50 mM HEPES pH 7.4
150 mM NaCl
1x complete protease inhibitors
1x PHOSStop complete phosphatase inhibitors

Cell freezing medium

Sf900 II SFM/DMEM/RPMI
50% FCS
10% DMSO

T cell hybridoma medium

DMEM
5% FCS
50 µM β-mercaptoethanol
100 U/ml penicillin
100 µg/ml streptomycin

Murine CD4⁺ T cell medium

IMDM
10% FCS
50 U/ml rmIL-2
100 U/ml penicillin
100 µg/ml streptomycin

Human CD4⁺ T cell medium

RPMI 1640
8% human serum
100 U/ml rhIL-2

2.1.6 Instruments

ÄKTA FPLC system	GE Healthcare Life Sciences, SE
Biometra Thermocycler T3	Chatel-St. Denis, CH
FACSCalibur	Becton Dickinson, US
BD LSR II	Becton Dickinson, US
BD Aria	Becton Dickinson, US
HPLC system (1525 Binary HPLC pump and 2998 Photodiode Array Detector)	Waters, US
Centrifuge 5810R	Eppendorf, DE
Centrifuge 5415D	Eppendorf, DE
Centrifuge 5417R	Eppendorf, DE
Mini-Protean 3 system	Bio-Rad, US
Ultracentrifuge Discovery M150SE	Thermo Scientific Sorvall, US
Ultrospec 3000 spectrophotometer	GE Healthcare Life Sciences, US
Epoch plate reader	Bio-Tek, CH
Countess cell counter	Invitrogen/Life Technologies, US
Semi-dry transfer unit Hoefer TE-70	GE Healthcare Life Sciences, US
UV lamps (312 and 365 nm)	Vilber Lourmat, FR

2.1.7 FPLC columns

Superdex S200	GE Healthcare Life Sciences, SE
HiPrep 26/10	GE Healthcare Life Sciences, SE
HisTrap HP 1ml	GE Healthcare Life Sciences, SE
MonoQ HR 5/5 1 ml	GE Healthcare Life Sciences, SE
Strep-Tactin Superflow high capacity 5 ml	IBA, DE

2.1.8 HPLC columns

Reverse phase C18, Grace Vydac, Hesperia CA, USA

2.1.9 Software

FlowJo 7.6	TreeStar	flow cytometry data analysis
ImageJ 1.46k	NIH	image analysis
Gen5 1.10	BioTek	ELISA data analysis
Prism 5	GraphPad Software	data analysis
Axiovision LE 4.8	Zeiss	image analysis
Unicorn 5.20	GE Healthcare Life Sciences	FPLC chromatogram data analyses
Vector NTI Advance 11	Invitrogen	DNA construct management
DeepView/Swiss PDB viewer v4.0.4	Swiss Institute for Bioinformatics	visualization of protein structure
EndNote X5	ThomsonReuters	reference manager
Word 2010	Microsoft	writing
Excel 2010	Microsoft	data storage
Photoshop CS3	Adobe	image analysis

2.1.10 Molecular biology methods

Preparation of chemically competent bacteria

E. coli XL-1 Blue cells were grown in 500 ml LB medium at 37 °C shaken at 250 rpm until mid-log phase was reached ($OD_{600}=0.6-0.8$). Cells were cooled on ice and harvested by centrifugation at 4000 rpm for 30 min at 4 °C. Bacterial pellets were resuspended in 25 ml ice-cold TSS solution, frozen in aliquots of 100 μ l in liquid nitrogen and stored at -80 °C.

Transformation of competent bacteria

Frozen competent XL-1 Blue bacteria (100 μ l) were thawed on ice and mixed with 5xKCM buffer and 1 μ g plasmid DNA or 5 μ l ligation mix, incubated 5 min at 37 °C and then incubated for 2 min on ice. Subsequently, 1 ml LB medium was added and the cells incubated for 1 h at 37 °C. Bacteria were plated on LB agar plates containing 100 μ g/ml ampicillin and then incubated overnight at 37 °C.

Plasmid preparation

For plasmid maxipreps (150 ml) or plasmid minipreps (3 ml), the appropriate volume of LB broth with 100 μ g/ml ampicillin was inoculated with transformed bacteria and allowed to grow overnight at 37 °C, while being shaken at 250 rpm. Bacterial cells were harvested by centrifugation at 4000 rpm for 30 min at 4 °C. Plasmids were purified with the MaxiPrep or MiniPrep kits according to the manufacturer's instructions. Plasmid preparations for transfections were dissolved in sterile EB buffer at 1-2 mg/ml.

Restriction enzyme digestion of plasmid DNA

Typically 10 μ g of plasmid DNA was digested in 50 μ l with appropriate restriction enzyme(s) and suitable 10x restriction buffer as recommended by the manufacturer, for 1 h at 37 °C. Digested plasmid DNA was loaded in the presence of loading buffer onto 1% agarose gels with 0.1 μ g/ml ethidium bromide and the appropriate DNA fragments isolated using the QiaQuick gel extraction kit according to the manufacturer's instructions.

DNA ligation

DNA ligation was carried out in 20 μ l containing 1 μ g digested and purified vector DNA, and an appropriate quantity of digested and purified insert DNA to achieve a 1:1 molar ratio. The Quick ligation kit (New England Biolabs) was used to perform the ligation in 5 min at room temperature. 5 μ l of this ligation mix was used for transformation of competent bacteria.

2.2 Materials and methods, Chapter I

Peptides

Sequence	Designation
PKYVKQNTLKLAT	HA ₃₀₆₋₃₁₈
PGVLLKEFTVSGNILTIRLTAADHR	NY-ESO-1 ₁₁₉₋₁₄₃
GFVFTLTVPSER	Flu-MP ₆₁₋₇₂
KKYFAATQFEPLAA	Oxy ₂₇₂₋₂₈₄
biotin-Ahx-CPKYVKQNTLKLAT	biotin-HA ₃₀₆₋₃₁₈
RQLQLSISCLQ	NY-ESO-1 ₁₄₃₋₁₅₄
HHHHHSGSGPKYVKQNTLKLAT	His-HA ₃₀₆₋₃₁₈
HHHHHSGSGPGVLLKEFTVSGNILTIRLTAADHR	His-NY-ESO-1 ₁₁₉₋₁₄₃
HHHHHSGSG-βNPPA-PKYVKQNTLKLAT	His-SGSG-βNPPA-PKYVKQNTLKLAT
PKYVKQNTLKLAT-βNPPA-SGSGHHHHH	PKYVKQNTLKLAT-βNPPA-SGSG-His
DTB-Ahx-CPKYVKQNTLKLAT	DTB-HA ₃₀₆₋₃₁₈
DTB-Ahx-CPGVLLKEFTVSGNILTIRLTAADHR	DTB-NY-ESO-1 ₁₁₉₋₁₄₃
pY-DDDDSGSGPKYVKQNTLKLAT	pY-D ₄ -SGSG-HA ₃₀₆₋₃₁₈
sY-DDDDDDSGSGPKYVKQNTLKLAT	sY-D ₆ -SGSG-HA ₃₀₆₋₃₁₈
pY-DDGGDDGGDDSGSGPKYVKQNTLKLAT	pY-(DDGG) ₂ DD-SGSG-HA ₃₀₆₋₃₁₈
pY-EEEEEEEEESGSGPKYVKQNTLKLAT	pY-E ₈ -SGSG-HA ₃₀₆₋₃₁₈
pY-EEEEEEEEESGSGPKYVKQNTLKLAT	pY-E ₈ -SGSG-HA ₃₀₆₋₃₁₈
FNNFTVSFWRVLPK	TT ₉₄₇₋₉₆₀
DTB-Ahx-CFNNFTVSFWRVLPK	DTB-TT ₉₄₇₋₉₆₀
HHHHHSGSGPKY-βNPG-QNTLKLAT	HA*2
HHHHHSGSGPKYV-βNPG-QNTLKLAT	HA*3
HHHHHSGSGPKYVKQ-βNPG-TLKLAT	HA*5
HHHHHSGSGPKYVKQNTL-βNPG-LAT	HA*8

MALDI-TOF of peptides

On a clean MALDI target plate, 0.8 µl of peptide in 50% water (0.1% TFA in water)/50% acetonitrile was applied per spot and allowed to air-dry. 0.8 µl of saturated methanol solution of α-cyano-4-hydroxycinnamic acid was added onto the spotted peptide and air-dried. Data were acquired with 200 pulses of the 337 nm laser; signals below 700 Da were excluded from the analysis due to species originating from matrix molecules.

Synthesis of NTA₄ biotin and SA-PE NTA₄

Tetra-NTA biotin was obtained by alkylation of the tetra-NTA peptide precursor, which was synthesized by conventional solid phase chemistry using chlorotriyl resins. Biotin-ε-aminocaproyl (Ahx) was used to incorporate biotin. Detailed protocols are reported in (Schmidt et al., 2011). Commercial SA-PE conjugates (Invitrogen Life Technologies) were saturated with a 10-fold molar excess of NTA₄ biotin and incubated with 100 mM NiSO₄ for 30 min at RT. Prior to use, excess reagents were removed with gel filtration spin columns and the concentration adjusted based on absorbance at 595 nm.

Antibodies

Mouse anti-human DR mAb L243 (ExBio, Czech Republic), mouse anti-human DP mAb B7.21.7, biotinylated mouse anti-BSP mAb 1.4.2.7 (a gift from G. De Libero, University Hospital Basel), FITC-labeled anti-CD4 mAb RPA-T4 (BD Pharmingen), mouse anti-phosphotyrosine mAb PY20 alkaline phosphatase conjugate (Calbiochem), mouse anti-sulfotyrosine mAb 1C-A2 (Merck Millipore).

Cells

10^6 PBMCs from a DRB1*0401⁺ healthy donor were stimulated with 2 μ M HA₃₀₆₋₃₁₈ and cultured in complete medium with 100 U rhIL-2/ml for at least 10 days before analysis. DR4/HA₃₀₆₋₃₁₈-specific clones were obtained by limiting dilution cloning of peptide-stimulated PBMC of the same donor after day 10 and cultured in RPMI 1640 medium supplemented with 8% human serum and 150 U/ml of rhIL-2 (complete medium). T2-DR4 cells were cultured in RPMI 1640 supplemented with 10% FCS. CD4⁺ T cells from DR1 transgenic mouse (referred to as AJ123 line) were maintained in IMDM supplemented with 10% FCS and 50 U/ml of recombinant mouse IL-2 (rmIL-2) (Peprotech). D.mel-2 were grown in Sf900 II SFM medium (Life Technologies/Invitrogen) in closed flasks at 26 °C without CO₂ or humidity. Puromycin-resistant lines and clones derived from original D.mel-2, used for the production of recombinant MHC class II molecules were maintained in Sf900 II SFM supplemented with 10 μ g/ml puromycin (Sigma).

Plasmids

MHC class II expression plasmids were derived from the pMT\BiP\V5-His A vector (Invitrogen). The restriction map of the plasmids containing the beta chain is shown in Fig. 2.1. The coding sequence for the human CLIP peptide (PVSKMRMATPLLMQA) was cloned between the BglII and NheI sites. The coding sequence for the thrombin cleavage site (LVPRGS), flanked on each side by linkers (GGGGS) was cloned between NheI and KpnI. The extracellular region of the mature beta chain (without the signal peptide) was cloned between KpnI and EcoRI. Alternatively, the extracellular region of the alpha chain was cloned between BglII and EcoRI, as the constructs for the alpha chains do not have the peptide and the thrombin cleavage site. Finally, coding sequences for acidic and basic leucine zippers were cloned between EcoRI and EcoRV sites. The alpha chain construct harbors the acidic leucine zipper, which in some cases was terminated by a tandem His-tag (HHHHHHGGGSGGGSGSHHHHH). The beta chain construct contains the basic leucine zipper and terminates with a biotinylation sequence peptide (BSP) tag, known also as Avi-Tag (LNDIFEAQKIEWHE).

The BglII-KpnI fragment was constructed by joining the CLIP-F and LTL-R oligonucleotides by PCR. The extracellular parts of the DR α (DRA1*0101) and DP α (DPA1*0103) chains were PCR amplified from plasmid constructs containing those chains cloned using the primers DRA-F and DRA-R for the DR α and DP4A-F and DP4A-R for DP α . The extracellular parts of the DRB1*0401 (DR4), DRB3*0202 (DR52b) and DPB1*0401 (DP4) were PCR amplified from respective plasmid constructs using primers DR4B-BglII-F (for DR4 with no covalently bound peptide) or DR4B-KpnI-F (with covalent CLIP peptide) and DR4B-R (DR4), DR4B-KpnI-F and DR4B-R (DR52b), and DP4B-F and DP4B-R (DP4). The coding sequences for the acidic and basic leucine zipper were PCR amplified from plasmid constructs with primers ALZ/BLZ-F (common primer for both leucine zippers) and

ALZ-R for acidic and BLZ-R for basic leucine zipper, respectively. The fragment containing the ALZ was extended with ALZ-His6-R and further with 2xHis-R to provide for the tandem His-tag.

For primer design, allele sequence data publicly available in the NIH dbMHC database (<http://www.ncbi.nlm.nih.gov/projects/gv/mhc>) were used.

The pBS-hs.PURO plasmid was a gift from K. Karjalainen (Seidl et al., 2001).

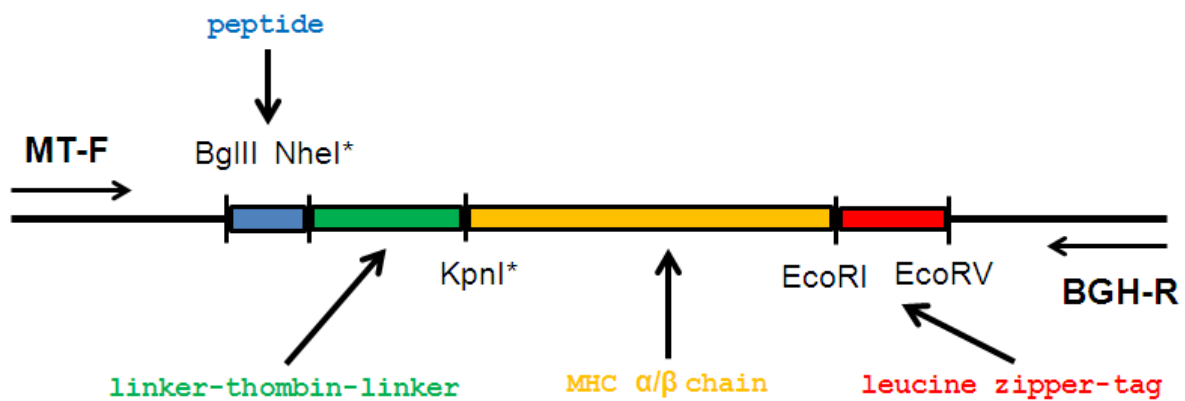


Figure 2.1 Schematic representation of the insert restriction map of the pMT plasmid constructs. The coding sequence for the peptide is cloned between BglII and NheI sites (blue). The thrombin cleavage site flanked by two linkers is cloned between NheI and KpnI (green). The extracellular region of the MHC class II α or β chain are between Kpn I or BglII and EcoRI. Note that for empty molecules the NheI and KpnI sites are omitted and the MHC chain is cloned into BglII/EcoRI. Finally, the acidic or basic leucine zipper (red) is cloned between EcoRI and EcoRV.

Primers and sequences

Primers

CLIP-F

5' CTTTAGATCTCCTGTGAGCAAGATGCGCATGGCCACCCCGCTGCTGATGCAGGCGGCTAG
CGGAGGTGGA3'

LTL-R

5' CTTTGGTACCTGAACCTCCACCTCCAGAGCCTCGGGGCACTAGTGAGCCTCCACCTCCGC
TAGCCGCCTGCAT3'

DRA-F

5' CTTTAGATCTATCAAAGAAGAACATGTGATC3'

DRA-R

5' CTTCGAATTCGTTCTCTGTAGTCTCTGGG3'

DP4A-F

5' CTTTAGATCTGCTGGAGCCATCAAGGCGGAC3'

DP4A-R

5' CTTTGAATTCCTCCGTTGTCTCAGGCATC3'

DR4B-BglII-F

5' CTTTAGATCTCGACCACGTTTCTTGGAGC3'

DR4B-KpnI-F

5' CTTTGGTACCCGACCACGTTTCTTGGAGC3'

DR4B-R

5' CTTTGAATTCCTTGCTCTGTGCAGATTCAG3'

DP4B-F

5' CTTTAGATCTCCAGAGAATTACCTTTTCC3'

DP4B-R

5' CTTTGAATTCCTTACTCCGGGCAGAATCAG3'

ALZ/BLZ-F

5' CTTTGAATTCGGTGGTGGATCAGGAGGTTCAACTACAGCTCCATCAGCTC3'

ALZ-R

5' CTTTGATATCTTACTGAGCCAGTTCCTTTTCC3'

BLZ-BSP-R

5' GATGTCGTTTCAGACCGCCACCACTGCCTCCCTGGGCGAGTTTCTTCTTGAG3'

ALZ-His6-R

5' CTTTGATATCTCAATGATGGTGGTGGTGGCCGGTGGCGCTGAGCCAGTTCCTTTTCC3'
,

ALZ-His6LinkerHis6-R

5' CTTTGATATCTCAGTGGTGGTGGTGGTGGCTGCCGCTGCCGCCGCCGCTGCCGCCGC
CATGATGGTGGTGGTGGCCGGTGGCG3'

Sequences

DR α

5' AGATCTATCAAAGAAGAACATGTGATCATCCAGGCCGAGTTCTATCTGAATCCTGACCAA
TCAGGCGAGTTTATGTTTGACTTTGATGGTGGTGGAGATTTCCATGTGGATATGGCAAAGAA
GGAGACGGTCTGGCGGCTTGAAGAATTTGGACGATTTGCCAGCTTTGAGGCTCAAGGTGCAT
TGGCCAAACATAGCTGTGGACAAAGCCAACCTGGAAATCATGACAAAGCGCTCCAACCTATACT
CCGATCACCAATGTACCTCCAGAGGTAACCTGTGCTCACGAACAGCCCTGTGGAACCTGAGAGA
GCCCAACGTCCTCATCTGTTTCATCGACAAGTTCACCCACAGTGGTCAATGTCACGTGGC
TTCGAAAATGGAAAACCTGTCCACACAGGAGTGTGACAGAGACAGTCTTCCCTGCCAGGGAAGAC
CACCTTTTCCGCAAGTTCCACTATCTCCCCTTCCCTGCCCTCAACTGAGGACGTTTACGACTG
CAGGGTGGAGCACTGGGGCTTGGATGAGCCTCTTCTCAAGCACTGGGAGTTTGATGCTCCAA
GCCCTCTCCCAGAGACTACAGAGAACGAATTCGGTGGTGGATCAGGAGTTCAACTACAGCT
CCATCAGCTCAGCTCGAAAAGAGCTCCAGGCCCTGGAGAAGGAAAATGCACAGCTGGAATG
GGAGTTGCAAGCACTGGAAAAGGAACTGGCTCAGTAAGATATC3'

RSIREEHVIIQAEFYLNPDQSGEFMFDFDGDEIFHVDMAKKETVWRLEEFGRFASFEAQGAL
ANIAVDKANLEIMTKRSNYTPITNVPPEVTVLTNLSPVELREPNVLICFIDKFTPPVNVNVTWL
RNGKPVTGTVSETVFLPREDHLFRKFHYLPFLPSTEDVYDCRVEHWGLDEPLLKHWEFDAPS
PLPETTENEFGGSGSSTTAPSAQLEKELQALEKENAQLWELQALEKELAQ

DR α 2xHis

5' AGATCTATCAAAGAAGAACATGTGATCATNCAGGCCGAGTTCTATCTGAATCCTGACCAA
TCAGGCGAGTTTATGTTTGACTTTGATGGTGGTGGAGATTTCCATGTGGATATGGCAAAGAA
GGAGACGGTCTGGCGGCTTGAAGAATTTGGACGATTTGCCAGCTTTGAGGCTCAAGGTGCAT

TGGCCAACATAGCTGTGGACAAAGCCAACCTGGAAATCATGACAAAGCGCTCCAACCTATACT
 CCGATCACCAATGTACCTCCAGAGGTAACCTGTGCTCACGAACAGCCCTGTGGAAGTGGAGAGA
 GCCCAACGTCTCATCTGTTTCATCGACAAGTTCACCCACCAGTGGTCAATGTCACGTGGC
 TTCGAAATGGAAAACCTGTCACCACAGGAGTGTGAGAGACAGTCTTCCTGCCAGGGGAAGAC
 CACCTTTTCCGCAAGTTCACCTATCTCCCTTTCCTGCCCTCAACTGAGGACGTTTACGACTG
 CAGGGTGGAGCACTGGGGCTTGGATGAGCCTCTTCTCAAGCACTGGGAGTTTGATGCTCCAA
 GCCCTCTCCCAGAGACTACAGAGAACGAATTCGGTGGTGGATCAGGAGGTTCAACTACAGCT
 CCATCAGCTCAGCTCGAAAAAGAGCTCCAGGCCCTGGAGAAGGAAAATGCACAGCTGGAATG
 GGAGTTGCAAGCACTGGAAAAGGAACTGGCTCAGCGCACCGGCCACCATCATCACCATCATG
 GCGGCGGCAGCGGCGGCGGCAGCGGCAGCCATCACCATCACCACCATTGAGATATC3'

RSIKEEHVIXQAEFYLNPDQSGEFMFDFDGDIEIFHVDMAKKETVWRLEEFGRFASF EAQ GAL
 ANIAVDKANLEIMTKRSNYTPITNVPPEVTVLTNSPVELREPNVLICFIDKFTPPVVNVTWL
 RNGKPVTTGVSETVFLPREDHLFRKFHYLPFLPSTEDVYDCRVEHWGLDEPLLKHWEFDAPS
 PLPETTENEFGGSGGSTTAPSAQLEKELQALEKENAQLEWELQALEKELAQRTHHHHHHG
 GSGGGSGSHHHHHH

DR4β CLIP

5' AGATCTCCTGTGAGCAAGATGCGCATGGCCACCCCGCTGCTGATGCAGGCGGCTAGCGGA
 GGTGGAGGCTCACTAGTGCCCGAGGCTCTGGAGGTGGAGGTTACAGTACCCGACCACGTTT
 CTTGGAGCAGGTTAAACATGAGTGTCAATTTCTTCAACGGGACGGAGCGGGTTCGGTTTCTGG
 ACAGATACTTCTATCACCAAGAGGAGTACGTGCGCTTTCGACAGCGACGTGGGGGAGTACCGG
 GCGGTGACGGAGCTGGGGCGGCCTGATGCCGAGTACTGGAACAGCCAGAAGGACCTCCTGGA
 GCAGAAGCGGGCCGCGGTGGACACCTACTGCAGACACAACCTACGGGGTTGGTGAGAGCTTCA
 CAGTGCAGCGGCGAGTCTATCCTGAGGTGACTGTGTATCCTGCAAAGACCCAGCCCCTGCAG
 CACCACAACCTCCTGGTCTGCTCTGTGAATGGTTTCTATCCAGGCAGCATTTGAAGTCAGGTG
 GTTCCGGAACGGCCAGGAAGAGAAGACTGGGGTGGTGTCCACAGGCCTGATCCAGAATGGAG
 ACTGGACCTTCCAGACCCTGGTGTGCTGGAAACAGTTCCTCGGAGTGGAGAGGTTTACACC
 TGCCAAGTGGAGCACCCAAGCCTGACGAGCCCTCTCACAGTGGAAATGGAGAGCACGGTCTGA
 ATCTGCACAGAGCAAGGAATTCGGTGGTGGATCAGGAGGTTCAACTACAGCTCCATCAGCTC
 AGTTGAAAAAGAAATTGCAAGCACTGAAGAAAAAGAACGCTCAGCTGAAGTGGAAACTTCAA
 GCCCTCAAGAAAAAACTCGCCCAGGGAGGCAGTGGTGGCGGTCTGAATGACATCTTCNAGGC
 TCAAAAAATCGAATGGCACGAATGAGATATC3'

RSPVSKMRMATPLLMQAASGGGGSLVPRSGGGGSGTRPRFLEQVKHECHFFNGTERVRF LD
 RYFYHQEEYVRFSDVGEYRAVTELGRPDAEYWN SQKDLLEQKRAAVDTYCRHNYGVGESFT
 VQRRVYPEVTVPYPAKTQPLQHNNLLVCSVNGFYPGSIEVRWFRNGQEEKTG VVSTGLIQNGD
 WTFQTLVMLETVPRSGEVYTCQVEHPSLTSPLTVEWRARSESAQSKEFGGGSGGSTTAPSAQ
 LKKKLQALKKKNAQLKWKLQALKKKLAQGGSGGGLNDIFEAQKIEWHE

DR1β

5' AGATCTCGACCACGTTTCTTGTGGCAGCTTAAGTTTGAATGTCATTTCTTCAATGGGACG
 GAGCGGGTTCGGTTGCTGGAAAGATGCATCTATAACCAAGAGGAGTCCGTGCGCTTCGACAG

CGACGTGGGGGAGTACCGGGCGGTGACGGAGCTGGGGCGGCCTGATGCCGAGTACTGGAACA
 GCCAGAAGGACCTCCTGGAGCAGAGGCGGGCCGCGGTGGACACCTACTGCAGACACA
 ACTACGGGTTGGTGGAGAGCTTACAGTGCAGCGGCGAGTTGAGCCTAAGGTGACTGTGTATCCTTC
 AAAGACCCAGCCCCTGCAGCACCACAACCTCCTGGTCTGCTCTGTGAGTGGTTTTCTATCCAG
 GCAGCATTGAAGTCAGGTGGTTCCGGAACGGCCAGGAAGAGAAGGCTGGGGTGGTGTCCACA
 GGCCTGATCCAGAATGGAGATTGGACCTTCCAGACCCTGGTGATGCTGGAAACAGTTCCTCG
 GAGTGGAGAGGTTTACACCTGCCAAGTGGAGCACCCAAGTGTGACGAGCCCTCTCACAGTGG
 AATGGAGAGCACGGTCTGAATCTGCACAGAGCAAGGAATTCGGTGGTGGATCAGGAGGTTCA
 ACTACAGCTCCATCAGCTCAGTTGAAAAAGAAATTGCAAGCACTGAAGAAAAAGAACGCTCA
 GCTGAAGTGGAAACTTCAAGCCCTCAAGAAGAACTCGCCCAGGGAGGCAGTGGTGGCGGTC
 TGAACGACATCTTCGAGGCTCAGAAAATCGAATGGCACGAATGAGATATC3'

RSRPRFLWQLKFECHFFNGTERVRLLERCIYNQEESVRFDSDVGEYRAVTELGRPDAEYWNS
 QKDLLEQRRAAVDITYCRHNYGVGESFTVQRRVEPKVTVYPSKTQPLQHHNLLVCSVSGFYPG
 SIEVRWFRNGQEEKAGVVSTGLIQNGDWTFFQTLVMLETVPRSGEVYTCQVEHPSVTSPLTVE
 WRARSESAQSKEFGGSGGSTTAPSAQLKKKLQALKKKNAQLKWKLQALKKKLAQGGSGGGL
 NDIFEAQKIEWHE

DR4β

5' AGATCTCGACCACGTTTCTTGGAGCAGGTTAAACATGAGTGTCAATTTCTTCAACGGGACG
 GAGCGGGTGC GGTTTCTGGACAGATACTTCTATCACCAAGAGGAGTACGTGCGCTTCGACAG
 CGACGTGGGGGAGTACCGGGCGGTGACGGAGCTGGGGCGGCCTGATGCCGAGTACTGGAACA
 GCCAGAAGGACCTCCTGGAGCAGAAGCGGGCCGCGGTGGACACCTACTGCAGACACA
 ACTACGGGTTGGTGGAGAGCTTACAGTGCAGCGGCGAGTCTATCCTGAGGTGACTGTGTATCCTGC
 AAAGACCCAGCCCCTGCAGCACCACAACCTCCTGGTCTGCTCTGTGAATGGTTTTCTATCCAG
 GCAGCATTGAAGTCAGGTGGTTCCGGAACGGCCAGGAAGAGAAGACTGGGGTGGTGTCCACA
 GGCCTGATCCAGAATGGAGACTGGACCTTCCAGACCCTGGTGATGCTGGAAACAGTTCCTCG
 GAGTGGAGAGGTTTACACCTGCCAAGTGGAGCACCCAAGCCTGACGAGCCCTCTCACAGTGG
 AATGGAGAGCACGGTCTGAATCTGCACAGAGCAAGGAATTCGGTGGTGGATCAGGAGGTTCA
 ACTACAGCTCCATCAGCTCAGTTGAAAAAGAAATTGCAAGCACTGAAGAAAAAGAACGCTCA
 GCTGAAGTGGAAACTTCAAGCCCTCAAGAAGAACTCGCCCAGGGAGGCAGTGGTGGCGGTC
 TGAACGACATCTTCGAGGCTCAGAAAATCGAATGGCACGAATGAGATATC3'

RSRPRFLEQVKHECHFFNGTERVRFLLDRYFYHQEEYVRFDSDVGEYRAVTELGRPDAEYWNS
 QKDLLEQKRAAVDITYCRHNYGVGESFTVQRRVYPEVTVYPAKTQPLQHHNLLVCSVNGFYPG
 SIEVRWFRNGQEEKTG VVSTGLIQNGDWTFFQTLVMLETVPRSGEVYTCQVEHPSLTSPLTVE
 WRARSESAQSKEFGGSGGSTTAPSAQLKKKLQALKKKNAQLKWKLQALKKKLAQGGSGGGL
 NDIFEAQKIEWHE

DR52bβ

5' AGATCTCGACCACGTTTCTTGGAGCTGCTTAAGTCTGAGTGTCAATTTCTTCAATGGGACG
 GAGCGGGTGC GGTTTCTGGAGAGACACTTCCATAACCAGGAGGAGTACGCGCGCTTCGACAG
 CGACGTGGGGGAGTACCGGGCGGTGAGGGAGCTGGGGCGGCCTGATGCCGAGTACTGGAACA

GCCAGAAGGACCTCCTGGAGCAGAAGCGGGGCCAGGTGGACAATTACTGCAGACACAACACTAC
 GGGGTTGGTGAGAGCTTCACAGTGCAGCGGCGAGTCCATCCTCAGGTGACTGTGTATCCTGC
 AAAGACCCAGCCCCTGCAGCACCACAACCTCCTGGTCTGCTCTGTGAGTGGTTTTCTATCCAG
 GCAGCATTGAAGTCAGGTGGTTCCGGAACGGCCAGGAAGAGAAGGCTGGGGTGGTGTCCACG
 GGCCTGATCCAGAATGGAGACTGGACCTTCCAGACCCTGGTGTGCTAGAAACAGTTCCCTCG
 GAGTGGAGAGGTTTACACCTGCCAAGTGGAGCACCCAAGCGTAACGAGCCCTCTCACAGTGG
 AATGGAGTGCACGGTCTGAATCTGCACAGAGCAAGGAATTCGGTGGTGGATCAGGAGGTTCA
 ACTACAGCTCCATCAGCTCAGTTGAAAAAGAAATTGCAAGCACTGAAGAAAAAGAACGCTCA
 GCTGAAGTGGAACTTCAAGCCCTCAAGAAGAACTCGCCCAGGGAGGCAGTGGTGGCGGTC
 TGAACGCATCTTCGAGGCTCAGAAAATCGAATGGCACGAATGAGATATC3'

RSRPRFLELLKSECHFFNGTERVRFLEHRHFHNQEEYARFDSVDVGEYRAVRELGRPDAEYWNS
 QKDLLEQKRGQVDNYCRHNYGVGESFTVQRRVHPQVTVYPAKTQPLQHHNLLVCSVSGFYPG
 SIEVRWFRNGQEEKAGVVSTGLIQNGDWTFFQTLVMLETVPRSGEVYTCQVEHPSVTSPLTVE
 WSARSESAQSKEFGGGSGGSTTAPSAQLKKKLQALKKKNAQLKWKLQALKKKLAQGGSGGGL
 NDIFEAQKIEWHE

DP α

5' AGATCTGCTGGAGCCATCAAGGCGGACCATGTGTCAACTTATGCCGCGTTTGTACAGACG
 CATAGACCAACAGGGGAGTTTATGTTTGAATTTGATGAAGATGAGATGTTCTATGTGGATCT
 GGACAAGAAGGAGACCGTCTGGCATCTGGAGGAGTTTGGCCAAGCCTTTTCCTTTGAGGCTC
 AGGGCGGGCTGGCTAACATTGCTATATTGAACAACAACCTTGAATACCTTGATCCAGCGTTCC
 AACCACACTCAGGCCACCAACGATCCCCCTGAGGTGACCGTGTTTCCCAAGGAGCCTGTGGA
 GCTGGGCCAGCCCAACACCCTCATCTGCCACATTGACAAGTTCTTCCCACCAGTGCTCAACG
 TCACGTGGCTGTGCAACGGGGAGCTGGTCACTGAGGGTGTGCTGAGAGCCTCTTCCTGCCC
 AGAACAGATTACAGCTTCCACAAGTTCCATTACCTGACCTTTGTGCCCTCAGCAGAGGACTT
 CTATGACTGCAGGGTGGAGCACTGGGGCTTGGACCAGCCGCTCCTCAAGCACTGGGAGGCCC
 AAGAGCCAATCCAGATGCCTGAGACAACGGAGGAATTCGGTGGTGGATCAGGAGGTTCAACT
 ACAGCTCCATCAGCTCAGCTCGAAAAAGAGCTCCAGGCCCTGGAGAAGGAAAAATGCACAGCT
 GGAATGGGAGTTGCAAGCACTGGAAAAGGAACTGGCTCAGTAAGATATC3'

RSAGAIKADHVSTYAAFVQTHRPTGEFMFEFDEDEMFYVDLDDKKEVWHLEEFQAFSFEAQ
 GGLANIAILNNNLNTLIQRSNHTQATNDPPEVTVPKPEVELGQPNTLICHIDKFFPPVLNV
 TWLCNGELVTEGVAESLFLPRTDYSFHKFHLYTFVPSAEDFYDCRVEHWGLDQPLLKHWEAQ
 EPIQMPETTEEFGGSGGSTTAPSAQLEKELQALEKENAQLEWELQALEKELAQ

DP α 2xHis

5' AGATCTGCTGGAGCCATCAAGGCGGACCATGTGTCAACTTATGCCGCGTTTGTACAGACG
 CATAGACCAACAGGGGAGTTTATGTTTGAATTTGATGAAGATGAGATGTTCTATGTGGATCT
 GGACAAGAAGGAGACCGTCTGGCATCTGGAGGAGTTTGGCCAAGCCTTTTCCTTTGAGGCTC
 AGGGCGGGCTGGCTAACATTGCTATATTGAACAACAACCTTGAATACCTTGATCCAGCGTTCC
 AACCACACTCAGGCCACCAACGATCCCCCTGAGGTGACCGTGTTTCCCAAGGAGCCTGTGGA
 GCTGGGCCAGCCCAACACCCTCATCTGCCACATTGACAAGTTCTTCCCACCAGTGCTCAACG

TCACGTGGCTGTGCAACGGGGAGCTGGTCACTGAGGGTGTGCGCTGAGAGCCTCTTCCTGCCC
 AGAACAGATTACAGCTTCCACAAGTTCCATTACCTGACCTTTGTGCCCTCAGCAGAGGACTT
 CTATGACTGCAGGGTGGAGCACTGGGGCTTGGACCAGCCGCTCCTCAAGCACTGGGAGGCCC
 AAGAGCCAATCCAGATGCCTGAGACAACGGAGGAATTCGGTGGTGGATCAGGAGGTTCAACT
 ACAGCTCCATCAGCTCAGCTCGAAAAAGAGCTCCAGGCCCTGGAGAAGGAAAATGCACAGCT
 GGAATGGGAGTTGCAAGCACTGGAAAAGGAACTGGCTCAGCGCACCGGCCACCATCATCACC
 ATCATGGCGGCGGCAGCGGCGGCGGCAGCGGCAGCCATCACCATCACCACCATTGAGATATC
 3'

RSAGAIKADHVSTYAAFVQTHRPTGEFMFEFDEDEMFYVDLDDKKEVWHLEEFQAFSFEAQ
 GGLANIAILNNNLNTLIQRSNHTQATNDPPEVTVPFKEPVELGQPNTLICHIDKFFPPVLNV
 TWLCNGELVTEGVAESLFLPRTDYSFHKFHLYLTFVPSAEDFYDCRVEHWGLDQPLLKHWEAQ
 EPIQMPETTEEFGGGSGGSTTAPSAQLEKELQALEKENAQLEWELQALEKELAQRTGHHHHH
 HGGGSGGGSGSHHHHHH

DP4β

5' AGATCTCCAGAGAATTACCTTTTCCAGGGACGGCAGGAATGCTACGCGTTTAATGGGACA
 CAGCGCTTCTGGAGAGATACATCTACAACCGGGAGGAGTTCGCGCGCTTCGACAGCGACGT
 GGGGGAGTTCCGGGCGGTGACGGAGCTGGGGCGGCCTGCTGCGGAGTACTGGAACAGCCAGA
 AGGACATCCTGGAGGAGAAGCGGGCAGTGCCGGACAGGATGTGCAGACACAACACTACGAGCTG
 GGCGGGCCCATGACCCTGCAGCGCCGAGTCCAGCCTAGGGTGAATGTTTCCCCCTCCAAGAA
 GGGGCCCTTGCAGCACCAACCTGCTTGTCTGCCACGTGACGGATTTCTACCCAGGCAGCA
 TTCAAGTCCGATGGTTCCTGAATGGACAGGAGGAAACAGCTGGGGTCGTGTCCACCAACCTG
 ATCCGTAATGGAGACTGGACCTTCCAGATCCTGGTGTGCTGGAAATGACCCCCCAGCAGGG
 AGATGTCTACACCTGCCAAGTGGAGCACACCAGCCTGGATAGTCTGTACCGTGGAGTGGA
 AGGCACAGTCTGATTCTGCCCCGAGTAAGGAATTCGGTGGTGGATCAGGAGGTTCAACTACA
 GCTCCATCAGCTCAGTTGAAAAAGAAATTGCAAGCACTGAAGAAAAAGAAGCTCAGCTGAA
 GTGGAAACTTCAAGCCCTCAAGAAGAAACTCGCCCAGGGAGGCAGTGGTGGCGGTCTGAATG
 ACATCTTCGAGGCTCAGAAAATCGAATGGCACGAATGAGATATC3'

RSPENYLFQGRQECYAFNGTQRFLERYIYNREEFARFDSVDVGEFRAVTELGRPAAEYWNSQK
 DILEEKRAVPDRMCRHNYELGGPMTLQRRVQPRVNVSPSKKGPLQHHNLLVCHVTDFYPGSI
 QVRWFLNGQEETAGVVSTNLIRNGDWTQILVMLEMTPOQGDVYTCQVEHTSLDSPVTVEWK
 AQSDSARSKEFGGGSGGSTTAPSAQLKKKLQALKKKNAQLKWKLQALKKKLAQGGSGGGLND
 IFEAQKIEWHE

Preparation of cDNA from EBVB cells

Total RNA was extracted from DR52b⁺ EBVB cells with RNAeasy Mini kit (Qiagen) and QIAshredder (Qiagen) according to manufacturer's instructions. cDNA was synthesized from 1 µg of total RNA using the OmniScript RT kit (Qiagen).

Liposomal transfection of insect cells

The day before transfection, D.mel-2 cells were plated at a subconfluent concentration of 0.5-1x10⁶ cells per well of a 24-well plate (Corning) in 0.5 ml of Sf900 II SFM medium. For transfection, in a well of a v-bottom 96-well plate, in 200 µl Sf900 II SFM medium, 20 µl of Cellfectin (Invitrogen) was added and 2.2 µg of plasmid DNA (1 µg of each pMT plasmid construct and 0.2 µg of pBS-hs.PURO plasmid to confer puromycin resistance) and mixed well. After 20 minutes at room temperature, the transfection mixture was pipetted dropwise onto the cells and after 24 hours puromycin was added. After 7 to 10 days, a puromycin-resistant cell line was obtained.

Generation of stably transfected insect cells for recombinant protein production

The day before plating, cells were split and diluted to 5x10⁵-10⁶ cells/ml. For limited dilution cloning a puromycin-resistant cell line is "spiked" (100 cells/ml) into untransfected D.mel-2 cells (3x10⁵ cells/ml) in Sf900 II SFM supplemented with 10% FCS and distributed by pipetting in flat-bottom 96-well plates (Corning) at 100 µl per well. Plates were wrapped in Saran wrap to prevent medium evaporation. After 24 hours, puromycin was added to the wells. Growth medium containing FCS and puromycin was replaced after 7 days and colonies scored after a further 7 days in culture. Colonies were transferred with a sterile pipette and expanded. Expression of recombinant MHC class II protein was tested by induction with 1 mM CuSO₄ and an ELISA assay after 3 to 5 days. Typically, clones obtained by this procedure were screened twice: first at an early stage to exclude all clones not expressing MHC class II protein and then a second selection where clones are induced at equal cell density to compare their specific productivity and choose the best producers for large scale supernatant production and protein purification. At least 10⁷ cells per vial were frozen in Sf900 II SFM-based freezing medium and kept in liquid nitrogen vapor phase for long term storage.

MHC class II ELISA

High-protein binding flat-bottom 96-well plates (Nunc Maxisorp) were coated with anti-DR L243 or anti-DP B7.21.7 antibodies (2 µg/ml) in 100 mM sodium carbonate buffer pH 8.3. Plates were blocked with incubation buffer and samples applied for 1 hour. For quantification, purified recombinant HLA-DR or DP protein were applied in a dilution series from 5000 ng/well in incubation buffer. After washes, bound recombinant MHC class II protein was detected with biotinylated anti-BSP antibody (0.2 µg/ml) and streptavidin-alkaline phosphatase (SA-AP) (Sigma). 100 µl of pNPP substrate was allowed to develop yellow color at room temperature, and color development stopped with equal volume of 1 M NaOH and read at 405 nm in a plate reader.

Scale-up of insect cell supernatants for protein purification

Roller bottles (Falcon) with closed caps were inoculated with 2×10^6 /cell in 500 ml of Sf900 II SFM without antibiotics. Cells were grown at room temperature (22-25 °C) turning at 6 rpm. Upon reaching densities from $0.5-1 \times 10^7$ cells/ml, cultures were induced with 1 mM CuSO_4 for 3 to 5 days. Supernatant was harvested by centrifugation at 2000 rpm for 5 min and filtered through a 0.22 μm filter and stored at 4 °C with 0.05% sodium azide and 2-iodoacetamide (4 mM).

Preparation of MHC class II-peptide complexes

Filtered supernatants from stably transfected insect cells containing soluble recombinant MHC class II molecules were purified on Chelating Sepharose FF columns if the molecules carried single or tandem His-tags. Alternatively, in the absence of His-tags, they were purified on CnBr Sepharose columns (20 ml) conjugated with anti-DR or anti-DP antibodies. Chelating Sepharose FF columns were washed with 10 mM imidazole in PBS and eluted with 200 mM imidazole in PBS. From anti-DR conjugated Sepharose columns, proteins were eluted with 50 mM glycine pH 11.5 and from anti-DP conjugated columns with 100 mM citrate pH 3.2. Chelating Sepharose FF columns were subsequently stripped of Cu^{2+} ions with 20 mM EDTA in PBS. Both types of columns were equilibrated in PBS with 0.05% sodium azide before the next purification cycle. The pH of eluates was corrected to neutral and concentrated in a nitrogen-pressurized Amicon concentration cell. Samples were further buffer-exchanged on a HiPrep 26/10 column into 100 mM sodium citrate, pH 6.0 and loaded with 100 μM peptide at 37 °C for 24 h in 1xprotease inhibitor mixture (Roche) and 0.2% octyl β -D-glucopyranoside. Excess unbound peptide was removed by buffer-exchange on a HiPrep 26/10 column. MHC class II-peptide complexes with untagged peptides were concentrated to < 2 ml and purified by gel filtration on a Superdex S200 column. MHC class II-peptide complexes containing peptide-bound His-tags were purified on a HisTrap HP 1 ml column and subsequently on a Superdex S200 column. Alternatively, MHC class II-peptide complexes with N-terminal polyanion tags were purified on MonoQ HR 5/5 columns over a 20 CV 0-1 M NaCl gradient. Complexes were eluted at 400-500 mM NaCl. Desthiobiotin-labeled complexes were purified on a 5 ml Strep-Tactin Superflow High-Capacity column (IBA). After elution with pH 7-buffered 50 mM desthiobiotin, excess desthiobiotin was eliminated with several concentration and dilution cycles in PBS. The streptactin column was regenerated with 1 mM 2-(4-hydroxyphenylazo)benzoic acid (HABA) in PBS and equilibrated with PBS to remove bound HABA and prepare the column for the next purification cycle.

Photocleavable peptides and generation of UV-exchangeable multimers

MHC class II complexes with peptides containing photocleavable amino-acid derivatives (βNPG) (1 μg in 100 μl PBS/well), were irradiated with a 30 W UV lamp (365 nm) on ice for 10 minutes (if not specified otherwise) in v-bottom 96-well plates. The amount of complexes harboring the tag is measured by an ELISA (see under *Peptide binding assays*). To make multimers from biotinylated photocleavable MHC class II complexes, UV irradiation was performed in 100 mM citrate pH 6.0 in the presence of 10 μM peptide (if not specified otherwise) and incubated overnight at 37 °C. Samples were brought to neutral pH with 10 μl Tris HCl pH 9.0. Subsequently, 3 μl (1 μg) of streptavidin-phycoerythrin (Invitrogen) were added and mixed and after 1h incubation, samples were used for staining cells.

Peptide binding assays

In a peptide competition assay, for each peptide, eight wells of a v-bottom 96-well plate (Greiner Bio-One) were filled with 50 μ l each of recombinant “empty” DR4 or DR52b protein (1 μ g) in a citrate saline buffer (100 mM citrate pH 6.0), with 0.2% β -octyl-glucopyranoside (Calbiochem), 1xcomplete protease inhibitors (Roche) and 2 μ M biotin-HA₃₀₆₋₃₁₈. Competitor peptides (10 mM DMSO solution) were added to each well to a final concentration of 100, 30, 10, 3, 1, 0.3 and 0.1 μ M. After incubation at 37 °C overnight, each reaction was diluted with a fourfold volume of 1xPBS pH 7.4, 0.1% BSA and 0.05% Tween 20 (PBT) and 100 μ l applied to a plate coated with anti-DR mAb L243 antibody (2 μ g/ml) and previously blocked with PBT. After 1 h of incubation at RT and three washes with 1xPBS pH 7.4, 0.05% Tween 20, streptavidin-alkaline phosphatase (SA-AP) conjugate (Sigma) was added as 1:10,000 in PBT. After 1 h, the plate was washed as previously described and developed with pNPP SigmaFAST substrate and absorbance read with the 405 nm filter.

To determine peptide occupancy, 500 μ g of purified “empty” DR4 was loaded with His-HA₃₀₆₋₃₁₈ or His-NY-ESO-1₁₁₉₋₁₄₃ peptides. For each time point, 0.5 ml was removed and subjected to gel filtration on a Superdex S200 column in PBS pH 7.4 to separate loaded DR4 from free peptide. The percentage of loaded DR4 was determined with two parallel sandwich ELISAs – anti-DR capture//His-Detector and anti-DR capture//anti-BSP biotin/SA-AP. Ni²⁺-NTA affinity chromatography was used to purify His-tagged DR4 complexes which were used as 100% standards in ELISA. Percentages of peptide occupancy were calculated as follows: peptide occupancy (%) = (amount of His-tagged DR4 complexes/amount of DR4 complexes)*100.

In a direct binding assay, 10 μ g purified DR4 protein or DR4 HA*5 complex and was dissolved in 500 μ l of 100 mM citrate buffer pH 6.0 with 10 μ M DTB-NY-ESO-1₁₁₉₋₁₄₃ peptide, 0.2% octyl-glucoside and complete protease inhibitor mix and were exposed to UV light (354 nm) for 10 min and incubated for 0, 6, 12 and 24 hours at 37 °C. At each time point, 100 μ l was withdrawn and frozen at -20 °C. After all samples were collected, they were diluted with an equal volume of the incubation buffer, captured on an anti-DR mAb L243 coated plates and detected with His-Detector (KPL).

Multimer binding assays

For binding studies, CD4⁺ T cell clones (5×10^4) or peptide-stimulated PBMCs (2×10^5) were incubated for 1 hour at 37 °C with graded concentrations of DR4/HA₃₀₆₋₃₁₈ multimers in 50 μ l FACS buffer. Peptide-stimulated PBMCs were counter-stained with FITC-labeled anti-CD4, APC-labeled anti-CD3 and 7-aminoactinomycin (7AAD). After washing, fluorescence associated with living cells (CD3⁺ 7AAD⁻ events) was analyzed on a FACSCalibur flow cytometer. In some experiments, washed cells were resuspended in FACS buffer supplemented with 100 mM imidazole and re-incubated for different periods of time.

Neuraminidase treatment

Prior to treatment, cells were washed in RPMI with 10% FCS and resuspended at 10^6 cells/ml. To a 50 μ l aliquot, neuraminidase from *Vibrio cholerae* was added to 0.2 U/ml and cells incubated for 30 min at 37 °C. After two washes in FACS buffer, cells were stained with multimers and analyzed by flow cytometry.

NTAmer dissociation kinetics

PBMCs from a DRB1*0401⁺ healthy donor were stimulated with HA₃₀₆₋₃₁₈ peptide for 10 days in complete medium. 10⁶ cells were pre-cooled on ice, and then stained for 2 hours at 4 °C with 4.5 µg/ml conventional or NTA-based multimers. Cells were analyzed on a FACSCalibur flow cytometer both prior to the addition of ice-cold 100 mM imidazole, and at 1, 2, 5 and 10 minutes after imidazole addition.

Fluorescence microscopy

Aliquots of 200 µl DR4/HA₃₀₆₋₃₁₈ clones (10⁶ cells/ml) were stained for 2 h at 4 °C, or for 1 h at 37 °C with 5 µg/ml PE-labeled DR4/HA₃₀₆₋₃₁₈ or DR4/Cy5-HA₃₀₆₋₃₁₈ multimers, washed, and incubated in growth medium for a further 4 h at 37 °C. For some experiments, they were subsequently surface-labeled with 0.02 µg/ml NHS-Cy5 for 5 min at 4 °C. Cells were fixed in 2% formaldehyde in PBS (v/v) for 10 min at room temperature and mounted on a microscope slide in 10 µl SlowFade medium (Invitrogen).

2.3 Materials and methods, Chapter II

Peptides

The *Plasmodium berghei* circumsporozoite 252-260 peptide (SYIPSAEKI) containing photoreactive 4-azidobenzoic acid on Lys-259 (PbCS(ABA)), its variant, PbCS(ABA) P255A and JAK1 non-receptor tyrosine kinase 355-363 (SYFPEITHI) (JAK1) peptides were synthesized using standard Fmoc chemistry, purified by reverse-phase C18 HPLC and verified by MALDI TOF mass spectrometry.

Antibodies

Rat anti-mouse CD8 α PE mAb 53.6.72, rat anti-mouse CD8 β PE mAb H35, anti-CD3 ϵ mAb 17A2, mouse anti-mouse V β 8.2 Alexa 647 mAb clone F23-2, rat anti-mouse anti-CD90.1 (Thy1.1) mAb HIS51 were from the antibody fluorescent conjugate collection of the Flow Cytometry Facility of LICR@UNIL. Rat anti-mouse CD8 α Cy5 mAb 53.6.72 and CD8 β Cy5 mAb KT112 were prepared from purified mAbs, conjugated with NHS-Cy5 at a dye/protein molar ratio 10:1 for 1 hour at RT and unreacted NHS-Cy5 removed with a PD-10 column (GE Healthcare Life Sciences/Amersham) previously equilibrated in 1xPBS. Final dye/protein ratios were 3.5 for anti-CD8 α Cy5 and 4.3 for anti-CD8 β Cy5 conjugate. For IP experiments, anti-CD8 α 53.6.72 and anti-CD8 β H35 were conjugated to CnBr Sepharose 4B beads according to manufacturer's instructions. To detect p56^{Lck} in Western blots, a primary rabbit polyclonal anti-Lck (sc-13, 2102) (Santa Cruz) was followed by HRP-conjugated goat anti-rabbit polyclonal antibody. To detect CD8 α and CD8 β in Western blots, a primary rat anti-mouse CD8 α 53.6.72 or rat anti-mouse CD8 β KT112 were followed by a secondary HRP-conjugated goat anti-rat polyclonal antibody (Southern Biotech). Supernatants containing rat anti-mouse CD16/32 mAb 2.4G2 were used to block Fc receptor binding (Fc γ RIII/II).

Multimers

PE-labeled K^d PbCS(ABA), K^d PbCS(ABA) 226/227, K^d PbCS(ABA) P255A multimers were kindly provided by Dr. Philippe Guillaume.

Plasmids

CD8 β -YFP was designed as full-length fusion of murine CD8 β (UniProt ID: P10300) with an enhanced variant of yellow fluorescent protein (eYFP) (Clontech) linked by GGGSGGGS. The construct for CD8 β -YFP was amplified from the PGK-driven pRRL vector with the primers for CD8B-EGFP-F and CD8B-EGFP-R and subcloned between BamHI and NotI sites of the pBMN-z vector. The pBMN-z CD3 ζ -CFP plasmid was a gift from the Dr. Nicolas Gascoigne lab (The Scripps Research Institute, San Diego, USA). Constructs for CD8 α (UniProt ID: P01731) and the CD8 α _{Tac} mutant were cloned in the CMV promoter-driven pSD-3 vector. Coding sequences for full length CD8 α were subcloned from the pLG449-2 plasmid by digestion with HindIII, followed by Klenow blunting of the site and digestion with XhoI. The pSD-3 vector was cut with BamHI, the site blunted with Klenow and then digested with Sall. The two DNA fragments were subsequently ligated. The Tac coding sequence was synthesized by creating a first synthetic DNA fragment from BgIII-tac-F and the tac-R primers, and then a with the tac-CD8a-F and SP6 primers. The two fragments were joined together, digested with BgIII and Sall and ligated into the BgIII and Sall digested

pLG449-2 plasmid. The fragment containing the CD8 α _{Tac} coding sequence was subcloned into the pBMN-z vector by PCR amplification with CD8 α -F and CD8 α -R primers from the pLG449-2 plasmid, digestion with HindIII and NotI and then ligated with the HindIII/NotI digested and purified pBMN-z vector.

Primers

CD8 α -F

5' AGGGAGACCCAAGCTTGCCA3'

CD8 α -R

5' TTTTGCGGCCGCTCACACAATTTTCTCTGAAGGTCTGGGC3'

SP6

5' ATTTAGGTGACACTATAG3'

BglII-tac-F

5' GGATTAGATCTCTGCGTAGCAGTGGCCGCCTGCGTGTTCC3'

tac-R

5' CCAGGTGAGGGCAGCCAGGAGGAGCACGGCGATGAGCAGGAACACGCAGGCCGGCCA3'

tac-CD8 α -F

5' TCCTGGCTGCCCTCACCTGGCACAGGAGCCGAAAGCGTGT3'

CD8B-EGFP-F

5' TTTAAGCTTTCTAGAGTCGACCTGCAGGG3'

CD8B-EGFP-R

5' AGTCGCGGCCGCTTTAGCCGGACTTGTACAGC3'

*Sequences***CD8 β -YFP**

5' GGATCCTCTAGAGTCGACCTGCAGGGGGGGGGGGGGGGGGTTTCAGTTGACAGAGCAC
 TGAGGGGAACAGTGTCCCCAAAAGCGCCAAG**ATG**CAGCCATGGCTCTGGCTGGTCTTCAGTA
 TGAAGCTGGCAGCTCTCTGGAGCAGCTCTGCCCTCATTTCAGACCCCTTCGTCCCTGCTGGTT
 CAAACCAACCATACGGCAAAGATGTCCTGTGAGGTTAAAAGCATCTCTAAGTTAACAAGCAT
 CTACTGGCTGCGGGAGCGCCAGGACCCCAAGGACAAGTACTTTGAGTTCTGGCCCTCCTGGA
 GTTCTTCCAAAGGAGTTTTGTATGGTGAAAGTGTGGACAAGAAAAGAAATATAATTCTTGAG
 TCTTCAGACTCAAGACGGCCCTTTCTCAGTATCATGAATGTGAAGCCAGAGGACAGTGACTT
 CTACTTCTGCGGACGGTTGGGAGCCCCAAGATGGTCTTTGGGACAGGGACGAAGCTGACTG
 TGGTTGATGTCTTCCCTACAACCTGCCCAACCAAGAAGACTACCCCTGAAGATGAAGAAGAAG
 AAGCAATGCCCGTTCCCCACCCAGAGACCCAGAAGGGCTGACATGCAGCCTTACCACCCT
 CAGCCTGCTGGTAGTCTGCATCCTGCTTCTGCTGGCATTCTCGGAGTGGCCGTCTACTTTT
 ACTGTGTGCGGAGGAGAGCCCGAATTCACTTCATGAAACAGTTTCACAAAGGAGGTGGATCA
 GGTGGAGGGAGCAAGGGCGAGGAGCTGTTACCCGGGGTGGTGCCCATCCTGGTTCGAGCTGGA
 CGGCGACGTAAACGGCCACAAGTTCAGCGTGTCCGGCGAGGGCGAGGGCGATGCCACCTACG
 GCAAGCTGACCCTGAAGTTCATCTGCACCACCGCAAGCTGCCCGTGCCCTGGCCACCCTC
 GTGACCACCTTCGGCTACGGCCTGCAGTGTTCGCCCGCTACCCCGACCACATGAAGCAGCA
 CGACTTCTTCAAGTCCGCCATGCCCGAAGGCTACGTCCAGGAGCGCACCATCTTCTTCAAGG
 ACGACGGCAACTACAAGACCCGCGCCGAGGTGAAGTTCGAGGGCGACACCCTGGTGAACCGC
 ATCGAGCTGAAGGGCATCGACTTCAAGGAGGACGGCAACATCCTGGGGCACAAGCTGGAGTA
 CAACTACAACAGCCACAACGTCTATATCATGGCCGACAAGCAGAAGAACGGCATCAAGGTGA
 ACTTCAAGATCCGCCACAACATCGAGGACGGCAGCGTGCAGCTCGCCGACCACTACCAGCAG
 AACACCCCATCGGCGACGGCCCCGTGCTGCTGCCCGACAACCACTACCTGAGCTACCAGTC
 CGCCCTGAGCAAAGACCCCAACGAGAAGCGCGATCACATGGTCTCTGCTGGAGTTCGTGACCG
 CCGCCGGGATCACTCTCGGCATGGACGAGCTGTACAAGTAAGCGGCCGC3'

MQPWLWLVFSMKLAALWSSSALIQTSSLLVQTNHTAKMSCEVKSISKLTSIYWLRRERQDPK
 DKYFEFLASWSSSKGVLYGESVDKRNIILESSDSRRPFLSIMNVKPEDSDFYFCATVGS PK
 MVFGTGTGLTVVDVLPPTAPTKKTTLMKMKKKQCFPHPETQKGLTCSLTTLSLLVVCILLL
 LAFLGVAVYFYCVRRRARIHFMKQFHKGGGSGGGGSKGEELFTGVVPIILVELDGDVNGHKFSV
 SGEGEDATYGLTTLKFICTTGKLPVPWPTLVTTFGYGLQCFARYPDHMKQHDFFKSAMPEG
 YVQERTIFFKDDGNYKTRAEVKFEKEDTLVNRIELKGI DFKEDGNILGHKLEYNYNSHNVYIM
 ADKQKNGIKVNFKIRHNIEDGSVQLADHYQQNTPIGDGPVLLPDNHLYSYQSALS KDPNEKR
 DHMVLLLEFVTAAGITLGMDELYK

CD8 α HA

5' AAGCTTGCCACC**ATG**GCCTCACCGTTGACCCGCTTTCTGTGCTGAACCTGCTGCTGCTG
 GGTGAGTCGATTATCCTGGGGAGTGGAGAAGCTAAGCCACAGGCACCCGAACCTCCGAATCTT
 TCCAAAGAAAATGGACGCCGAACCTGGTCAGAAGGTGGACCTGGTATGTGAAGTGTGGGGT
 CCGTTTTCGCAAGGATGCTCTTGGCTCTTCCAGAACTCCAGCTCCAAACTCCCCAGCCACC
 TTCGTTGTCTATATGGCTTCATCCCACAACAAGATAACGTGGGACGAGAAGCTGAATTCGTC

GAAACTGTTTTCTGCCATGAGGGACACGAATAATAAGTACGTTCTCACCTGAACAAGTTCA
 GCAAGGAAAACGAAGGCTACTATTTCTGCTCAGTCATCAGCAACTCGGTGATGTACTTCAGT
 TCTGTCTGTCAGTCCCTTCAGAAAGTGAAGTCTACTACTACCAAGCCAGTGCTGCGAACTCC
 CTCACCTGTGCACCCTACCGGGACATCTCAGCCCCAGAGACCAGAAGATTGTCTGGCCCCGTG
 GCTCAGTGAAGGGGACCGGATTAGATCTCTGCCTGTGATATTTACATCTGGGCACCCTTGCC
 GGAATCTGCGTGGCCCTTCTGCTGTCCTTGATCATCACTCTCATCTGCTACCACAGGAGCCG
 AAAGCGTGTTTGCAAATGTCCCAGGCCGCTAGTCAGACAGGAAGGCAAGCCCAGACCTTCAG
 AGAAAATTGTGGTCTGACTATCCATATGACGTGCCAAACTACGCATGAACTAGTGCGGCCGCT
 CGAG3'

MASPLTRFLSLNLLLLGESIIILGSGEAKPQAPELRIFPKKMDAELGQKVDLVCEVLGSVSQG
 CSWLFQNSSSKLPQPTFVVYMASSHNKITWDEKLNSSKLF SAMRDTN NKYVLT LNKF SKENE
 GYFCSVISNSVMYFSSVVPVLQKVNSTTTKPVLRTPSPVHPTGTSQPQRPEDCRPRGSVKG
 TGLDLACDIYIWAPLAGICVALLLSLIITLICYHRSRKRKRVCKCPRPLVRQEGKPRPSEKIVV
 DYPYDVPNYA

CD₈ tac HA

5' AAGCTTGCCACC**ATG**GCCTCACCGTTGACCCGCTTTCTGTCTGCTGAACCTGCTGCTGCTG
 GGTGAGTCGATTATCCTGGGGAGTGGAGAAGCTAAGCCACAGGCACCCGAACTCCGAATCTT
 TCCAAAGAAAATGGACGCCGAACTTGGTCAGAAGGTGGACCTGGTATGTGAAGTGTGGGGT
 CCGTTTCGCAAGGATGCTCTTGGCTCTTCCAGAACTCCAGCTCCAAACTCCCCAGCCCACC
 TTCGTTGTCTATATGGCTTCATCCCACAACAAGATAACGTGGGACGAGAAGCTGAATTCGTC
 GAAACTGTTTTCTGCCATGAGGGACACGAATAATAAGTACGTTCTCACCTGAACAAGTTCA
 GCAAGGAAAACGAAGGCTACTATTTCTGCTCAGTCATCAGCAACTCGGTGATGTACTTCAGT
 TCTGTCTGTCAGTCCCTTCAGAAAGTGAAGTCTACTACTACCAAGCCAGTGCTGCGAACTCC
 CTCACCTGTGCACCCTACCGGGACATCTCAGCCCCAGAGACCAGAAGATTGTCTGGCCCCGTG
 GCTCAGTGAAGGGGACCGGATTAGATCTCTGCGTAGCAGTGGCCGCCTGCGTGTTCCTGCTC
 ATCGCCGTGCTCCTCCTGGCTGCCCTCACCTGGCACAGGAGCCGAAAGCGTGTGGCAAATG
 TCCCAGGCCGCTAGTCAGACAGGAAGGCAAGCCCAGACCTTCAGAGAAAATTGTGGTCTGACT
 ATCCATATGACGTGCCAAACTACGCATGAACTAGTGCGGCCGCTCGAG3'

MASPLTRFLSLNLLLLGESIIILGSGEAKPQAPELRIFPKKMDAELGQKVDLVCEVLGSVSQG
 CSWLFQNSSSKLPQPTFVVYMASSHNKITWDEKLNSSKLF SAMRDTN NKYVLT LNKF SKENE
 GYFCSVISNSVMYFSSVVPVLQKVNSTTTKPVLRTPSPVHPTGTSQPQRPEDCRPRGSVKG
 TGLDLCVAVAACVFLLIIVLALLAALTWHRSRKRKRVCKCPRPLVRQEGKPRPSEKIVVDYPYDV
 PNYA

Cells

Phoenix Eco packaging cells, 293T cells and P815 mastocytoma cells were grown in DMEM with 10% FCS, 50 U/ml penicillin and 50 µg/ml streptomycin. T cell hybridomas were grown in DMEM supplemented with 5% FCS, 50 µM β-mercaptoethanol, 50 U/ml penicillin and 50 µg/ml streptomycin.

Lentivirus production

For production of lentiviral supernatants, HEK 293-derived cell lines were transfected with plasmid constructs by the calcium phosphate method. For constructs derived from the pRRL vector (CD8α, CD8α_{Tac}), 293T cells were used. Alternatively, for constructs derived from the pBMN-z vector (CD8β-eYFP, CD3ζ-eCFP), Phoenix Eco packaging cells were used. The day before transfection, 10 cm tissue culture dishes with 5x10⁶ cells were prepared in 8 ml of growth medium. At least 30 min prior to transfection, the old growth medium was exchanged for 4.5 ml fresh growth medium with chloroquine (25 µM). To generate viral supernatants from pRRL-based constructs, 5 µg pMD2.VSVG, 15 µg pCMVΔR8.91 plasmids and 20 µg proper pRRL construct, or alternatively, 30 µg pBMN-z-based constructs were mixed well with 250 µl sterile water and 250 µl CaCl₂ (0.5 M). To this solution, 500 µl 2xHeBS was added dropwise with vigorous agitation (pipette bubbling or vortexing). After 20 min incubation, the solution was added to the cell monolayer. After 24 hours, growth medium was exchanged and viral supernatant harvested 48 hours post-transfection. Supernatants were 0.22 µm-filtered and used immediately or frozen at -80 °C.

Infection, cloning and selection of hybridoma cells

To infect the T1 TCR T cell hybridoma, 2x10⁵ cells/well were resuspended in 2 ml growth medium in a 6-well plate. Polybrene (4 µg/ml) was added before the addition of 2 ml viral supernatant. After 5 days of incubation, single cells were FACS sorted for high expression of a particular surface protein or fluorescent protein (CD8α/CD8α Tac/CD8β-YFP/CD8ζ-CFP) on BD Aria cell sorter in flat-bottom 96-well plates at 0.5 cells/well. After 7-10 days, clones were analyzed for 1) surface expression of T1 TCR, CD8α, CD8β and YFP/CFP fluorescence by flow cytometry, 2) morphology and localization of YFP and CFP fluorescence by fluorescence microscopy, 3) IL-2 production when stimulated with PbCS(ABA)-pulsed P815 cells by IL-2 ELISA. Successive rounds of infection were used to introduce CD8α/CD8α Tac, CD8β-YFP and CD3ζ-CFP. Resulting cloned cells were named T1.wt, T1.tac, T1.wt.bYFP, T1.Tac.bYFP, T1.wt.bYFP.zCFP and T1.Tac.bYFP.zCFP.

Conjugate formation assay

One day before the assay, P815 cells were harvested, washed twice with 1xPBS, resuspended in PBS at 10⁶/ml and labeled with 10 µg/ml NHS-Cy5 (Amersham/GE Healthcare Life Sciences) for 5 min. For conjugate formation, 2x10⁵ of P815 for each time point were loaded with 1 µM peptide for 1 h in a humidified incubator at 37 °C in DMEM, 0.5% FCS, 2 µg/ml hβ2m. Unbound peptide was removed by washing and cells were mixed with a T cell hybridoma at a 1:1 ratio in 200 µl of DMEM, 5% FCS, 50 µM β-mercaptoethanol. The time course was started after spinning at 1000 rpm for 1 min at room temperature. At each time point, cells were fixed with PBS buffered 2% formaldehyde and later analyzed on the FACSCalibur. Calculation of the percentage of conjugates was performed with the following formula: conjugate (%) = (2xYFP⁺Cy5⁺)/[(YFP⁺Cy5⁻+YFP⁻Cy5⁺+2xYFP⁺Cy5⁺)].

Calcium flux

P815 cells (10^6 cells/ml) were pulsed with 1 μ M PbCS(ABA) for 1 h at 37 °C in DMEM supplemented with 0.5% FCS and 2 μ g/ml h β 2m. T1 TCR hybridomas (10^6 cells/ml) were incubated with 5 μ M Indo-1 acetate ester (Sigma) at 37 °C for 45 min, washed in DMEM and mixed with peptide-loaded P815 cells at an E/T ratio of 1:4. After incubation in a waterbath at 37 °C for 1 min, calcium-dependent Indo-1 cell-associated fluorescence was measured on a LSR II flow cytometer equipped with a 355 nm solid-state laser. During acquisition, the sample temperature was maintained at 37 °C with a solid-state heating jacket around the sample tube. Emissions at 405 nm (E_{405}) and 525 nm (E_{525}) after excitation at 355 nm were recorded over time. Calcium flux was calculated as the E_{405}/E_{525} ratio.

TCR downregulation

To measure TCR downregulation, P815 cells were pulsed with 1 μ M peptide for 1 h at 37 °C in DMEM, 0.5% FCS, 2 μ g/ml h β 2m. After the removal of unbound peptide with DMEM washes, 10^5 of peptide-loaded P815 cells were brought into contact with an equal number of T cell hybridoma cells and centrifuged gently at 1000 rpm for 1 minute at RT. After different times of incubation at 37 °C, cells were fixed in ice-cold PBS-buffered 2% formaldehyde. Samples were treated with anti-CD16/32 mAb 2.4G2 supernatants before staining for the TCR receptor with PE-labeled anti-Vb8.2. Data were collected on FACSCalibur flow cytometer.

FACS and FRET analysis

For FACS analyses, aliquots of 5×10^5 cells were incubated in 100 μ l of FACS buffer in v-bottom 96-well plates (Greiner Bio-One) with fluorescently labeled antibodies (20 μ g/ml) for 15 min at 4 °C; or with PE-labeled multimers of K^d PbCS(ABA), K^d PbCS(ABA) P255A, K^d PbCS(ABA) 226/227 for 30 min at room temperature in the presence or absence of anti-CD8 β mAb H35 (20 μ g/ml). After two washes, cell-associated fluorescence was assessed on a FACSCalibur. For FRET analyses, aliquots of 10^5 cells were incubated in 100 μ l FACS buffer in v-bottom 96-well plates with 20 μ g/ml Cy5-labeled anti-CD8 α 53.6.72, anti-CD8 β KT112; PE-labeled anti-CD3 ϵ mAb 17A2, anti-TCR β mAb H57, anti-CD90.1 mAb HIS51 or PE-labeled K^d/PbCS(ABA) multimers. After 45 min of incubation at 4 °C, cells were washed and fixed with formaldehyde (2% w/v in FACS buffer) for 10 min at room temperature, and cell-associated fluorescence was measured on a FACSCalibur at 580 nm upon excitation at 488 nm (FL2), at 670 nm upon excitation at 630 nm (FL4) and at 670 nm after excitation at 488 nm (FL3). The FRET intensity was calculated as “FRET units” as follows: FRET unit = $[(FL3_{\text{both}} - FL3_{\text{none}}) - ((FL3_{\text{Cy5}} - FL3_{\text{none}}) \times (FL4_{\text{both}}/FL4_{\text{Cy5}}))] - [(FL3_{\text{PE}} - FL3_{\text{none}}) \times (FL2_{\text{both}}/FL2_{\text{PE}})]$ as previously described (Doucey et al., 2003). Mean fluorescence intensities were measured on unlabeled cells (FL_{none}), or cells labeled only with Cy5 (FL_{Cy5}), PE (FL_{PE}), or Cy5 and PE (FL_{both}).

IL-2 assay

To measure IL-2 production, 10^4 T cell hybridoma cells were mixed with peptide-pulsed P815 cells per well in a 1:4 E/T ratio and incubated in T cell hybridoma growth medium overnight in a v-bottom 96-well plate. 100 μ l of supernatant was used in an IL-2 ELISA assay which was performed according to manufacturer’s instructions (Mabtech).

Isolation of detergent-insoluble membranes (DIMs), co-immunoprecipitation and immunoblotting

T1 TCR hybridomas (1.5×10^7 cells) were lysed on ice for 30 min in lysis buffer (TBS (20 mM Tris HCl, pH 8.0, 100 mM NaCl) containing 1% Brij96 and 1x complete protease inhibitors (Roche Molecular Biochemicals)). The lysates were spun at 10,000 *g* for 10 min, and supernatants were immunoprecipitated using Sepharose-bound monoclonal antibodies specific for CD8 α (53.6.72) or CD8 β (H35). Alternatively, T cell hybridomas (5×10^7) were lysed in 1 ml cell lysis buffer with Triton X-100 for 30 min on ice. The samples were centrifuged at 100,000 *x g* for 60 min at 4°C, and the supernatant was collected (membrane (M) fraction). The pellet was homogenized in 1 ml cell lysis buffer with Brij96 and incubated for 60 min on ice. After centrifugation for 20 min at 12,000 *x g* and 4 °C, the supernatant was collected (DIM fraction), as described in (Arcaro et al., 2000). Membrane and DIM fractions were immunoprecipitated with anti-CD8 α mAb 53.6.72 (20 μ g) coupled to Sepharose. The samples were analyzed by SDS-PAGE and Western blotting with anti-CD8 β Abs KT112 and goat anti-rat HRP secondary reagent.

The immune complexes were washed twice with lysis buffer. Subsequently, they were boiled 5 min at 95 °C in reducing Laemmli sample buffer and resolved on 4-15% gradient SDS-PAGE (Bio-Rad), transferred onto a nitrocellulose membrane, and Western blotted using anti-CD3 δ and anti-p56^{Lck} antibodies. For detection the enhance chemiluminescence (ECL) kit (GE Healthcare Life Sciences) was used according to manufacturer's instructions.

FRET microscopy

FRET microscopy was performed on the Axio Observer.Z1 (Zeiss) inverted fluorescence microscope with filters for Cy5, YFP, CFP and YFP/CFP FRET (Chroma). Samples were prepared in the same way as for conjugate formation but they were formaldehyde fixed after 20 min of incubation at 37 °C. Samples were mounted after formaldehyde removal with PBS in the glycerol-based Slowfade medium (Invitrogen) on standard microscope slides. Coverslips were sealed with nail polish and slides used within a week of mounting. Images were processed with the AxioVision 4.8 (Zeiss) and ImageJ software and final FRET values calculated with MS Excel according to (Mallaun et al., 2008). Microscope setup G value was measured with CFP-YFP cells exposed to different levels of donor (CFP) bleaching by exposure to excitation light according to (Zal and Gascoigne, 2004).

Mathematical methods

It is assumed that a streptavidin conjugate has four binding sites for biotin and that a biotinylated MHC-peptide complex is occupied with the desired peptide with a probability p or with any other peptide with a probability $q=1-p$.

The probability of the formation of a tetramer with all four cognate MHC-peptide complexes is :

$$1. \quad \binom{4}{4} p^4 q^0 = p^4$$

For the trimer, i.e. three right MHC-peptide and one irrelevant can be obtained in four different arrangements. Therefore, it is assigned the probability of :

$$2. \quad \binom{4}{3} p^3 q^1 = 4p^3 q$$

Because of the tetrahedral arrangement of MHC-peptides in a streptavidin conjugate, it can be considered that a tetramer and a trimer of the correct MHC-peptides are the proper staining reagents. This gives its probability as a sum of 1 and 2 or :

$$3. \quad p^4 + 4p^3 q = 4p^3 - 3p^4$$

The distribution of streptavidin MHC-peptide oligomers obeys a binomial distribution where the probability of forming a dimer, monomer and a conjugate with no desired peptide-MHC (i.e. all four sites are occupied by irrelevant peptide-MHCs) is given by :

$$\text{dimer } \binom{4}{2} p^2 q^2, \text{ monomer } \binom{4}{1} p^1 q^3, \text{ and with all irrelevant MHC-peptides } \binom{4}{0} p^0 q^4$$

Sum over all probabilities of different oligomers is 1.

CHAPTER I

3. Detection of antigen-specific CD4⁺ T cells by novel types of MHC class II-peptide complexes

3.1 Results

3.1.1 State of the art of MHC-peptide multimer staining of specific CD4⁺ T cells

Despite similarities in structural features, recombinant MHC class II-peptide complexes are characterized by more complex biochemistry and conformational dynamics than their MHC class I-peptide counterparts (Belmares et al., 2003; Georges et al., 2000; Lovitch and Unanue, 2005; Rötzschke et al., 1999; Schmitt et al., 1999). Therefore, it is necessary to validate MHC class II-peptide multimers on T cell lines or clones that are: i) specific for the peptide studied, and ii) stringently HLA typed.

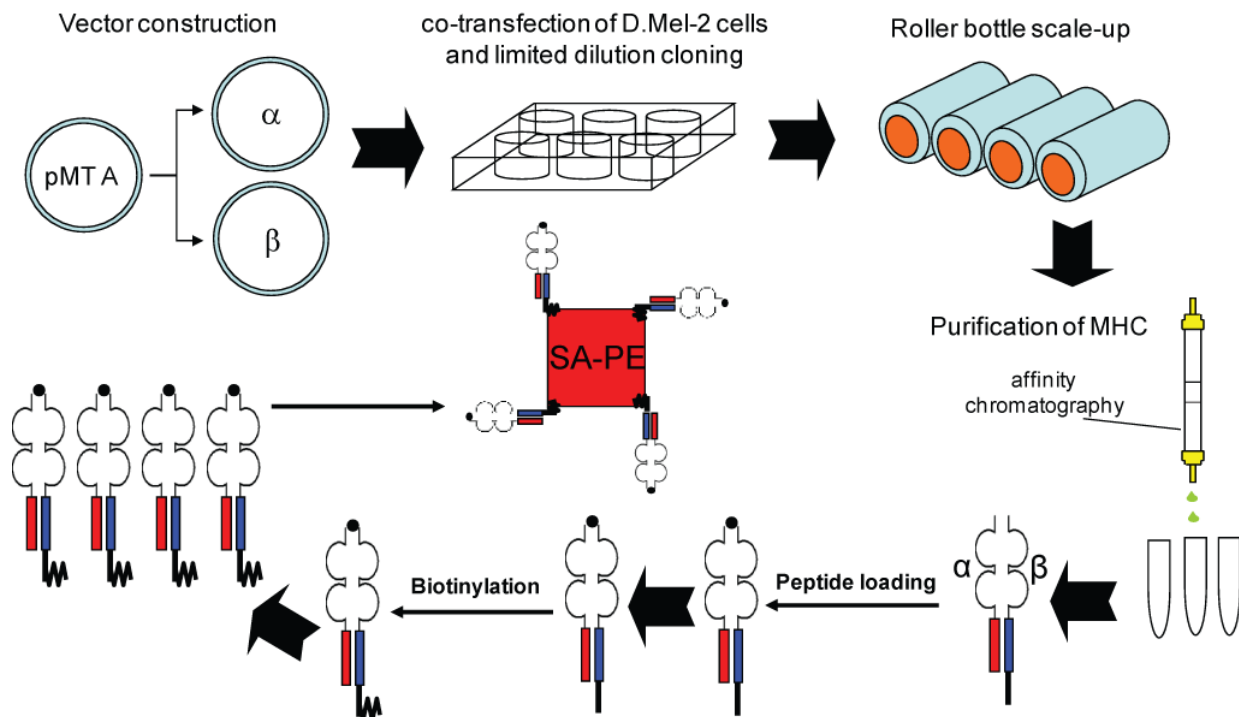


Figure 3.1 *Production of conventional MHC class II-peptide multimers.* Separate constructs for the MHC α and β chain in expression plasmids containing a metallothionein promoter are co-transfected with a plasmid conferring antibiotic resistance (e.g. puromycin) into S2 cells. After antibiotic selection, lines or clones were derived by limiting dilution, expanded and cultured in roller bottles at room temperature. After induction with 1 mM CuSO₄ for 3-5 days, recombinant MHC class II proteins are purified from supernatants by immunoaffinity chromatography on an anti-MHC class II antibody column, loaded with a peptide of interest and enzymatically biotinylated with BirA. After gel filtration chromatography, MHC-peptide complexes are multimerized with a fluorescent streptavidin conjugate at a 4:1 ratio.

There are two main strategies to produce soluble recombinant MHC class II-peptide complexes: i) “Empty” (without a nominal peptide cargo) MHC molecules are loaded *in vitro* with a peptide of interest, and ii) The peptide of interest is tethered onto the MHC class II β chain via a long and flexible linker (Fremont et al., 1996a). This latter strategy is commonly used for the production of recombinant murine MHC class II-peptide complexes, mainly because “empty” mouse MHC class II molecules are not stable. The two strategies can be combined, by expressing MHC class II molecules with tethered on CLIP peptide and subsequent peptide exchange after proteolytic cleavage of the CLIP peptide (Day et al., 2003)

With respect to MHC class II-peptide complexes obtained by peptide loading of “empty” MHC class II molecules, we and others have observed that efficient peptide binding is limited to native molecules (Carven et al., 2004; Natarajan et al., 1999a; Rabinowitz et al., 1998). By adding a low molecular weight tag N-terminally to the peptide, correct MHC class II-peptide complexes can be isolated by means of this peptide tag (Day et al., 2003; Demotz et al., 1991; Nag et al., 1994). This is a reliable method to ensure the biochemical integrity of MHC class II-peptide multimers. In the following sections of this chapter, several such strategies will be presented. Multimer staining of antigen-specific CD4⁺ T cells differs in several aspects from multimer staining of CD8⁺ T cells, such as: i) MHC class II-peptide multimer staining is preferably performed at elevated temperatures, usually 37°C. Although some CD4⁺ T cells can also be efficiently stained in the cold, others are stained poorly or not at all (Fig. 3.2) (Reichstetter et al., 2000); ii) Longer incubation periods (1 hour or longer) are needed for

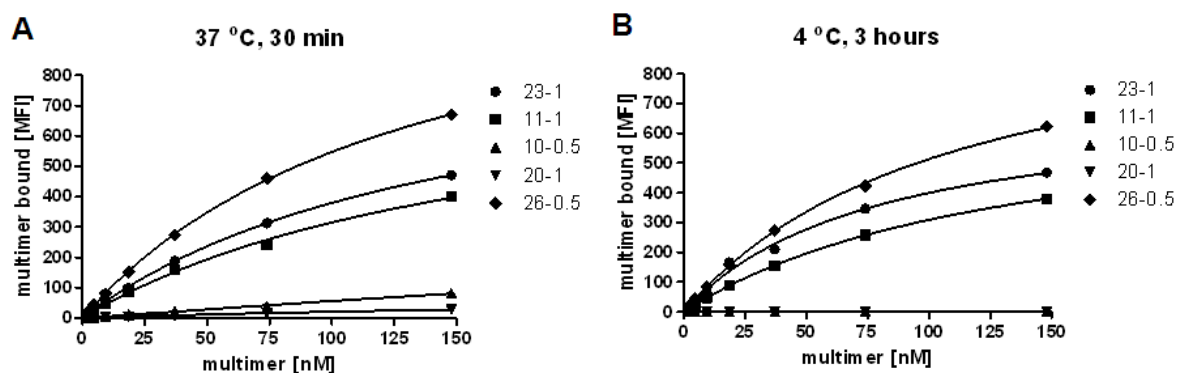


Figure 3.2 *Staining parameters of MHC class II-peptide multimers.* DR4/HA₃₀₆₋₃₁₈ clones were stained with the conventional SA-PE DR4/HA₃₀₆₋₃₁₈ multimer for 30 min at 37 °C (A) or 3 hours at 4 °C (B), washed, and cell-associated fluorescence measured by flow cytometry. Data were fitted by nonlinear regression from two experiments.

efficient staining, which is explained, at least in part, by accumulation of MHC class II-peptide multimers due to endocytosis (Fig. 3.3) (Cameron et al., 2001) and iii) The avidity of MHC class II-peptide multimer binding is typically lower than the binding of MHC class I-peptide multimers. Unlike CD8, the CD4 coreceptor does not significantly increase MHC-peptide binding to the TCR (Xiong et al., 2001). Moreover, data comparing the binding avidity of MHC class I and class II-peptide complexes to their cognate TCR showed on average weaker binding for the latter (Cole et al., 2007). MHC class II-peptide multimers therefore have to be titrated up to high concentrations (e.g. 100 nM/approx. 50 µg/ml). Even then, some antigen-specific CD4+ T cells, namely those specific for self-antigens, remain un- or barely detectable by MHC class II-peptide multimer staining.

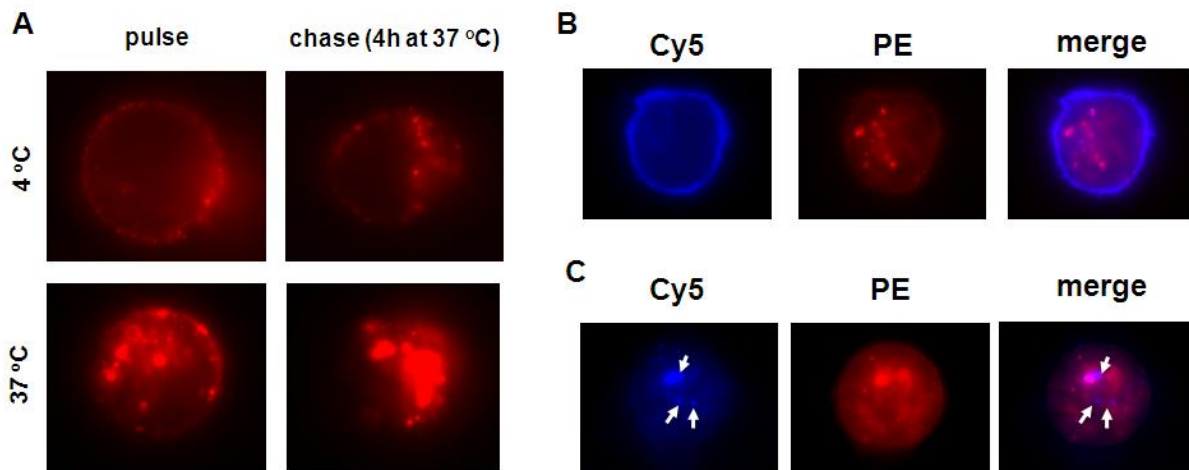


Figure 3.3 *MHC class II-peptide multimers are internalized at physiological temperatures.* A, DR4/HA₃₀₆₋₃₁₈ clone was stained with 5 µg/ml SA-PE DR4/HA₃₀₆₋₃₁₈ multimer for 1 hour at 4 °C (top) or 37 °C (bottom) - (pulse), washed and incubated at 37 °C for 4 hours (chase). B, DR4/HA₃₀₆₋₃₁₈ clone was stained with 5 µg/ml SA-PE DR4/HA₃₀₆₋₃₁₈ multimer for 1 hour at 37 °C (red), washed and then surface labeled with NHS-Cy5 (blue). C, DR4/HA₃₀₆₋₃₁₈ clone was stained with 5 µg/ml SA-PE DR4/Cy5-HA₃₀₆₋₃₁₈ multimer for 4 hours at 37 °C. Cells were fixed with formaldehyde and imaged by fluorescence microscopy. Red indicates signals from PE and blue from Cy5. White arrows indicate accumulation of Cy5 fluorescence without PE fluorescence.

(Gebe et al., 2003; Kwok, 2003; Sabatino et al., 2011). This is explained, at least in part, by a combination of very low TCR avidity and rapid TCR down-modulation. Dasatinib, a Src kinase inhibitor, has been reported to inhibit TCR down-modulation and thus to increase multimer staining (Lissina et al., 2009). Moreover, we and others have observed that enzymatic desialylation with neuraminidase from *Vibrio cholerae* or *Clostridium perfringens* can increase MHC class II-peptide multimer staining several-fold (Fig. 3.4) (Massilamany et al., 2011; Reddy et al., 2003).

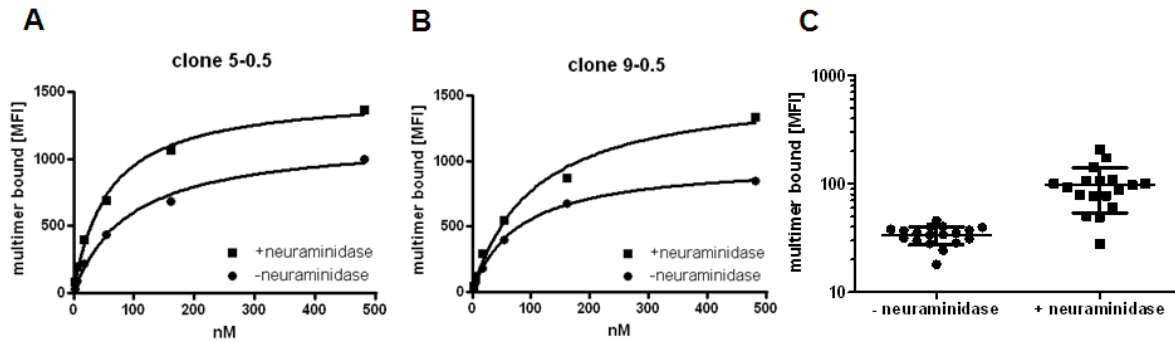


Figure 3.4 *Neuraminidase pre-treatment enhances multimer binding.* A, B, DR4/HA₃₀₆₋₃₁₈ clones 5-0.5 and 9-0.5 were pretreated (squares) or not (circles) with 0.2 U/ml neuraminidase for 30 min at 37 °C, washed and stained with SA-PE DR4/HA₃₀₆₋₃₁₈ multimer for 1 h at 37 °C. Experiments were performed at least twice. C, 18 DR4/HA₃₀₆₋₃₁₈ clones were pretreated (squares) or not (circles) with 0.2 U/ml neuraminidase for 30 min at 37 °C, washed and stained with 3.7 nM (2 µg/ml) SA-PE DR4/HA₃₀₆₋₃₁₈ multimer for 1 h at 37 °C and analyzed by flow cytometry. Non-specific binding was determined on a DR4/Flu-MP₆₁₋₇₂-specific clone and subtracted. Error bars represent SD.

3.1.2 Loading of “empty” MHC class II molecules with specific peptides and impact of peptide loading efficiency on multimer staining

Commonly used protocols to prepare human MHC class II-peptide multimers (Kwok et al., 2002) involve loading of “empty” recombinant MHC class II molecules with high peptide concentrations (up to 100 µM) under acidic conditions (pH 5.2-6.0) for up to 72 hours at elevated temperatures (37 °C), followed by size exclusion chromatography to recover monomeric MHC class II-peptide complexes. To investigate whether peptide binding affinity correlates with the degree of loading, we compared relative affinities of DR4-binding peptides by means of a binding competition assay (Fig. 3.5A) and their loading efficiency after 6, 24 and 48 hours (Fig. 3.5B). The HA₃₀₆₋₃₁₈ and NY-ESO-1₁₁₉₋₁₄₃ peptides both exhibited high affinities for DR4 (DRA*0101, DRB1*0401), with IC₅₀ values for half-maximal binding of 4.43±1.22 µM for HA₃₀₆₋₃₁₈ and 14.84±13.96 µM for NY-ESO-1₁₁₉₋₁₄₃, respectively, which is in concordance with published data (Zarour et al., 2002). In contrast, when peptide occupancy was determined after 24 h of incubation with peptides on DR4 complexes, >80% of monomeric DR4 had bound the HA₃₀₆₋₃₁₈ peptide, but only 25% of monomeric DR4 had bound the NY-ESO-1₁₁₉₋₁₄₃ peptide.

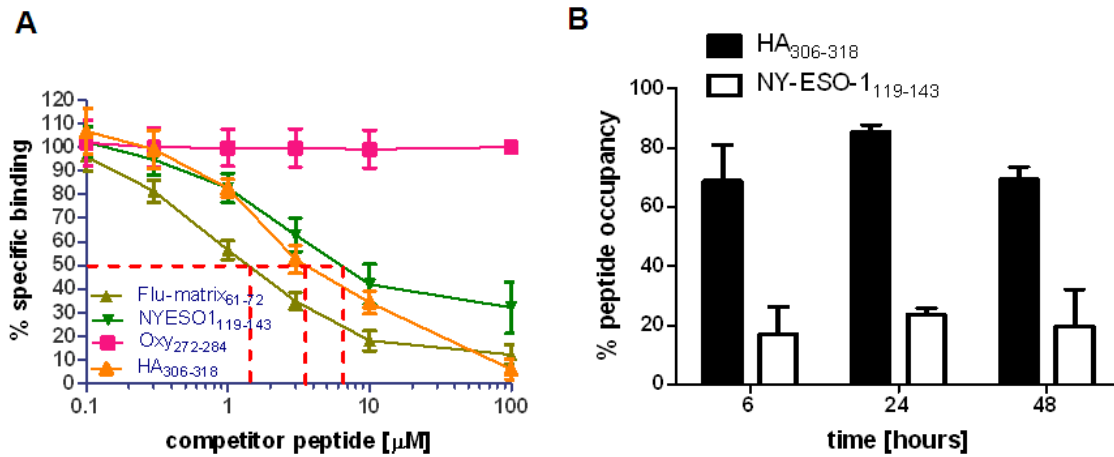


Figure 3.5 Extent of peptide loading and binding affinity are two separate parameters. **A**, Peptide binding of HA₃₀₆₋₃₁₈ (orange triangles) and NY-ESO-1₁₁₉₋₁₄₃ (inverted dark green triangles) peptides to recombinant soluble DR4 (10 μg/ml) was measured by competition with 2 μM biotin-HA₃₀₆₋₃₁₈ peptide. Flu-MP₆₁₋₇₂ (olive green triangles) served as the positive control, and Oxy₂₇₂₋₂₈₄ (magenta squares) as the negative control. Data were normalized to signals from the uncompeteted samples, which were taken as 100%. Red dashed lines indicate 50% binding. Mean values and SD were calculated from three experiments. **B**, Peptide occupancy of DR4 with His-HA₃₀₆₋₃₁₈ (black bars) or His-NY-ESO-1₁₁₉₋₁₄₃ (white bars) for 6, 24 and 48 hours at 37 °C at pH 6. Peptide occupancy was calculated as follows: (amount of His-peptide bound to the DR4 molecule)/(amount of total DR4). Samples were gel-filtered to remove unbound peptide and quantitated by ELISA using affinity-purified complexes as 100%. Mean values and SD were calculated from at least two experiments.

Similar results were obtained with recombinant DR52b molecules (DRA*0101, DRB3*0202); in which case the affinities of the NY-ESO-1₁₁₉₋₁₄₃ peptide were higher (0.62 ± 0.06 μM for NY-ESO-1₁₁₉₋₁₄₃ and 2.54 ± 0.13 μM for HA₃₀₆₋₃₁₈) (Fig. 3.8B). After loading of “empty” DR52b with Cy5-labeled NY-ESO-1₁₁₉₋₁₄₃ under the same conditions and purification by gel filtration, the dye/protein (D/P) ratio of the MHC-peptide monomer was $\leq 20\%$ (data not shown).

To investigate the correlation between peptide loading onto MHC class II molecules and multimer binding, we compared binding of mixed multimers to antigen-specific CD4⁺ T-cell clones. To form mixed multimers, cognate and non-specific MHC-peptide complexes were mixed and multimerized on a PE-labeled streptavidin conjugate. For the sake of simplicity, we assumed that all four binding sites on a streptavidin molecule were equally occupied. Fractions of cognate tetramers, trimers, dimers and monomers were calculated as a function of the proportion of cognate peptide-MHC complexes in tetramers are shown in Fig. 3.6A. If all MHC-peptide complexes are cognate, the resulting tetramer is *bona fide*. However, if half of the MHC-peptide monomers are cognate, the “tetramer” preparation consists mostly of dimers (37.5 %), equal proportions of trimers and monomers (25%) and only 6.25% *bona*

fide tetramers. If only 20% of MHC-peptide complexes are specific, the reagent consists mostly of monomers (41%), of dimers (~15%) and traces of true trimers (~3%) and tetramers (~0.2%).

In tetramer binding to T cells, cell-associated fluorescence derives from molecular species of different valence. We defined the effective reagent fraction as the sum of fractions of different MHC-peptide species contributing to staining (Fig. 3.6A). Thus, four theoretical curves can be generated, depending on the binding avidity of the TCR. As shown in Fig. 3.6B, when the avidity is low, only *bona fide* tetramers can stably bind ($x=4$). As the avidity gradually increases tetramers and trimers ($x=4+3$), then tetramers, trimers and dimers ($x=4+3+2$) and finally tetramers, trimers, dimers and even monomers ($x=4+3+2+1$) can bind stably. To determine whether there is a threshold, below which tetramer binding is negligible, i.e. where the effective reagent fraction is close to zero, mixed tetramers containing graded fractions of DR4/His-HA₃₀₆₋₃₁₈ and DR4/CLIP monomers were prepared. Their binding profiles were assessed on seven DR4/HA₃₀₆₋₃₁₈-specific CD4⁺ T cell clones (Fig. 3.6C). According to similarities of the binding profiles of clones with the theoretical binding curves (Fig. 3.6B), the observed binding data were grouped in three categories - very high avidity (Fig. 3.6D), high avidity (Fig. 3.6E) and low avidity (Fig. 3.6F). These categories exhibit differently shaped binding curves; the very high avidity curves are concave, the high avidity nearly linear and the low avidity convex. On very high avidity clones tetramer binding stays relatively constant to about 50% of specific complexes and then rapidly decreases at higher fractions of non-specific complexes. For high-avidity clones this decrease starts already at ~80% of specific complexes. For low-avidity clones, however, the monomer purity is paramount, as their staining strictly depends on the reagent's content of *bona fide* tetramers, as seen by the nearly exponential decrease with the fraction of cognate complexes.

This analysis highlights the importance of using affinity purified complexes for detection of low avidity CD4⁺ T-cells that are frequently those specific for self-antigens, including cancer antigens. Another important conclusion of our analysis is that binding diminishes dramatically when the fraction of specific complexes decreases to 20% or less (Figs. 3.6D-F, vertical light blue dashed line). As elaborated below, this explains why in the case of the NY-ESO-1₁₁₉₋₁₄₃ peptide, tetramers prepared by using conventional procedures exhibited no significant staining of clones or populations.

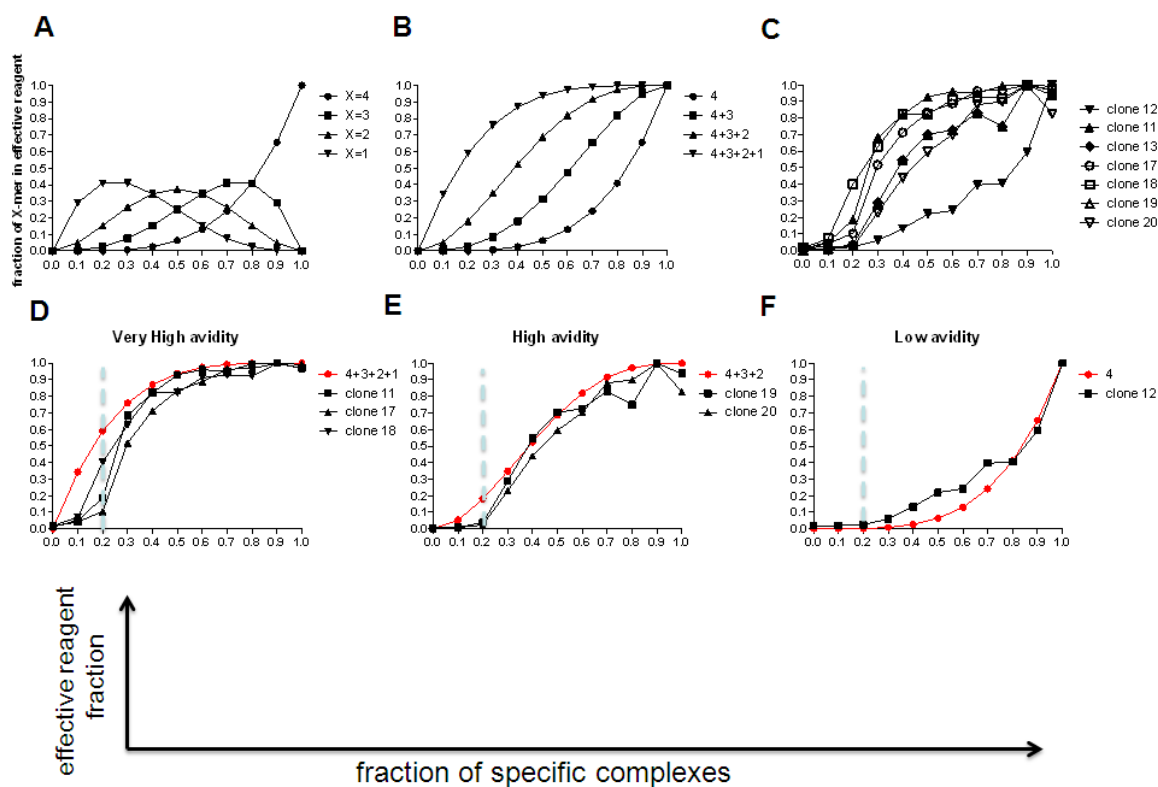


Figure 3.6 *Dependence of tetramer staining on their cognate MHC-peptide content* A, Cognate and irrelevant MHC-peptide monomers were mixed in different ratios (x-axis; fraction of specific monomers) and reacted with streptavidin to make tetramers. The binominal distributions of X-mers, i.e. complexes containing X=1,2,3 or 4 cognate monomers, were calculated and plotted on the y-axis as fraction of 1. B, Theoretical effective reagent fraction, defined as the sum of the fractions of X-mers that bind stably to antigen-specific cells. Four curves were calculated reflecting different TCR avidities. C, Different PE-labeled tetramers were prepared by reacting PE-streptavidin with mixtures of cognate biotinylated DR4/His-HA₃₀₆₋₃₁₈ complexes and irrelevant biotinylated DR4/CLIP complexes. The fraction of cognate monomers is shown on the x-axis. The indicated DR4/HA₃₀₆₋₃₁₈-specific CD4⁺ T cells clones were stained with the different tetramers (18.5 nM; i.e 10 µg/ml) for 1 hour at 37 °C, washed and analyzed by flow cytometry. The observed mean fluorescence intensities were normalized to the staining observed for *bona fide* DR4/His-HA₃₀₆₋₃₁₈ tetramers, which was defined as 100% and represented at effective reagent fraction on the y-axis. Averages of two experiments are shown. D-F, DR4/HA₃₀₆₋₃₁₈-specific clones from C) are grouped in three categories (very high avidity (D), high avidity (E), low avidity (F) based on their ability to bind X-mers. The vertical dashed line in light blue represents a critical staining threshold. One out of two-three experiments is shown.

3.1.3 Purification of *bona fide* MHC class II-peptide complexes and impact on staining of antigen-specific CD4⁺ T cells

3.1.3.1 Purification via a His-tag at the peptide N-terminus

Purification of MHC class II-peptide monomers can be accomplished by means of a hexahistidine tag (His-tag) added to the peptide of interest via a SGSG linker. After peptide loading and biotinylation, MHC-peptide complexes were bound to a Ni²⁺-NTA chelating column and then eluted in a single sharp peak (Fig. 3.7A). Imidazole and eventual aggregates

were removed by subsequent gel filtration chromatography on a Superdex S200 column (Fig. 3.7B). Purity and biotinylation state of the MHC-peptide monomers were verified by non-denaturing SDS-PAGE (Fig. 3.7C) in the presence and absence of avidin.

As peptide binding sites of MHC class II molecules are open-ended, permitting accommodation of peptide ligands of various lengths (Lippolis et al., 2002), we reasoned that the His-tag is located outside of the peptide binding groove and hence may not affect peptide binding to the MHC molecule. To verify this, N-terminally His-tagged NY-ESO-1₁₁₉₋₁₄₃ peptide was compared with the wild-type peptide in a binding competition assay. This assay was performed on soluble DR4 (Fig. 3.8A) and DR52b (Fig. 3.8B). Only modest differences were observed between the IC₅₀ values of the His-tagged peptide and the unmodified peptide, with a tendency for the His-tagged peptide to exhibit slightly higher IC₅₀ values.

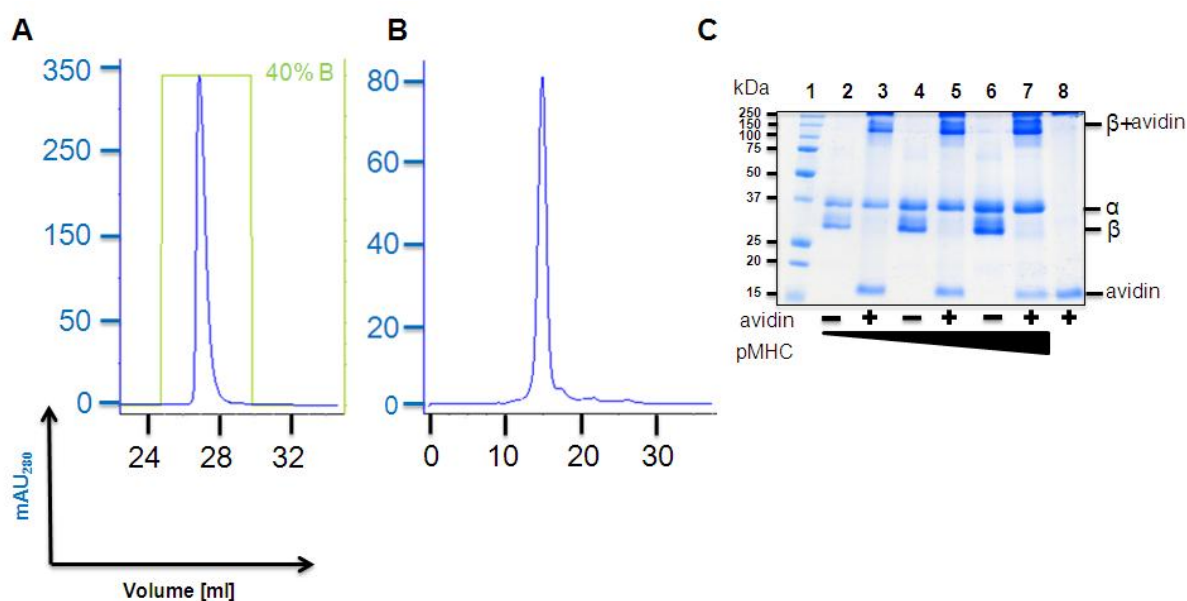


Figure 3.7 *Purification and SDS-PAGE analysis of His-tagged MHC class II-peptide complexes.* A, Representative Ni²⁺-NTA column chromatogram of a MHC class II-peptide complex with a N-terminal peptide His-tag (here DR4/His-NY-ESO-1₁₁₉₋₁₄₃). His-tagged complexes elute in a sharp peak with 200 mM imidazole. B, Representative gel filtration chromatogram of DR4/His-NY-ESO-1₁₁₉₋₁₄₃ monomer eluted from the Ni²⁺-NTA column. C, Non-reducing SDS-PAGE (12%) of the DR4/His-NY-ESO-1₁₁₉₋₁₄₃ monomers after gel filtration. Molecular weight marker (lane 1) with the appropriate molecular weights in kDa shown on the left. Lanes 2, 4 and 6 were loaded with 2, 5 and 10 µg of monomers and lanes 3, 5 and 7 likewise but with the addition of 10 µg avidin. Lane 8 contains avidin only.

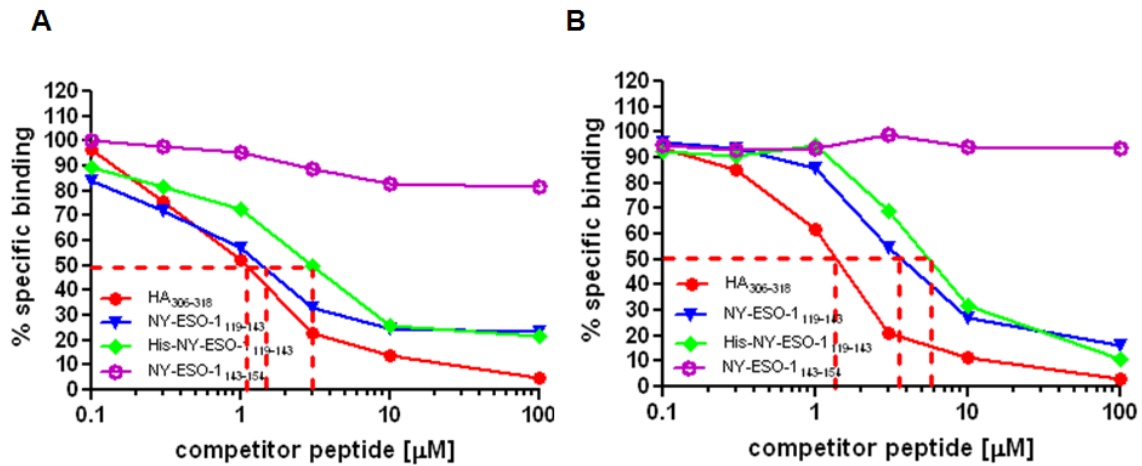


Figure 3.8 *N-terminal His-tag barely alters peptide binding to DR4 and DR52b.* Peptide binding of NY-ESO-1₁₁₉₋₁₄₃ (triangles) and His-NY-ESO-1₁₁₉₋₁₄₃ (diamonds) peptides to recombinant DR4 (A) and recombinant DR52b (B) was determined by competition against biotin-HA₃₀₆₋₃₁₈. HA₃₀₆₋₃₁₈ is the positive control (red circles) and NY-ESO-1₁₄₃₋₁₅₄ is the negative control (pink circles). The red dashed line marks IC₅₀ values as the competitor peptide concentration needed to reduce the amount of biotin-HA₃₀₆₋₃₁₈-containing complexes to 50%. The IC₅₀ values were 1.6 μ M and 3.0 μ M for the wild-type and His-tagged NY-ESO-1₁₁₉₋₁₄₃ peptides on DR4 and 3.6 μ M and 5.9 μ M for the wild-type and His-tagged NY-ESO-1₁₁₉₋₁₄₃ peptides on DR52b, respectively. Experiments were performed at least twice. Representative experiments are shown.

To illustrate the impact of MHC-peptide monomer purity on the staining of fluorescent MHC-peptide tetramers, the binding of affinity purified DR4/His-NY-ESO-1₁₁₉₋₁₄₃ complexes was compared with the binding of conventional DR4/NY-ESO-1₁₁₉₋₁₄₃ complexes on NY-ESO-1-specific CD4⁺ T cell line (Fig. 3.9A). Conventional DR4/NY-ESO-1₁₁₉₋₁₄₃ multimers failed to detect specific cells at any concentration tested. By contrast, DR4/His-NY-ESO-1₁₁₉₋₁₄₃ multimers detected up to 8.2% specific CD4⁺ T cells. We then analyzed a NY-ESO-1₁₁₉₋₁₄₃-specific, DR52b-restricted CD4⁺ T cell clone and observed IFN γ production upon stimulation with the NY-ESO-1₁₁₉₋₁₄₃ peptide (Fig. 3.9B). This clone was not significantly stained with conventional DR52b/NY-ESO-1₁₁₉₋₁₄₃ multimers, but was stained avidly with multimers containing “immunopure” (molecularly defined) DR52b/His-NY-ESO-1₁₁₉₋₁₄₃ monomers (Fig. 3.9C).

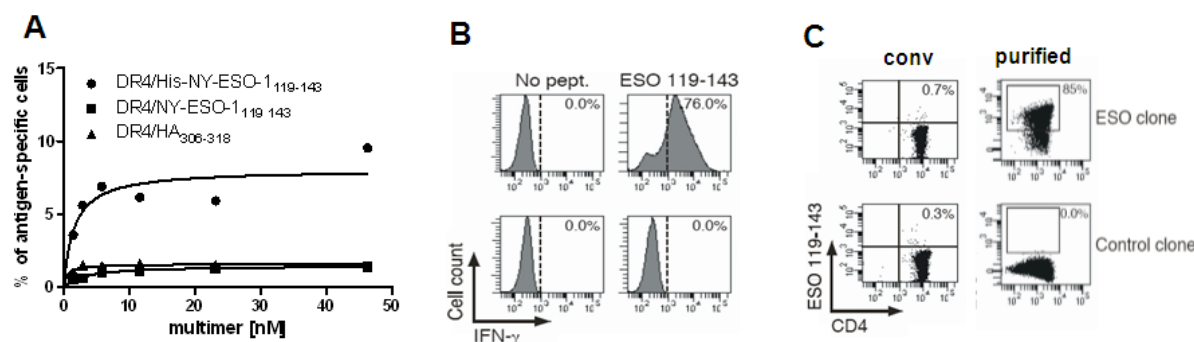


Figure 3.9 Improved staining with “immunopure” DR4 and DR52b/His-NY-ESO-1₁₁₉₋₁₄₃ multimers. **A**, Binding isotherm on a DR4/NY-ESO-1₁₁₉₋₁₄₃-specific CD4⁺ T cell line stained with SA-PE multimers containing biotinylated affinity-purified DR4/His-NY-ESO-1₁₁₉₋₁₄₃ monomers (circles), conventionally loaded DR4/NY-ESO-1₁₁₉₋₁₄₃ monomers (squares) or DR4/CLIP monomers (triangles). Cells were stained with the indicated concentrations of multimers for 1 hour at 37 °C and analyzed by flow cytometry. **B**, Intracellular production of IFN γ in a DR52b/NY-ESO-1₁₁₉₋₁₄₃-specific clone stimulated with 2 μ M NY-ESO-1₁₁₉₋₁₄₃ peptide (ESO clone, top); nonspecific background was evaluated on a DR52b-restricted clone specific for the SSX2 antigen (Control clone, bottom). **C**, Staining of the clones as in **B** with 5.6 nM (3 μ g/ml) conventional (left) and “immunopure” DR52b/NY-ESO-1₁₁₉₋₁₄₃ multimers (right).

Moreover, “immunopure” DR52b/His-NY-ESO-1₁₁₉₋₁₄₃ tetramers detected specific CD4⁺ T-cells from vaccinated melanoma patients directly *ex vivo* (Fig. 3.10), i.e. without anti-PE based enrichment techniques or peptide stimulation of the T cells *in vitro*. This is of great significance, because for the first time this allowed conclusive analysis of tumor antigen-specific CD4⁺ T cells without biasing the results and conclusions.

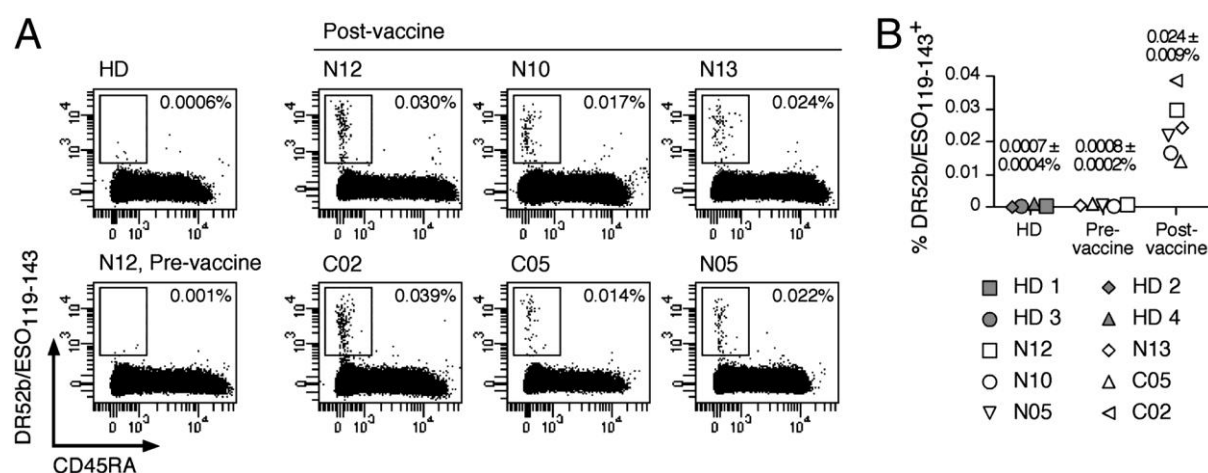


Figure 3.10 *Ex vivo* detection of DR52b/NY-ESO-1₁₁₉₋₁₄₃-specific CD4⁺ T cells from vaccinated cancer patients. **A**, CD4⁺ T cells purified from PBMC from DR52b⁺ healthy donors and from pre- and postvaccine samples from DR52b⁺ patients stained *ex vivo* with DR52b/His-NY-ESO-1₁₁₉₋₁₄₃ tetramers (5.6 nM or 3 μ g/ml) for 2 h at 37 °C and then stained with anti-CD45RA mAb HI100 and analyzed by flow cytometry. Dot plots for one HD, one pre-vaccine sample, and all postvaccine samples are shown in **A** and data for all samples tested are summarized in **B**. Numbers in dot plots correspond to the percentage of tetramer-positive cells among memory CD45RA⁻ CD4⁺ T cells (from (Ayyoub et al., 2010a)).

3.1.3.2 Reversible N-terminal peptide tags

Our and others results support the notion that the binding of peptides to MHC class II molecules readily tolerates N- and C-terminal extensions from the binding nonamer core (Chicz et al., 1992; Hunt et al., 1992; Rudensky et al., 1991). However, several reports have implicated N- and C-terminal residues adjacent to the nonamer core, termed “peptide-flanking residues”, in modulating TCR binding (Arnold et al., 2002; Carson et al., 1997; Sant’Angelo et al., 2002), and influencing TCR repertoire selection (Cole et al., 2012). In view of the large diversity of TCR:MHC-peptide binding configurations, it is difficult to predict what effect modifications of peptide-flanking sequences might have on TCR recognition. We therefore established a strategy that allows easy removal of the peptide tag after its use for monomer purification, in order to avoid its potential interference with TCR recognition. To this end, we synthesized two variants of the HA₃₀₆₋₃₁₈ peptide bearing a His-tag either at the N- or the C-terminal end via a GSGS linker and a photocleavable residue, β -nitrophenylglycine (β NPG) (Fig. 3.11A,B). The β NPG undergoes a photolytic reaction resulting in cleavage at its C-N bond. After cleavage, the indicated chemical entities (Fig. 3.11B) remain on the N- and C-terminal portions. We prepared affinity-purified N- and C-terminally tagged DR4 complexes and subjected them to irradiation with UV light at 365 nm for up to 60 minutes and observed the His-tag bound to the MHC molecules by ELISA. The half-lives of these complexes under these conditions were 0.51 min for the N-terminal and 0.57 min for the C-terminal complex. In 10 minutes the photocleavage reaction was essentially complete (Figs. 3.11C-D).

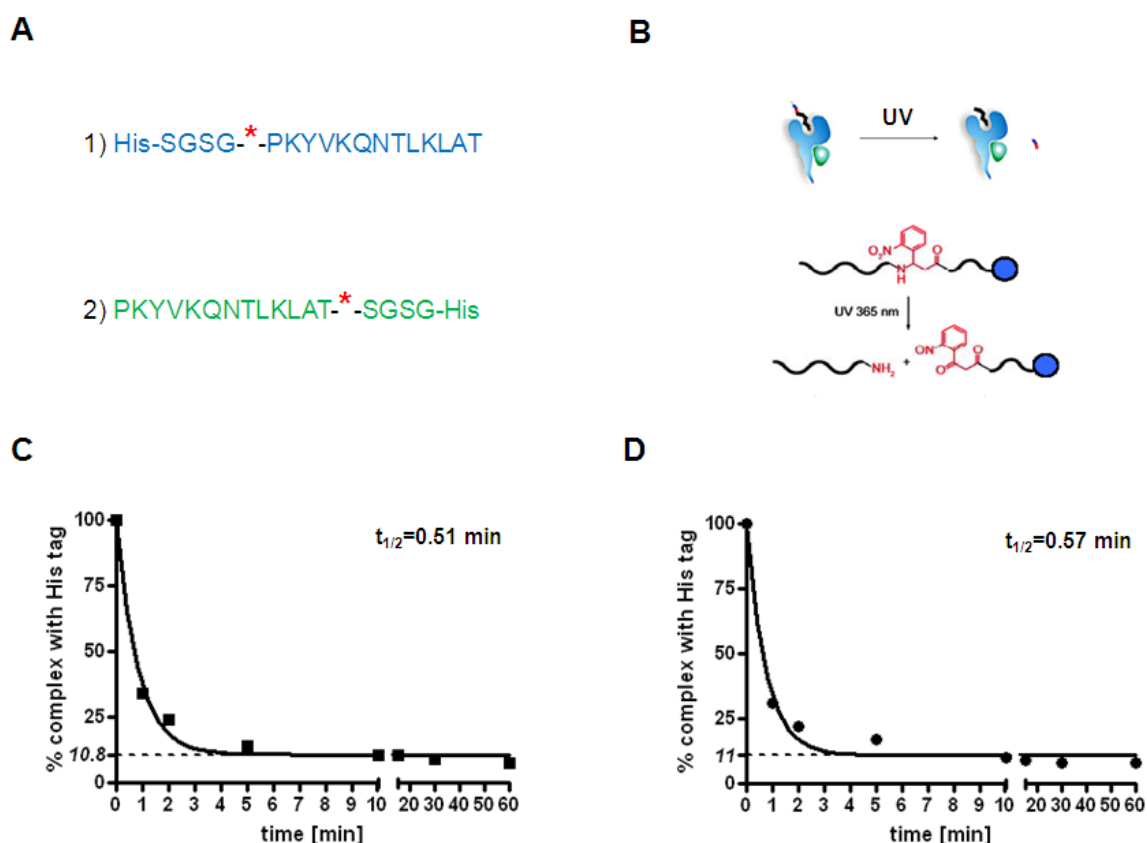


Figure 3.11 Kinetics of photolytic tag removal. A, Sequences of HA₃₀₆₋₃₁₈-peptide derivatives containing a photolabile β -nitrophenylglycine residue between the His-tag on the N-terminus (peptide 1) or C-terminus (peptide 2) of the MHC class II-binding peptide. B, Cartoon of the photocleavage reaction (top). Photochemical reaction of the β -nitrophenylglycine residue, induced by UV light at 365 nm (bottom), resulting in the cleavage of the adjacent peptide bond. C-D, Kinetics of His-tag photocleavage induced by UV light, as measured by ELISA on DR4 monomers containing peptide 1 (C) or peptide 2 (D). The half-lives of the photocleavage were 0.51 min and the 0.57 min for the N-terminally and C-terminally labeled peptides, respectively. One representative experiment (out of \geq two) is shown.

To test and validate this strategy, we either UV-irradiated or not immunopure, biotinylated DR4/HA₃₀₆₋₃₁₈ monomers containing a N- or C-terminal conditional peptide His-tag for 10 minutes, prepared PE-labeled multimers and performed binding isotherms on four different DR4/HA₃₀₆₋₃₁₈-specific clones (Figs 3.12A-D and Table 3.1). Clones 2 and 9 were of high and clones 15 and 8 were of low avidity. Levels of surface-expressed TCR, CD4 and their functional avidities are listed in Table 3.2. Multimers from N-terminally His-tagged DR4/HA₃₀₆₋₃₁₈ complexes stained more efficiently in all cases than the C-terminally His-tagged complexes and both stained more avidly than conventional multimers.

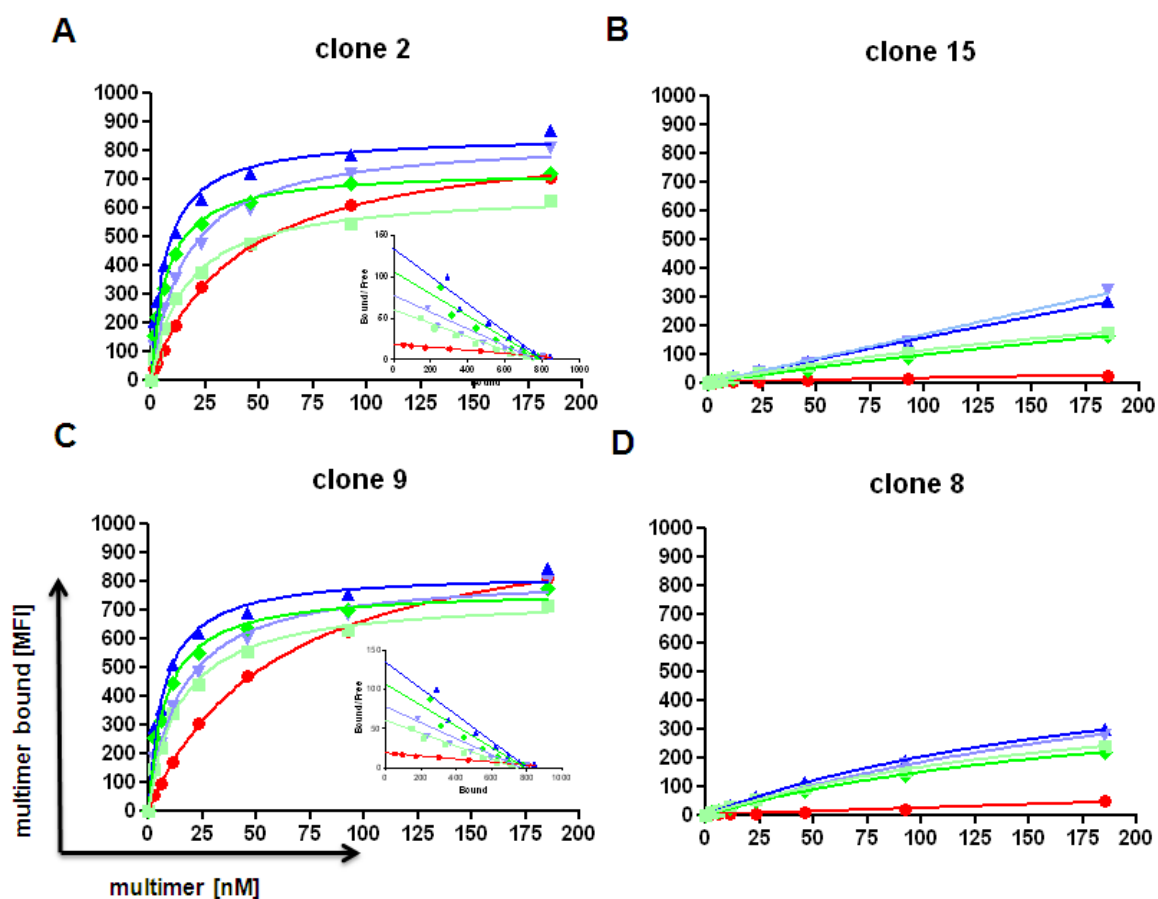


Figure 3.12 *Photolytic removal of peptide His-tag and its impact on multimer binding.* A-D, Binding isotherms of “immunopure” DR4/HA₃₀₆₋₃₁₈ multimers (blue and green), and conventional multimers (red) on DR4/HA₃₀₆₋₃₁₈-specific clones. Binding of multimers prepared from non-irradiated complexes with N-terminal His-tags (dark blue) and irradiated N-terminal complexes (light blue), were compared to binding of multimers prepared from non-irradiated C-terminal His-tagged complexes (bright green) and UV-irradiated C-terminal His-tagged complexes (light green). Multimer binding was performed for 1 hour at 37 °C. Scatchard plots are displayed as inserts in graphs A and C. Due to low binding, no conclusive Scatchard plots could be derived for B and D. A DR4/Flu-MP₆₁₋₇₂ clone was used to evaluate non-specific background binding for each reagent and the value of this background was subtracted. Inferred K_D and B_{max} values are compiled in Table 3.1. Experiments were performed twice. Representative experiments are shown.

Table 3.1 K_D and B_{max} values from Fig. 3.12

clone 2	K_D (nM)	B_{max} (MFI)	clone 9	K_D (nM)	B_{max} (MFI)
conventional	45.5	955	conventional	46.3	863
N-term +UV	5.2	728	N-term +UV	5.4	728
N-term -UV	11.8	676	N-term -UV	10.2	658
C-term +UV	6.7	679	C-term +UV	6.1	666
C-term -UV	12.4	563	C-term -UV	11.3	643

Moreover, there was a slight, but significant decrease in staining efficiency in multimer staining from UV-irradiated complexes, as reflected in slight changes in K_D and B_{max} values (Table 3.1). For the low binding affinity clones 8 and 15 reliable nonlinear regression and Scatchard analyses were not feasible because saturation was not reached. In conclusion, our comparative tetramer binding studies indicated that: i) compared to conventional tetramers, those made of “immunopure” monomers stained antigen-specific CD4+ T cells much more efficiently, in particular low avidity ones; and ii) N-terminal and to a lesser degree C-terminal His-tags may artificially increase binding and that this can be circumvented by photochemical removal of the tags.

Table 3.2 Characterization of DR4/HA₃₀₆₋₃₁₈ clones from Fig. 3.12

clone	TCR (MFI)	CD4 (MFI)	IFN γ EC ₅₀ (nM)
8	35	185	88
9	25	167	37
2	22	157	43
15	33	187	65

3.1.3.3 Purification of MHC-peptide monomers via N-terminal acidic tags

While the isolation of “immunopure” MHC-peptide monomers by means of peptide His-tag has advantages such as providing good peptide solubility and gentle isolation procedures, it necessitated purification of recombinant MHC class II molecules by immunoaffinity chromatography and conjugate formation via irreversible biotin-streptavidin interactions. As this is not compatible with the novel staining reagents referred to as NTAmers (presented in section 3.1.4), it was necessary to establish another strategy to purify cognate MHC-peptide monomers.

Polyanion tags containing multiple glutamate and/or aspartate residues have been used successfully to purify recombinant proteins by anion exchange chromatography (Le Borgne et al., 1995; Stubenrauch et al., 2000; Suominen et al., 1992). As a model system to test the feasibility of using polyanionic tags for purification of MHC-peptide monomers of interest, Cy5.5, a blue fluorescent moiety containing four negatively charged SO_3^- groups, was tested as a purification tag (Fig. 3.13). After loading of the soluble DR4 molecules with the Cy5.5-HA₃₀₆₋₃₁₈ peptide, the blue DR4/Cy5.5-HA₃₀₆₋₃₁₈ complexes (peak 2) were clearly resolved from colorless material (peak 1) (Fig. 3.13A). The blue DR4/Cy5.5-HA₃₀₆₋₃₁₈ complexes were characterized by a strong absorption of Cy5.5 at 675 nm (Fig. 3.13B). The DR4/Cy5.5-HA₃₀₆₋₃₁₈ complexes were predominantly monomeric as verified by gel filtration

chromatography (Fig. 3.13C) and SDS-PAGE analysis (Fig. 3.13D). Fluorescent multimers prepared from these monomers bound more avidly to a DR4/HA₃₀₆₋₃₁₈-specific CD4⁺ T cell clone (Fig. 3.13E) and also elicited a stronger IL-2 response when bound to a plastic surface at the same concentration than DR4/HA₃₀₆₋₃₁₈ complexes prepared by conventional peptide loading (Fig. 3.13F). However, use of Cy5.5 as a purification tag had serious disadvantages, such as: i) solubility problems and non-specific binding; ii) the use of photosensitive linkers for subsequent removal of the peptide tag was not applicable, due to the high UV absorption of Cy5.5 and iii) highly expensive and often difficult syntheses.

To determine the minimal peptidic polyanionic tag length allowing effective separation of specific MHC-peptide complexes of interest from the remaining MHC molecules, we examined the different variants of the HA₃₀₆₋₃₁₈ peptide shown in Table 3.3. To facilitate detection of the tagged MHC-peptide monomers in chromatographic fractions by ELISA, the peptide's N-terminus was capped with a phosphotyrosine (pY) or sulfotyrosine (sY), for which there exist antibodies. After loading, excess peptide was eliminated by gel filtration and MHC-peptide monomers resolved on anion-exchange chromatography. Fractions were assayed for peptide (pY, red and sY, purple) and DR protein in two separate ELISA. Peptide tags carrying four (Fig. 3.14A) and six aspartates (Fig. 3.14B) insufficiently separated specific (peak 2) and non-specific MHC-peptide complexes (peak 1), i.e. the peaks largely overlapped. By spacing the six negatively charged aspartates over ten residues (Fig. 3.14C) or by using eight glutamate residues (Fig. 3.14C-E), a clear separation of specific MHC-peptide monomers from the irrelevant MHCs was achieved. The octaglutamate tag (E₈), irrespectively of glutamate linkage via the α -carbon (pY-E₈) or via the γ -carbon atom (pY-E₈) gave the best separation. The functionality of the complexes was verified by multimer staining (Fig. 3.14G). However, the usefulness of the E₈ peptide tag was found to be limited to very stable complexes, e.g. DR4 (or DR1)/HA₃₀₆₋₃₁₈. For less stable complexes, such as DR1 or DR4/NY-ESO-1₁₁₉₋₁₄₃, aggregate formation was observed after purification due to the high salt conditions (>0.5M) needed for elution (data not shown). Another drawback of this strategy was the frequently high contamination of the thus isolated cognate monomers with diverse impurity, especially when the MHC class II molecules were isolated first by chelation and not by immunoaffinity chromatography (data not shown).

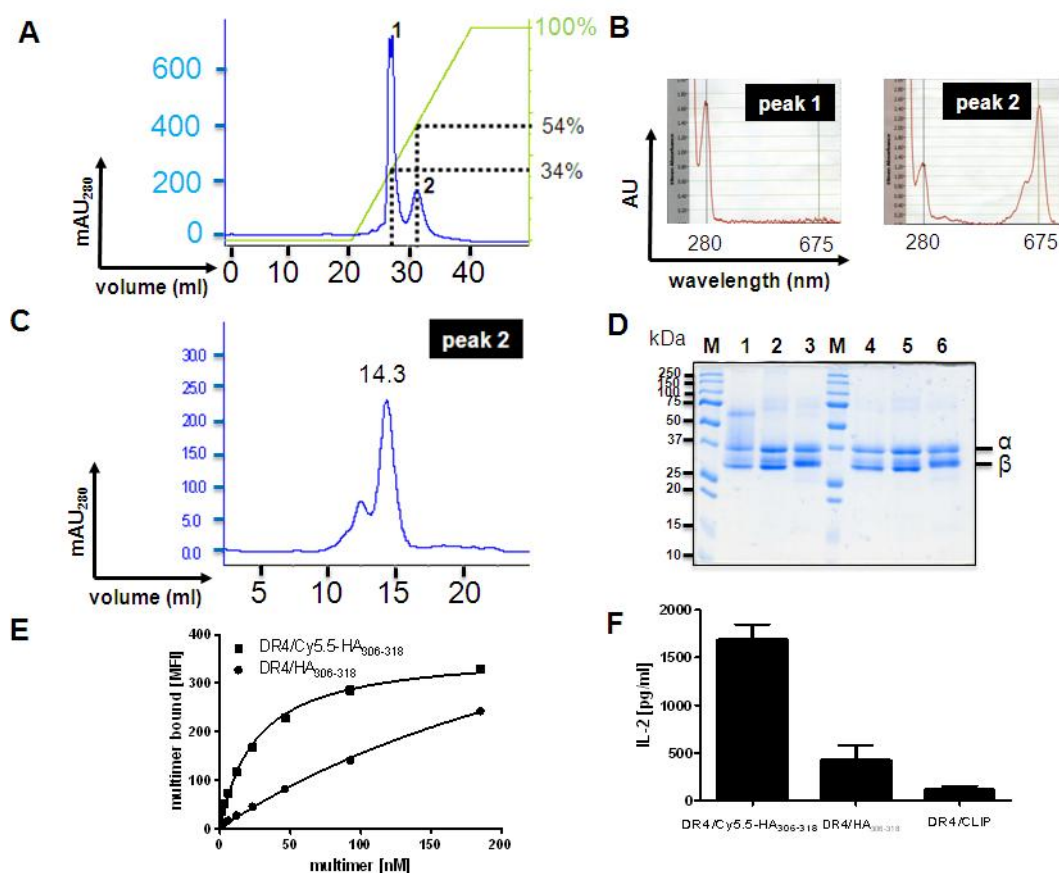


Figure 3.13 *Purification of DR4/Cy5.5-HA₃₀₆₋₃₁₈ complexes and their properties.* A, Resolution of DR4/Cy5.5-HA₃₀₆₋₃₁₈ from non-specific complexes by anion-exchange chromatography, referred to as peak 1 and 2, respectively. B, UV/VIS spectrophotometric analysis of peak 1 and 2. C, Gel filtration on a Superdex S200 column of the material corresponding to peak 2. D, SDS-PAGE (12%) of DR4/Cy5.5-HA₃₀₆₋₃₁₈ (lanes 1,4), DR4/HA₃₀₆₋₃₁₈ (lanes 2,5), DR4/CLIP (lanes 3,6) complexes under non-reducing (lanes 1,2,3) and reducing (lanes 4,5,6) conditions. M labels the molecular weight marker. E, Binding isotherm at 37 °C on a DR4/HA₃₀₆₋₃₁₈-specific clone with PE-labeled DR4/Cy5.5-HA₃₀₆₋₃₁₈ multimers (squares) and DR4/HA₃₀₆₋₃₁₈ multimers (circles). F, IL-2 production from a CD4⁺ T-cell DR4/HA₃₀₆₋₃₁₈ clone stimulated with plate-bound (100 ng/well) biotinylated complexes. IL-2 quantification was performed by ELISA. A representative experiment is shown out of two. Error bars represent SEMs from triplicates.

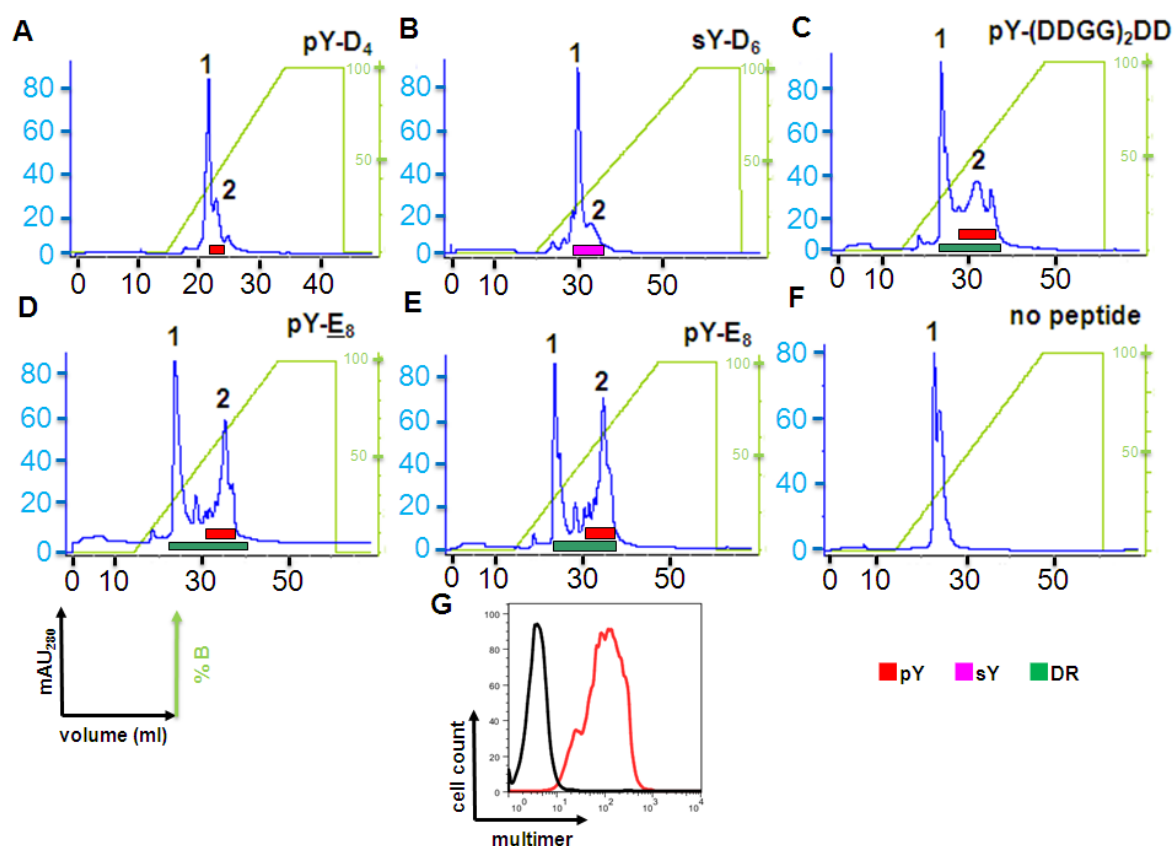


Figure 3.14 Isolation of “immunopure” MHC-peptide complexes via peptide polyanion tags. A-E, Empty DR4 molecules were loaded with HA₃₀₆₋₃₁₈ peptides with the negatively charged N-terminal extensions listed in Table 3.3. After elimination of unbound peptide, DR4/peptide complexes were separated with anion-exchange chromatography on a NaCl gradient (0-1 M, 20 CV). F, As the negative control, the empty DR4 protein was subjected to anion-exchange chromatography under the same conditions. G, Staining of a DR4/HA₃₀₆₋₃₁₈-specific CD4⁺ T cell line with PE-labeled DR4/pY-E₈-HA₃₀₆₋₃₁₈ (9.3 nM or 5 μg/ml) (red histogram). The black histogram represents cells stained with the same concentration of PE-labeled DR4/CLIP multimer. On all chromatograms, peak 1 represents DR4 without the peptide of interest, and peak 2 corresponds to DR4 complexes with the target peptides. Peak assignment was based on the ELISA analysis of fractions for the presence of the N-terminal pY (red) or sY (magenta) tag or the DR4 protein (green).

Table 3.3 Polyanion tags for purification of MHC class II-peptide complexes. pY and sY stands for phosphotyrosine and sulfotyrosine, respectively. E stands for glutamate where peptide linkage is achieved through the γ-carbon. All other letters are standard amino-acids.

polyanion tag	separation power	negative charges
Cy5.5-SGSG-HA ₃₀₆₋₃₁₈	++	4
pY-D ₄ -SGSG-HA ₃₀₆₋₃₁₈	+	4+2
sY-D ₆ -SGSG-HA ₃₀₆₋₃₁₈	++	6+2
pY-(DDGG) ₂ DD-SGSG-HA ₃₀₆₋₃₁₈	+++	6+2
pY-E ₈ -SGSG-HA ₃₀₆₋₃₁₈	++++	8+2
pY-E _{γ8} -SGSG-HA ₃₀₆₋₃₁₈	++++	8+2

3.1.3.4 MHC-peptide monomer purification via a N-terminal DTB tag

To find an alternative peptide tag that permits simple peptide synthesis and gentle MHC-peptide complex isolation, we tested desthiobiotin (DTB). Desthiobiotin is a biotin analog, missing the sulfur atom (Fig. 3.15A). It binds less avidly to streptavidin ($K_D=2 \times 10^{-9}$ M versus 4×10^{-14} M for biotin, (Green, 1970) and is easily dissociated at room temperature or 37 °C or displaced with biotin. Streptactin, an engineered mutant of streptavidin (Korndörfer and Skerra, 2002; Voss and Skerra, 1997), is preferentially used for protein purification of streptag- or desthiobiotin-tagged proteins (Wu and Wong, 2004) as it can be easily displaced with 2-(4-hydroxyphenylazo)benzoic acid (HABA) and regenerated for repeated cycles of purification (Fig. 3.15B,C).

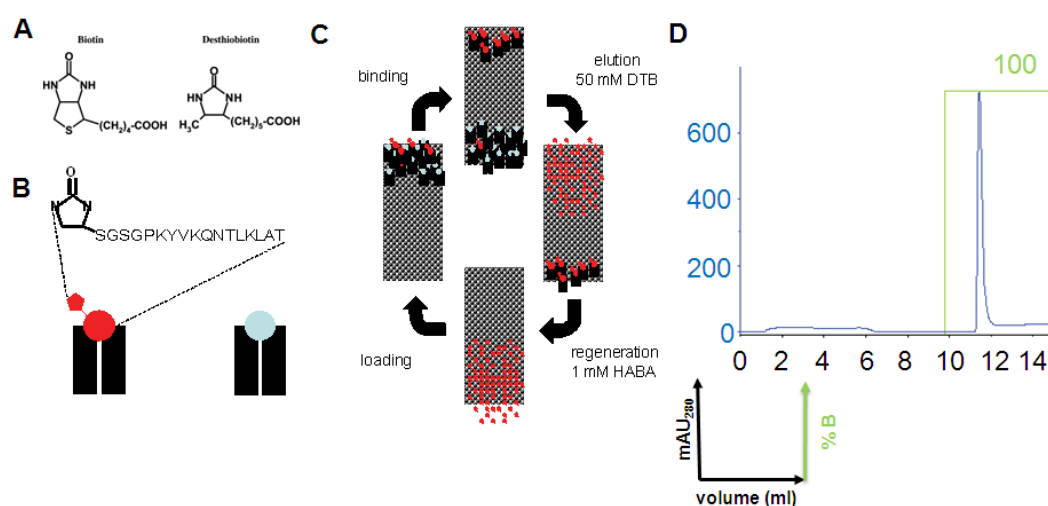


Figure 3.15 Isolation of MHC class II-peptide complexes via DTB-labeled peptides. **A**, Molecular structure of biotin and desthiobiotin. **B**, Cartoon representation of the DTB-HA₃₀₆₋₃₁₈ peptide (red) or an irrelevant peptide (light blue) bound to the DR4 protein (black). **C**, Purification cycle of DTB-labeled MHC-peptide complexes on a streptactin column. **D**, Chromatogram of DR4/DTB-HA₃₀₆₋₃₁₈ monomers eluted from a streptactin Sepharose column. Free DTB (50 mM) was used to elute DTB-labeled complexes from streptactin Sepharose.

For a proof-of-principle, we synthesized HA₃₀₆₋₃₁₈ with a N-terminal DTB residue separated from the HA₃₀₆₋₃₁₈ peptide by a flexible GSGS peptide linker and loaded this onto recombinant DR4 protein. Elution of the DR4/DTB-HA₃₀₆₋₃₁₈ complexes with excess ligand (50 mM DTB) at neutral pH was efficient (>70% recovery) and resulted in a sharp peak (Fig. 3.15D). The validity of this strategy was confirmed by extending this experiment to DR1, DR4 and DP4 MHC class II complexes with a wide range of different peptides.

3.1.4 NTAmers: a novel class of reversible MHC class II-peptide staining reagents

Several reasons prompted us to develop a novel strategy for the preparation of MHC class II-peptide multimers. First, the commonly used immunoaffinity purification is not only tedious and costly, but also a major source of MHC protein denaturation due to the typically harsh elution conditions required (pH=11.3 or 3.2 depending on the mAb). Purification via His-tags and chelating columns is more attractive, as it does not cause MHC II denaturation, and is universally applicable, economic and scalable. Second, conventional multimer preparation based on enzymatic biotinylation of soluble recombinant MHC-peptide complexes and subsequent multimer formation by conjugation with fluorescent streptavidin derivatives is irreversible and provides no versatility in conjugate formation. Third, besides flow cytometric analysis of antigen-specific CD4⁺ T cells, many studies require sorting of such cells.

Sorting of antigen-specific T cells by means of conventional multimers may cause diverse difficulties. Upon avid binding of cell-surface TCR, MHC class I-peptide tetramers and dimers strongly induce T cell activation, provoking cell death and functional alterations in CD8⁺ T cells (Cebecauer et al., 2005a; Guillaume et al., 2006; Knabel et al., 2002; Schmidt et al., 2011). Even if the binding is performed in the cold, multimers stay on the cell surface and upon subsequent culturing of cells internalize and strongly activate CD8⁺ T cells. Furthermore, peptides from multimers can be transferred to cell-associated MHC molecules and thus enable potentially adverse T cell-T cell interactions (Ge et al., 2002; Schott et al., 2002; Walden and Eisen, 1990). Desthiobiotin and streptactin-based reagents are stable only in the cold (0-4 °C), and hence are not applicable for sorting of CD4⁺ T cells, comprehensible staining of which requires elevated temperatures. Because there are growing interests in sorting antigen-specific CD4⁺ T cells for adoptive transfer in therapeutic settings, we devised a new strategy, based on the reversible Ni²⁺ NTA-His tag interaction.

3.1.4.1 Principles of the new strategy

The first step in building a reversible reagent was to replace the essentially irreversible biotin-streptavidin interaction ($K_D \sim 10^{-15}$ M) between the biotinylated MHC-peptide monomers and the fluorescent streptavidin conjugate. As basis for this reversible interaction we chose the well-characterized Ni^{2+} NTA:His-tag chelate complexes that are widely used, not only for protein purification, but also for binding of proteins to various surfaces (such as Biacore sensor chips or glass surfaces for protein microarrays) or even cell-surface for protein conjugation (Guignet et al., 2004). However, the interaction of one His-tag with Ni^{2+} NTA groups is not very strong ($K_D \sim 10^{-6}$ M) and thus not adequate for stable conjugate formation. To strengthen this interaction, the hexahistidine tag was duplicated via a flexible GSGSGGGG spacer (Schmidt et al., 2011) (Fig. 3.16A). Moreover, four NTA groups were clustered as a dimer-of-a-dimer containing the same GSGSGGGG spacer in a linear peptide carrying an N-terminal biotin (Fig. 3.16C). This molecule we designated biotin-NTA₄. By saturating the biotin binding sites of a streptavidin-phycoerythrin and adding nickel ions, the reversible scaffold was prepared (Fig. 3.16B). In this way, binding affinities up to 10^{-12} M were achieved for the Ni^{2+} NTA₄:2xHis pair. The tandem His-tag was appended to the C-terminus of the MHC class II α chain, while on the β chains the C-terminal BirA-tag (BSP) was kept, providing an alternative tag for detection by antibody or enzymatic biotinylation (Fig. 3.16A). To purify correctly formed MHC-peptide monomers, DTB was used as a peptide tag of choice on the peptide's N-terminus. Fluorescent streptavidin conjugates were prepared by mixing monomers with excess biotin-NTA₄ ligands charged with NiSO_4 and subsequently dialyzed to eliminate unbound reagents. Such fluorescent conjugates are referred to as SA-PE NTA₄. The workflow of NTamer preparation is outlined in Fig. 3.17. This strategy allows gently purification of delicate “empty” MHC class II molecules by chelating chromatography on IDA (iminodiacetic acid) columns, which is universally applicable, inexpensive and scalable. In addition, it includes reversible use of the DTB peptide tag to isolate cognate MHC class II-peptide complexes after peptide loading. The sequential combination of these two different affinity chromatographies provides cognate MHC class II-peptide monomers of remarkably high purity. Finally in this strategy the tandem His-tag is again used for conjugate formation with SA-PE NTA₄. While these conjugates are highly stable in the absence of imidazole, they very rapidly decay in its presence, i.e. they are fully switchable.

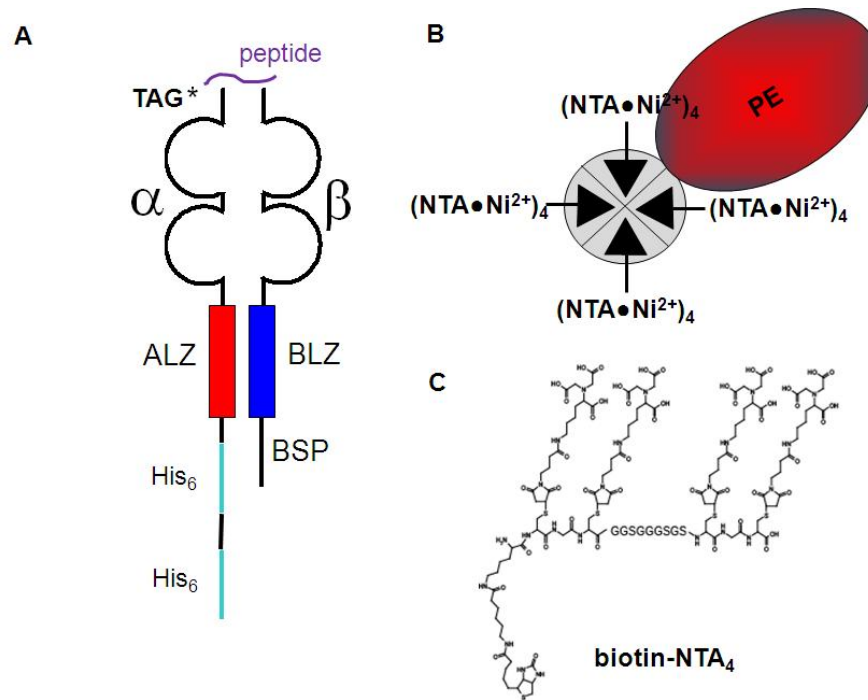


Figure 3.16 *Components of the NTamer.* A, Cartoon representation of the 2xHis-tagged MHC complex loaded with a tag-labeled peptide. B, Cartoon representation of PE-labeled streptavidin saturated with biotin-NTA₄ groups. C, Structure of biotin-NTA₄ from (Schmidt et al., 2011).

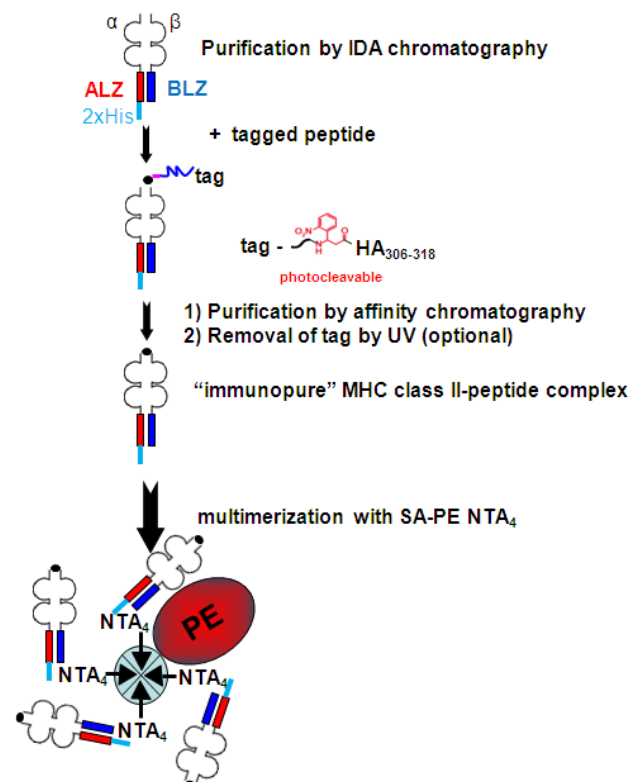


Figure 3.17 *Workflow of NTamer preparation.* “Empty” MHC class II proteins are purified from insect cell culture supernatants by means of IDA columns and subsequently loaded with DTB-tagged peptides. DTB-labeled MHC class II-peptide monomers are purified on streptactin columns and multimerized by mixing with SA-PE NTA₄.

3.1.4.2 Staining performance of reversible NTAmers and staining reversibility

We wished to test binding of reversible NTAmers on cells. To this end, we prepared SA-PE NTA₄-based multimers incorporating DR4_{2xHis}/DTB-HA₃₀₆₋₃₁₈ complexes, by mixing MHC-peptide monomers with SA-PE NTA₄. Concentrations of DR4_{2xHis}/DTB-HA₃₀₆₋₃₁₈ and DR4/His-HA₃₀₆₋₃₁₈ multimers were equalized according to their PE content and binding isotherms assessed on a DR4/HA₃₀₆₋₃₁₈-specific high avidity clone 9 (Fig. 3.18A,B) and a low avidity clone 8 (Fig. 3.18C,D). Whereas conventional SA-PE DR4/His-HA₃₀₆₋₃₁₈ multimers displayed a higher binding avidity (K_D) than SA-PE NTA₄ DR4_{2xHis}/DTB-HA₃₀₆₋₃₁₈ multimers on clone 9, the inverse was true on clone 8 (Table 3.4). On both clones maximum binding (B_{max}) was considerably higher for NTAmer as compared to conventional multimers.

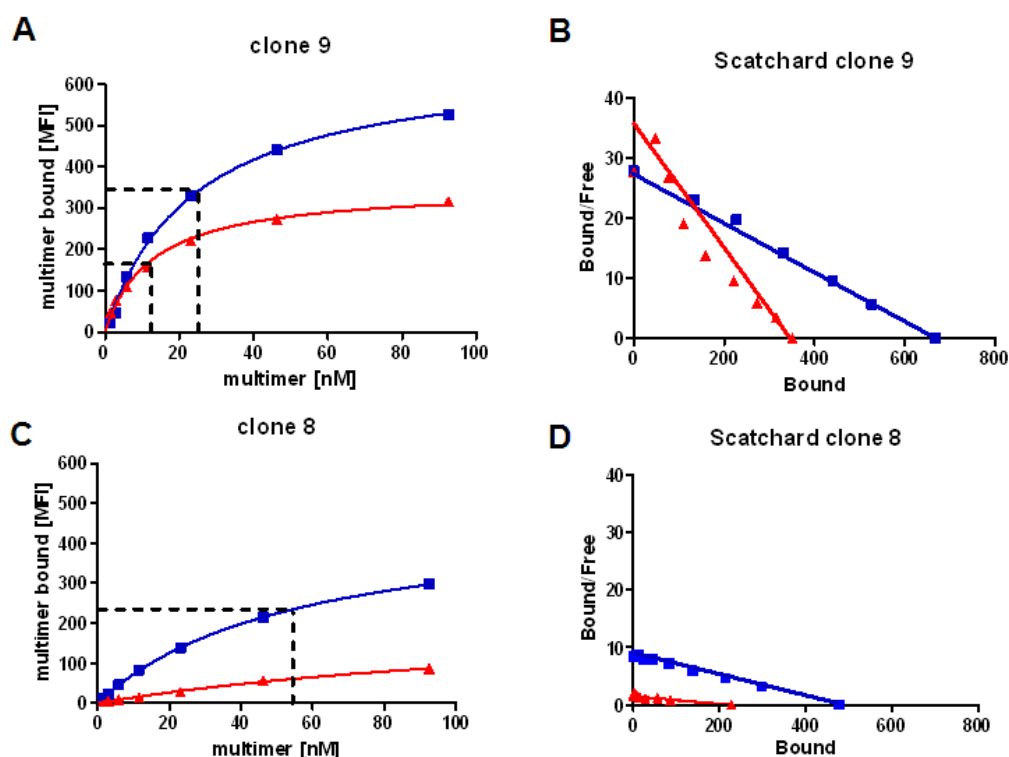


Figure 3.18 *Binding of conventional (BSP) and NTAmer (NTA) on CD4⁺ T cell clones.* A and C, Binding isotherms of DR4_{2xHis}/DTB-HA₃₀₆₋₃₁₈ NTAmer (blue squares) and BSP multimers prepared from (red triangles). B and D, Scatchard plots for binding curves (A) and (C), respectively. Cells were stained at 37 °C for 1 hour with the respective multimers and cell-associated fluorescence was analyzed by flow cytometry. Concentrations of multimers were adjusted for PE content, by measuring absorbance at 565 nm. A DR4/Flu-MP₆₁₋₇₂ clone was used to assess non-specific binding for each reagent and the value of this background was subtracted. Curves were fit by non-linear regression. Resulting B_{max} and K_D values are reported in Table 3.4. Experiments were performed twice. Representative experiments are shown.

We then extended such an analysis to DR4/HA₃₀₆₋₃₁₈-specific CD4⁺ T cells from a heterogeneous population. We compared the frequency of multimer positive cells on PBMC from a DR4⁺ healthy donor previously stimulated with the HA₃₀₆₋₃₁₈ peptide and stained with NTA and conventional BSP multimers (Fig. 3.19A). For comparison we assessed IFN γ intracellular staining (Fig. 3.18B). A higher frequency (4% versus 3.1%) of antigen-specific cells was detected over a wide range of concentrations (up to 95 nM or ~50 μ g/ml) with the SA-PE NTA₄ DR4_{2xHis}/DTB-HA₃₀₆₋₃₁₈ multimer compared to the immunopure DR4/His-HA₃₀₆₋₃₁₈ BSP multimer. NTAMers stained more avidly and detected higher frequencies of antigen-specific CD4⁺ T cells when tested at the same concentration than conventional multimers, at both 37 °C (6.23% NTA versus 4.52% BSP) and RT (5.35 NTA versus 3.30% BSP) (Fig. 3.19C). Similar results were observed when comparing DP4_{2xHis}/DTB-TT₉₄₇₋₉₆₀ NTAMers and conventional DP4/TT₉₄₇₋₉₆₀ multimers (2.65% NTA versus 2.14% BSP in specific cells) on peptide stimulated PBMC (Figs. 3.19D) or with the corresponding DR1/NY-ESO-1₁₁₉₋₁₄₃ multimers on a DR1/NY-ESO-1₁₁₉₋₁₄₃ specific CD4⁺ T cell line (MFI 284 versus 52.1) (3.19E). It should be noted that higher non-specific staining was observed with SA-PE NTA₄-based multimers than with the BSP multimers in the experiment shown in Fig. 3.19C. This may be explained, at least in part, by the fact that the PBMC of this particular donor had significant frequency of DR4/TT₉₄₇₋₉₆₀-specific CD4⁺ T cells.

Table 3.4 B_{max} and K_D values from Fig. 3.18

	multimer	K_D (nM)	B_{max} (MFI)
clone 9	NTA	24.0	667
	BSP	12.7	352
clone 8	NTA	56.4	478
	BSP	>100	227

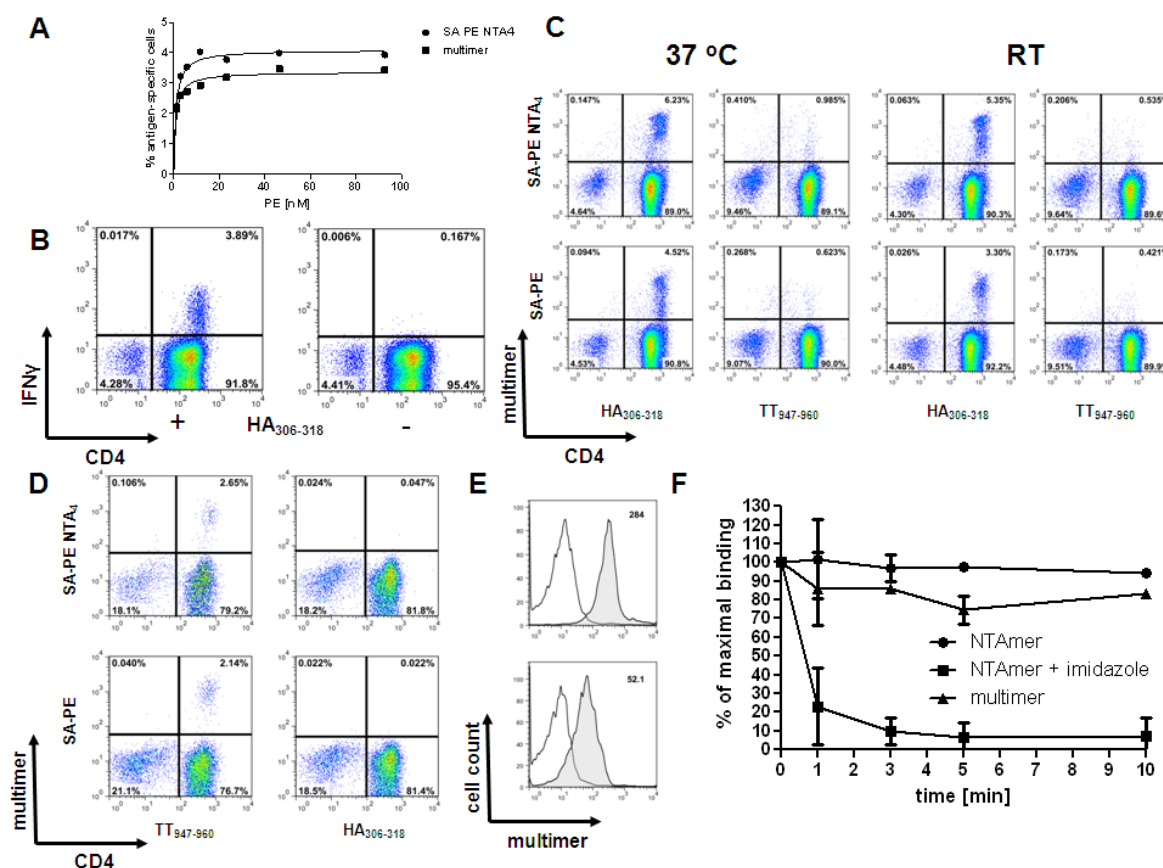


Figure 3.19 Comparative staining of NTamer and BSP multimer. A, Binding isotherms were assessed at 37 °C on HA₃₀₆₋₃₁₈-stimulated PBMC from a DR4⁺ healthy donor with conventional SA-PE DR4/His-HA₃₀₆₋₃₁₈ multimers (squares) and SA-PE NTA₄ DR4_{2xHis}/DTB-HA₃₀₆₋₃₁₈ (circles). B, Intracellular IFN γ staining of DR4/HA₃₀₆₋₃₁₈-peptide stimulated PBMC. C, Staining of PBMC stimulated previously with 2 μ M of HA₃₀₆₋₃₁₈ or TT₉₄₇₋₉₆₀ peptide with conventional SA-PE DR4/His-HA₃₀₆₋₃₁₈ multimers (multimer) and SA-PE NTA₄ DR4_{2xHis}/DTB-HA₃₀₆₋₃₁₈ (SA-PE NTA₄) at 18.5 nM (10 μ g/ml) for 1 hour at 37 °C or room temperature (RT). D, Staining of PBMC stimulated with 2 μ M HA₃₀₆₋₃₁₈ or TT₉₄₇₋₉₆₀ peptide with conventional SA-PE DP4/TT₉₄₇₋₉₆₀ multimers (multimer) and SA-PE NTA₄ DP4_{2xHis}/DTB-TT₉₄₇₋₉₆₀ (SA-PE NTA₄) at 18.5 nM (10 μ g/ml) for 1 hour at 37°C. E, Staining of a DR1/NY-ESO-1₁₁₉₋₁₄₃ cell line with conventional SA-PE DR1/His-NY-ESO-1₁₁₉₋₁₄₃ multimers (multimer) and SA-PE NTA₄ DR1_{2xHis}/DTB-NY-ESO-1₁₁₉₋₁₄₃ (SA-PE NTA₄) at 18.5 nM (10 μ g/ml) for 1 hour. F, PBMC stimulated with 2 μ M HA₃₀₆₋₃₁₈ peptide (from C) were stained with 18.5 nM (10 μ g/ml) conventional SA-PE DR4/His-HA₃₀₆₋₃₁₈ multimer (triangles) or SA-PE NTA₄ DR4_{2xHis}/HA₃₀₆₋₃₁₈ multimer (squares), washed and analyzed by flow cytometry. The initial frequency of tetramer+ cells was normalized to 100%. Upon the addition of 100 mM imidazole, the frequency of tetramer+ events was measured at 1, 3, 5 and 10 minutes and converted to percentages of initial frequencies. As a control, cells were stained with SA-PE NTA₄ DR4_{2xHis}/HA₃₀₆₋₃₁₈ multimer and left untreated (circles). Mean values and SD were calculated from two experiments.

A key feature of the NTA-based multimers is their reversibility, i.e. they quickly disintegrate upon addition of 100 mM imidazole in the cold (4 °C), which allows sorting of “untouched” T cells. To confirm staining reversibility with SA-PE NTA₄ DR4_{2xHis}/DTB-HA₃₀₆₋₃₁₈ multimers, we subjected cold-stained peptide-stimulated PBMC to imidazole treatment and assessed the count of antigen-specific cells over time (Fig. 3.19F). After one minute of incubation, >90% of NTA-mer stained cells disappeared and complete loss of specific

staining was reached after 5 minutes. In the absence of imidazole, staining remained stable. Conventional multimers were insensitive to the presence of imidazole, as expected.

3.1.5 Improving peptide loading of MHC class II molecules via conditional peptide ligands

As described above (section 3.1.2) loading of “empty” MHC class II molecules with some peptides, namely viral epitopes, is quite efficient (~80%), whereas for others, many of which derived from tumor-associated antigens, is inefficient (~20%). Because MHC proteins are precious, we explored whether the loading efficiency of the latter peptides can be significantly increased by means of conditional peptide ligands. The idea was to design a photocleavable peptide that can be efficiently loaded onto given MHC class II molecules and subsequently be exchanged with a peptide of interest by means of photocleavage of the conditional peptide.

3.1.5.1 Design of conditional photocleavable peptide ligands

The crystal structure of DR4 with the HA₃₀₆₋₃₁₈ peptide bound to the HA1.7 TCR (Hennecke and Wiley, 2002) was used to design suitable photocleavable peptide ligands. HA₃₀₆₋₃₁₈ is a peptide derived from the influenza A virus hemagglutinin protein with a low nanomolar affinity for many HLA-DR proteins (e.g. DR1, DR4, DR7, DR52b and many others (Posch et al., 1996)) ensuring a broad applicability of an optimal photocleavable ligand, unlike the photosensitive MBP-P4* derivative of MBP₈₅₋₉₉ peptide which is specific only for DR2 (Grotenbreg et al., 2007). Peptides bound to MHC class II proteins assume a poly-proline II helix-like, extended conformation and form a network of hydrogen bonds with the MHC protein backbone. In addition, several side chains act as “anchors” occupying deep pockets, namely P1, P4, P6 and P9.

In the DR4\HA₃₀₆₋₃₁₈ complex the Tyr308 side chain occupies the principal, deep hydrophobic pocket P1, and those of Gln311, Thr313 and Leu316 the pockets P4, P6 and P9 respectively. Residues Lys307, Val309, Lys310, Asn312, Leu 314 and Lys315 are oriented towards the TCR (Fig. 3.20A).

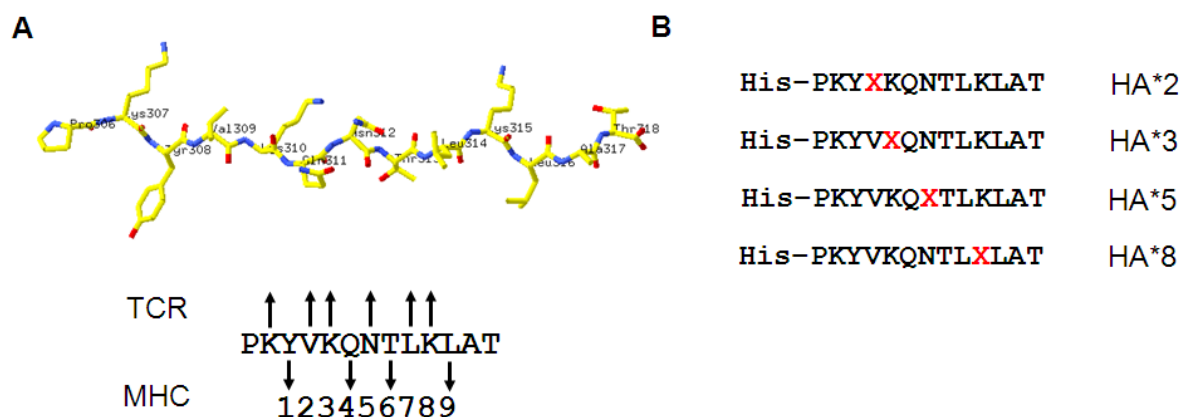


Figure 3.20 Design of photocleavable peptide ligands. A, Structure of the HA₃₀₆₋₃₁₈ peptide from the DR4/HA₃₀₆₋₃₁₈:HA1.7 TCR crystal structure (PDB file ID code 1J8H) with TCR and MHC-facing side-chains indicated by arrows. Carbon atoms are yellow, nitrogen atoms blue and oxygen atoms red. B, Peptide variants generated from the HA₃₀₆₋₃₁₈ peptide where a photolabile β -(2-nitro)phenylglycine residue (represented by a red X) was introduced in positions 2,3,5 or 8.

Based on this, we replaced amino acid residues at positions 2 (Val309), 3 (Lys310), 5 (Asn312) or 8 (Leu 314) by β -(2-nitro)phenylglycine (β NPG), a UV-labile residue, generating a set of four photocleavable HA₃₀₆₋₃₁₈-derived peptides referred to as HA*2, HA*3, HA*5 and HA*8 (Fig. 3.20B). We selected the residues whose side chains are solvent-exposed and whose replacement hence should not interfere with the binding of the peptide to the DR4 protein. Upon irradiation at 365 nm, β NPG undergoes a rearrangement resulting in the cleavage of the N-proximal peptide bond (Fig. 3.11B). The aim was to generate, upon photolysis, two peptide fragments that have dramatically reduced binding to DR4 and hence can be readily exchanged for a peptide of interest. Hexahistidine tags were added to the N-terminus of the photocleavable ligands through a SGSG spacer to allow isolation of homogeneous DR4/HA* complexes.

3.1.5.2 Relative affinity of conditional peptide ligands for DR4 and efficiency of photocleavage

To determine the best candidate for the photosensitive DR4 complexes, we performed a competition assay to determine the relative binding affinities of the conditional peptide ligands for the DR4 protein (Fig. 3.21A). Two peptides, HA*3 and HA*5, had equal ($\sim 6 \mu\text{M}$) or better ($\sim 2 \mu\text{M}$) affinity (IC_{50}), respectively, for DR4 than the wild-type HA₃₀₆₋₃₁₈ peptide. Another two candidate peptides (HA*2, HA*8) bound ~ 10 -fold less avidly (as judged by their IC_{50}) than the parental peptide and were excluded from further analyses. The HA*3 ligand was also excluded from further analyses due to its inability to be exchanged after UV

irradiation (data not shown). To verify that UV light induced fragmentation of the HA*5 peptide ligand occurred as expected (Fig. 3.21B), the HA*5 peptide (2676 Da) (Fig. 3.21C) was UV-irradiated for an extended period of time to ensure completion of UV-induced fragmentation (60 min); this indeed resulted in the appearance of the expected fragments (1870 Da and 806 Da) as detected by MALDI-TOF (Fig. 3.21D).

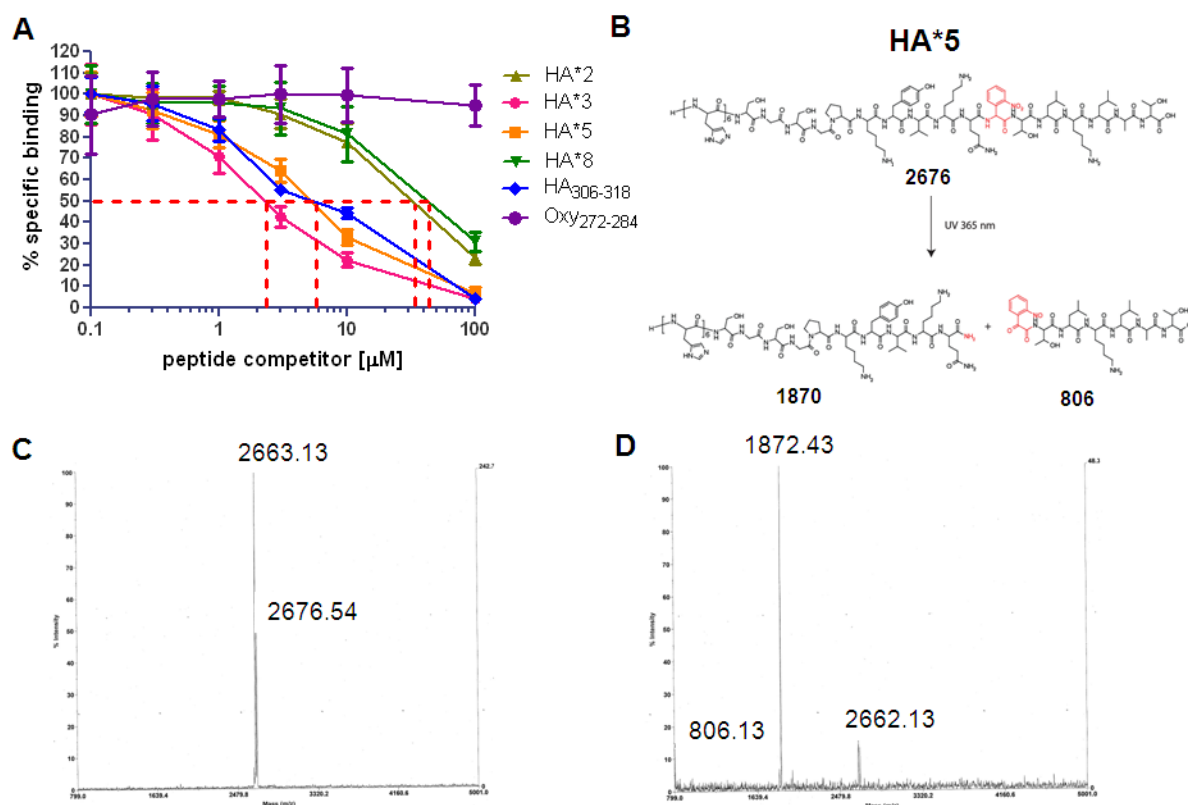


Figure 3.21 *Characterization of photocleavable peptide ligands.* **A**, Four photosensitive HA₃₀₆₋₃₁₈ peptide derivatives (HA*2, HA*3, HA*5, HA*8) were compared to the HA₃₀₆₋₃₁₈ peptide for their ability to compete with biotin-HA₃₀₆₋₃₁₈ for binding to DR4. Oxy₂₇₂₋₂₈₄ is the negative control. Data are an average of three experiments. Error bars represent SD. **B**, Structure of the HA*5 peptide and the predicted photocleavage fragments resulting after UV irradiation. Inserted numbers indicate the predicted molecular weights. Molecular structure drawn by Julien Schmidt. **C**, Verification of molecular weight of HA*5 with MALDI MS. **D**, Detection of HA*5 photocleavage fragments after 1 hour of irradiation with UV at 365 nm by MALDI MS. The mass spectrometry data were collected by Julien Schmidt. The experiment was performed twice. A representative experiment is shown.

3.1.5.3 Dissociation of photocleaved peptide depends on temperature and pH

Loading of a peptide of interest onto the MHC molecule harboring a conditional peptide ligand is expected to depend on the dissociation of the peptide fragments upon its photolytic cleavage. UV-induced decay kinetics was first examined on free HA*5 peptide in PBS (Fig. 3.22A), exhibiting a half-life ($t_{1/2}$) of 2.05 min. The UV-induced decay was rapid, with the

peptide being >98% fragmented after 10 minutes of irradiation and not detectable after 30 minutes.

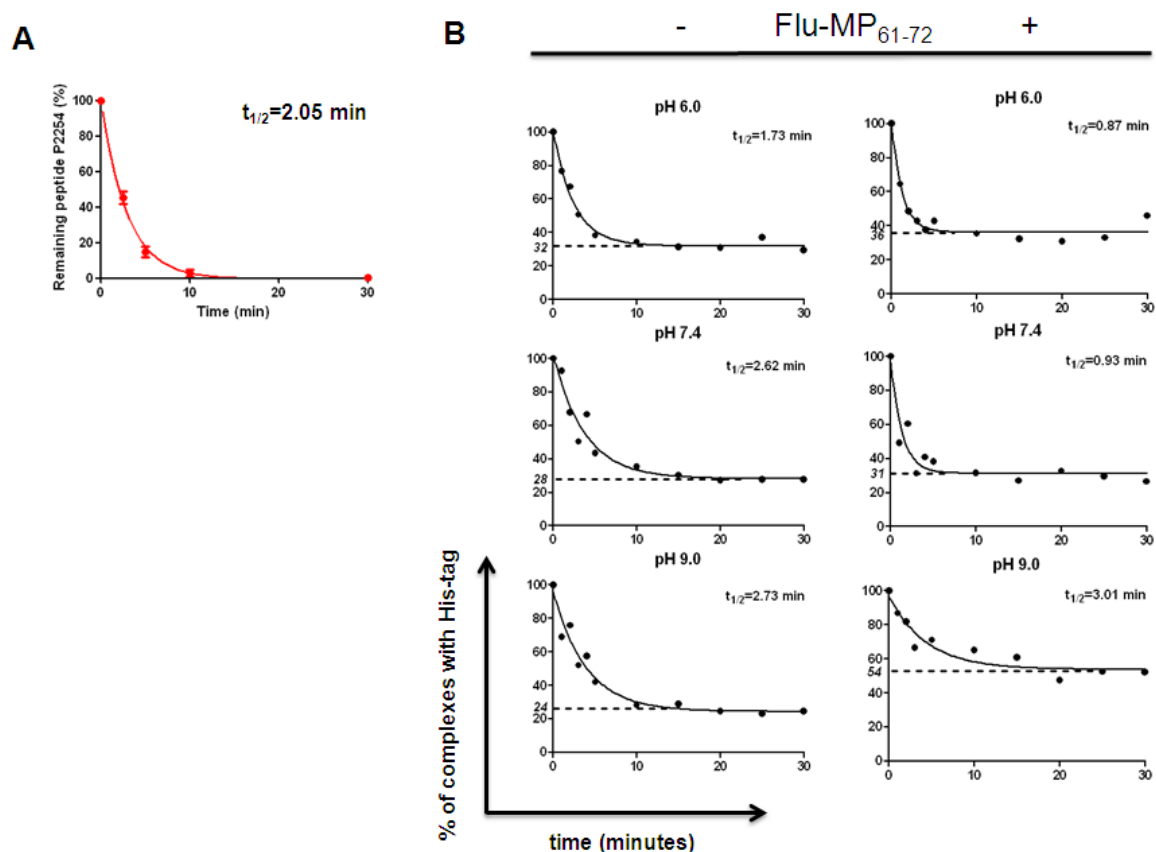


Figure 3.22 Photocleavage kinetics of HA*5 peptide. A, Photocleavage kinetics of the free HA*5 peptide measured by HPLC on C18 columns. Area under the peaks corresponding to the intact HA*5 peptide were integrated at designated time points, and normalized to those of non-irradiated HA*5 peptide. B, Photocleavage kinetics of DR4/HA*5 complexes, where the His-tag is detected by ELISA. Kinetics experiments were performed in the presence (right) or the absence (left) of 10 μ M Flu-MP₆₁₋₇₂ peptide at pH 6.0, 7.4, 9.0. The percentage of residual DR4-bound, heavier His-tag peptide fragment, is indicated in *italics*. Peptide half-lives (free and in complex with DR4), were calculated by fitting the data with an exponential decay curve and are indicated as $t_{1/2}$. The experiments were performed twice. Representative experiments are shown.

To assess the photocleavage kinetics of His-tagged HA*5 bound to an MHC protein, the DR4/HA*5 monomers were prepared, purified over Ni²⁺-NTA column to homogeneity and subjected to UV irradiation for indicated periods of time in the presence or absence of Flu-MP₆₁₋₇₂ peptide at three different pH. The remaining DR4-associated His-tag peptide fragment was detected by ELISA using serial dilutions (Fig. 3.22B). The half-lives of HA*5 bound to DR4 ($t_{1/2}$ from 0.87 to 3.01 min) were comparable to the half-life measured on the free peptide. The observed half-lives were pH dependent, namely were shorter at low than at high pH. Furthermore, in the presence of a strongly binding competitor, the half-lives were

shorter at pH 6 and pH 7.4, but not at pH 9, where the peptide exchange is scant. Although photocleavage of the free peptide was complete after 10 minutes, 24-53% of the His-tagged HA*5 peptide fragment remained DR4-associated after UV irradiation. Possible explanations for this include: i) the photocleavage of DR4-bound, as opposed to free, HA*5 peptide may not be complete; ii) the His-tagged N-terminal HA*5 peptide fragment, being rather large (1870 Da), may not completely dissociate at room temperature. Indeed, it is generally accepted that efficient peptide loading requires elevated temperatures and this may be due to more efficient dissociation of MHC-bound peptides.

3.1.5.4 Increased peptide binding of UV-irradiated, photosensitive DR4/HA*5 peptide complexes

Recombinant MHC class II proteins without covalently bound peptide cargo expressed by *Drosophila* cells are capable of binding antigenic peptides. However, as described above (see section 3.1.2), direct loading of such “empty” MHC class II molecules with peptides of interest, namely peptides derived from tumor-associated or self-antigens, is often remarkably inefficient. This may be explained by that they have either bound unknown peptides or are conformationally heterogeneous, i.e. contain peptide-receptive and non-receptive conformers that can interconvert. To find out whether loading of such peptides can be improved by means of conditional peptide ligands, DR4/HA*5 complexes were incubated with DTB-NY-ESO-1₁₁₉₋₁₄₃ peptide and the desthiobiotin (DTB) bound to DR4 measured by ELISA (Fig. 3.23). After UV-irradiation of DR4/HA*5 complexes extensive DTB-NY-ESO-1₁₁₉₋₁₄₃ peptide binding was observed, whereas barely detectable binding was detected in the absence of UV-irradiation (Fig. 3.23). By comparison, peptide binding on “empty” DR4 molecules was slower and less efficient, with no differences between UV-irradiated and non-irradiated molecules.

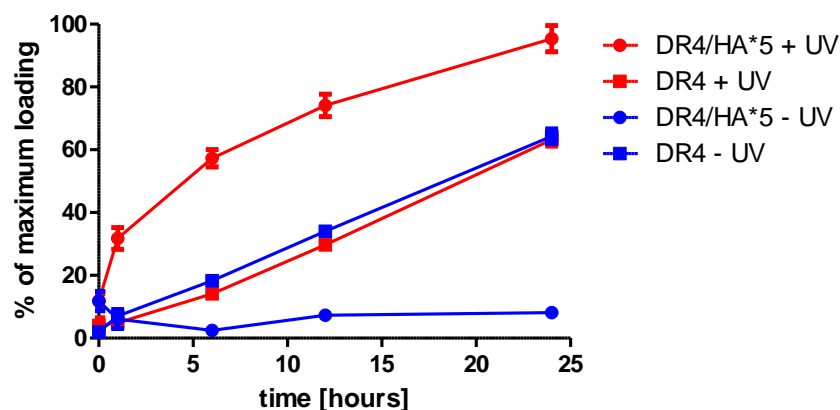


Figure 3.23 *Binding kinetics of the DTB-NY-ESO-1₁₁₉₋₁₄₃ peptide onto UV-irradiated DR4/HA*5 complexes.* Kinetics of DTB-NY-ESO-1₁₁₉₋₁₄₃ peptide binding on DR4/HA*5 complexes (circles) or “empty” DR4 molecules (squares), UV-irradiated (red) or not (blue) for 10 minutes on ice and subsequently incubated 1, 6, 12 and 24 hours at 37 °C in the presence of 10 μM DTB-NY-ESO-1₁₁₉₋₁₄₃ peptide. The percentages of DTB-containing DR4 complexes were measured by ELISA specific for DTB. Data were normalized to the signal from DR4/DTB-NY-ESO-1₁₁₉₋₁₄₃ complexes after 24 hours taken as 100%. A representative experiment out of three is shown. Error bars represent SEM from triplicates.

3.1.5.5 Detection of antigen-specific T cells with peptide exchange multimers

To optimize time and temperature parameters for peptide exchange, affinity-purified DR4 HA*5 complexes were UV-irradiated or not and incubated with 10 μM Flu-MP₆₁₋₇₂ peptide for up to 24 hours. After incubations of the samples they were diluted with FACS buffer, multimers prepared with SA-PE, and the sample directly used to stain DR4/Flu-MP₆₁₋₇₂-specific cloned cells (Fig. 3.24). The optimal conditions for peptide exchange were clearly 24h at 37 °C. To test whether DR4-peptide complexes created by peptide exchange via the UV-irradiated photolabile precursor can be used to produce functional fluorescent multimers, as previously demonstrated on MHC class I HLA-A1, -A3, -A11 and -B7 alleles (Bakker et al., 2008), biotinylated DR4/HA*5 complexes were irradiated and exchanged with Flu-MP₆₁₋₇₂, HA₃₀₆₋₃₁₈ or NY-ESO-1₁₁₉₋₁₄₃ peptides, multimerized with SA-PE and used to stain specific CD4⁺ T cells (Fig. 3.24 A-C).

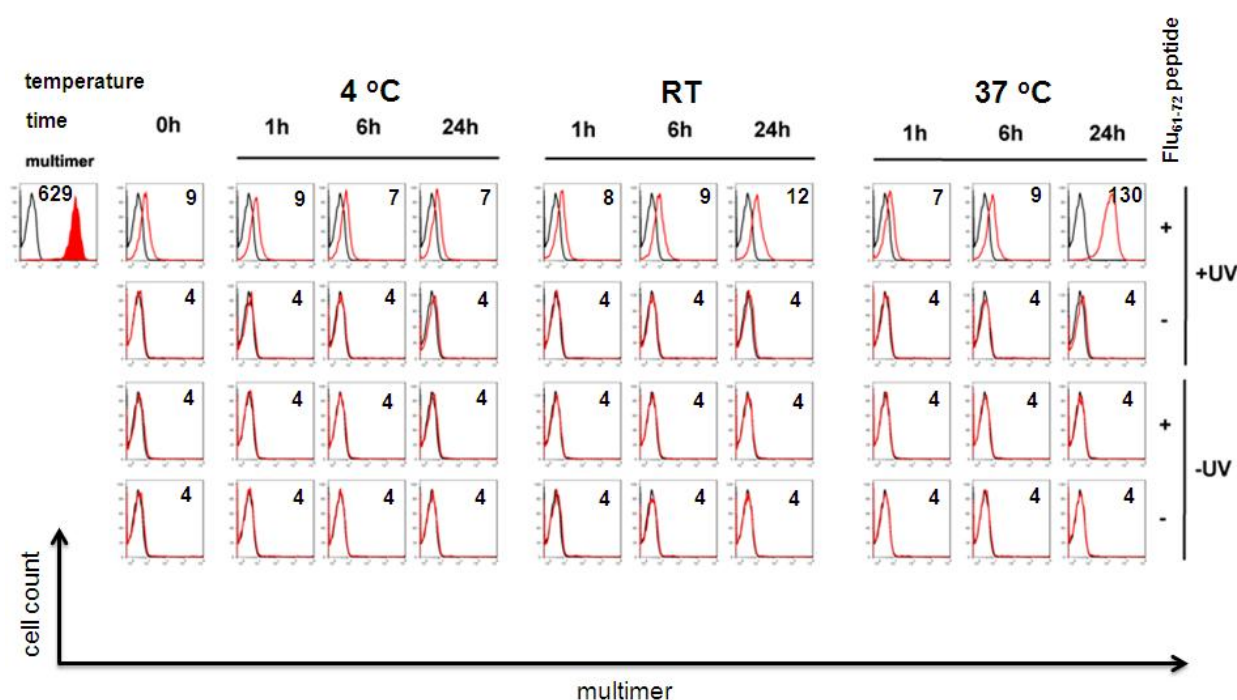


Figure 3.24 Optimization of peptide exchange conditions of DR4/HA*5 complexes by multimer staining. A, 1 μ g biotinylated DR4/HA*5 complexes in 50 μ l at pH 6.0 were irradiated (+UV) or not (-UV) for 10 min at 365 nm on ice and incubated for 1, 6 or 24 hours at 4 °C, RT or 37 °C with 10 μ M Flu-MP₆₁₋₇₂ peptide at pH 6.0, diluted with 50 mM Tris pH 9.0 and multimerized with SA-PE. A DR4/Flu-MP₆₁₋₇₂-specific clone was stained with the resulting multimers for 1 hour at 37 °C and analyzed by flow cytometry. Inserted numbers indicate mean fluorescence intensities of cell-associated multimer. Black histograms refer to the DR4/CLIP multimer staining. The experiment was performed twice. A representative experiment is shown.

Multimers prepared with affinity-purified DR4 complexes via N-terminal peptide His-tags were used for comparison. Peptide-exchanged DR4 multimers were less efficient in staining specific cells than multimers made from affinity-purified DR4 complexes used at the same concentration. Peptide-exchanged multimers prepared with peptides at 0.1, 1 and 10 μ M had nearly identical staining patterns when applied at the same concentration, while more efficient staining was obtained when the exchange peptide at 100 μ M was used (Fig. 3.25).

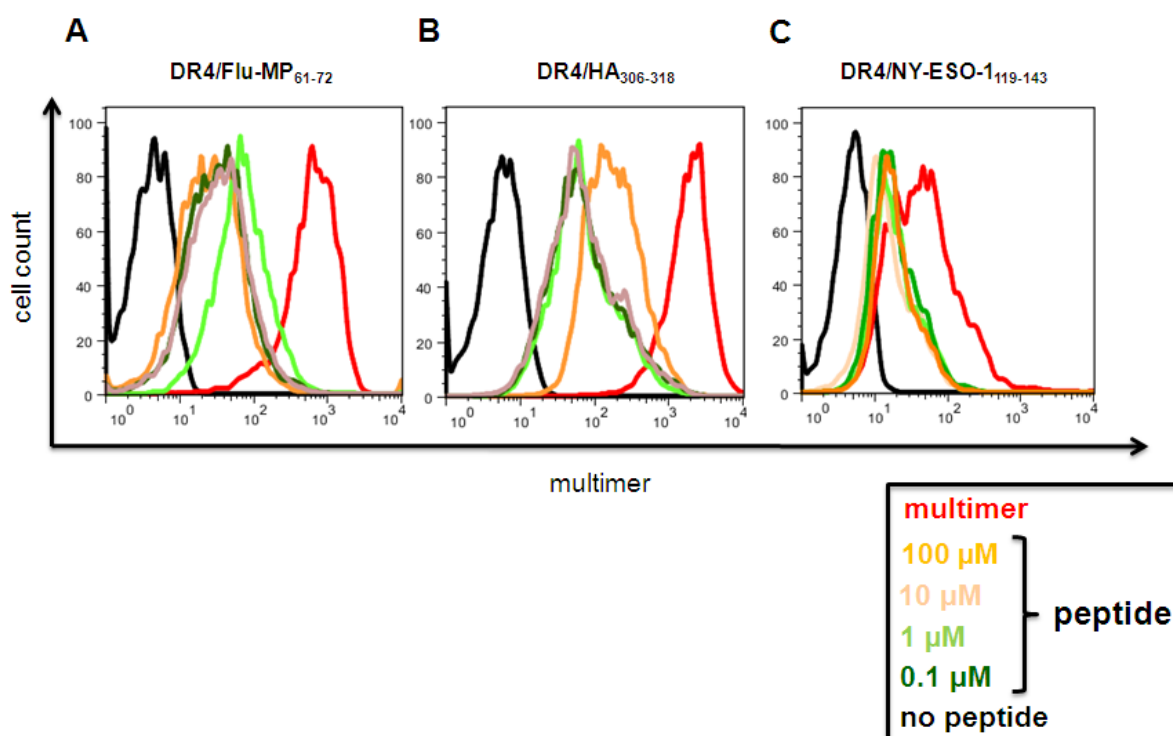


Figure 3.25 Staining of antigen-specific CD4⁺ T cell clones with peptide-exchanged multimers. A-C, 3 $\mu\text{g}/\text{ml}$ of SA-PE multimers prepared with photosensitive biotinylated DR4/HA*5 complexes and loaded with different concentrations of Flu-MP₆₁₋₇₂ (left), HA₃₀₆₋₃₁₈ (center), or NY-ESO-1₁₁₉₋₁₄₃ (right) peptides (from 0.1 μM in dark green to 100 μM in yellow). Non-specific background staining was assessed by using 3 $\mu\text{g}/\text{ml}$ DR4/HA*5 multimers (black histograms). As positive controls immunopure multimers were used (red histograms). A representative experiment out of two is shown.

Taken collectively these results indicate that the use of conditional peptide ligands is a viable and attractive means to substantially increase loading of peptides to MHC class II molecules, especially of peptides that inefficiently bind to empty molecules. We argue that combination of this strategy with the use of conditional N-terminal DTB peptide tags and affinity purification of *bona fide* cognate MHC class II-peptide monomers is a preferred method to produce high quality MHC class II-peptide multimers.

3.2 Discussion

The present study unequivocally demonstrates that peptide loading of “empty” recombinant HLA class II proteins is erratic and for some peptides (e.g. NY-ESO-1₁₁₉₋₁₄₃) remarkably inefficient and that this can dramatically impair staining performance of fluorescent multimers prepared with such monomers (Fig. 3.9). Factors that contribute to incomplete and erratic peptide loading of “empty” HLA class II molecules include: 1) MHC class II molecules are typically purified by immunoaffinity chromatography, which require extreme pH for elution (pH=11.5 or pH 3.2, depending on the antibody). MHC class II proteins, especially “empty” ones, are prone to rapidly denature under such conditions and thereby lose their ability to bind peptide. 2) The ability of antigenic peptides to be loaded onto “empty” MHC molecules can vary considerably from peptide to peptide and may not correlate with the binding affinity of the peptide (Fig. 3.5).

In order to produce homogenous MHC class II-peptide complexes, small tags, such as dinitrophenyl (DNP), His-tag or biotin were added onto the peptide to allow affinity purification of correctly peptide-loaded complexes (Day et al., 2003; Demotz et al., 1991; Nag et al., 1994). However, none of these techniques gained broader acceptance for the preparation of fluorescent MHC-peptide multimers, partly because some tags (e.g. DNP) tended to worsen peptide solubility and caused concerns for MHC and/or TCR binding.

Based on these findings and in order to produce high quality MHC class II-peptide staining reagents we examined different peptide tags for their suitability to isolate molecularly defined, also referred to as “immunopure”, MHC class II-peptide monomers. From those published previously, only the His-tag turned out to be practically useful. Using a His-tag added on the peptide’s N- or C-termini, homogeneous complexes could be purified (referred to as “immunopure”) and staining of specific cells with resulting multimers was improved, sometimes dramatically, as demonstrated in the case of DR4 or DR52b/His-NY-ESO-1₁₁₉₋₁₄₃ (Fig. 3.9). By analyzing binding of mixed multimers (Fig 3.6) and multimer binding isotherms (Fig 3.12) on a panel of DR4/HA₃₀₆₋₃₁₈-specific clones, we demonstrated MHC class II-peptide complex heterogeneity, due to incomplete peptide loading of MHC molecules, precluded reliable detection of low-avidity clonotypes, which can be very frequent in CD4⁺ T-cell responses (Gebe et al., 2003; Sabatino et al., 2011).

We successfully applied this strategy to different HLA class II alleles (DR1, DR4, DR52b and DP4) and peptides, demonstrating the general applicability of this strategy (Fig. 3.9) and

unpublished data (Ayyoub et al., 2010a; Ayyoub et al., 2010b). As shown for DR52b/His-NY-ESO₁₁₉₋₁₄₃, the use of immunopure multimer could dramatically improve staining of NY-ESO-1-specific CD4⁺ T cells in PBMC from melanoma patients as compared to conventional multimers (Fig. 3.9, 3.10) (Ayyoub et al., 2010a). In particular, it made possible for the first time a direct analysis of *ex vivo* analysis of such cells.

Because it has been shown that peptide residues flanking the core of CD4⁺ T cell epitopes could influence TCR recognition (Carson et al., 1997), as well as peptide binding to MHC class II molecules (Adams and Humphreys, 1995; Rötzschke et al., 1999), a caveat of this strategy is that the added peptide tag may bias multimer staining. To circumvent this, we linked the His-tag to the peptide via a linker containing photosensitive β -(2-nitro)phenylglycine to allow its removal by irradiation at 365 nm (Fig. 3.11). This UV irradiation is safe for MHC class II peptide complexes, which do not absorb light at this wavelength, as demonstrated by multimer binding experiments (Fig. 3.12).

It is noteworthy that we unsuccessfully tried to apply the same strategy to murine MHC class II molecules, namely I-A^b. Unlike HLA class II molecules, especially HLA-DR, I-A^b was found not to be stable as “empty” molecule. In fact, to our knowledge, not a single murine MHC class II peptide complex has ever been made via peptide loading of “empty” soluble recombinant H-2 molecules. The only strategy that allows preparation of H-2 class II tetramers consist in tethering the peptide of interest on the N-terminus of the MHC class II β -chain via a long and flexible linker (Fremont et al., 1996a). It should be cautioned, however, that although this way the peptide is part of the molecule, this is no guarantee that it is properly nested in the MHC peptide binding groove (Landais et al., 2009). Therefore, this strategy has the same problem of not knowing the extent of nominal peptide loading, as has the conventional peptide loading of empty HLA class II molecules.

We successfully adapted the NTamer multimer format (Figs. 3.16, 3.17) (Schmidt et al., 2011) for MHC class II-peptide complexes and thus created reversible MHC class II-peptide multimers, providing equal or better staining than the conventional or “immunopure” SA-PE multimers (Figs. 3.18, 3.19). The use of a tandem His-tag to bind MHC class II-peptide monomers to the SA-PE NTA₄ precluded the use of the His-tag for MHC-peptide isolation. We therefore tested various N-terminal polyanion sequences (Fig. 3.14 and Table 3.3) and desthiobiotin (Fig. 3.15), as alternative purification tags; both of which have been used successfully to isolate recombinant proteins (Stubenrauch et al., 2000; Suominen et al., 1992; Wu and Wong, 2004). The polyanionic tags (E₈ and E₈) were able to well separate MHC-

peptide complexes of interest, but required elution conditions which proved to be deleterious for their integrity. In addition, the synthesis of peptides with polyanionic tags was often difficult, costly and with poor yields. On the other hand, we demonstrated that the desthiobiotin tag was best suited because of mild elution conditions (pH 7.4) which preserved the integrity of the MHC-peptide complexes; in addition the synthesis of DTB-tagged peptides was facile. We found the MHC class II NTAmers to be stable at a wide range of temperatures, unlike reversible multimer formats developed for the MHC class I-peptides which can be used only at 4 °C (Guillaume et al., 2006; Knabel et al., 2002). We and others have confirmed that optimal MHC class II-peptide multimer staining requires plasma membrane fluidity, active cellular processes and desialylation (Figs. 3.2, 3.3, 3.4) (Cameron et al., 2001; Cecconi et al., 2008; Novak et al., 2001; Reddy et al., 2003). It is interesting to note that human DR4/HA₃₀₆₋₃₁₈-specific cells are able to separate Cy5-labeled HA₃₀₆₋₃₁₈ from internalized DR4/Cy5-HA₃₀₆₋₃₁₈ complexes (Fig. 3.3). This indicated that these cells could potentially cross-present the internalized peptide and induce adverse T cell-T cell interactions. NTAmers could therefore prove especially useful for isolation of untouched antigen-specific CD4⁺ T cells for basic research and clinical applications.

While the use of conditional peptide tags allows the preparation of “immunopure”, *bona fide* HLA class II-peptide complexes, depending on the allele and peptide can be low ($\leq 20\%$) due to inefficient peptide loading. We therefore investigated whether peptide loading can be substantially increased by means of conditional peptide ligands. For HLA class I molecules, UV-mediated ligand exchange technology is well established (Bakker et al., 2008; Toebes et al., 2006) and allows the generation of a vast diversity of MHC-peptide multimers with minimal effort. We reasoned that this strategy should also be applicable to HLA class II peptide complexes and should allow substantial increase of peptide loading efficiency of some peptides (e.g. NY-ESO-1₁₁₉₋₁₄₃) when using a strongly loading conditional peptide (e.g. a HA₃₀₆₋₃₁₈ peptide derivative HA*5 (Figs. 3.20, 3.21)). Suitable conditional, i.e. UV-photocleavable ligands should fulfill the following criteria: i) they should bind to given HLA class II molecules with high efficiency and should exhibit broad binding specificity, i.e. should bind to multiple alleles, e.g. like the HA₃₀₆₋₃₁₈ peptide that very efficiently binds to nearly all HLA-DR molecules; ii) upon UV irradiation they should disintegrate, i.e. photolyse rapidly; iii) photolysis fragments should dissociate rapidly to generate intermediate “empty” HLA class II molecules that avidly binding peptides. As a proof of principle a structure-based approach was used to identify a suitable photocleavable derivative of the HA₃₀₆₋₃₁₈ peptide,

similar as has been described for DR2/MBP₈₅₋₉₉ (Grotenbreg et al., 2007). Out of four candidate peptide variants examined, only one satisfied all three criteria (Figs 3.27, 3.28, 3.29). However, the third criterion was satisfied only partially, because 24-54% of the peptide remained bound to the DR4 protein, even though the photolysis was apparently complete. Systematic evaluation of peptide loading conditions indicated as optimal ones incubated for 24 hours at 37 °C and pH 6.0, which facilitate peptide exchange due to the “open” conformation of MHC class II molecules (Boniface et al., 1996; Runnels et al., 1996; Sette et al., 1992). DR4/HA*5 complexes allowed for substantially improved loading of problematic peptides, as demonstrated for DTB-NY-ESO-1₁₁₉₋₁₄₃ (Fig. 3.29). For the HA₃₀₆₋₃₁₈, Flu-MP₆₁₋₇₂ and NY-ESO-1₁₁₉₋₁₄₃ peptides it was possible to obtain peptide-exchanged multimers that stained specific cells, and the quality of staining depended on the concentration of the peptide used for exchange.

3.3 Conclusion and perspectives

MHC class II-peptide multimers are important tools for detection, enumeration and isolation of antigen-specific CD4⁺ T-cells. Their erratic performance prevented widespread use and consequently they had limited impact on the study of CD4⁺ T cell responses. We found that a major obstacle for this was in the quality of recombinant MHC class II-peptide complexes, frequently prepared by peptide loading. We observed that the affinity of the peptide for the MHC class II molecule is not necessarily related to the extent of peptide loading. By adding a His-tag or desthiobiotin to the N-terminus of the MHC class II-binding peptides and subsequently isolating “immunopure” MHC class II-peptide monomers by affinity chromatography we could significantly, sometimes dramatically, improve staining of antigen-specific CD4⁺ T cells. Inserting a photolabile β-(2-nitro)phenylglycine residue between the tag and the MHC-binding peptide, allowed the removal of the tag from the “immunopure” MHC class II-peptide complex, thereby eliminating potential concerns for interference with TCR binding. We also successfully adapted the NTAmer multimer format, originally developed for MHC class I-peptide multimers for MHC class II-peptide complexes. Finally, by replacing the Asn312 in the HA₃₀₆₋₃₁₈ peptide from influenza A hemagglutinin we generated a broadly applicable photocleavable peptide, HA*5, and showed that DR4/HA*5 complexes exhibit improved, UV-dependent loading, opening new perspectives for the future. Currently developed for the fluorescence-based flow cytometry, NTAmers can be easily modified to suit the needs of the emerging, more powerful, time-of-flight cytometry

(Newell et al., 2012). With the ever-greater realization of the role that CD4⁺ T cells play in cancer and antiviral immunity, and in particular cytotoxic CD4⁺ T cells (Quezada et al., 2010; Xie et al., 2010), the reversible “immunopure” NTAmers should be most useful tools for future CD4⁺ T cell sorting and analysis.

CHAPTER II

4. Essential role of the CD8 α transmembrane domain for efficient CD8 coreceptor function

4.1 Results

4.1.1 Role of transmembrane domains for CD8 coreceptor function

Transmembrane domains (TMDs) of membrane proteins play important roles besides providing anchors for the lipid bilayer of the plasma membrane. Assembly or oligomerization of receptors is at least in part driven by TMD-TMD interactions and is important for their signaling function; inhibition of such interactions can lead to different pathological disorders (Fink et al., 2012). Assembly of MHC class II proteins (Cosson and Bonifacio, 1992), the TCR:CD3 complex (Call and Wucherpfennig, 2005) and CD8 (Hennecke and Cosson, 1993) are all driven by TMD-TMD interactions. Such interactions are mediated mainly by Van der Waals contacts, but hydrogen bonds bridging polar residues and aromatic residues capable of π - π stacking provide important contributions. Analyses of TMD sequences revealed the existence of numerous motifs mediating such interactions: i) the most common, GxxxG motif; ii) leucine heptad motif; iii) the Polar-xx-Polar motif, where polar amino acids can be Ser, Thr, Glu, Gln, Asp and Asn; iv) Aromatic-xx-Aromatic motif; v) a Gly zipper (GxxxGxxxG) motif; vi) Leu zipper and vii) Ser/Thr rich sequences. A special motif present in immune receptors encompassing the combination of polar and aromatic residues, called CART, has been postulated to play a role in T cell signaling (Campbell et al., 1994). It has been previously shown that for homodimerization of murine CD8 α , the TMD of CD8 α plays an important role together with the extracellular part of CD8 α (Hennecke and Cosson, 1993). Conversely, formation of the CD8 $\alpha\beta$ heterodimer is entirely driven by interactions of the chain's extracellular domains, which is also true for the human CD8 $\alpha\beta$ (Pang et al., 2007). The TMD of CD8 β apparently is not involved in CD8 β homo- or heterodimerization. Thus, in a CD8 $\alpha\beta$ heterodimer, the CD8 α TMD is free to interact with CD8 α TMD of another CD8 $\alpha\beta$ and to thus form CD8 $\alpha\beta$ dimers. To investigate the functional significance of CD8 α TMD, we generated a mutant, CD8 α_{Tac} , in which the CD8 α TMD was replaced with the one from the partially monomerizing ($44.5 \pm 14\%$ monomer) interleukin-2 receptor α chain (Tac) (Hennecke and Cosson, 1993). We investigated molecular and functional implications using T1 T cell hybridomas. The T1 TCR has been cloned from CD8 $^+$ CTLs derived from mice immunized with the PbCS(ABA) peptide (SYIPSAE(ABA)I). In this system, UV-irradiation

at 312 nm the ABA group (4-azido-benzoic acid) to cross-link to bound TCR (photoaffinity labeling), which allows binding studies with monomers to be performed on living cells. The T1 TCR is CD8-independent for the recognition of the PbCS(ABA) peptide, but not for its weak agonist P255A (Luescher et al., 1995a; Luescher et al., 1992; Luescher et al., 1991).

4.1.2 Cell surface expression of CD8 α and CD8 α_{Tac} on T1 T cell hybridomas

Alignment of the CD8 α TMDs for a variety of mammalian species (Fig. 4.1A) revealed highly conserved sequence motifs. The alignment of CD8 β TMDs, conserved to a modest degree, is shown for comparison (Fig. 4.1B). Sequence conservation is visualized by the sequence logo of each alignment (Fig. 4.1C).

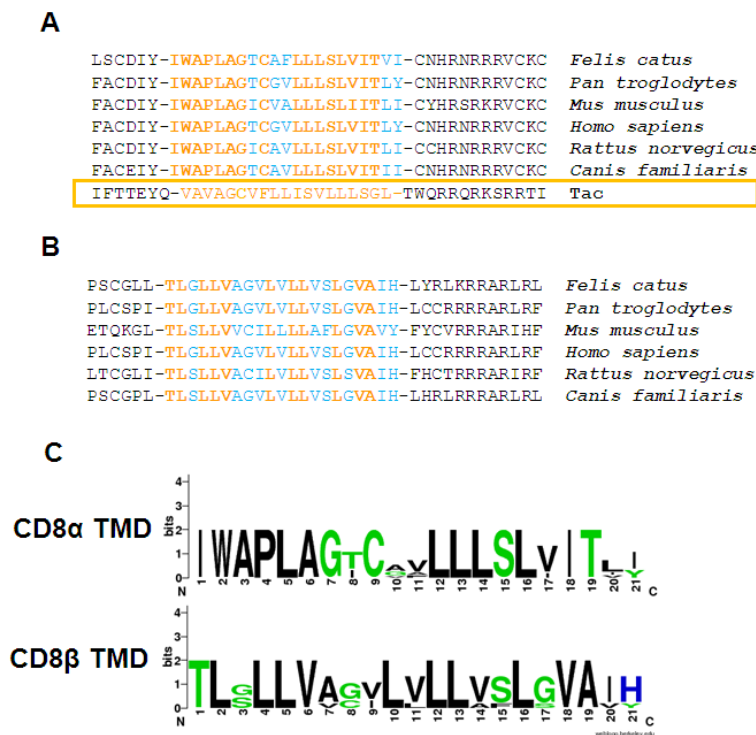


Figure 4.1 Sequence alignments of transmembrane domains of CD8 α and CD8 β . Transmembrane domains of CD8 α (A), and CD8 β (B) from selected mammalian species. Completely conserved residues are shown in orange, while differing residues are shown in blue. C, The consensus sequence is shown in logo cartoon format with black capital letters indicating absolutely conserved residues, and smaller sized letters in black, green and blue indicating a lesser degree of sequence conservation.

The expression of wild type CD8 α and mutant CD8 α_{Tac} was examined on the T1.4 (T1 TCR+ CD8 α - CD8 β -) T cell hybridoma transduced with lentiviral constructs for CD8 α and CD8 α_{Tac} , respectively and FACS sorted. The CD8 α and CD8 α_{Tac} were expressed at comparable, high levels (Fig. 4.2A). The expression of CD8 α insignificantly affected TCR expression, while the cells remained negative for CD8 β . Following introduction of a lentiviral

construct for CD8 β -YFP into cells expressing CD8 α or CD8 α_{Tac} and subsequent FACS sorting, cells expressing similar levels of YFP were obtained (Fig. 4.2B). Thus, a set of four cell types was generated to investigate the role of TMD replacement. All cells derived from T1.4 maintained similar levels of the T1 TCR, CD8 α and CD8 β (Table 4.1).

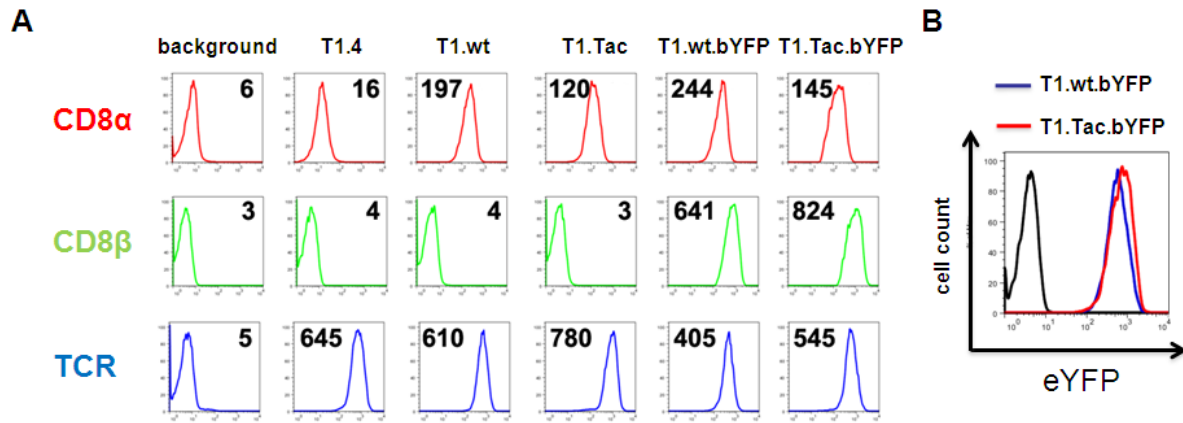


Figure 4.2 *Characterization of T1 hybridomas expressing CD8 α or CD8 α_{Tac} .* **A**, Cells were stained with PE-labeled anti-CD8 α , anti-CD8 β , or Alexa 647-labeled anti-V β 8.2 antibodies and fluorescence levels measured by flow cytometry. T1.4 cells express the T1 TCR but no CD8 α or CD8 β chains. Cells expressing the CD8 α or CD8 α_{Tac} , but no CD8 β , are referred to as T1.wt and T1.Tac, respectively. Alternatively, if CD8 β is expressed in the form of the CD8 β -eYFP fusion protein, cells are referred to as T1.wt.bYFP and T1.Tac.bYFP. A representative experiment is shown out of at least two independent ones. Errors in Table 4.1 represent SD. **B**, Levels of eYFP measured by flow cytometry are shown in histograms. A representative experiment is shown out of at least two independent ones.

Table 4.1 *Surface expression of CD8 α , CD8 β and TCR on T1 hybridomas.*

	T1.4	T1.wt	T1.Tac	T1.wt.bYFP	T1.Tac.bYFP
CD8α	12.6 \pm 5	170.0 \pm 38.2	152.5 \pm 46	293.5 \pm 70	169 \pm 34
CD8β	3.4 \pm 0.2	3.7 \pm 0.1	3.3 \pm 0.1	612.5 \pm 40	718.5 \pm 149
TCR	652.5 \pm 11	627.5 \pm 25	835.0 \pm 78	509.0 \pm 147	551.5 \pm 9

4.1.3 K^d/PbCS(ABA) multimer binding

To examine whether replacement of the CD8 α TMD affected ligand binding, we measured multimer binding at room temperature on CD8 β ⁺ cells expressing CD8 α (T1.wt.bYFP) or CD8 α_{Tac} (T1.Tac.bYFP). To this end, the cells were incubated with PE-labeled K^d/peptide multimers. Two different peptide ligands were used; the high affinity PbCS(ABA) ligand and its variant, P255A, which has a lower affinity for the T1 TCR (Luescher et al., 1995a). To

gauge the contribution of CD8 to multimer binding, we used complexes of CD8-binding deficient K^d Q226A/D227K ($K^d_{226/227}$) mutant multimers containing PbCS(ABA) (Fig. 4.3A, D) or blocking anti-CD8 β mAb H35 (Fig. 4.3B,C,E,F). Dissociation constants (K_D) were determined by nonlinear regression analysis of the MFI values of bound multimers (Table 4.2). CD8 $\alpha_{Tac}\beta$ hybridomas bound K^d /PbCS(ABA) multimers with modestly weaker avidity as compared to CD8 $\alpha\beta$ hybridomas ($K_D=3.0\pm 0.3$ versus 2.5 ± 0.3). Moreover, the difference in binding avidity (ΔK_D) between the K^d wild-type PbCS(ABA) and $K^d_{226/227}$ /PbCS(ABA) multimers was greater for CD8 $\alpha\beta$ hybridomas (3.8-fold) than for CD8 $\alpha_{Tac}\beta$ hybridomas (1.5-fold), indicating a lesser contribution of the CD8 coreceptor to multimer binding. The difference in maximal binding of K^d /PbCS(ABA) P255A multimers was dramatic, as CD8 $\alpha_{Tac}\beta$ hybridomas exhibited only ~8% of maximal binding of K^d /PbCS(ABA) multimers (Fig. 4.3F) while the CD8 $\alpha\beta$ hybridomas reached ~50% of maximal binding of K^d /PbCS(ABA) multimers (Fig. 4.3C). The binding experiments were repeated in the presence of an anti-CD8 β blocking antibody (H35). The H35 mAb strongly reduced maximal binding (B_{max}) of K^d /PbCS(ABA) multimers, which was essentially halved in CD8 $\alpha\beta$ (53%) and CD8 $\alpha_{Tac}\beta$ hybridomas (46%) with little changes of K_D values (3.1 ± 0.2 and 4.0 ± 0.2 for CD8 $\alpha\beta$ and CD8 $\alpha_{Tac}\beta$ hybridomas, respectively) (Fig. 4.3B,E and Table 4.2). For K^d /PbCS(ABA) P255A multimers, the binding difference between the two hybridomas was dramatic (Figs. 4.3C,F) and completely ablated in the presence of H35 mAb, indicating that the binding of K^d /PbCS(ABA) P255A multimers was entirely CD8 β -dependent. Collectively our data indicated that replacement of the TMD of the CD8 α with the one of Tac, reduced the CD8 $\alpha\beta$ -mediated increase in multimer binding, in particular of the weak agonist K^d /PbCS(ABA) P255A multimers; in other words this mutation affected the ability of CD8 to strengthen the MHC-peptide binding, which is an important aspect of CD8 coreceptor function.

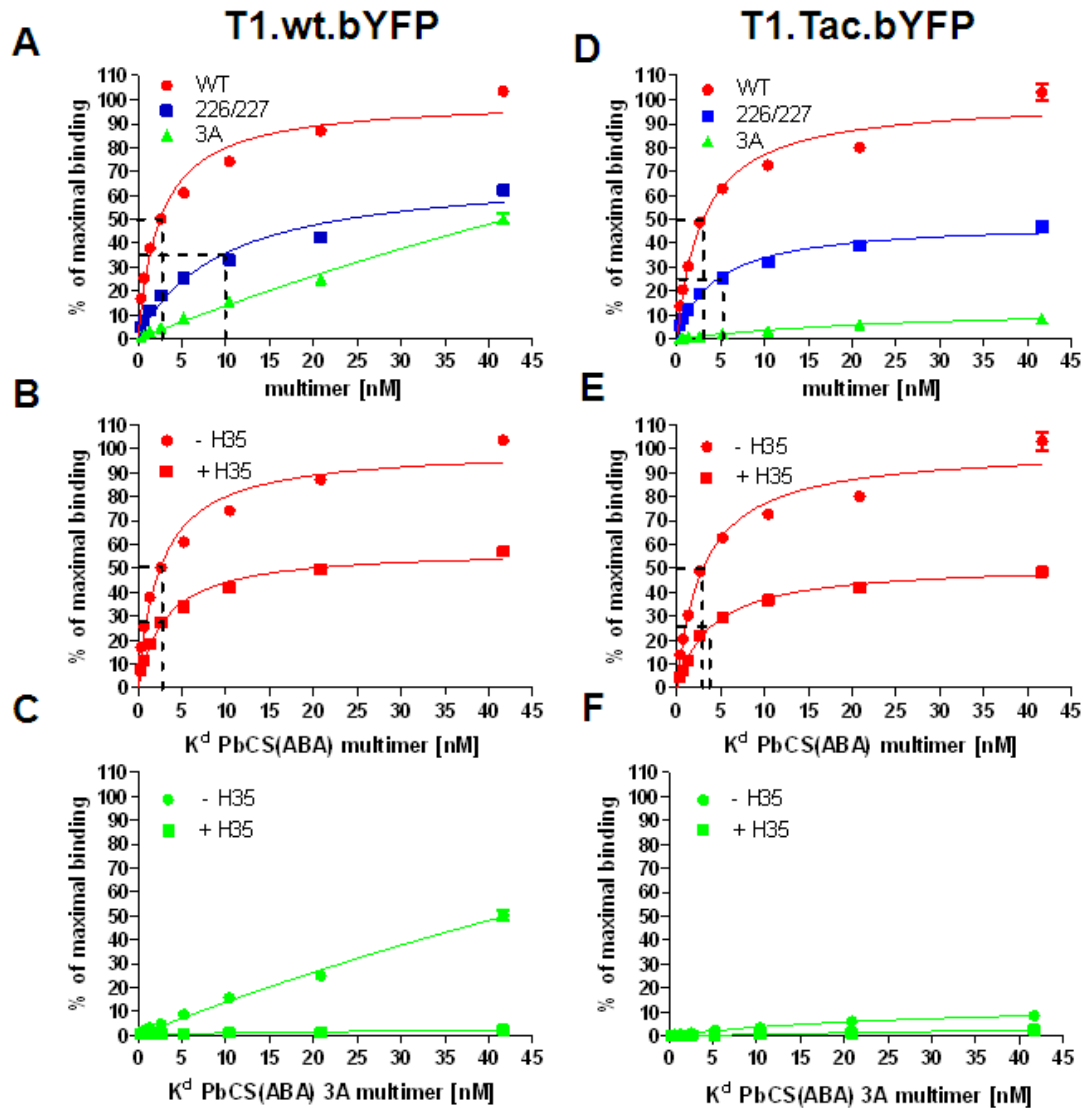


Figure 4.3 K^d /*PbCS(ABA)* multimer binding on *T* cell hybridomas. Room temperature binding isotherms of PE-labeled multimeric K^d /*PbCS(ABA)*, $K^d_{226/227}$ /*PbCS(ABA)* and K^d /*PbCS(ABA)* P255A ligands labeled WT (red), 226/227 (blue) and 3A (green) on T1.wt.bYFP (A-C) and T1.Tac.bYFP (D-F). Binding data were normalized by taking B_{max} of the K^d /*PbCS(ABA)* multimer binding isotherm as 100%. Room temperature binding isotherms of K^d /*PbCS(ABA)* (B and E) and K^d /*PbCS(ABA)* P255A (C and F) in the presence (squares) or absence (circles) of anti-CD8 β mAb H35 blocking antibody (20 μ g/ml) on T1.wt.bYFP and T1.Tac.bYFP cells. Representative data from two experiments are shown. Error bars represent SEM from duplicates.

Table 4.2 K_D and B_{max} values from K^d /PbCS(ABA) multimer binding.

K_D [nM]	K^d PbCS(ABA) - H35	K^d PbCS(ABA) + H35	$K^d_{226/227}$ PbCS(ABA)
T1.wt.bYFP	2.5±0.3	3.1±0.2	9.6±1.5
T1.Tac.bYFP	3.0±0.3	4.0±0.2	4.4±0.5

B_{max}	K^d PbCS(ABA) - H35	K^d PbCS(ABA) + H35	$K^d_{226/227}$ PbCS(ABA)
T1.wt.bYFP	100±2.9	57.8±1.2	70.3±4.2
T1.Tac.bYFP	100±3.0	51.7±0.7	48.9±1.7

4.1.4 Calcium flux and IL-2 production is impaired on hybridomas expressing $CD8\alpha_{Tac}$

To examine the effect of $CD8\alpha$ TMD replacement on functional responses, we measured intracellular calcium flux upon incubation of the hybridomas with PbCS(ABA)-pulsed P815 cells. $CD8\beta^+$ T1 hybridomas expressing wild type $CD8\alpha$ (T1.wt.bYFP) exhibited high intracellular Ca^{2+} flux (67% positive cells), whereas $CD8\beta^+$ hybridoma expressing the $CD8\alpha_{Tac}$ mutant (T1.Tac.bYFP) displayed a significantly reduced response (41% positive cells) and T1.4 ($CD8\alpha^- CD8\beta^-$) hybridoma even less (11% positive cells) (Fig. 4.4A). We next assessed the IL-2 responses of the $CD8\beta^+$ hybridomas upon incubation with P815 cells pulsed with graded concentrations of the PbCS(ABA) peptide. As shown in Fig. 4.4B and Table 4.3, the $CD8\alpha_{Tac}\beta$ hybridoma were less responsive than the $CD8\alpha\beta$ hybridoma ($EC_{50}=764.8$ pM versus 25.9 pM, respectively). The presence of the anti- $CD8\beta$ mAb H35 significantly impaired sensitivity of IL-2 production by $CD8\alpha\beta$ hybridomas ($EC_{50}=465.7$ pM, $\Delta EC_{50}\sim 18$ -fold), and to a lesser degree in $CD8\alpha_{Tac}\beta$ hybridomas ($EC_{50}=4545$ pM, $\Delta EC_{50}\sim 6$ -fold). We previously observed that CD8 was essential for K^d /PbCS(ABA) P255A multimer binding, and therefore we expected IL-2 production to follow suit. This proved to be indeed the case. $CD8\alpha\beta$ hybridomas produced IL-2 upon incubation with PbCS(ABA) P255A peptide pulsed APCs, however considerably less efficiently as compared to PbCS(ABA) pulsed APC ($EC_{50}=1160$ pM) (Fig. 4.4B). By contrast, $CD8\alpha_{Tac}\beta$ hybridomas failed to produce any detectable IL-2 in response to any concentration of the PbCS(ABA) P255A peptide tested, regardless of the presence or absence of the anti- $CD8\beta$ mAb H35.

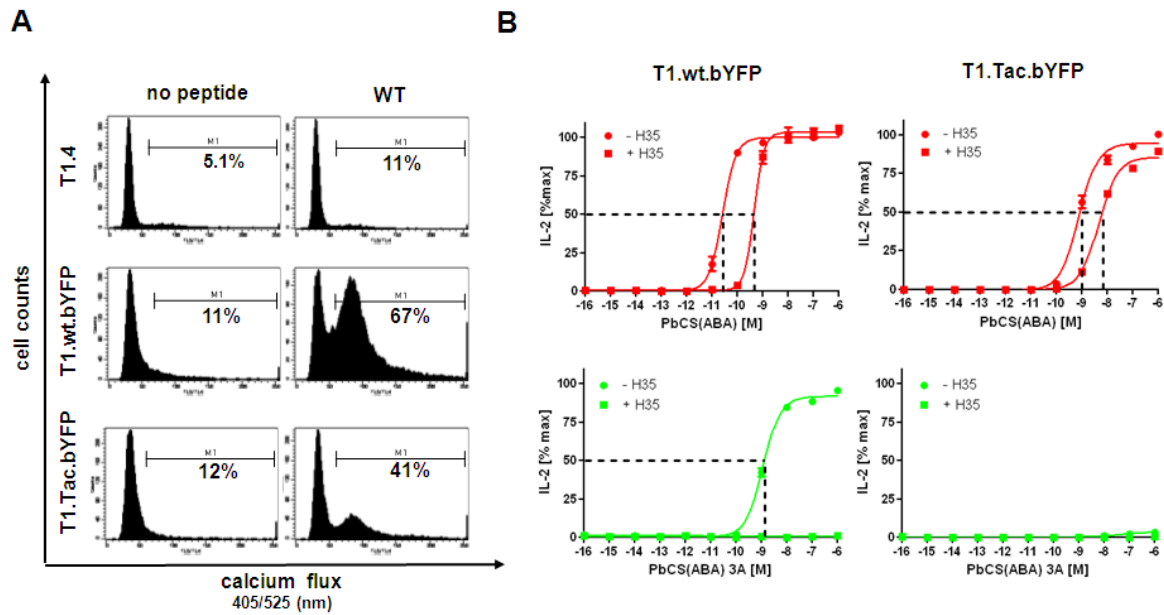


Figure 4.4 *Intracellular calcium flux and IL-2 production of CD8 $\alpha_{Tac\beta}$ hybridomas are impaired.* **A**, Calcium flux of Indo-1 loaded T1.4, T1.wt.bYFP and T1.Tac.bYFP cells when stimulated with P815 cells pulsed (WT) or not (no peptide) with 1 μ M PbCS(ABA) peptide. **B**, IL-2 production of T1.wt.bYFP and T1.Tac.bYFP cells with P815 cells pulsed with graded concentrations of PbCS(ABA) (WT) or its P255A variant (3A) peptide in the presence (squares) or absence (circles) of anti-CD8 β mAb H35 blocking antibody was measured by ELISA. Representative experiments from at least two independent experiments are shown. Values are normalized to maximal IL-2 secretion of T1.wt.bYFP cells taken as 100%.

Table 4.3 *EC₅₀ values of IL-2 secretion*

EC ₅₀ [pM]	K ^d PbCS(ABA) - H35	K ^d PbCS(ABA) + H35	K ^d PbCS(ABA) P255A - H35
T1.wt.bYFP	25.9	465.7	1160
T1.Tac.bYFP	764.8	4545	-

4.1.5 Assessment of the proximity of CD8 and TCR:CD3 by FRET

We wished to assess the proximity of CD8 to TCR:CD3 by FRET on CD8 β^+ T1 hybridomas expressing CD8 α or CD8 α_{Tac} . First, the proximity was measured in the absence of MHC-peptide (Fig. 4.5A) by co-staining CD8 $\alpha\beta$ and CD8 $\alpha_{Tac\beta}$ hybridomas with the PE-labeled anti-CD3 ϵ mAb 17A2 or anti-TCR β mAb H57 and Cy5-labeled anti-CD8 β mAb KT112. We observed more CD3 ϵ -CD8 β FRET (FRET units=3.7 \pm 0.1) and TCR-CD8 β (FRET units=2.3 \pm 0.2) on CD8 $\alpha\beta$ hybridomas than on CD8 $\alpha_{Tac\beta}$ hybridomas (CD3 ϵ -CD8 β FRET units=2.0 \pm 0.1 and TCR-CD8 β FRET units=1.1 \pm 0.1). Moreover, when PE-labeled K^d/PbCS(ABA) multimers were used as FRET donors, much stronger FRET was observed between the multimer and CD8 β than between the multimer and CD8 α in both CD8 $\alpha\beta$

hybridomas (multimer-CD8 β FRET units=126.6 \pm 27.4 versus multimer-CD8 α FRET units=50.2 \pm 11.8) and CD8 $\alpha_{\text{Tac}}\beta$ hybridoma (multimer-CD8 β FRET units=65.7 \pm 25.2 versus multimer-CD8 α FRET units=34.6 \pm 13.1) (Fig. 4.5B). Importantly, multimer-CD8 β FRET observed on CD8 $\alpha_{\text{Tac}}\beta$ hybridomas was significantly weaker than on the CD8 $\alpha\beta$ hybridomas, indicating that CD8 $\alpha_{\text{Tac}}\beta$ associates with the TCR:CD3 less efficiently.

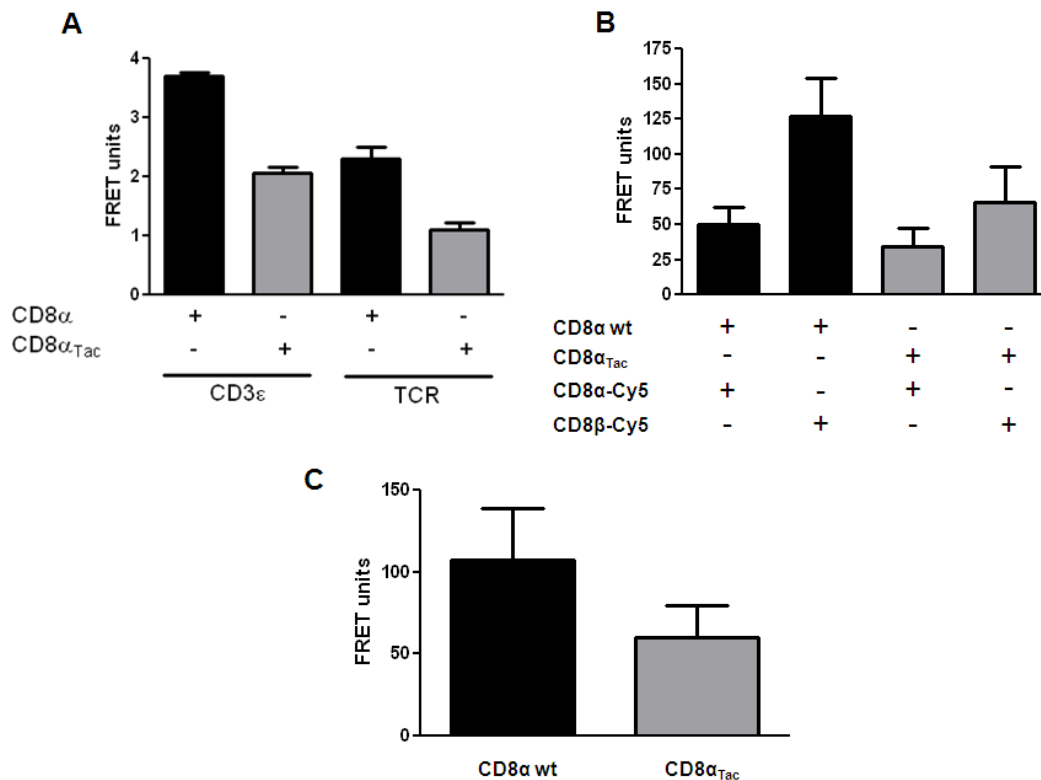


Figure 4.5 *CD8 $\alpha_{\text{Tac}}\beta$ associates inefficiently with TCR:CD3.* **A**, T1 hybridomas expressing CD8 β -eYFP and CD8 α or CD8 α_{Tac} were stained in the cold with PE-labeled anti-CD3 ϵ mAb 17A2 or anti-TCR β mAb H57 and Cy5-labeled anti-CD8 β mAb KT112. **B**, Alternatively, staining was performed with PE-labeled K^d/PbCS(ABA) multimers and Cy5-labeled anti-CD8 β mAb KT112 or anti-CD8 α mAb 53.6.72. **C**, T1 hybridomas expressing wild-type CD8 α or CD8 α_{Tac} were stained with PE-labeled anti-CD90.1 mAb HIS51 and Cy5-labeled CD8 α mAb 53.6.72. Cells were analyzed by FACS using excitation at 488 and 630 nm. FRET units were calculated from the fluorescence emissions at 580 and 670 nm (see “Materials and methods”). For **B** and **C**, mean values and SD were calculated from three experiments, each performed in duplicate, while for **A** from two experiments.

By virtue of palmitoylation at its tail cysteine residue (Cys198), CD8 β confers lipid raft association to the CD8 $\alpha\beta$, thus strengthening its association with p56^{Lck} that also partitions to lipid rafts by virtue of its N-terminal palmitoyl and myristoyl modifications (Arcaro et al., 2000). CD8 α_{Tac} confers partial monomerization of CD8 α normally present in CD8 $\alpha\alpha$ homodimers or CD8 $\alpha\beta$ heterodimers at the cell surface. To compare the extent of raft association of CD8 $\alpha\beta$ and CD8 $\alpha_{\text{Tac}}\beta$, we measured FRET between Thy-1.1 (PE-labeled anti-

Thy-1.1 (CD90.1) mAb HIS51), a constitutive raft marker and CD8 α (Cy5-labeled anti-CD8 α mAb 53.6.72). Indeed, the Thy-1.1-CD8 α FRET was lower on CD8 α_{Tac} hybridomas (FRET units=107.4 \pm 31.7) than on CD8 α hybridomas (FRET units=60.2 \pm 19.5) (Fig. 4.5C).

4.1.6 Multimer and CD8 β co-localize on CD8 $\alpha\beta$ and CD8 $\alpha_{\text{Tac}}\beta$ hybridomas

While co-localization does not necessarily imply interaction between two proteins, the reverse holds true, i.e. if there is no association, two proteins do not co-localize. Having measured more intense FRET between PE-labeled K^d/PbCS(ABA) multimers and Cy5-labeled anti-CD8 β mAb KT112, we examined co-localization of PE and YFP fluorescence on the plasma membrane (Fig. 4.6). To this end, CD8 $\alpha\beta$ and CD8 $\alpha_{\text{Tac}}\beta$ hybridomas were stained with PE-labeled K^d/PbCS(ABA) multimers in the cold and fixed. Membrane distribution of PE and YFP was imaged by fluorescence microscopy. Examination of fluorescence micrographs showed that multimers induced large patches on T1.wt.bYFP and T1.Tac.bYFP hybridomas in which CD8 β -YFP and multimers co-localized to comparable degrees (Fig. 4.6A). This was confirmed by co-localization metrics, indicating similar Pearson's correlation coefficient (0.999 for T1.wt.bYFP and 0.987 for the T1.Tac.bYFP) between YFP and PE pixels and the cytofluorogram showed no difference in co-localization (Fig. 4.6B). The population of pixels parallel to the diagonal, but shifted towards higher YFP values came from multimer patches containing with more accumulated CD8 β -YFP.

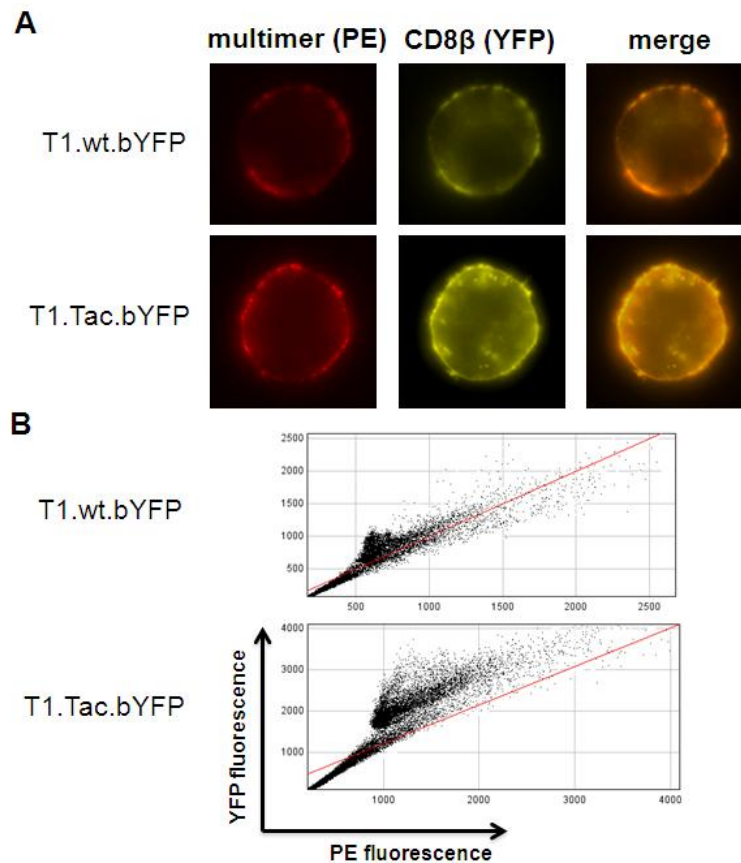


Figure 4.6 *Similar co-localization of K^d /PbCS(ABA) multimer and $CD8\beta$ on $CD8\alpha\beta$ and $CD8\alpha_{Tac}\beta$ cells.* A, T1.wt.bYFP and T1.Tac.bYFP hybridomas were stained with ~40 nM PE-labeled K^d PbCS(ABA) multimer at 4 °C, fixed and imaged by fluorescence microscopy where PE and YFP fluorescence were recorded in separate channels. B, Cytofluorograms of each image are labeled appropriately; images were processed so that only pixels representing cell-surface features were taken into account. Pearson's correlation coefficients were 0.999 for the T1.wt.bYFP image and 0.987 for the T1.Tac.bYFP image. Cytofluorograms and Pearson's correlation coefficients were calculated by the JACoP plugin of the ImageJ program. A representative experiment is shown out of the two.

4.1.7 Expression of $CD3\zeta$ -CFP in hybridomas harboring $CD8\beta$ -YFP and $CD8\alpha$ or $CD8\alpha_{Tac}$

Multimer binding, calcium flux and IL-2 production data indicated a functional impairment of hybridomas expressing $CD8\alpha_{Tac}\beta$ compared to those expressing $CD8\alpha\beta$. Because interaction of the CD8 coreceptor with TCR:CD3 is crucial for initiation of TCR signaling, we wished to assess this interaction in contact areas (immunological synapses) between the hybridoma cell and the peptide-pulsed APC. To this end, we transduced T1 TCR hybridomas expressing $CD8\beta$ -YFP and $CD8\alpha$ or $CD8\alpha_{Tac}$ with the $CD3\zeta$ -eCFP fusion protein. The resulting T cell hybridomas were FACS-sorted and cloned. Clones were selected for comparable surface expression of the T1 TCR, $CD8\alpha$, $CD8\beta$ -YFP and $CD3\zeta$ -CFP (Fig. 4.7A). We next analyzed these cells by flow cytometry for $CD3\zeta$ -CFP and $CD8\beta$ -YFP

fluorescence and found that while the latter exhibited comparable expression, the former showed clearly higher expression on T1.Tac.bYFP.zCFP (Fig. 4.7B,C). This seems at variance with the TCR surface expression, this divergence is explained, at least in part by that CD3 ζ -CFP transfectants express endogenous CD3 ζ and that only a fraction of CD3 ζ is associated with TCR (Yachi et al., 2005b). Moreover, examination by fluorescence microscopy of the hybridomas showed that most of the CD3 ζ -CFP and CD8 β -YFP fluorescence was membrane-associated on both cell types, but that on the T1.Tac.bYFP.zCFP cells there was also a significant fraction of intracellular, perinuclear fluorescence.

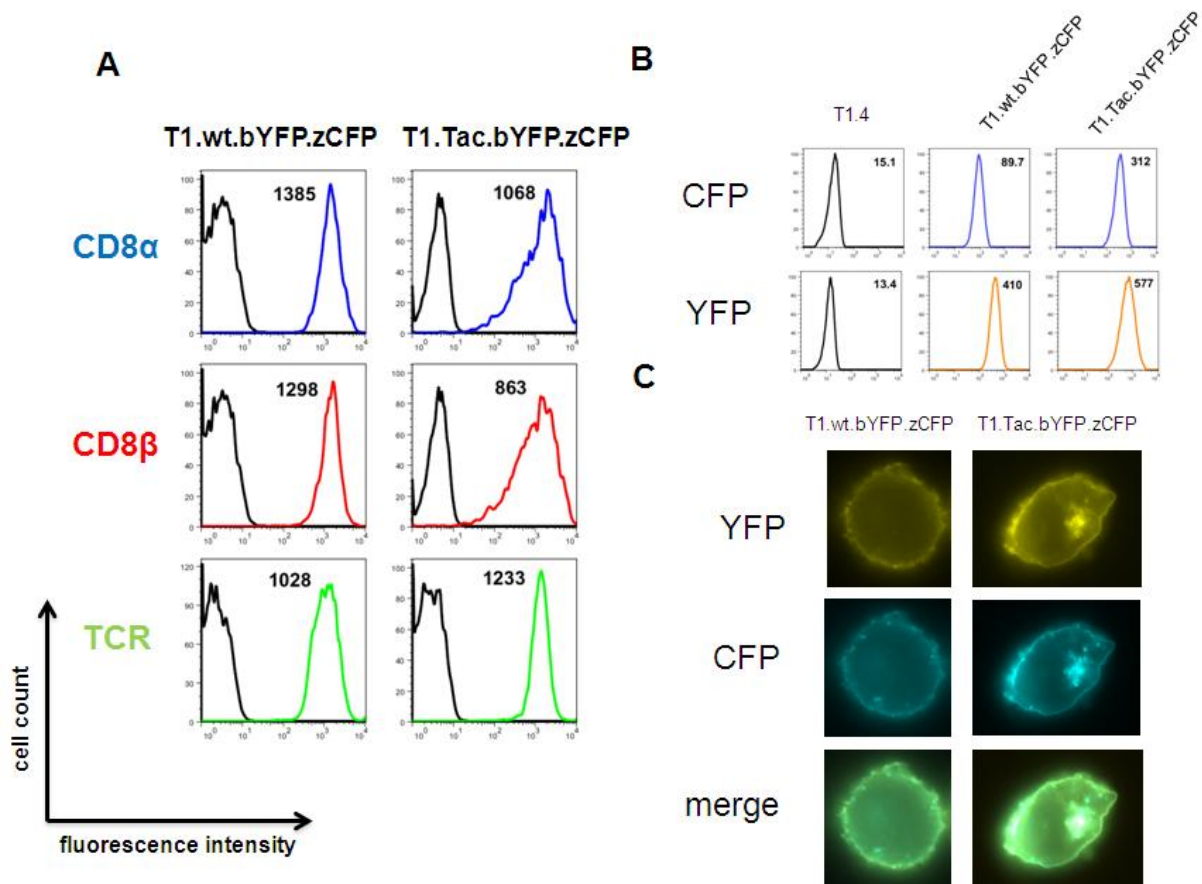


Figure 4.7 *Characterization of CD3 ζ -CFP⁺ CD8 β -YFP⁺ hybridomas.* A, Surface expression of CD8 α , CD8 β and the T1 TCR on T1.wt.bYFP.zCFP and T1.Tac.bYFP.zCFP hybridomas by staining with PE-labeled anti-CD8 α mAb 53.6.72, PE-labeled anti-CD8 β H35 and Alexa 647 labeled anti-V β 8.2. B, Levels of expression of CFP and YFP on T1.wt.bYFP.zCFP and T1.Tac.bYFP.zCFP hybridomas measured by flow cytometry. C, Fluorescence micrographs of CFP and YFP in T1.wt.bYFP.zCFP and T1.Tac.bYFP.zCFP hybridoma. Cells were fixed before imaging. YFP and CFP channels were recorded separately. Calculated MFI values are displayed in the associated histograms. Representative data of two or more experiments.

4.1.8 Antigen-dependent responses of hybridomas expressing CD8 β -YFP, CD3 ζ -CFP and CD8 α or CD8 α_{Tac}

To assess functionality of a new pair of hybridoma cells and to verify whether the introduction of CD3 ζ -CFP altered previous conclusions, we tested fluorescent CD3 ζ -CFP+ T1 TCR hybridomas for their ability to form conjugates, internalize plasma membrane-bound TCRs and to produce IL-2 upon incubation with peptide-loaded APCs. As APCs, P815 cells were used. CD8 $\alpha\beta$ hybridomas (T1.wt.bYFP.zCFP) were able to form conjugates with P815 cells pulsed with the wild-type (WT) peptide, PbCS(ABA), in a time-dependent manner, attaining a maximal frequency of 40% \pm 11% after 10 minutes, followed by a gradual decrease after 20 minutes to 28% \pm 7% at 60 minutes (Fig. 4.8A). With the weak agonist peptide, PbCS(ABA) P255A (3A), the maximal frequency of conjugates was significantly reduced (25% \pm 2%) and was reached only after 20 minutes, thereafter rapidly falling to 11% \pm 3% after 60 minutes (Fig. 4.8A).

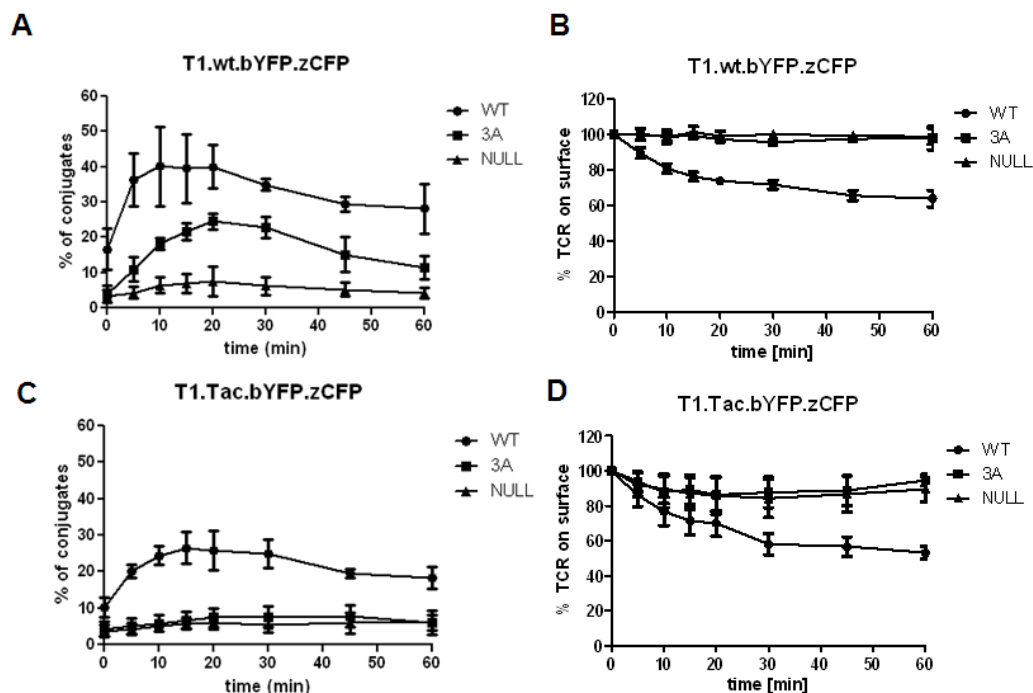


Figure 4.8 Conjugate formation, but not TCR downregulation is impaired in T1.Tac.bYFP.zCFP hybridomas. A,C Time course of conjugate formation of T1.wt.bYFP.zCFP (A) or T1.Tac.bYFP.zCFP (C) with NHS-Cy5 surface labeled P815 cells pulsed with 1 μ M of PbCS(ABA) (WT, circles), PbCS(ABA) P255A (3A, squares) or JAK1 (NULL, triangles). Data are an average of three independent experiments. Error bars represent SD. B,D TCR downregulation of T1.wt.bYFP.zCFP (B) or T1.Tac.bYFP.zCFP (D) with P815 cells pulsed with 1 μ M of PbCS(ABA) (WT, circles), PbCS(ABA) P255A (3A, squares) or JAK1 (NULL, triangles). Average of three independent experiments is shown. Error bars represent SD.

P815 pulsed with the irrelevant JAK1 peptide (NULL) also formed conjugates, albeit inefficiently, in a time dependent manner, peaking after 20 minutes ($7\% \pm 4\%$) and slowly decreasing to $4\% \pm 1\%$. These conjugates reflected non-specific adhesion that is at least in part CD8-mediated. CD8 $\alpha_{\text{Tac}}\beta$ hybridomas (T1.Tac.bYFP.zCFP) attained the maximal frequency of conjugates with the PbCS(ABA)-pulsed P815 cells (WT) after 15 minutes, i.e. 5 minutes later than the cells with wild-type CD8 α , and at lower frequency ($26\% \pm 4\%$) than their wild-type CD8 α counterparts, which fell to $18\% \pm 3\%$ after 60 minutes (Fig. 4.8C). The conjugate frequencies with P815 cells pulsed with the PbCS(ABA) P255A (3A) peptide were similar ($7\% \pm 2\%$ after 20 minutes) to P815 cells pulsed with JAK1 peptide ($6\% \pm 2\%$ after 20 minutes) and changed very little 30 minutes later ($6\% \pm 2\%$ for 3A and $6\% \pm 3\%$ for JAK1). These findings are in accordance with the multimer binding, calcium flux and IL-2 data (Figs 4.3 and 4.4). The high affinity ligand, PbCS(ABA) (WT), pulsed on P815 cells induced endocytosis of $\sim 36\%$ and $\sim 47\%$ of cell surface TCR after 60 minutes of incubation on wild-type CD8 α and CD8 α_{Tac} cells, respectively (Fig. 4.8B, D).

The low affinity PbCS(ABA) P255A and the non-cognate JAK1 peptide failed to induce any significant internalization of surface TCR on the hybridomas tested. For a late functional response, IL-2 secretion was examined. The strong peptide agonist, PbCS(ABA) (WT) induced IL-2 production from T1.wt.bYFP.zCFP hybridoma ($EC_{50}=39.5$ pM), and with weaker sensitivity ($EC_{50}=5042$ pM) and lower maximal levels ($\sim 80\%$ of maximum observed in T1.wt.bYFP.zCFP hybridoma) from CD8 $\alpha_{\text{Tac}}\beta$ hybridoma (Fig. 4.9C and Table 4.4). In accordance with previous results, while hybridoma expressing CD8 α produced IL-2 when stimulated with the weaker P255A ligand ($EC_{50}=2051$ pM) at lower maximal levels ($\sim 75\%$ of maximum of wild-type CD8 α hybridoma with WT peptide), no detectable IL-2 was produced in hybridomas expressing CD8 α_{Tac} .

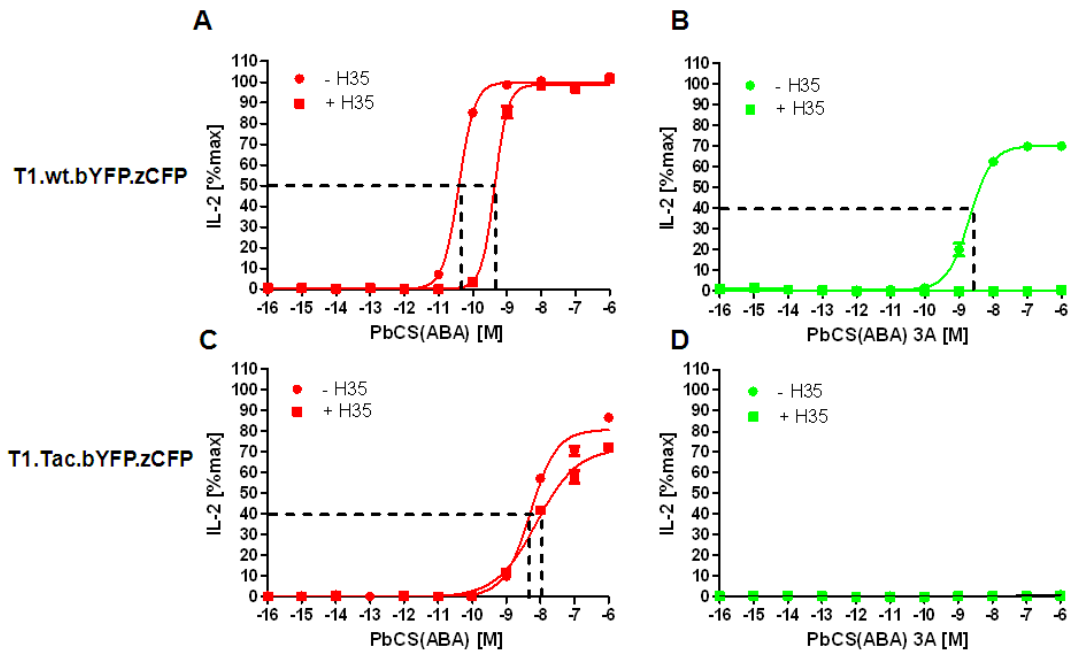


Figure 4.9 *IL-2* production is impaired in *CD3 ζ -CFP+ CD8 α_{Tac}* hybridomas. Production of *IL-2* from T1.wt.bYFP.zCFP (A,B) or T1.Tac.bYFP.zCFP (C,D) with P815 cells pulsed with graded amounts of PbCS(ABA) (WT – A,C) or PbCS(ABA) P255A (3A – B,D) in the presence (+H35) or absence (-H35) of the anti-CD8 β blocking mAb clone H35. Maximal attained levels of *IL-2* by T1.wt.bYFP.zCFP hybridoma in contact with PbCS(ABA)-peptide pulsed P815 cells. Representative data are shown out of two independent experiments. Error bars represent SEM from duplicates.

Table 4.4 EC_{50} values of *IL-2* secretion of *CD3 ζ -CFP+ T1* hybridomas

EC_{50} [pM]	K^d PbCS(ABA) - H35	K^d PbCS(ABA) + H35	K^d PbCS(ABA) P255A - H35
T1.wt.bYFP	39.5	437.1	2051
T1.Tac.bYFP	5042	7772	-

4.1.9 Antigen-induced CD8-CD3 ζ interaction is reduced on CD8 α_{Tac} hybridoma

We measured CD8-CD3 ζ FRET in synapses/contact sites of T1 CD3 ζ -CFP+ CD8 β -YFP+ hybridomas expressing CD8 α or CD8 α_{Tac} with peptide-loaded P815 cells after 20 minutes of incubation at 37 °C (Fig. 4.10A). Two different peptide ligands were examined: the wild type PbCS(ABA) and PbCS(ABA) P255A. Hybridomas expressing CD8 α and CD8 α_{Tac} had increased CD8 β -CD3 ζ FRET to similar amounts (3.1% \pm 0.9% and 2.9% \pm 1.1%, respectively) in the contact site with P815 cells pulsed with the PbCS(ABA) peptide (Fig. 4.10B). Conversely, CD8 β -CD3 ζ FRET was lower on either hybridomas in contact with the PbCS(ABA) P255A-loaded P815 cells, with CD8 α_{Tac} cells displaying less intense FRET (1.8% \pm 0.3%) than their CD8 α counterparts (2.6% \pm 0.5%).

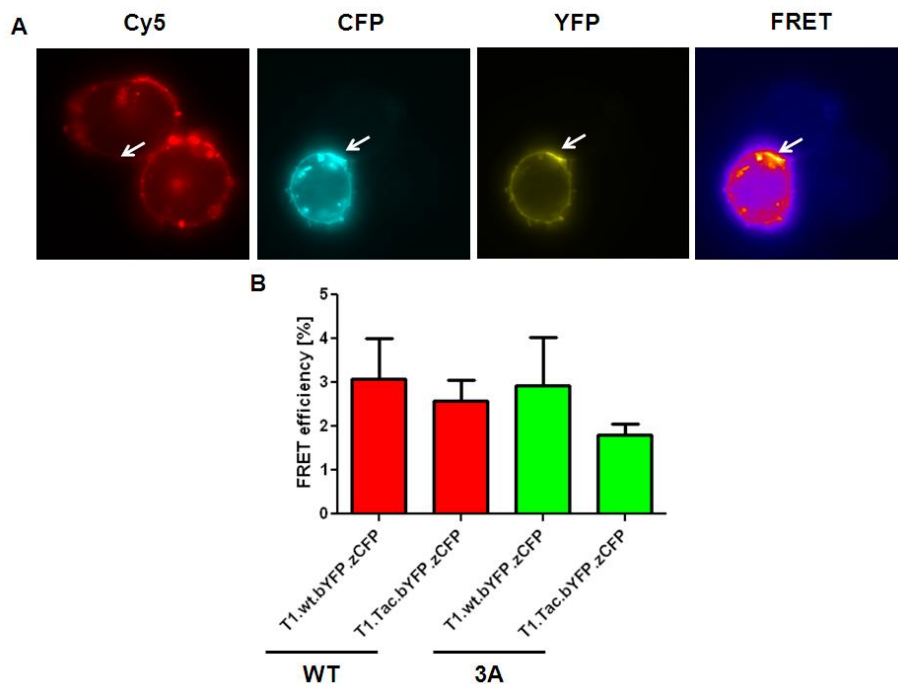


Figure 4.10 *CD8 $\alpha_{Tac}\beta$ associates inefficiently with CD3 ζ .* A, FRET microscopy of a conjugate between a PbCS(ABA)-pulsed, NHS-Cy5 surface labeled P815 cell (red) and a T1.wt.bYFP.zCFP cell. The white arrows indicate contact sites/synapses. The image is shown in four channels – Cy5, YFP, CFP and FRET. Intensity of FRET is shown by a color gradient ranging from blue (lowest) to white (highest). B, Quantification of FRET from synapses of T1.wt.bYFP.zCFP or T1.Tac.bYFP.zCFP cells with NHS-Cy5 surface labeled P815 cells pulsed with the PbCS(ABA) or PbCS(ABA) P255A peptide after 20 minutes of incubation. Error bars represent SD. Experiments were repeated twice. A representative experiment is shown.

4.1.10 CD8 $\alpha_{Tac}\beta$ associates with less p56^{Lck} and partitions less in rafts than the CD8 $\alpha\beta$

Critical for CD8 coreceptor function is its ability to bring p56^{Lck}, a Src tyrosine kinase, into close proximity of TCR-associated CD3 units, in particular the CD3 ζ chains. The p56^{Lck} phosphorylates ITAMs on the CD3, namely ζ chains and thus initiates the TCR signal transduction cascade. To find out whether in addition to impaired TCR-CD8 association there are other functional defects intrinsic to the CD8 $\alpha_{Tac}\beta$, we compared the amount of p56^{Lck} associated to the CD8 β chain in hybridomas expressing CD8 α or CD8 α_{Tac} . Western blot analysis of immunoprecipitates with anti-CD8 α or anti-CD8 β (Fig. 4.11A) revealed markedly lower amounts of p56^{Lck} associated with CD8 β in hybridomas expressing CD8 α_{Tac} than in hybridomas expressing wild-type CD8 α . Moreover, less CD8 β was immunoprecipitated with anti-CD8 α in hybridomas expressing CD8 α_{Tac} than in those expressing wild-type CD8 α . When p56^{Lck} was immunoprecipitated with anti-CD8 β antibody, the same differences were observed. To examine whether weaker association of p56^{Lck} with CD8 $\alpha_{Tac}\beta$ is related to

differential partitioning of $CD8\alpha_{Tac}\beta$ in lipid rafts (where $p56^{Lck}$ is mainly located), we immunoprecipitated $CD8\beta$ with anti- $CD8\alpha$ antibody from detergent soluble (M) and detergent insoluble fractions (DIM) of plasma membranes of cells expressing $CD8\alpha$ or $CD8\alpha_{Tac}$ (Fig. 4.11B). We detected $CD8\beta$ in immunoprecipitates from DIM from wild-type $CD8\alpha$ cells, but observed little or no $CD8\beta$ in immunoprecipitates from DIM from T1 hybridoma expressing $CD8\alpha_{Tac}$.

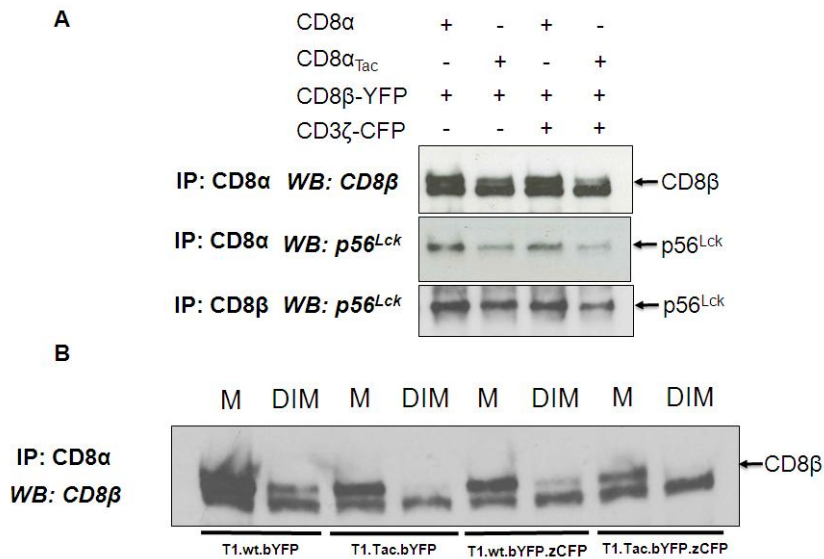


Figure 4.11 $CD8\alpha_{Tac}\beta$ associates with less $p56^{Lck}$ than $CD8\alpha\beta$ because of weaker partitioning in lipid rafts. **A**, Western blots with anti- $CD8\beta$ mAb KT112 and anti- $p56^{Lck}$ polyclonal antibody of reducing SDS-PAGE-resolved immunoprecipitates with anti- $CD8\alpha$ mAb 53.6.72 or anti- $CD8\beta$ H35 from T1 hybridoma. In all lanes of the Western blot for $CD8\beta$ there is a non-specific band at 50 kDa. The specific band of the $CD8\beta$ -eYFP fusion protein can be seen on top of the non-specific band. **B**, Western blot with anti- $CD8\beta$ mAb KT112 of reducing SDS-PAGE-resolved of detergent-soluble (M) and detergent insoluble (DIM) fractions of cellular extracts immunoprecipitated with anti- $CD8\alpha$ mAb 53.6.72. The arrows indicate specific bands.

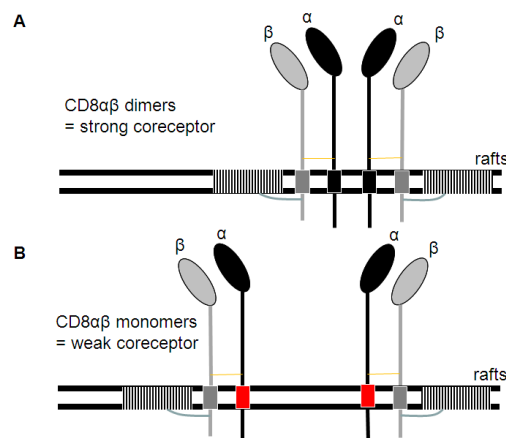


Figure 4.12 The $CD8\alpha\beta$ dimers are bona fide $CD8$ coreceptors. **A**, $CD8\alpha\beta$ forms dimers-of-dimers, held together by $CD8\alpha$ TMD interactions. **B**, The $CD8\alpha_{Tac}$ mutant is greatly impaired in dimerization and such forms of $CD8$ associate weakly with lipid rafts.

4.2 Discussion

The key finding of our study is that replacement of the strongly dimerizing CD8 α TMD with the one of the IL-2 receptor α chain (Tac) resulted in substantial reduction of T1 hybridomas' ability to form conjugates with APCs (Fig. 4.8), to flux intracellular Ca²⁺ and to produce IL-2 (Fig. 4.4 and 4.9) and to bind MHC-peptide multimers (Fig. 4.3). This replacement did not alter significantly the surface expression of CD8 $\alpha\alpha$ homodimers or CD8 $\alpha\beta$ heterodimers (Fig. 4.2), which rules out impaired subunit chain assembly and/or intercellular transport as explanations for the observed defects.

There are two major aspects of CD8 coreceptor function: **First**, the association of CD8 with TCR:CD3. We and others have shown previously that binding of MHC-peptide complexes (monomers and tetramers) to CD8+ T cells is greatly strengthened by coordinate binding of CD8 to TCR-associated complexes (Cawthon and Alexander-Miller, 2002; Luescher et al., 1995b; Renard et al., 1996). This binding avidity enhancement critically depends on association of CD8 with TCR:CD3 (Gallagher et al., 1989; Mallaun et al., 2008; Naehrer et al., 2002; Takada and Engleman, 1987). Similar findings to ours were obtained on CD8+ T cells that i) lack the CD3 δ chain (i.e. from CD3 δ KO mice) (Dave et al., 1998; Delgado et al., 2000); ii) express the α CPM variant of TCR (α IV/ β III) (Bäckström et al., 1996) or iii) express tailless CD8 β (Arcaro et al., 2001; Irie et al., 1998; Itano et al., 1994). There is evidence that CD8 β couples with the TCR:CD3 via CD3 δ (Doucey et al., 2003; Suzuki et al., 1992). Indeed on CD8+ T cells expressing TCR containing the α CPM mutation, i.e. lacking the highly conserved (FETDXNLN) motif in the connecting peptide of the TCR α chain, CD3 δ cannot stably associate (Bäckström et al., 1996). While the molecular nature of the putative association of CD8 with CD3 δ remains to be elucidated, it seems unlikely the CD8 α TMD plays a role, because CD8 $\alpha\alpha$ does not significantly associate with TCR:CD3 (Doucey et al., 2003; Naehrer et al., 2002). In the present study we observed that K^d/PbCS(ABA) multimer binding on CD8 $\alpha_{\text{Tac}}\beta$ cells was less efficient than on CD8 $\alpha\beta$ T1 hybridomas (Fig. 4.3). Binding differences were particularly striking for multimers containing the weak agonist peptide Kd/PbCS(ABA) P255A, whose binding was critically dependent on CD8 (Fig. 4.3). Moreover and importantly, we observed that CD8 $\alpha_{\text{Tac}}\beta$ associated less strongly with TCR:CD3 than CD8 $\alpha\beta$ as demonstrated by the lower FRET signals (Fig. 4.5). This was observed in the absence as well as in the presence of the MHC-peptide ligand, arguing that

replacement of the CD8 α the one of Tac severely impairs the ability of CD8 $\alpha\beta$ to associate with TCR:CD3. This defect is especially notable in the case of low avidity MHC-peptide ligands, consistent with the well-established notion that CD8 $\alpha\beta$ increases the breadth and sensitivity of ligand recognition by the TCR:CD3.

Second, efficient CD8 coreceptor function requires CD8 partitioning in lipid rafts and CD8 association with p56^{Lck} (Arcaro et al., 2001; Doucey et al., 2001; Pang et al., 2007). These two aspects are intimately related, because CD8 association with Lck occurs mainly in rafts, due to their high p56^{Lck} content (Janes et al., 1999; Montixi et al., 1998; Moran and Miceli, 1998; Xavier et al., 1998). Antigen-specific T cell activation is initiated by MHC-peptide mediated cross-linking of TCR:CD3 and CD8, resulting in activation of CD8-associated p56^{Lck} (Arcaro et al., 2001; Doucey et al., 2001). Because lipid rafts exclude the abundant phosphatases (namely CD45), they are the sites where initial p56^{Lck}-mediated phosphorylation of CD3 ITAM take place (Arcaro et al., 2001; Doucey et al., 2001). CD8 raft-association has been shown to be mediated by CD8 β , namely by its cytoplasmic domain (Arcaro et al., 2000). On one hand the CD8 β cytoplasmic tail harbors a membrane proximal palmitoylation site that when palmitoylated conveys strong raft-association (Arcaro et al., 2000). On the other hand the short CD8 β tail is extremely basic and hence promotes CD8 raft association by binding to acidic lipids that are highly abundant on the inner leaflet of rafts (Lingwood and Simons, 2010). Our results demonstrate that replacement of the CD8 α TMD severely impairs the association of CD8 $\alpha\beta$ with Lck and with lipid rafts (Fig. 4.11). Consistent with this is the observation that CD8 $\alpha_{\text{Tac}}\beta$ T1 hybridomas exhibited substantially less intracellular Ca²⁺ flux as compared to CD8 $\alpha\beta$ cells (Fig. 4.4A). Intracellular Ca²⁺ flux on CD8⁺ T cells has been shown to critically depend on activation of CD8-associated Lck, Lck-mediated ITAM phosphorylation and subsequent triggering of the canonical ZAP70-LAT-PLC γ pathway (Artyomov et al., 2010; Purbhoo et al., 2001). This activation pathway and intracellular Ca²⁺ elevation are also required for IL-2 production of CD8⁺ T cells (Stanley et al., 1990). This is consistent with our observation that CD8 $\alpha_{\text{Tac}}\beta$ T1 hybridomas displayed reduced IL-2 responses compared to their CD8 $\alpha\beta$ counterparts (Figs. 4.4B and 4.9). Again this difference was most striking for the weak agonist PbCS(ABA) P255A, whose IL-2 response was entirely CD8 $\alpha\beta$ dependent, i.e. was ablated by the CD8 α_{Tac} mutation (Figs. 4.4B and 4.9).

It remains to be explained why replacement of the CD8 α TMD with the one of Tac impairs partitioning of CD8 $\alpha\beta$ in lipid rafts. It has been shown that a (VIL) sequence motif as present in the outer leaflet of the TMD of the influenza hemagglutinin protein cooperates with palmitoyled cysteine residues in conveying raft association (Engel et al., 2012). The CD8 α TMD contains no such VIL motif (Fig. 4.1). Another study reported the existence of a (VXXTLXXIY) motif in the inner leaflet of the TMD of the COPI protein p24. This motif was found to bind to sphingosine, a lipid abundant in rafts (Contreras et al., 2012). The CD8 α TMD contains a highly conserved IWAPLAG sequence spanning the outer and the equally conserved LLLSLVIT sequence in the inner leaflet (Fig. 4.1). One may argue that these might have analogous properties due to their similarity to cholesterol and sphingosine-binding motifs, both lipids highly enriched in lipid rafts (Ernst et al., 2010). This, however, seems not plausible because CD8 $\alpha\alpha$ does not partition in lipid rafts, unless one speculates that a putative CD8 α TMD lipid-binding motifs might be (self)masked in CD8 $\alpha\alpha$ homodimers, while in CD8 $\alpha\beta$ heterodimer they might be accessible for lipid binding.

Alternatively and more convincingly, our results are consistent with a model according to which the CD8 α TMD mediates the dimerization of CD8 $\alpha\beta$ heterodimers (Fig. 4.12). As it has been demonstrated that CD8 $\alpha\beta$ partitioning in lipid rafts is mediated by CD8 β (Arcaro et al., 2000), such putative “dimers-of-dimers” containing two CD8 β chains therefore are expected to partition in lipid rafts more effectively than CD8 $\alpha\beta$ monomers. Since CD8 $\alpha_{\text{Tac}}\beta$ is unable to form such putative dimers-of-dimers, this would explain the observed reduced partitioning into lipid rafts (Fig. 4.11). Moreover, CD8 $\alpha\beta$, but not CD8 $\alpha\alpha$ have been shown to associate with the TCR:CD3, and that this is mediated by CD8 β (Doucey et al., 2003). According to our model CD8 $\alpha\beta$ dimers-of-dimers, containing CD8 β are thus expected to associate with TCR:CD3 more avidly than CD8 $\alpha\beta$ monomers. This view is consistent with the observation that there was less FRET between CD8 and TCR:CD3 on T1 hybridomas expressing CD8 $\alpha\beta$ than on those expressing CD8 $\alpha_{\text{Tac}}\beta$ (Fig. 4.5). There is biochemical evidence that CD8 $\alpha\beta$ can form dimers, which is at variance with other studies (Ledbetter et al., 1981a; Ledbetter et al., 1981b). It should be noted, however, that classical biochemical analysis, e.g. immunoprecipitation, SDS-PAGE and Western blotting fail to detect such CD8 $\alpha\beta$ dimers-of-dimers. An intriguing implication of our CD8 $\alpha\beta$ dimer-of-dimer model is

that these should promote dimerization of TCR:CD3, especially upon co-engagement on CD8 and TCR:CD3 by MHC-peptide ligands, including monomers. There is indeed a substantial body of evidence that TCR:CD3 can form dimers (and higher oligomers) and this is critical for TCR triggering (Kumar et al., 2011; Minguet et al., 2007; Schamel et al., 2005).

4.3 Conclusion and perspectives

The CD8 $\alpha\beta$ coreceptor plays crucial roles in thymic selection and CD8⁺ T cell development, differentiation and effector function. The CD8 $\alpha\beta$ isoform expressed on the surface of CD8⁺ T cells, not the CD8 $\alpha\alpha$, promotes an increase in functional avidity of the TCR:CD3 complex by cooperatively binding to the MHC class I-peptide ligand, thereby increasing the breadth and sensitivity of ligand recognition by the TCR:CD3. For the coreceptor function of the CD8 $\alpha\beta$ heterodimer it is important: 1) its ability to partition to lipid rafts where p56^{Lck} resides; 2) its capacity to associate with TCR:CD3. In murine CD8 $\alpha\beta$, raft partitioning is achieved by the palmytoilation and the cluster of basic arginine residues at the C-terminal tail of the CD8 β chain. We have found that by replacing the highly evolutionary conserved TMD of CD8 α with the partially monomerizing TMD of IL-2 receptor α -chain (Tac) on T cell hybridoma expressing the T1 TCR, we obtained surface-expressed CD8 $\alpha_{\text{Tac}}\beta$ heterodimers that are severely impaired in coreceptor function. We relate this functional defect to: 1) reduced ability of the CD8 $\alpha_{\text{Tac}}\beta$ to associate with TCR:CD3; 2) its diminished association with p56^{Lck} as a consequence of perturbed lipid rafts partitioning. We postulate that the replacement of CD8 α TMD disrupts the formation of CD8 $\alpha\beta$ dimer-of-dimers, whose existence would be consistent with current findings. Further studies to investigate in detail the contribution of the conserved sequence motifs of the CD8 α TMD would be needed to provide conclusive evidence, uncovering yet further structural feature(s) of CD8 $\alpha\beta$.

5. REFERENCES

- Adams, S., and Humphreys, R.E. (1995). Invariant chain peptides enhancing or inhibiting the presentation of antigenic peptides by major histocompatibility complex class II molecules. *Eur. J. Immunol.* *25*, 1693-1702.
- Altman, J.D., Moss, P.A.H., Goulder, P.J.R., Barouch, D.H., McHeyzer-Williams, M.G., Bell, J.I., McMichael, A.J., and Davis, M.M. (1996). Phenotypic analysis of antigen-specific T lymphocytes. *Science* *274*, 94-96.
- Anel, A., Martinez-Lorenzo, M., Schmitt-Verhulst, A., and Boyer, C. (1997). Influence on CD8 of TCR/CD3-generated signals in CTL clones and CTL precursor cells. *J. Immunol.* *158*, 19-28.
- Arcaro, A., Grégoire, C., Bakker, T.R., Baldi, L., Jordan, M., Goffin, L., Boucheron, N., Wurm, F., van der Merwe, P.A., Malissen, B., and Luescher, I.F. (2001). CD8 β endows CD8 with efficient coreceptor function by coupling T cell receptor/CD3 to raft-associated CD8/p56lck complexes. *J. Exp. Med.* *194*, 1485-1495.
- Arcaro, A., Gregoire, C., Boucheron, N., Stotz, S., Palmer, E., Malissen, B., and Luescher, I.F. (2000). Essential role of CD8 palmitoylation in CD8 coreceptor function. *J. Immunol.* *165*, 2068-2076.
- Arnold, P.Y., La Gruta, N.L., Miller, T., Vignali, K.M., Adams, P.S., Woodland, D.L., and Vignali, D.A.A. (2002). The majority of immunogenic epitopes generate CD4⁺ T cells that are dependent on MHC class II-bound peptide-flanking residues. *J. Immunol.* *169*, 739-749.
- Artyomov, M.N., Lis, M., Devadas, S., Davis, M.M., and Chakraborty, A.K. (2010). CD4 and CD8 binding to MHC molecules primarily acts to enhance Lck delivery. *Proc. Natl. Acad. Sci.* *107*, 16916-16921.
- Ayyoub, M., Dojcinovic, D., Pignon, P., Raimbaud, I., Schmidt, J., Luescher, I., and Valmori, D. (2010a). Monitoring of NY-ESO-1 specific CD4⁺ T cells using molecularly defined MHC class II/His-tag-peptide tetramers. *Proc. Nat. Acad. Sci.* *107*, 7437-7442.
- Ayyoub, M., Pignon, P., Dojcinovic, D., Raimbaud, I., Old, L.J., Luescher, I., and Valmori, D. (2010b). Assessment of vaccine-induced CD4 T cell responses to the 119-143 immunodominant region of the tumor-specific antigen NY-ESO-1 using DRB1*0101 tetramers. *Clin. Cancer Res.* *16*, 4607-4615.
- Bacchetta, R., Gregori, S., and Roncarolo, M.-G. (2005). CD4⁺ regulatory T cells: Mechanisms of induction and effector function. *Autoimm. Rev.* *4*, 491-496.
- Bäckström, B.T., Milia, E., Peter, A., Jaureguierry, B., Baldari, C.T., and Palmer, E. (1996). A motif within the T cell receptor α chain constant region connecting peptide domain controls antigen responsiveness. *Immunity* *5*, 437-447.
- Bakker, A.H., Hoppes, R., Linnemann, C., Toebe, M., Rodenko, B., Berkens, C.R., Hadrup, S.R., van Esch, W.J.E., Heemskerk, M.H.M., Ovaas, H., and Schumacher, T.N.M. (2008).

- Conditional MHC class I ligands and peptide exchange technology for the human MHC gene products HLA-A1, -A3, -A11, and -B7. *Proc. Nat. Acad. Sci.* *105*, 3825-3830.
- Belmares, M.P., Busch, R., Mellins, E.D., and McConnell, H.M. (2003). Formation of two peptide/MHC II isomers is catalyzed differentially by HLA-DM. *Biochemistry* *42*, 838-847.
- Bluemel, C., Hausmann, S., Fluhr, P., Sriskandarajah, M., Stallcup, W., Baeuerle, P., and Kufer, P. (2010). Epitope distance to the target cell membrane and antigen size determine the potency of T cell-mediated lysis by BiTE antibodies specific for a large melanoma surface antigen. *Cancer Immunol. Immunoth.* *59*, 1197-1209.
- Boniface, J.J., Lyons, D.S., Wettstein, D.A., Allbritton, N.L., and Davis, M.M. (1996). Evidence for a conformational change in a class II major histocompatibility complex molecule occurring in the same pH range where antigen binding is enhanced. *J. Exp. Med.* *183*, 119-126.
- Bosselut, R., Kubo, S., Guinter, T., Kopacz, J.L., Altman, J.D., Feigenbaum, L., and Singer, A. (2000). Role of CD8 β domains in CD8 coreceptor function: importance for MHC I binding, signaling, and positive selection of CD8 $^+$ T cells in the thymus. *Immunity* *12*, 409-418.
- Call, M.E., and Wucherpfennig, K.W. (2004). Molecular mechanisms for the assembly of the T cell receptor-CD3 complex. *Mol. Immunol.* *40*, 1295-1305.
- Call, M.E., and Wucherpfennig, K.W. (2005). The T cell receptor: critical role of the membrane environment in receptor assembly and function. *Ann. Rev. Immunol.* *23*, 101-125.
- Cameron, T.O., Cochran, J.R., Yassine-Diab, B., Sekaly, R.-P., and Stern, L.J. (2001). Cutting edge: Detection of antigen-specific CD4 $^+$ T cells by HLA-DR1 oligomers is dependent on the T cell activation state. *J. Immunol.* *166*, 741-745.
- Campbell, K.S., Bäckström, B.T., Tiefenthaler, G., and Palmer, E. (1994). CART: a conserved antigen receptor transmembrane motif. *Sem. Immunol.* *6*, 393-410.
- Carson, R.T., Vignali, K.M., Woodland, D.L., and Vignali, D.A.A. (1997). T cell receptor recognition of MHC class II bound peptide flanking residues enhances immunogenicity and results in altered TCR V region usage. *Immunity* *7*, 387-399.
- Carven, G.J., Chitta, S., Hilgert, I., Rushe, M.M., Baggio, R.F., Palmer, M., Arenas, J.E., Strominger, J.L., Horejsi, V., Santambrogio, L., and Stern, L.J. (2004). Monoclonal antibodies specific for the empty conformation of HLA-DR1 reveal aspects of the conformational change associated with peptide binding. *J. Biol. Chem.* *279*, 16561-16570.
- Carven, G.J., and Stern, L.J. (2005). Probing the ligand-induced conformational change in HLA-DR1 by selective chemical modification and mass spectrometric mapping. *Biochemistry* *44*, 13625-13637.
- Casrouge, A., Beaudoin, E., Dalle, S., Pannetier, C., Kanellopoulos, J., and Kourilsky, P. (2000). Size estimate of the $\alpha\beta$ TCR repertoire of naive mouse splenocytes. *J. Immunol.* *164*, 5782-5787.

- Cauley, L.S., Cookenham, T., Miller, T.B., Adams, P.S., Vignali, K.M., Vignali, D.A.A., and Woodland, D.L. (2002). Cutting edge: virus-specific CD4+ memory T cells in nonlymphoid tissues express a highly activated phenotype. *J. Immunol.* *169*, 6655-6658.
- Cawthon, A.G., and Alexander-Miller, M.A. (2002). Optimal colocalization of TCR and CD8 as a novel mechanism for the control of functional avidity. *J. Immunol.* *169*, 3492-3498.
- Cebecauer, M., Guillaume, P., Hozák, P., Mark, S., Everett, H., Schneider, P., and Luescher, I.F. (2005a). Soluble MHC-peptide complexes induce rapid death of CD8+ CTL. *J. Immunol.* *174*, 6809-6819.
- Cebecauer, M., Guillaume, P., Mark, S., Michielin, O., Boucheron, N., Bezard, M., Meyer, B.H., Segura, J.-M., Vogel, H., and Luescher, I.F. (2005b). CD8+ cytotoxic T lymphocyte activation by soluble major histocompatibility complex-peptide dimers. *J. Biol. Chem.* *280*, 23820-23828.
- Cecconi, V., Moro, M., Del Mare, S., Dellabona, P., and Casorati, G. (2008). Use of MHC class II tetramers to investigate CD4+ T cell responses: Problems and solutions. *Cytometry* *73A*, 1010-1018.
- Cecconi, V., Moro, M., Del Mare, S., Sidney, J., Bachi, A., Longhi, R., Sette, A., Protti, M.P., Dellabona, P., and Casorati, G. (2010). The CD4+ T-cell epitope-binding register is a critical parameter when generating functional HLA-DR tetramers with promiscuous peptides. *Eur. J. Immunol.* *40*, 1603-1616.
- Chang, H.-C., Tan, K., Ouyang, J., Parisini, E., Liu, J.-h., Le, Y., Wang, X., Reinherz, E.L., and Wang, J.-h. (2005). Structural and mutational analyses of a CD8 $\alpha\beta$ heterodimer and comparison with the CD8 $\alpha\alpha$ homodimer. *Immunity* *23*, 661-671.
- Cheroutre, H., and Lambolez, F. (2008). Doubting the TCR coreceptor function of CD8 $\alpha\alpha$. *Immunity* *28*, 149-159.
- Chicz, R.M., Urban, R.G., Lane, W.S., Gorga, J.C., Stern, L.J., Vignali, D.A.A., and Strominger, J.L. (1992). Predominant naturally processed peptides bound to HLA-DR1 are derived from MHC-related molecules and are heterogeneous in size. *Nature* *358*, 764-768.
- Choudhuri, K., Parker, M., Milicic, A., Cole, D.K., Shaw, M.K., Sewell, A.K., Stewart-Jones, G., Dong, T., Gould, K.G., and van der Merwe, P.A. (2009). Peptide-major histocompatibility complex dimensions control proximal kinase-phosphatase balance during T cell activation. *J. Biol. Chem.* *284*, 26096-26105.
- Choudhuri, K., Wiseman, D., Brown, M.H., Gould, K., and van der Merwe, P.A. (2005). T-cell receptor triggering is critically dependent on the dimensions of its peptide-MHC ligand. *Nature* *436*, 578-582.
- Cochran, J.R., Aivazian, D., Cameron, T.O., and Stern, L.J. (2001). Receptor clustering and transmembrane signaling in T cells. *Trends in Biochemical Sciences* *26*, 304-310.
- Cole, D.K., Gallagher, K., Lemercier, B., Holland, C.J., Junaid, S., Hindley, J.P., Wynn, K.K., Gostick, E., Sewell, A.K., Gallimore, A.M., *et al.* (2012). Modification of the carboxy-

- terminal flanking region of a universal influenza epitope alters CD4⁺ T-cell repertoire selection. *Nat. Commun.* *3*, 665.
- Cole, D.K., Pumphrey, N.J., Boulter, J.M., Sami, M., Bell, J.I., Gostick, E., Price, D.A., Gao, G.F., Sewell, A.K., and Jakobsen, B.K. (2007). Human TCR-binding affinity is governed by MHC class restriction. *J. Immunol.* *178*, 5727-5734.
- Constant, S.L., and Bottomly, K. (1997). Induction of T_H1 and T_H2 CD4⁺ T cell responses: The alternative approaches. *Ann. Rev. Immunol.* *15*, 297-322.
- Contreras, F.X., Ernst, A.M., Haberkant, P., Bjorkholm, P., Lindahl, E., Gonen, B., Tischer, C., Elofsson, A., von Heijne, G., Thiele, C., *et al.* (2012). Molecular recognition of a single sphingolipid species by a protein's transmembrane domain. *Nature* *481*, 525-529.
- Cosson, P., and Bonifacio, J. (1992). Role of transmembrane domain interactions in the assembly of class II MHC molecules. *Science* *258*, 659-662.
- Cunliffe, S.L., Wyer, J.R., Sutton, J.K., Lucas, M., Harcourt, G., Klenerman, P., McMichael, A.J., and Kelleher, A.D. (2002). Optimization of peptide linker length in production of MHC class II/peptide tetrameric complexes increases yield and stability, and allows identification of antigen-specific CD4⁺ T cells in peripheral blood mononuclear cells. *Eur. J. Immunol.* *32*, 3366-3375.
- Dardalhon, V., Awasthi, A., Kwon, H., Galileos, G., Gao, W., Sobel, R.A., Mitsdoerffer, M., Strom, T.B., Elyaman, W., Ho, I.C., *et al.* (2008). IL-4 inhibits TGFβ-induced Foxp3⁺ T cells and, together with TGFβ, generates IL-9⁺ IL-10⁺ Foxp3⁻ effector T cells. *Nat. Immunol.* *9*, 1347-1355.
- Dave, V.P., Keefe, R., Berger, M.A., Drbal, K., Punt, J.A., Wiest, D.L., Alarcon, B., and Kappes, D.J. (1998). Altered functional responsiveness of thymocyte subsets from CD3δ-deficient mice to TCR-CD3 engagement. *Int. Immunol.* *10*, 1481-1490.
- Day, C.L., Seth, N.P., Lucas, M., Appel, H., Gauthier, L., Lauer, G.M., Robbins, G.K., Szczepiorkowski, Z.M., Casson, D.R., Chung, R.T., *et al.* (2003). Ex vivo analysis of human memory CD4 T cells specific for hepatitis C virus using MHC class II tetramers. *J. Clin. Invest.* *112*, 831-842.
- de Jong, E.C., Smits, H.H., and Kapsenberg, M.L. (2005). Dendritic cell-mediated T cell polarization. *Springer Sem. Immunopath.* *26*, 289-307.
- Delgado, P., Fernandez, E., Dave, V., Kappes, D., and Alarcon, B. (2000). CD3δ couples T-cell receptor signalling to ERK activation and thymocyte positive selection. *Nature* *406*, 426-430.
- Demotte, N., Stroobant, V., Courtoy, P.J., Van Der Smissen, P., Colau, D., Luescher, I.F., Hivroz, C., Nicaise, J., Squifflet, J.-L., Mourad, M., *et al.* (2008). Restoring the association of the T cell receptor with CD8 reverses anergy in human tumor-infiltrating lymphocytes. *Immunity* *28*, 414-424.

- Demotz, S., Sette, A., Sakaguchi, K., Buchner, R., Appella, E., and Grey, H.M. (1991). Self peptide requirement for class II major histocompatibility complex allorecognition. *Proc. Nat. Acad. Sci.* 88, 8730-8734.
- Dong, C., and Flavell, R.A. (2001). Th1 and Th2 cells. *Curr. Opin. Hematol.* 8, 47-51.
- Doucey, M.-A., Goffin, L., Naeher, D., Michielin, O., Baumgärtner, P., Guillaume, P., Palmer, E., and Luescher, I.F. (2003). CD3 δ establishes a functional link between the T cell receptor and CD8. *J. Biol. Chem.* 278, 3257-3264.
- Doucey, M.-A., Legler, D.F., Boucheron, N., Cerottini, J.-C., Bron, C., and Luescher, I.F. (2001). CTL activation is induced by cross-linking of TCR/MHC-peptide-CD8/p56lck adducts in rafts. *Eur. J. Immunol.* 31, 1561-1570.
- Durinovic-Bello, I., Rosinger, S., Olson, J.A., Congia, M., Ahmad, R.C., Rickert, M., Hampl, J., Kalbacher, H., Drijfhout, J.W., Mellins, E.D., *et al.* (2006). DRB1*0401-restricted human T cell clone specific for the major proinsulin 73-90 epitope expresses a down-regulatory T helper 2 phenotype. *Proc. Natl. Acad. Sci.* 103, 11683-11688.
- Engel, S., de Vries, M., Herrmann, A., and Veit, M. (2012). Mutation of a raft-targeting signal in the transmembrane region retards transport of influenza virus hemagglutinin through the Golgi. *FEBS Lett.* 586, 277-282.
- Ernst, A.M., Contreras, F.X., Brügger, B., and Wieland, F. (2010). Determinants of specificity at the protein–lipid interface in membranes. *FEBS Lett.* 584, 1713-1720.
- Fink, A., Sal-Man, N., Gerber, D., and Shai, Y. (2012). Transmembrane domains interactions within the membrane milieu: Principles, advances and challenges. *Biochim. Biophys. Acta* 1818, 974-983.
- Föhse, L., Suffner, J., Suhre, K., Wahl, B., Lindner, C., Lee, C.-W., Schmitz, S., Haas, J.D., Lamprecht, S., Koenecke, C., *et al.* (2011). High TCR diversity ensures optimal function and homeostasis of Foxp3+ regulatory T cells. *Eur. J. Immunol.* 41, 3101-3113.
- Frayser, M., Sato, A.K., Xu, L., and Stern, L.J. (1999). Empty and peptide-loaded class II major histocompatibility complex proteins produced by expression in *Escherichia coli* and folding in vitro. *Prot. Expr. Purif.* 15, 105-114.
- Fremont, D.H., Hendrickson, W.A., Marrack, P., and Kappler, J. (1996a). Structures of an MHC class II molecule with covalently bound single peptides. *Science* 272, 1001-1004.
- Fremont, D.H., Rees, W.A., and Kozono, H. (1996b). Biophysical studies of T-cell receptors and their ligands. *Curr. Opin. Immunol.* 8, 93-100.
- Gallagher, P.F., Fazekas de St Groth, B., and Miller, J.F. (1989). CD4 and CD8 molecules can physically associate with the same T-cell receptor. *Proc. Nat. Acad. Sci.* 86, 10044-10048.
- Garboczi, D.N., Ghosh, P., Utz, U., Fan, Q.R., Biddison, W.E., and Wiley, D.C. (1996). Structure of the complex between human T-cell receptor, viral peptide and HLA-A2. *Nature* 384, 134-141.

- Garcia, K.C., Degano, M., Stanfield, R.L., Brunmark, A., Jackson, M.R., Peterson, P.A., Teyton, L., and Wilson, I.A. (1996a). An $\alpha\beta$ T cell receptor structure at 2.5 Å and Its orientation in the TCR-MHC complex. *Science* 274, 209-219.
- Garcia, K.C., Scott, C.A., Brunmark, A., Carbone, F.R., Peterson, P.A., Wilson, I.A., and Teyton, L. (1996b). CD8 enhances formation of stable T-cell receptor/MHC class I molecule complexes. *Nature* 384, 577-581.
- Ge, Q., Stone, J.D., Thompson, M.T., Cochran, J.R., Rushe, M., Eisen, H.N., Chen, J., and Stern, L.J. (2002). Soluble peptide-MHC monomers cause activation of CD8+ T cells through transfer of the peptide to T cell MHC molecules. *Proc. Nat. Acad. Sci.* 99, 13729-13734.
- Gebe, J.A., Falk, B.A., Rock, K.A., Kochik, S.A., Heninger, A.K., Reijonen, H., Kwok, W.W., and Nepom, G.T. (2003). Low-avidity recognition by CD4+ T cells directed to self-antigens. *Eur. J. Immunol.* 33, 1409-1417.
- Georges, B., Loing, E., Neveu, R., Melnyk, O., Gras-Masse, H., and Auriault, C. (2000). Structural diversity of human class II histocompatibility molecules induced by peptide ligands. *FEBS Lett.* 481, 249-254.
- Geppert, T., and Lipsky, P. (1987). Accessory cell independent proliferation of human T4 cells stimulated by immobilized monoclonal antibodies to CD3. *J. Immunol.* 138, 1660-1666.
- Geppert, T.D., and Lipsky, P.E. (1991). Association of various T cell-surface molecules with the cytoskeleton. Effect of cross-linking and activation. *J. Immunol.* 146, 3298-3305.
- Glebov, O.O., and Nichols, B.J. (2004). Lipid raft proteins have a random distribution during localized activation of the T-cell receptor. *Nat. Cell. Biol.* 6, 238-243.
- Grazia Roncarolo, M., Gregori, S., Battaglia, M., Bacchetta, R., Fleischhauer, K., and Levings, M.K. (2006). Interleukin-10-secreting type 1 regulatory T cells in rodents and humans. *Imm. Rev.* 212, 28-50.
- Green, N. (1970). Spectrophotometric determination of avidin and biotin. *Meth. Enzymol.* 18, 418-424.
- Grotenbreg, G.M., Nicholson, M.J., Fowler, K.D., Wilbuer, K., Octavio, L., Yang, M., Chakraborty, A.K., Ploegh, H.L., and Wucherpfennig, K.W. (2007). Empty class II major histocompatibility complex created by peptide photolysis establishes the role of DM in peptide association. *J. Biol. Chem.* 282, 21425-21436.
- Guignet, E.G., Hovius, R., and Vogel, H. (2004). Reversible site-selective labeling of membrane proteins in live cells. *Nat. Biotech.* 22, 440-444.
- Guillaume, P., Baumgaertner, P., Angelov, G.S., Speiser, D., and Luescher, I.F. (2006). Fluorescence-activated cell sorting and cloning of bona fide CD8+ CTL with reversible MHC-peptide and antibody Fab' conjugates. *J. Immunol.* 177, 3903-3912.

- Guillaume, P., Dojcinovic, D., and Luescher, I.F. (2009). Soluble MHC-peptide complexes: tools for the monitoring of T cell responses in clinical trials and basic research. *Cancer Immun.* *9*, 7.
- Guillaume, P., Legler, D.F., Boucheron, N., Doucey, M.-A., Cerottini, J.-C., and Luescher, I.F. (2003). Soluble major histocompatibility complex-peptide octamers with impaired CD8 binding selectively induce Fas-dependent apoptosis. *J. Biol. Chem.* *278*, 4500-4509.
- Harty, J.T., Tvinnereim, A.R., and White, D.W. (2000). CD8(+) T cell effector mechanisms in resistance to infection. *Ann. Rev. Immunol.* *18*, 275-308.
- Hashimoto-Tane, A., Yokosuka, T., Ishihara, C., Sakuma, M., Kobayashi, W., and Saito, T. (2010). T-cell receptor microclusters critical for T-cell activation are formed independently of lipid raft clustering. *Mol. Cel. Biol.* *30*, 3421-3429.
- Hennecke, J., and Wiley, D.C. (2002). Structure of a complex of the human α/β T Cell Receptor (TCR) HA1.7, influenza hemagglutinin peptide, and major histocompatibility complex class II molecule, HLA-DR4 (DRA0101 and DRB10401): insight into TCR cross-restriction and alloreactivity. *J. Exp. Med.* *195*, 571-581.
- Hennecke, S., and Cosson, P. (1993). Role of transmembrane domains in assembly and intracellular transport of the CD8 molecule. *J. Biol. Chem.* *268*, 26607-26612.
- Hunt, D., Michel, H., Dickinson, T., Shabanowitz, J., Cox, A., Sakaguchi, K., Appella, E., Grey, H., and Sette, A. (1992). Peptides presented to the immune system by the murine class II major histocompatibility complex molecule I-Ad. *Science* *256*, 1817-1820.
- Huse, M. (2009). The T-cell-receptor signaling network. *J. Cell Sci.* *122*, 1269-1273.
- Irie, H.Y., Mong, M.S., Itano, A., Crooks, M.E.C., Littman, D.R., Burakoff, S.J., and Robey, E. (1998). The cytoplasmic domain of CD8 β regulates Lck kinase activation and CD8 T cell development. *J. Immunol.* *161*, 183-191.
- Irles, C., Symons, A., Michel, F., Bakker, T.R., van der Merwe, P.A., and Acuto, O. (2003). CD45 ectodomain controls interaction with GEMs and Lck activity for optimal TCR signaling. *Nat. Immunol.* *4*, 189-197.
- Irvine, D.J., Purbhoo, M.A., Krogsgaard, M., and Davis, M.M. (2002). Direct observation of ligand recognition by T cells. *Nature* *419*, 845-849.
- Itano, A., Cado, D., Chan, F.K.M., and Robey, E. (1994). A role for the cytoplasmic tail of the β chain of CD8 in thymic selection. *Immunity* *1*, 287-290.
- James, S.E., Greenberg, P.D., Jensen, M.C., Lin, Y., Wang, J., Till, B.G., Raubitschek, A.A., Forman, S.J., and Press, O.W. (2008). Antigen sensitivity of CD22-specific chimeric TCR is modulated by target epitope distance from the cell membrane. *J. Immunol.* *180*, 7028-7038.
- Janes, P.W., Ley, S.C., and Magee, A.I. (1999). Aggregation of lipid rafts accompanies signaling via the T cell antigen receptor. *J. Cell Biol.* *147*, 447-461.

- Jiang, N., Huang, J., Edwards, L.J., Liu, B., Zhang, Y., Beal, C.D., Evavold, B.D., and Zhu, C. (2011). Two-stage cooperative T cell receptor-peptide major histocompatibility complex-CD8 trimolecular interactions amplify antigen discrimination. *Immunity* 34, 13-23.
- Kane, L.P., Lin, J., and Weiss, A. (2000). Signal transduction by the TCR for antigen. *Curr. Opin. Immunol.* 12, 242-249.
- Kern, P., Hussey, R.E., Spoerl, R., Reinherz, E.L., and Chang, H.-C. (1999). Expression, purification, and functional analysis of murine ectodomain fragments of CD8 $\alpha\alpha$ and CD8 $\alpha\beta$ dimers. *J. Biol. Chem.* 274, 27237-27243.
- Klein, L., Münz, C., and Lünemann, J.D. (2010). Autophagy-mediated antigen processing in CD4⁺ T cell tolerance and immunity. *FEBS Lett.* 584, 1405-1410.
- Klenerman, P., Cerundolo, V., and Dunbar, P.R. (2002). Tracking T cells with tetramers: new tales from new tools. *Nat. Rev. Immunol.* 2, 263-272.
- Knabel, M., Franz, T.J., Schiemann, M., Wulf, A., Villmow, B., Schmidt, B., Bernhard, H., Wagner, H., and Busch, D.H. (2002). Reversible MHC multimer staining for functional isolation of T-cell populations and effective adoptive transfer. *Nat. Med.* 8, 631-637.
- Koch, U., and Radtke, F. (2011). Mechanisms of T cell development and transformation. *Ann. Rev. Cell Dev. Biol.* 27, 539-562.
- Korndörfer, I.P., and Skerra, A. (2002). Improved affinity of engineered streptavidin for the Strep-Tag II peptide is due to a fixed open conformation of the lid-like loop at the binding site. *Prot. Sci.* 11, 883-893.
- Kosugi, A., Sakakura, J., Yasuda, K., Ogata, M., and Hamaoka, T. (2001). Involvement of SHP-1 tyrosine phosphatase in TCR-mediated signaling pathways in lipid rafts. *Immunity* 14, 669-680.
- Krogsgaard, M., Li, Q.-j., Sumen, C., Huppa, J.B., Huse, M., and Davis, M.M. (2005). Agonist/endogenous peptide-MHC heterodimers drive T cell activation and sensitivity. *Nature* 434, 238-243.
- Kuhns, M.S., Girvin, A.T., Klein, L.O., Chen, R., Jensen, K.D.C., Newell, E.W., Huppa, J.B., Lillemeier, B.F., Huse, M., Chien, Y.-h., *et al.* (2010). Evidence for a functional sidedness to the $\alpha\beta$ TCR. *Proc. Nat. Acad. Sci.* 107, 5094-5099.
- Kumanovics, A., Takada, T., and Lindahl, K.F. (2003). Genomic organization of the mammalian Mhc. *Ann. Rev. Immunol.* 21, 629-657.
- Kumar, R., Ferez, M., Swamy, M., Arechaga, I., Rejas, María T., Valpuesta, Jose M., Schamel, Wolfgang W.A., Alarcon, B., and van Santen, Hisse M. (2011). Increased sensitivity of antigen-experienced T cells through the enrichment of oligomeric T cell receptor complexes. *Immunity* 35, 375-387.
- Kwok, W.W. (2003). Challenges in staining T cells using HLA class II tetramers. *Clin. Immunol.* 106, 23-28.

- Kwok, W.W., Ptacek, N.A., Liu, A.W., and Buckner, J.H. (2002). Use of class II tetramers for identification of CD4⁺ T cells. *J. Immunol. Meth.* 268, 71-81.
- Landais, E., Romagnoli, P.A., Corper, A.L., Shires, J., Altman, J.D., Wilson, I.A., Garcia, K.C., and Teyton, L. (2009). New design of MHC class II tetramers to accommodate fundamental principles of antigen presentation. *J. Immunol.* 183, 7949-7957.
- Le Borgne, S., Graber, M., and Condoret, J. (1995). Experimental and theoretical analysis of the chromatographic behaviour of protein purification fusions carrying charged tails. *Bioseparation* 5, 53-64.
- Ledbetter, J.A., Evans, R.L., Lipinski, M., C, C.-R., Good, R.A., and Herzenberg, L.A. (1981a). Evolutionary conservation of surface molecules that distinguish T lymphocyte helper/inducer and cytotoxic/suppressor subpopulations in mouse and man. *J. Exp. Med.* 153, 310-323.
- Ledbetter, J.A., Seaman, W.E., Tsu, T.T., and Herzenberg, L.A. (1981b). Lyt-2 and lyt-3 antigens are on two different polypeptide subunits linked by disulfide bonds. Relationship of subunits to T cell cytolytic activity. *J. Exp. Med.* 153, 1503-1516.
- Lederman, S., Cleary, A.M., Yellin, M.J., Frank, D.M., Karpusas, M., Thomas, D.W., and Chess, L. (1996). The central role of the CD40-ligand and CD40 pathway in T-lymphocyte-mediated differentiation of B lymphocytes. *Curr. Opin. Hematol.* 3, 77-86.
- Levisetti, M.G., Suri, A., Petzold, S.J., and Unanue, E.R. (2007). The insulin-specific T cells of nonobese diabetic mice recognize a weak MHC-binding segment in more than one form. *J. Immunol.* 178, 6051-6057.
- Lin, J., and Weiss, A. (2003). The tyrosine phosphatase CD148 is excluded from the immunologic synapse and down-regulates prolonged T cell signaling. *J. Cell Biol.* 162, 673-682.
- Lingwood, D., and Simons, K. (2010). Lipid rafts as a membrane-organizing principle. *Science* 327, 46-50.
- Lippolis, J.D., White, F.M., Marto, J.A., Luckey, C.J., Bullock, T.N.J., Shabanowitz, J., Hunt, D.F., and Engelhard, V.H. (2002). Analysis of MHC class II antigen processing by quantitation of peptides that constitute nested sets. *J. Immunol.* 169, 5089-5097.
- Lissina, A., Ladell, K., Skowera, A., Clement, M., Edwards, E., Seggewiss, R., van den Berg, H.A., Gostick, E., Gallagher, K., Jones, E., *et al.* (2009). Protein kinase inhibitors substantially improve the physical detection of T-cells with peptide-MHC tetramers. *J. Immunol. Meth.* 340, 11-24.
- Livnah, O., Stura, E.A., Middleton, S.A., Johnson, D.L., Jolliffe, L.K., and Wilson, I.A. (1999). Crystallographic evidence for preformed dimers of erythropoietin receptor before ligand activation. *Science* 283, 987-990.
- LoGrasso, P.V., Hawkins, J., Frank, L.J., Wisniewski, D., and Marcy, A. (1996). Mechanism of activation for Zap-70 catalytic activity. *Proc. Nat. Acad. Sci.* 93, 12165-12170.

- Lovitch, S.B., Pu, Z., and Unanue, E.R. (2006). Amino-terminal flanking residues determine the conformation of a peptide-class II MHC complex. *J. Immunol.* *176*, 2958-2968.
- Lovitch, S.B., and Unanue, E.R. (2005). Conformational isomers of a peptide-class II major histocompatibility complex. *Immunol. Rev.* *207*, 293-313.
- Luescher, I.F., Anjuère, F., Peitsch, M.C., Jongeneel, C.V., Cerottini, J.-C., and Romero, P. (1995a). Structural analysis of TCR-ligand interactions studied on H-2Kd-restricted cloned CTL specific for a photoreactive peptide derivative. *Immunity* *3*, 51-63.
- Luescher, I.F., Lóez, J.A., Malissen, B., and Cerottini, J.C. (1992). Interaction of antigenic peptides with MHC class I molecules on living cells studied by photoaffinity labeling. *J. Immunol.* *148*, 1003-1011.
- Luescher, I.F., Romero, P., Cerottini, J.-C., and Maryanski, J.L. (1991). Specific binding of antigenic peptides to cell-associated MHC class I molecules. *Nature* *351*, 72-74.
- Luescher, I.F., Vivier, E., Layer, A., Mahiou, J., Godeau, F., Malissen, B., and Romero, P. (1995b). CD8 modulation of T-cell antigen receptor-ligand interactions on living cytotoxic T lymphocytes. *Nature* *373*, 353-356.
- Ma, Z., Sharp, K.A., Janmey, P.A., and Finkel, T.H. (2008). Surface-anchored monomeric agonist pMHCs alone trigger TCR with high sensitivity. *PLoS Biol.* *6*, e43.
- Maekawa, A., Schmidt, B., Fazekas de St. Groth, B., Sanejouand, Y.-H., and Hogg, P.J. (2006). Evidence for a domain-swapped CD4 dimer as the coreceptor for binding to class II MHC. *J. Immunol.* *176*, 6873-6878.
- Maile, R., Siler, C.A., Kerry, S.E., Midkiff, K.E., Collins, E.J., and Frelinger, J.A. (2005). Peripheral "CD8 tuning" dynamically modulates the size and responsiveness of an antigen-specific T cell pool in vivo. *J. Immunol.* *174*, 619-627.
- Mallaun, M., Naeher, D., Daniels, M.A., Yachi, P.P., Hausmann, B., Luescher, I.F., Gascoigne, N.R.J., and Palmer, E. (2008). The T cell receptors α -chain connecting peptide motif promotes close approximation of the CD8 coreceptor allowing efficient signal initiation. *J. Immunol.* *180*, 8211-8221.
- Massilamany, C., Gangaplara, A., Chapman, N., Rose, N., and Reddy, J. (2011). Detection of cardiac myosin heavy chain- α -specific CD4 cells by using MHC class II/IAk tetramers in A/J mice. *J. Immunol. Meth.* *372*, 107-118.
- Medzhitov, R. (2007). Recognition of microorganisms and activation of the immune response. *Nature* *449*, 819-826.
- Merwe, P.A.v.d., and Davis, S.J. (2003). Molecular interactions mediating T cell antigen recognition. *Annu. Rev. Immunol.* *21*, 659-684.
- Meyer, A.L., Trollmo, C., Crawford, F., Marrack, P., Steere, A.C., Huber, B.T., Kappler, J., and Hafler, D.A. (2000). Direct enumeration of Borrelia-reactive CD4 T cells ex vivo by using MHC class II tetramers. *Proc. Nat. Acad. Sci.* *97*, 11433-11438.

- Minguet, S., Swamy, M., Alarcón, B., Luescher, I.F., and Schamel, W.W.A. (2007). Full activation of the T cell receptor requires both clustering and conformational changes at CD3. *Immunity* 26, 43-54.
- Mohan, J.F., Levisetti, M.G., Calderon, B., Herzog, J.W., Petzold, S.J., and Unanue, E.R. (2010). Unique autoreactive T cells recognize insulin peptides generated within the islets of Langerhans in autoimmune diabetes. *Nat. Immunol.* 11, 350-354.
- Mohan, J.F., Petzold, S.J., and Unanue, E.R. (2011). Register shifting of an insulin peptide–MHC complex allows diabetogenic T cells to escape thymic deletion. *J. Exp. Med.* 208, 2375-2383.
- Mohan, J.F., and Unanue, E.R. (2012). Unconventional recognition of peptides by T cells and the implications for autoimmunity. *Nat. Rev. Immunol.* *advance online publication*.
- Montixi, C., Langlet, C., Bernard, A.-M., Thimonier, J., Dubois, C., Wurbel, M.-A., Chauvin, J.-P., Pierres, M., and He, H.-T. (1998). Engagement of T cell receptor triggers its recruitment to low-density detergent-insoluble membrane domains. *EMBO J.* 17, 5334-5348.
- Moody, A.M., Chui, D., Reche, P.A., Priatel, J.J., Marth, J.D., and Reinherz, E.L. (2001). Developmentally regulated glycosylation of the CD8 $\alpha\beta$ coreceptor stalk modulates ligand binding. *Cell* 107, 501-512.
- Moon, J.J., Chu, H.H., Pepper, M., McSorley, S.J., Jameson, S.C., Kedl, Ross M., and Jenkins, M.K. (2007). Naive CD4⁺ T cell frequency varies for different epitopes and predicts repertoire diversity and response magnitude. *Immunity* 27, 203-213.
- Moran, M., and Miceli, M.C. (1998). Engagement of GPI-linked CD48 contributes to TCR signals and cytoskeletal reorganization: a role for lipid rafts in T cell activation. *Immunity* 9, 787-796.
- Naeher, D., Daniels, M.A., Hausmann, B., Guillaume, P., Luescher, I., and Palmer, E. (2007). A constant affinity threshold for T cell tolerance. *J. Exp. Med.* 204, 2553-2559.
- Naeher, D., Luescher, I.F., and Palmer, E. (2002). A role for the α -chain connecting peptide motif in mediating TCR-CD8 cooperation. *J. Immunol.* 169, 2964-2970.
- Nag, B., Mukku, P.V., Arimilli, S., Kendrick, T., Deshpande, S.V., and Sharma, S.D. (1994). Separation of complexes of major histocompatibility class II molecules and known antigenic peptide by metal chelate affinity chromatography. *J. Immunol. Meth.* 169, 273-285.
- Nakayama, M., Abiru, N., Moriyama, H., Babaya, N., Liu, E., Miao, D., Yu, L., Wegmann, D.R., Hutton, J.C., Elliott, J.F., and Eisenbarth, G.S. (2005). Prime role for an insulin epitope in the development of type 1 diabetes in NOD mice. *Nature* 435, 220-223.
- Natarajan, S.K., Assadi, M., and Sadegh-Nasseri, S. (1999a). Stable peptide binding to MHC class II molecule is rapid and is determined by a receptive conformation shaped by prior association with low affinity peptides. *J. Immunol.* 162, 4030-4036.

- Natarajan, S.K., Stern, L.J., and Sadegh-Nasseri, S. (1999b). Sodium dodecyl sulfate stability of HLA-DR1 complexes correlates with burial of hydrophobic residues in pocket 1. *J. Immunol.* *162*, 3463-3470.
- Neefjes, J., Jongstra, M.L.M., Paul, P., and Bakke, O. (2011). Towards a systems understanding of MHC class I and MHC class II antigen presentation. *Nat. Rev. Immunol.* *11*, 823-836.
- Newell, Evan W., Sigal, N., Bendall, Sean C., Nolan, Garry P., and Davis, Mark M. (2012). Cytometry by time-of-flight shows combinatorial cytokine expression and virus-specific cell niches within a continuum of CD8⁺ T cell phenotypes. *Immunity* *36*, 142-152.
- Novak, E.J., Masewicz, S.A., Liu, A.W., Lernmark, A., Kwok, W.W., and Nepom, G.T. (2001). Activated human epitope-specific T cells identified by class II tetramers reside within a CD4high, proliferating subset. *Int. Immunol.* *13*, 799-806.
- O'Rourke, A.M., Apgar, J.R., Kane, K.P., Martz, E., and Mescher, M.F. (1991). Cytoskeletal function in CD8- and T cell receptor-mediated interaction of cytotoxic T lymphocytes with class I protein. *J Exp. Med.* *173*, 241-249.
- O'Rourke, A.M., Rogers, J., and Mescher, M.F. (1990). Activated CD8 binding to class I protein mediated by the T-cell receptor results in signalling. *Nature* *346*, 187-189.
- Palacios, E.H., and Weiss, A. (2004). Function of the Src-family kinases, Lck and Fyn, in T-cell development and activation. *Oncogene* *23*, 7990-8000.
- Palmer, E. (2003). Negative selection - clearing out the bad apples from the T-cell repertoire. *Nat. Rev. Immunol.* *3*, 383-391.
- Palmer, E., and Naeher, D. (2009). Affinity threshold for thymic selection through a T-cell receptor-co-receptor zipper. *Nat. Rev. Immunol.* *9*, 207-213.
- Pang, D.J., Hayday, A.C., and Bijlmakers, M.-J. (2007). CD8 raft localization is induced by its assembly into CD8 $\alpha\beta$ heterodimers, not CD8 $\alpha\alpha$ homodimers. *J. Biol. Chem.* *282*, 13884-13894.
- Pitcher, L.A., and van Oers, N.S.C. (2003). T-cell receptor signal transmission: who gives an ITAM? *Trends Immunol.* *24*, 554-560.
- Pizzo, P., Giurisato, E., Tassi, M., Benedetti, A., Pozzan, T., and Viola, A. (2002). Lipid rafts and T cell receptor signaling: a critical re-evaluation. *Eur. J. Immunol.* *32*, 3082-3091.
- Porter, G.W., Yi, W., and Denzin, L.K. (2011). TLR agonists downregulate H2-O in CD8 α -dendritic cells. *J. Immunol.* *187*, 4151-4160.
- Posch, P.E., Hastings, A.E., Rosen-Bronson, S., Richert, J.R., and Hurley, C.K. (1996). The relative importance of individual DR binding motif positions as defined by peptide anchor analysis of influenza hemagglutinin peptide 306-318 and human myelin basic protein peptide 152-165 binding to several DR molecules: definition of a common extended DR binding motif. *Eur. J. Immunol.* *26*, 1884-1891.

- Pu, Z., Carrero, J.A., and Unanue, E.R. (2002). Distinct recognition by two subsets of T cells of an MHC class II-peptide complex. *Proc. Nat. Acad. Sci.* *99*, 8844-8849.
- Pu, Z., Lovitch, S.B., Bikoff, E.K., and Unanue, E.R. (2004). T cells distinguish MHC-peptide complexes formed in separate vesicles and edited by H2-DM. *Immunity* *20*, 467-476.
- Purbhoo, M.A., Boulter, J.M., Price, D.A., Vuidepot, A.-L., Hourigan, C.S., Dunbar, P.R., Olson, K., Dawson, S.J., Phillips, R.E., Jakobsen, B.K., *et al.* (2001). The human CD8 coreceptor effects cytotoxic T cell activation and antigen sensitivity primarily by mediating complete phosphorylation of the T cell receptor ζ chain. *J. Biol. Chem.* *276*, 32786-32792.
- Purbhoo, M.A., Irvine, D.J., Huppa, J.B., and Davis, M.M. (2004). T cell killing does not require the formation of a stable mature immunological synapse. *Nat. Immunol.* *5*, 524-530.
- Quezada, S.A., Simpson, T.R., Peggs, K.S., Merghoub, T., Vider, J., Fan, X., Blasberg, R., Yagita, H., Muranski, P., Antony, P.A., *et al.* (2010). Tumor-reactive CD4⁺ T cells develop cytotoxic activity and eradicate large established melanoma after transfer into lymphopenic hosts. *J. Exp. Med.* *207*, 637-650.
- Qui, H.Z., Hagymasi, A.T., Bandyopadhyay, S., St. Rose, M.-C., Ramanarasimhaiah, R., Ménoret, A., Mittler, R.S., Gordon, S.M., Reiner, S.L., Vella, A.T., and Adler, A.J. (2011). CD134 plus CD137 dual costimulation induces eomesodermin in CD4 T cells to program cytotoxic Th1 differentiation. *J. Immunol.* *187*, 3555-3564.
- Rabinowitz, J.D., Vrljic, M., Kasson, P.M., Liang, M.N., Busch, R., Boniface, J.J., Davis, M.M., and McConnell, H.M. (1998). Formation of a highly peptide-receptive state of class II MHC. *Immunity* *9*, 699-709.
- Randolph, D.A., and Fathman, C.G. (2006). CD4⁺CD25⁺ Regulatory T Cells and Their Therapeutic Potential. *Ann. Rev. Med.* *57*, 381-402.
- Reddy, J., Bettelli, E., Nicholson, L., Waldner, H., Jang, M.-H., Wucherpfennig, K.W., and Kuchroo, V.K. (2003). Detection of autoreactive myelin proteolipid protein 139-151-specific T cells by using MHC II (IAs) tetramers. *J. Immunol.* *170*, 870-877.
- Reich, Z., Boniface, J.J., Lyons, D.S., Borochoy, N., Wachtel, E.J., and Davis, M.M. (1997). Ligand-specific oligomerization of T-cell receptor molecules. *Nature* *387*, 617-620.
- Reichstetter, S., Ettinger, R.A., Liu, A.W., Gebe, J.A., Nepom, G.T., and Kwok, W.W. (2000). Distinct T cell interactions with HLA class II tetramers characterize a spectrum of TCR affinities in the human antigen-specific T cell response. *J. Immunol.* *165*, 6994-6998.
- Reinhardt, R.L., Kang, S.-J., Liang, H.-E., and Locksley, R.M. (2006). T helper cell effector fates — who, how and where? *Curr. Opin. Immunol.* *18*, 271-277.
- Renard, V., Romero, P., Vivier, E., Malissen, B., and Luescher, I.F. (1996). CD8beta increases CD8 coreceptor function and participation in TCR-ligand binding. *J. Exp. Med.* *184*, 2439-2444.

- Rettig, L., McNeill, L., Sarner, N., Guillaume, P., Luescher, I., Tolaini, M., Kioussis, D., and Zamoyska, R. (2009). An essential role for the stalk region of CD8 β in the coreceptor function of CD8. *J. Immunol.* *182*, 121-129.
- Robins, H.S., Campregher, P.V., Srivastava, S.K., Wachter, A., Turtle, C.J., Kahsai, O., Riddell, S.R., Warren, E.H., and Carlson, C.S. (2009). Comprehensive assessment of T-cell receptor β -chain diversity in $\alpha\beta$ T cells. *Blood* *114*, 4099-4107.
- Romero, P., Cerottini, J.-C., and Luescher, I.F. (2005). On the significance of CD8 $\alpha\alpha$ expression for T cell memory. *Eur. J. Immunol.* *35*, 3092-3094.
- Rötzschke, O., Falk, K., Mack, J., Lau, J.M., Jung, G., and Strominger, J.L. (1999). Conformational variants of class II MHC/peptide complexes induced by N- and C-terminal extensions of minimal peptide epitopes. *Proc. Nat. Acad. Sci.* *96*, 7445-7450.
- Rudensky, A.Y., Preston-Hurlburt, P., Hong, S.-C., Barlow, A., and Janeway, C.A. (1991). Sequence analysis of peptides bound to MHC class II molecules. *Nature* *353*, 622-627.
- Rudolph, M.G., Luz, J.G., and Wilson, I.A. (2002). Structural and thermodynamic correlates of T cell signaling. *Ann. Rev. Biophys. Biomol. Struct.* *31*, 121-149.
- Rudolph, M.G., Stanfield, R.L., and Wilson, I.A. (2006). How TCRs bind MHCs, peptides, and coreceptors. *Ann. Rev. Immunol.* *24*, 419-466.
- Runnels, H.A., Moore, J.C., and Jensen, P.E. (1996). A structural transition in class II major histocompatibility complex proteins at mildly acidic pH. *J. Exp. Med.* *183*, 127-136.
- Sabatino, J.J., Huang, J., Zhu, C., and Evavold, B.D. (2011). High prevalence of low affinity peptide-MHC II tetramer-negative effectors during polyclonal CD4⁺ T cell responses. *J. Exp. Med.* *208*, 81-90.
- Sant'Angelo, D.B., Robinson, E., Janeway, J.C.A., and Denzin, L.K. (2002). Recognition of core and flanking amino acids of MHC class II-bound peptides by the T cell receptor. *Eur. J. Immunol.* *32*, 2510-2520.
- Schamel, W.W.A., Arechaga, I., Risueno, R.M., van Santen, H.M., Cabezas, P., Risco, C., Valpuesta, J.M., and Alarcon, B. (2005). Coexistence of multivalent and monovalent TCRs explains high sensitivity and wide range of response. *J. Exp. Med.* *202*, 493-503.
- Schamel, W.W.A., Risueño, R.M., Minguet, S., Ortíz, A.R., and Alarcón, B. (2006). A conformation- and avidity-based proofreading mechanism for the TCR-CD3 complex. *Trends Immunol.* *27*, 176-182.
- Schmidt, J., Guillaume, P., Irving, M., Baumgaertner, P., Speiser, D., and Luescher, I.F. (2011). Reversible major histocompatibility complex I-peptide multimers containing Ni²⁺-nitrilotriacetic acid peptides and histidine tags improve analysis and sorting of CD8⁺ T cells. *J. Biol. Chem.* *286*, 41723-41735.
- Schmitt, L., Boniface, J.J., Davis, M.M., and McConnell, H.M. (1999). Conformational isomers of a class II MHC-peptide complex in solution. *J. Mol. Biol.* *286*, 207-218.

- Schott, E., Bertho, N., Ge, Q., Maurice, M.M., and Ploegh, H.L. (2002). Class I negative CD8 T cells reveal the confounding role of peptide-transfer onto CD8 T cells stimulated with soluble H2-Kb molecules. *Proc. Nat. Acad. Sci.* *99*, 13735-13740.
- Seidl, T., Rolink, A., and Melchers, F. (2001). The VpreB protein of the surrogate light-chain can pair with some μ heavy-chains in the absence of the $\lambda 5$ protein. *Eur. J. Immunol.* *31*, 1999-2006.
- Sette, A., Southwood, S., O'Sullivan, D., Gaeta, F., Sidney, J., and Grey, H.M. (1992). Effect of pH on MHC class II-peptide interactions. *J. Immunol.* *148*, 844-851.
- Shore, D., Wilson, I., Dwek, R., and Rudd, P. (2005). Glycosylation and the function of the T cell co-receptor CD8. In *Glycobiology and Medicine*, J. Axford, ed. (Springer Netherlands), pp. 71-84.
- Smith-Garvin, J.E., Koretzky, G.A., and Jordan, M.S. (2009). T cell activation. *Ann. Rev. Immunol.* *27*, 591-619.
- Stadinski, B.D., Zhang, L., Crawford, F., Marrack, P., Eisenbarth, G.S., and Kappler, J.W. (2010). Diabetogenic T cells recognize insulin bound to IA2 in an unexpected, weakly binding register. *Proc. Nat. Acad. Sci.* *107*, 10978-10983.
- Stanley, J.B., Gorczynski, R., Huang, C.K., Love, J., and Mills, G.B. (1990). Tyrosine phosphorylation is an obligatory event in IL-2 secretion. *J. Immunol.* *145*, 2189-2198.
- Stubenrauch, K., Bachmann, A., Rudolph, R., and Lilie, H. (2000). Purification of a viral coat protein by an engineered polyionic sequence. *J. Chrom. B* *737*, 77-84.
- Suominen, I., Nurmela, H., Heimo, H., Ford, C., Stachon, D., and Glatz, C. (1992). Use of charged tails in protein-purification fusions. *Ann. New York Acad. Sci.* *672*, 106-113.
- Susan L, S. (1999). Helper T cell differentiation. *Curr. Opin. Immunol.* *11*, 180-185.
- Suzuki, S., Kupsch, J., Eichmann, K., and Saizawa, M.K. (1992). Biochemical evidence of the physical association of the majority of CD3 δ chains with the accessory/co-receptor molecules CD4 and CD8 on nonactivated T lymphocytes. *Eur. J. Immunol.* *22*, 2475-2479.
- Takada, S., and Engleman, E.G. (1987). Evidence for an association between CD8 molecules and the T cell receptor complex on cytotoxic T cells. *J. Immunol.* *139*, 3231-3235.
- Tato, C.M., Laurence, A., and O'Shea, J.J. (2006). Helper T cell differentiation enters a new era: Le Roi est mort; vive le Roi! *J. Exp. Med.* *203*, 809-812.
- Toebes, M., Coccoris, M., Bins, A., Rodenko, B., Gomez, R., Nieuwkoop, N.J., van de Kastele, W., Rimmelzwaan, G.F., Haanen, J.B.A.G., Ovaa, H., and Schumacher, T.N.M. (2006). Design and use of conditional MHC class I ligands. *Nat. Med.* *12*, 246-251.
- Varma, R., Campi, G., Yokosuka, T., Saito, T., and Dustin, M.L. (2006). T cell receptor-proximal signals are sustained in peripheral microclusters and terminated in the central supramolecular activation cluster. *Immunity* *25*, 117-127.

- Veldhoen, M., Uyttenhove, C., van Snick, J., Helmby, H., Westendorf, A., Buer, J., Martin, B., Wilhelm, C., and Stockinger, B. (2008). Transforming growth factor- β 'reprograms' the differentiation of T helper 2 cells and promotes an interleukin 9-producing subset. *Nat. Immunol.* *9*, 1341-1346.
- Viner, N.J., Nelson, C.A., Deck, B., and Unanue, E.R. (1996). Complexes generated by the binding of free peptides to class II MHC molecules are antigenically diverse compared with those generated by intracellular processing. *J. Immunol.* *156*, 2365-2368.
- Vollers, S.S., and Stern, L.J. (2008). Class II major histocompatibility complex tetramer staining: progress, problems, and prospects. *Immunology* *123*, 305-313.
- Voss, S., and Skerra, A. (1997). Mutagenesis of a flexible loop in streptavidin leads to higher affinity for the Strep-tag II peptide and improved performance in recombinant protein purification. *Prot. Engin.* *10*, 975-982.
- Wahl, S., and Chen, W. (2005). Transforming growth factor-beta-induced regulatory T cells referee inflammatory and autoimmune diseases. *Arthritis Res. Ther.* *7*, 62-68.
- Walden, P.R., and Eisen, H.N. (1990). Cognate peptides induce self-destruction of CD8+ cytolytic T lymphocytes. *Proc. Nat. Acad. Sci.* *87*, 9015-9019.
- Wang, R., Natarajan, K., and Margulies, D.H. (2009). Structural basis of the CD8 $\alpha\beta$ /MHC class I interaction: focused recognition orients CD8 β to a T cell proximal position. *J. Immunol.* *183*, 2554-2564.
- Wu, S.-C., and Wong, S.-L. (2004). Development of an enzymatic method for site-specific incorporation of desthiobiotin to recombinant proteins in vitro. *Anal. Biochem.* *331*, 340-348.
- Wulfing, C., Sumen, C., Sjaastad, M.D., Wu, L.C., Dustin, M.L., and Davis, M.M. (2002). Costimulation and endogenous MHC ligands contribute to T cell recognition. *Nat. Immunol.* *3*, 42-47.
- Xavier, R., Brennan, T., Li, Q., McCormack, C., and Seed, B. (1998). Membrane compartmentation is required for efficient T cell activation. *Immunity* *8*, 723-732.
- Xie, Y., Akpınarlı, A., Maris, C., Hipkiss, E.L., Lane, M., Kwon, E.-K.M., Muranski, P., Restifo, N.P., and Antony, P.A. (2010). Naive tumor-specific CD4+ T cells differentiated in vivo eradicate established melanoma. *J. Exp. Med.* *207*, 651-667.
- Xiong, Y., Kern, P., Chang, H.-C., and Reinherz, E.L. (2001). T cell receptor binding to a pMHCII ligand is kinetically distinct from and independent of CD4. *J. Biol. Chem.* *276*, 5659-5667.
- Xiu, F., Côté, M.-H., Bourgeois-Daigneault, M.-C., Brunet, A., Gauvreau, M.-É., Shaw, A., and Thibodeau, J. (2011). Cutting edge: HLA-DO impairs the incorporation of HLA-DM into exosomes. *J. Immunol.* *187*, 1547-1551.
- Yachi, P.P., Ampudia, J., Gascoigne, N.R.J., and Zal, T. (2005). Nonstimulatory peptides contribute to antigen-induced CD8-T cell receptor interaction at the immunological synapse. *Nat. Immunol.* *6*, 785-792.

- Yamasaki, S., Ishikawa, E., Sakuma, M., Ogata, K., Sakata-Sogawa, K., Hiroshima, M., Wiest, D.L., Tokunaga, M., and Saito, T. (2006). Mechanistic basis of pre-T cell receptor-mediated autonomous signaling critical for thymocyte development. *Nat. Immunol.* *7*, 67-75.
- Yamazaki, S., Inaba, K., Tarbell, K.V., and Steinman, R.M. (2006). Dendritic cells expand antigen-specific Foxp3⁺CD25⁺CD4⁺ regulatory T cells including suppressors of alloreactivity. *Imm. Rev.* *212*, 314-329.
- Yin, Y., Wang, X.X., and Mariuzza, R.A. (2012). Crystal structure of a complete ternary complex of T-cell receptor, peptide–MHC, and CD4. *Proc. Nat. Acad. Sci.* *109*, 5405-5410.
- Yokosuka, T., Sakata-Sogawa, K., Kobayashi, W., Hiroshima, M., Hashimoto-Tane, A., Tokunaga, M., Dustin, M.L., and Saito, T. (2005). Newly generated T cell receptor microclusters initiate and sustain T cell activation by recruitment of Zap70 and SLP-76. *Nat. Immunol.* *6*, 1253-1262.
- Zal, T., and Gascoigne, N.R.J. (2004). Photobleaching-corrected FRET efficiency imaging of live cells. *Biophys. J.* *86*, 3923-3939.
- Zarour, H.M., Maillere, B., Brusica, V., Coval, K., Williams, E., Pouvelle-Moratille, S., Castelli, F., Land, S., Bennouna, J., Logan, T., and Kirkwood, J.M. (2002). NY-ESO-1 119–143 is a promiscuous major histocompatibility complex class II T-helper epitope recognized by Th1- and Th2-type tumor-reactive CD4⁺ T cells. *Cancer Res.* *62*, 213-218.
- Zarutskie, J.A., Sato, A.K., Rushe, M.M., Chan, I.C., Lomakin, A., Benedek, G.B., and Stern, L.J. (1999). A conformational change in the human major histocompatibility complex protein HLA-DR1 induced by peptide binding. *Biochemistry* *38*, 5878-5887.
- Zhu, M., Shen, S., Liu, Y., Granillo, O., and Zhang, W. (2005). Cutting edge: Localization of linker for activation of T cells to lipid rafts is not essential in T cell activation and development. *J. Immunol.* *174*, 31-35.